Spectroscopic studies on the liquid phase dynamics and interactions of acetonitrile

Kevin Eric Arnold

Spectroscopic Studies on the Liquid Phase Dynamics and Interactions of Acetonitrile.

by

Kevin Eric Arnold, B.Sc. (Durham)

(Grey College)

A thesis submitted for the degree of Doctor of Philosophy in the University of Durham, 1981

Declaration

The material described in this thesis was carried out by the author in the department of chemistry ,University of Durham, University College of Wales Edward Davies Chemical Laboratories , Aberystwyth and the Institüt für Physikalische Chemie der Technischen Universtät, Braunschweig between October 1978 and October 1981. It has not been submitted for any other degree. The work is my own work except where acknowledged by reference.

Acknowledgements

I am grateful to Dr. Jack Yarwood for providing the opportunity to pursue this work, and the constant encouragement given throughout; also to the Chemistry Department's technical staff and the staff of Durham University Computer Unit.

I am indebted to Dr. Alun Price at U.C.W. Aberystwyth, for the use of the microwave equipment and for the help and advice he gave; and to Professor Gottfried Döge at the Technical University, Braunschweig, for the use of the Raman equipment.

Many thanks to Albrecht Khuen and Manfred Possiel for their help and hospitality, to Graham O'Neill and Peter James for some useful discussions, and to Barbara Janik for sending me some microwave measurements on the pure liquid CH_3CN from Poland.

Thanks are also due to the SRC for funding the three years' research and to NATO for paying for the trip to Braunschweig.

Finally, thanks to Dr. Ian Burdess of Durham University Microprocessor Centre for the use of the word processor facilities in getting this thesis into print, and to Wanda Malinowski for helping to type and proof read it.

Abstract

Spectroscopic studies on the liquid phase dynamics and interactions of acetonitrile.

Microwave and far-infrared spectra were used to study the angular motion of CH_3CN molecules in the pure liquid and in the non-polar solvents carbon tetrachloride, benzene and n-heptane. The spectral data were analysed to give information on the static angular structure of the liquid and the rates of reorientational motion of the CH_3CN molecules. The use of these two experimental techniques enabled the short and long time parts of the angular motion to be studied together using Fourier transform analysis of the combined microwave/far-infrared spectrum. Band moment analysis was performed on the microwave/far-infrared band in order to obtain information on intermolecular torques. Gordon's sum rule was applied to the spectra in an attempt to estimate what proportion of the band is due to the presence of collision induced dipoles in the CH_3CN molecules. The reorientational relaxation rates and static angular correlation factors obtained from the microwave/far-infrared spectra were compared with literature data on similar solutions obtained by depolarised light scattering experiments.

The model for reorientational motion developed by Evans on the Mori formalism was fitted to the experimental spectrum of the pure liquid and the results discussed in terms of the parameters of the model.

The ν_1 vibrational band of CH_3CN was analysed when the molecule was subject to 'hydrogen bonding' interactions with methanol. An attempt was made to elucidate the processes which cause the vibrational band to be broadened in these solutions. The vibrational line shapes were analysed using the Kubo line shape theory for the rapid modulation limit.

To my family and friends.

Contents

Chapter I.

Introduction

I.1 General Introduction

The structure and dynamics of simple molecules in the liquid state can be studied using various spectroscopic techniques. These include microwave dielectric measurements[1], infrared and light scattering line shape analysis[2,3], neutron scattering line shape analysis[4], nuclear spin relaxation[5] and X-ray and neutron diffraction[6]. The work presented in this thesis is on microwave, far-infrared and Raman spectra of acetonitrile: these spectra yield information about the intermolecular forces and torques which determine the motion and the nature of the motion itself[2]. The microwave and far-infrared studies are on the rotational motion of CH_3CN in different chemical environments and the Raman analysis is on the ν_1(C-H symmetric stretch) vibration band of CH_3CN when the molecule is subject to hydrogen bonding interactions with methanol.

I.2 Rotational Motion in Liquids

Acetonitrile is a prolate symmetric top molecule belonging to the C_{3v} point group (see Fig.I.1). Rotation of the molecule in the condensed liquid state can occur in two ways:

a) Rotation perpendicular to the C_3 axis. In a liquid complete free rotation is prevented because the molecules are closely packed together. This motion is therefore restricted to small angle reorientational or 'tumbling' motion.

b) 'Spinning' about the C_3 axis.

Orientational motion is largely determined by the nature of the molecular environment and so is expected to be very sensitive to the overall structural dynamics occuring on the same time scale (10^{-10}-10^{-12} seconds)[2]. Since the electric dipole moment of CH_3CN lies along the C_{3v}

FIG. I.1

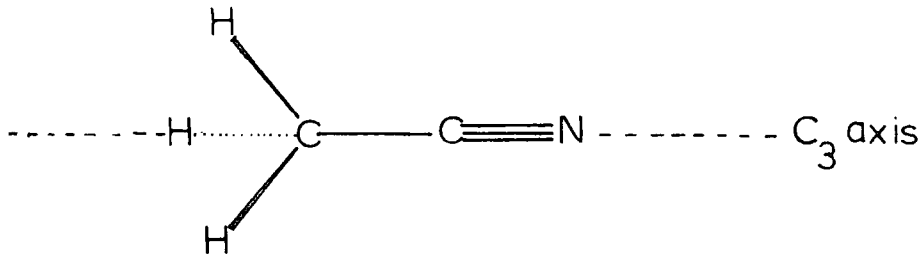

a) Diagram of the bonding in the acetonitrile molecule

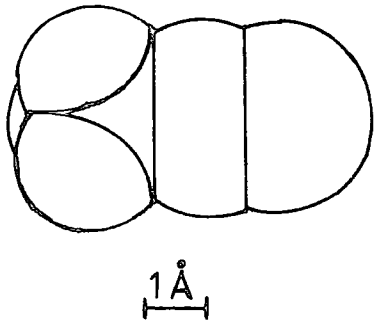

b) Diagram of the space filling molecule for acetonitrile[104]

axis reorientational motion causes a change in direction of the electric dipole moment which then, according to classical electrodynamics[7], leads to an absorption of electromagnetic radiation from an applied electric field. This is observed in the microwave/far-infrared region of the electromagnetic spectrum. Vibrationally excited molecules are also subject to reorientation enabling mid-infrared and Raman bands to be used in principle to study this motion (see section I.5). The associated fluctuation in the molecular polarisability tensor leads to scattering of visible radiation enabling depolarised Rayleigh scattering and Raman spectroscopy to be employed in the study of reorientational motion (see section I.5).

The spinning motion does not lead to a change in direction or magnitude of the electric dipole moment or polarisability tensor; however, this motion will affect perpendicular vibrations of the molecule and so can be studied using the degenerate E-bands of CH_3CN combined with N.M.R. spin relaxation data. This has been done by Possiel et al[8].

I.3 Dielectric Relaxation

Debye[9] began the study of dipolar orientational motion by observing the polarisation P, of the liquid in a weak applied electric field : this is given by

$$\mathbf{P}(\omega)=\chi(\omega)\mathbf{E}_m(\omega) \qquad \text{.....I.1}$$

where P is the polarisation (moment per unit volume), $\chi(\omega)$ the electric susceptibility and E_m the average Maxwell field throughout the sample. ω is the field frequency in radians per second. The permittivity of the sample is given by

$$\epsilon(\omega)=1+4\pi\chi(\omega) \qquad \text{.....I.2}$$

All quantities are field frequency dependent and hence complex. The polarisation consists of an induced part, due to electron cloud deformation by the electric field and an orientational part, due to the relaxation of the dipoles in the field. The complex permittivity can be written as

$$\epsilon(\omega)=\epsilon'(\omega) - i\epsilon''(\omega) \qquad \text{.....I.3}$$

The complex permittivity consisits of an in phase dispersive part, ϵ' and an out of phase dissipative componant, ϵ'' called the 'dielectric loss' because this quantity controls the rate at which energy is lost to the dielectric from the field[1]. Assuming instantaneous induced polarisation and that the relaxation process is exponential i.e.

$$P_{or.}=(P_{total}-P_{ind.})[1-\exp(-t/\tau)] \qquad \text{.....I.4}$$

the following equations can be obtained[1];

$$\epsilon'(\omega)=\epsilon_{\infty}+(\epsilon_0-\epsilon_{\infty})/1+\omega^2\tau^2 \qquad \text{.....I.5}$$

and

$$\epsilon''(\omega)=(\epsilon_0-\epsilon_{\infty})\omega\tau/1+\omega^2\tau^2 \qquad \text{.....I.6}$$

with

$$\epsilon''(\omega)_{max.}=(\epsilon_0-\epsilon_{\infty})/2 \qquad \text{.....I.7}$$

where ϵ_0 is the permittivity of zero frequency and ϵ_{∞} is the permittivity when the field is oscillating at such a high frequency that the molecular forces opposing dipole orientation dominate and only distortion polarisation remains. Equations I.5 and I.6 are commonly called the Debye equations. τ is the relaxation time given by $\omega_{max.}\tau=1$. It is the time required for the orientation polarisation to fall to 1/e of its original value (or reach 1/e of its maximum value). For simple organic polar liquids $\omega_{max.}$ ranges from 10-100 GHz[1,7]. i.e. in the microwave spectroscopic region. However, dielectric absorption often

extends up to 1000GHz. so in order to study the complete frequency dependence of orientation polarisation a combination of microwave and far-infrared techniques is required.

Simple organic polar liquids (CH_3CN) included do not obey the simple equations I.5 and I.6[1,7] (see Fig.I.2). The $\epsilon''(\omega)$ curves are broader and flatter than predicted and have a high frequency bulge. The deviations from equations I.5 and I.6 (though not the high frequency bulge which had not been observed at this time) were understood by Frölich[13] and Fuoss and Kirkwood[14] to be due to a distribution of relaxation times throughout the liquid , and by Rocard[15] and Powles[16] as being due to the neglect of molecular inertia in the Debye[9] treatment (see chapter II). The high frequency bulge which can only be seen using far-infrared spectroscopy does show that the short time part (up to $1x10^{-12}$s.) of the dipolar orientational motion is non-exponential.

The work presented here is an analysis of microwave measurements made on CH_3CN in the non-polar solvents CCl_4, benzene and n-heptane made at U.C.W. Aberystwyth in collaboration with Dr. Alun Price, in terms of a single relaxation time obtained from $1/\omega_{max.}$. The microwave data is then combined with far-infrared spectra measured on a Michelson interferometer at Durham and used to examine the time dependence of the orientational motion (see chapter II). The far-infrared spectra also provide a very sensitive test of the various models for reorientational motion; also this region of the spectrum yields information on the energy of the rotation and intermolecular torques through band moment analysis.

I.4 Macroscopic - Microscopic relation

One of the most important problems in dielectric studies is in

Fig.I.2 $\epsilon''(\nu)$ and $\epsilon'(\nu)$ data for pure CH_3CN

△ Data from ref. 10.

⊠ Data from ref. 11.

⊙ Data from ref. 12.

——Calculated using equations I.5 and I.6 (see footnote I.1).

---Obtained from far-infrared measurements (see chapters IV and V).

Footnote I.1

This curve was calculated using the Debye equations (I.5 and I.6) with τ=6.0p.s., ϵ_0=37.5 (see chapter III) and ϵ_∞=2.25. This value of τ was taken from the measurements of Mansingh[11]. It was done on the basis of the temperature dependence of the $\epsilon''(\nu)$ points. The points at 9.95 and 20.8 GHz. increase with increasing temperature while those at 32.0GHz. decrease with temperature. This means that the peak in $\epsilon''(\nu)$ must lie between 20.8 and 32.0GHz. Therefore, τ must have a value between 7.7 and 5.0p.s. Looking at this data plotted in Fig.I.2 a value of 6.0p.s. appears to be a reasonable value. The value of ϵ_∞ was chosen on the basis of Vaughan's[10] estimate made by taking the mean of the known values for HCN and C_2H_6. The justification for this value came from the Kramers-Krönig analysis in chapter V which suggests that 2.25 is a reasonable estimate for ϵ_∞.

Fig.I.2. $\varepsilon'(\nu)$ and $\varepsilon''(\nu)$ data for pure CH_3CN

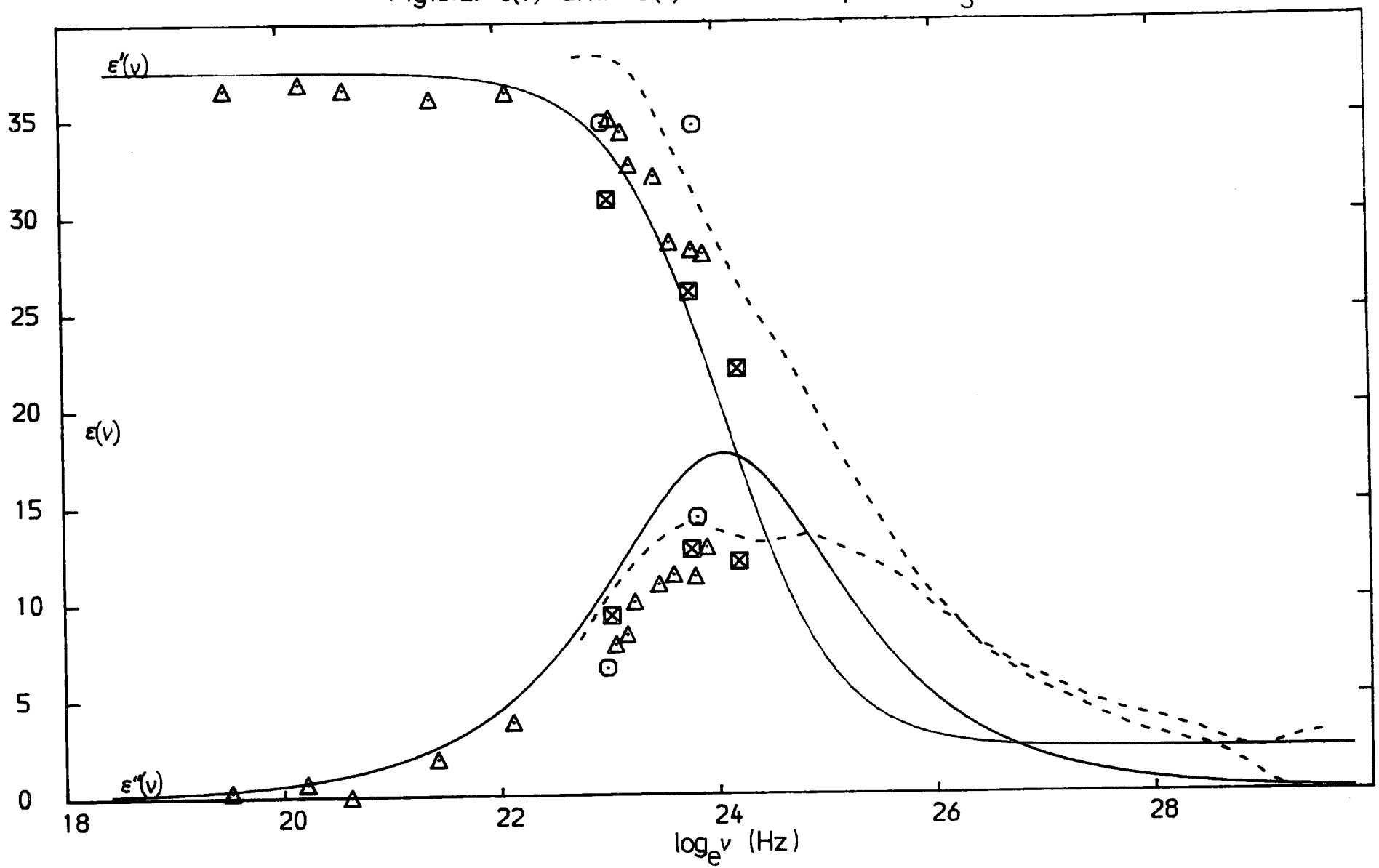

calculating the relation between the macroscopic observed quantities (τ, ϵ) and the underlying molecular quantities of molecular relaxation time and molecular dipole moment. This is often done by calculating the 'local' or 'internal' field acting at a molecular dipole in terms of the external or applied field and the fields due to the dipoles themselves. The external field (E_0) is related to the average internal Maxwell(E_m) field by (in e.s.u system)

$$E_m(\omega) = E_0(\omega) - \lambda P(\omega) \qquad \text{.....I.8}$$

λ is the shape dependent depolarisation factor[17]. $P(\omega)$ is then related to $E_0(\omega)$ via the quasi-susceptibility:

$$P(\omega) = \chi^0(\omega) E_0(\omega) \qquad \text{.....I.9}$$

This means that the calculation of the internal field has to have the shape of the sample specified; this is a consequence of the long-range nature of electrostatic forces[17]. Calculations are usually modelled on a spherical sample embedded in an infinite continuum of the same material[7] for which[18]

$$4\pi\chi^0(\omega) = \{[\epsilon(\omega)-1][2\epsilon(\omega)+1]\}/3\epsilon(\omega) \qquad \text{.....I.10}$$

Debye[9] first calculated the static dielectric constant by considering the local field acting at a point dipole at the centre of a spherical region within the dielectric which is small compared with the whole dielectric but large compared with molecular dimensions. He used the Lorentz[19] method whereby the local field is obtained by summing the fields due to the external field and the field due to polarisation at the surface of the sphere but neglecting the fields produced by the dipoles themselves, and obtained;

$$\epsilon_0 - 1/\epsilon_0 + 2 = 4\pi N(\alpha + \mu^2/3kT)/3 \qquad \text{.....I.11}$$

where α is the average of the three mutually perpendicular

polarisabilities of the molecule, k is Boltzman's constant, T is the temperature in degrees Kelvin, μ the dipole moment and N the number of molecules per cm^3. Debye applied the Lorentz field to an oscillating applied field and assuming expontial relaxation of the dipoles he obtained the molecular single particle relaxation time from the macroscopic relaxation time from:

$$\tau_{sp.} = \tau\ (\epsilon_{\infty}+2)/(\epsilon_0+2) \qquad \text{.....I.12}$$

The neglect of the field inside the sphere due to the molecules themselves limits this equation to gases and dilute solutions of polar solutes in non polar solvents where $\epsilon_0 \approx \epsilon_{\infty}$ in which case $\tau_{sp.} \approx \tau$.

Onsager[20] did include the fields produced by the polarisation of the surroundings by the central molecule. His model was different to that of Debye in that the spherical cavity contained only one molecule surrounded by a continuum of uniform dielectric constant equal to the macroscopic dielectric constant. Kirkwood[21] and Frolich[13] extended this model using a more rigorous statistical mechanical method in which the embedded sphere consists of a central molecule surrounded by its first shell of nearest neighbours embedded in an infinite continuum of macroscopic dielectric constant. The Kirkwood-Frolich equation for polarisable dipoles is

$$\frac{(\epsilon_0-\epsilon_{\infty})(2\epsilon_{\infty}+\epsilon_0)}{\epsilon_0(\epsilon_{\infty}+2)^2} = \pi 4N\mu^2 g/9kT \qquad \text{.....I.13}$$

This is identical with Onsager's equation except for the factor g. This is the average value of the cosine of the angle between dipoles and is a measure of static orientational ordering. For reviews on these theories see Bottcher[7] and Hill[1].

Glarum[22] and Cole[23] used linear response theory (see section I.5) to

derive a relation between the frequency dependent permittivity and the autocorrelation function of a dipole at the centre of a Kirkwood type embedded sphere, from which the single particle relaxation time can be extracted. Glarum and Cole considered the surrounding continuum to have a frequency-independent dielectric constant equal to the static dielectric constant of the inner sphere and they obtained:

$$\tau_{sp.} = \tau\ (2\epsilon_o + \epsilon_\infty)/3\epsilon_o \qquad \text{.....I.14}$$

which is identical with Powles result[24]. Fatuzzo and Mason[25] performed a similar calculation but considered the two regions to have equal (frequency dependent) dielectric constants which then yielded:

$$\tau_{sp.} \approx \tau \qquad \text{.....I.15}$$

Titulaer and Deutch[26] have reviewed and assessed these two approaches and come out in favour of the Fatuzzo-Mason result as being more physically realistic. However, this is difficult to justify for solutions of polar solutes in non-polar solvents wherin the permittivity of the embedded spherical region will not be equal to that of the outer continuum. Deutch[27] and Kivelson and Madden[18] do, however, point out that since the embedded sphere under consideration is microscopic but not molecular in dimension, truly single particle quantities cannot be obtained from them. In addition, molecular intercorrelations may be present because the internal energy of the medium (kT) is of the same order of magnitude as the rotational energy of the molecules[17] and so multimolecular relaxation may contribute to the macroscopic relaxation times. In this study it is hoped that single particle relaxation times can be obtained from measurements on dilute solutions of CH_3CN in the non-polar solvents.

Keyes and Kivelson[28] and Madden and Kivelson[18] have developed a

theory called the Corresponding Macroscopic Microscopic Relation which does not entail the calculation of local fields at a small microscopic cavity. Their result, again assuming that both the macroscopic and molecular relaxation times are exponential, is that

$$\tau_{sp.} = \tau \ (1+N\dot{F})/(1+NG) \qquad .....I.16$$

G is the equilibrium correlation factor where (1+NG) is the Kirkwood g-factor. $\dot{F}$ is a dynamic correlation factor. It is a measure of the correlation between the angular momentum of adjacent molecules. Assuming $\dot{F}=0$[18] i.e. dynamic correlations are not present, for a spherical sample in an infinite continuum of the same material equation I.16 becomes

$$\tau_{sp.} = \tau \ \frac{(\epsilon_0-\epsilon_\infty)(2\epsilon_\infty+\epsilon_0)9kT}{\epsilon_0(\epsilon_\infty+2)^2 \qquad 4\pi N\langle\mu\rangle^2} \qquad .....I.17$$

$\langle\mu\rangle^2$ is the mean square dipole moment which Kivelson and Madden estimated using

$$N\langle\mu\rangle^2/3kT=4.85\mu_g\rho/m(T/300) \qquad .....I.18$$

ρ is the mass density, m the molecular weight and μ_g the gas phase dipole moment.

The Cole , Glarum, Powles result (CGP) will be applied to the microwave data presented in this thesis in order to show the quantitative effect of applying internal field correction factors. In addition the Keyes-Kivelson equation will be applied to the pure liquid result. However, it must be clearly stated that all the above theories assume that both the macroscopic and molecular relaxation times are exponential in time behaviour, which is not true for the short time part of the motion (see chapter V). A further problem is that if the embedded region contained only one molecule it would not be spherical in the case of CH_3CN which has a ratio of short to long axis of 0.6 (see Fig.I.1).

Connected with this is the fact that the CH_3CN molecule will not have equal polarisabilities in all three mutually perpendicular axes of the molecule. Also implicit in these models is the location of the dipole at the centre of the molecule which is also unlikely in reality. If an ellipsoidal cavity is employed in the calculation of the internal fields each of the three mutually perpendicular polarisibilities ($\alpha_{11}.\alpha_{22}.\alpha_{33}$) of the molecule have to be evaluated as do the dimensions of the ellipsoid. The latter can be taken as the dimensions of the molecule or its free volume of rotation in the liquid[7,29], both of which are different. In addition, the charge distribution throughout the ellipsiod is required[7]. The difficulties and approximations involved in making these evaluations have led to no corrections for non-sphericity of the embedded region being applied in this thesis.

I.5 Correlation Functions

The combined microwave/far-infrared data was analysed in order to obtain the dipole-dipole correlation function. In this approach the behaviour of the appropriate dynamic quantity with respect to time (dipole moment vector of CH_3CN) is obtained by Fourier transformation of the experimental frequency spectrum. This enables both the short and long time angular motion to be looked at together. Kubo[30] developed this formalism which is based on two related hypotheses:[31,32]

a) Linear response theory.

b) Fluctuation dissipation theory.

Linear response theory describes the behaviour of two weakly coupled systems i.e. electromagnetic radiation with dipolar fluctuations. Because the coupling is weak the response of the system can be calculated from a knowledge of its behaviour in the absence of the

stimulus. The behaviour of the dynamic variables is described in terms of correlation functions which are equilibrium averages over the whole liquid.

Fluctuation dissipation theory is based on a hypopthesis by Onsager that every system at equilibrium exhibits small departures from equilbrium which regress with time at a rate governed by the system's usual motional processes. The latter hypothesis is also at the root of Debye dielctric theory[31].

The time dependent dipole-dipole multimolecular correlation function for the microwave/far-infrared rotational spectrum is given by[17]:

$$g(t)=\sum_{i,j}\langle P_1[\mu_i(0).\mu_j(t)]\rangle = \sum_{i,j}\langle \cos\theta_{i,j}(t)\rangle \quad ...I.19$$

μ_i is a unit vector in the permanent dipole moment axis of the i'th molecule. P_1 is the 1st order Legendre polynomial which means that the function is the cosine of the angle between μ_i and μ_j. The angle brackets indicate an equilibrium ensemble average in the absence of an electric field. The correlation time is the area under the correlation function. However, it is often the case that the correlation functions are unreliable at long enough times to enable this integration to be made. If the band is purely Lorentzian then its value at 1/e is equal to the correlation time. The correlation time for the long time part of the motion is also equal to slope of the natural log. of the function. A comparison of this value with that from the 1/e drop will give a good indication of how pure a Lorentzian a band is. In addition, $1/\Delta\omega_{1/2}$ is equal to the relaxation time for a pure lorentzian band where $\Delta\omega_{1/2}$ is the band width at half its height. The function can be separated into 'self' and 'distinct' terms.

$$g(t)=\underbrace{\langle \mu_i(0).\mu_i(t)\rangle}_{\text{'self'}} + \underbrace{\sum_{i\neq j}\langle \mu_i(0).\mu_j(t)\rangle}_{\text{'distinct'}} \quad \text{.....I.20}$$

At zero time this is equivalent to the Kirkwood g-factor:

$$g(0)=1 + \sum_{i\neq j}\langle \cos\theta_{i,j}\rangle \quad \text{.....I.21}$$

The correlation function is obtained by Fourier transformation of the frequency spectrum which for an even symmetric function is given by[36]

$$g(t)=6hc/\pi^2 N\mu_g^2 4\int_0^\infty \epsilon''(\omega)D(\omega)\cos\omega t\ d\omega/\ [1-\exp(-h\omega/kT)] \quad \text{...I.22}$$

The exponential term in the denominator can then be expanded. Only the first and second terms are considered since the higher terms are less than one, this then gives:[17]

$$g(t)=6kT/4\pi^2 N\mu^2\int_0^\infty \epsilon''(\omega)\ D(\omega)\ \cos\omega t\ d\omega\ /\omega \quad \text{.....I.23}$$

$D(\omega)$ is the frequency dependent internal field correction factor. The form of this factor used in the analysis will be $D(\omega)=1$ (ie no correction) and those of Hill[33] and Klug, Kranbuel and Vaughan[34] (KKV) which is the same as that proposed by Nee and Zwanzig[35] (NZ), as used by Strauss et al[36] in their paper on chloroform. These equations are all extensions of the Fatuzzo and Mason[25] hypothesis to polarisable dipoles and therefore strictly only applicable to single particle correlation functions of pure liquids (see section I.4) and so cannot really be applied to the pure liquid or solution spectra since solutions are not pure liquids and there may be molecular intercorrelations in the pure liquid. However, they will be used in this thesis to show their qualitative effect. In addition, in assuming exponential relaxation their application at high frequencies (far-infrared) is likely to cause errors (see chapter V).

The KKV and NZ derivations (of which the latter was formulated to include the effects of dielectric friction) both yield

$$D(\omega)=[3/(\epsilon_{\infty}+2)]^2\ 2|\epsilon|^2+\epsilon_{\infty}{}^2/3|\epsilon|^2 \qquad \text{.....I.24}$$

Hill's model was designed to separate contributions from induced moments in the surrounding sphere it is,

$$D(\omega)=[3/(\epsilon_{\infty}+2)]^2[(2\epsilon_0+\epsilon_{\infty})/(2\epsilon_0+1)]\ 2|\epsilon|^2+\epsilon_{\infty}/3|\epsilon|^2 \qquad \text{...I.25}$$

As mentioned in the general introduction mid-infrared and Raman vibration-rotation bands can be used to study reorientational motion. The appropriate correlation functions are as follows[2,3,37]:

a. Infrared correlation functions

The correlation functions for a mid-infrared vibration-rotation band are given by[2,3]

$$\Phi_v(t).\Phi_{1r}(t)=\langle Q_l(0).Q_l(t)\rangle\langle P_1[\mu_l(0).\mu_l(t)\rangle \qquad \text{.....I.26}$$

Φ_v is the the vibrational correlation function, Φ_{1r} the infrared rotational correlation function and μ_l is a unit vector along the direction of the transition moment corresponding to the normal coordinate Q_l of the l'th molecule; this lies along the C_3 axis of CH_3CN for parallel vibrations of the molecule (eg ν1,2,3 and 4 of CH_3CN). Single particle correlation functions are used in the assumption that molecules become vibrationally excited independently of each other. The correlation function is obtained from

$$\Phi_v(t).\Phi_{1r}(t) = \int_{\text{band}} I(\omega)\ \cos\omega t\ d\omega \qquad \text{.....I.27}$$

where $I(\omega)$ is the normalised (to unit area) absorption spectrum of a band. The bands are normalised so that at zero time the correlation functions equal one. $\omega=(\omega-\omega_0)$, where ω_0 is the proper frequency of vibration. Several workers [37,38] have neglected vibrational relaxation

and assumed that the intrinsic line width is very narrow enabling Φ_{1r} to be extracted from the band. This assumption cannot be made for the ν_1 and ν_3 bands of CH_3CN[71].

b) Raman correlation functions

Raman band shapes (observed by inelastic light scattering) arise from the interaction of visible radiation with fluctuations of the polarisability tensor of the molecule via the formation of induced dipoles[40].

For a totally symmetric vibration-rotation Raman band[41]

$$\Phi_v(t).\Phi_{2r}(t) = \langle Q_i(0).Q_i(t)\rangle \langle P_2[\mu_i(0).\mu_i(t)]\rangle \quad .....I.27$$

P_2 is the second order Legendre polynomial given by $1/2(3\cos^2\theta(t)-1)$. In the laser Raman experiment the vibrational and rotational functions can be separated by way of the polarisation of the scattered light as compared to the polarisation of the incident laser light[40]. As in the infrared case single particle correlation functions are assumed. The parallel(VV) (polarisation compared to the polarisation of the laser light) and perpendicular(VH) components of the scattered light are related to the isotropic and anisotropic parts of the scattering tensor by

$$I_{iso}(\omega)=I_{vv}(\omega) - 4/3I_{vh}(\omega) \quad .....I.28$$

$$I_{aniso}(\omega)=I_{vh}(\omega) \quad .....I.29$$

where

$$\Phi_v(t) = \int_{band} I_{iso}(\omega) \cos\omega t \, d\omega \quad .....I.30$$

and

$$\Phi_v(t).\Phi_{2r}(t) = \int_{band} I_{aniso}(\omega) \cos\omega t \, d\omega \quad .....I.31$$

then assuming

$$\Phi_v(t)[\text{infra-red}]=\Phi_v(t)[\text{iso}]=\Phi_v(t)[\text{aniso}] \qquad \ldots\text{I.32}$$

we have

$$\Phi_{1r}(t)=\int_{\text{band}} I_{1r}(\omega)\ \cos\omega t\ d\omega \ /\ \int_{\text{band}} I_{iso}(\omega)\ \cos\omega t\ d\omega \qquad \ldots\ldots\text{I.33}$$

and

$$\Phi_{2r}(t)=\int_{\text{band}} I_{aniso}(\omega)\ \cos\omega t\ d\omega \ /\ \int_{\text{band}} I_{iso}(\omega)\ \cos\omega t\ d\omega \qquad \ldots\ldots\text{I.34}$$

All the intensities are normalised to unit area.

There are theoretical arguments that the equivalence in equation I.32 is not valid if intermolecular vibrational coupling is present[42]. It has been shown that the effects of the coupling make different contributions to each of the three correlation functions. This is one explanation of the fact that each of the three bands has a different peak frequency by several wavenumbers. A further problem is the neglect of the vibration-rotation coupling which is known to be important in the gas phase spectra of CH_3CN[43], which does show quite strong effects of Coriolis coupling.

c) Depolarised Rayleigh scattering correlation functions

Depolarised Rayleigh bands are observed as the depolarised component of the broadening of the central exciting laser line at 90° to incident beam. The line shape is approximately proportional to $\epsilon''(\omega)/\omega$[32]. The line shape includes contributions from the fluctuations of dipoles induced in the polarisability tensor by the laser light and from those induced by intermolecular collisions. The latter have to be removed by band fitting procedures[44] in order to obtain the reorientational correlation function. For a molecule with at least a three fold axis of

symmetry[45,46]

$$I(\omega)=CNE_i^2(\alpha_{par}-\alpha_{per})^2\int_o^{\infty} g^{(2)}(t)\ \exp(-\omega t)\ dt \qquad .....I.35$$

where

$$g^{(2)}(t)=\sum_{i,j}\langle P_2\cos_{i,j}\theta(t)\rangle \qquad .....I.36$$

C is a constant, N is the number of particles per unit volume, E_i is the local field strength of the incident light, α_{par} and α_{per} are the two principal polarisability components (parallel and perpendicular to the C_3 axis).At zero time we have the second order orientational structure factor $g^{(2)}$ given by

$$g^{(2)}(0)=1 + \sum_{i\neq j}\langle P_2[\cos\theta_{i,j}(0)]\rangle \qquad .....I.37$$

which is closely related to the first order factor (the Kirkwood g-factor) through the Legendre polynomials[44].

Versmold[44] has made a valuable study of CH_3CN in a range of CCl_4 solutions using depolarised Rayleigh scattering which will be used in comparison with the results presented in this thesis.

I.6 Band Moment Analysis

Gordon[37] and Brot[17] showed that the correlation function can be expanded in a (time) power series, the coefficients of which may be identified with the frequency moments of the spectrum. For the microwave/far-infrared rotational band the moments are defined as

$$g(t)=\int_o^{\infty}(it)^n M(n)\ dn\ /n! \qquad .....I.38$$

where the spectral moments, M(n), are given by

$$M(n) = \int_o^{\infty} I(\omega)\ \omega^n\ d\omega \qquad .....I.39$$

$I(\omega)$ is the spectral intensity and $\omega=\omega-\omega_0$ where ω_0 is the band origin

which=0.0 for the microwave far-infrared absorption. For a classical system only even values of n are considered. Each coefficient is an equilibrium property of the system so can be evaluated without the need to solve equations of motion[37]. The lower moments of the spectrum are simple properties of the system because they describe the short-time motion of the system. The higher moments reflect more complicated motion and are difficult to evaluate. The lower moments have been evaluated as follows for a symmetric top molecule[47]:

$$g(t)=g(0) - 2kT/I_b((t^2/2)) + 8(kT/I_b)^2[1+I_a/I_b + \langle O(v)^2\rangle/4(kT)^2] (t^4/4!) + \_\_\_\_\_ \quad .....I.40$$

I_b = moment of inertia perpendicular to C_3 axis. I_a = moment of inertia parallel to C_3 axis. $\langle O(v)^2\rangle$ is the mean square intermolecular torque, v is the angle dependent part of intermolecular potential and O is the associated operator. It can be seen that the first and third terms in this expansion are multimolecular quantities whereas the second moment is a purely single molecule property. It is a measure of the molecule's rotational kinetic energy. This means that the second moment of the band intensity is independent of interactions. Thus, as M_2 is proportional to $\omega^2\epsilon''(\omega)/\omega = \epsilon''(\omega)\omega = n(\omega)\alpha(\omega)$ (see I.7) then if the refractive index is constant as it is in the region 20-250 cm^{-1} (see Chapter V) this means that the integrated $\alpha(\omega)$ intensity is independent of interactions. Thus, there is the interisting consideration that as $\alpha(\omega)$ has most of its weighting in the far-infrared region then the integrated far-infrared intensity is independent of interactions.

Higher moments are also difficult to measure (as well as calculate) because as ω^n increases the higher frequency parts of the spectrum

become more important to the integral I.38 and in the case of far-infrared absorption interference from vibrational bands of either solvent or solute will occur. In addition collision induced dipolar absorption is thought to become more important at higher frequencies[48].

Once again the intensities must be corrected for the effects of the internal fields. The factors used in equations I.24 and I.25 only apply to the low frequency (microwave region) part of the spectrum and the band moments are weighted by the far-infrared parts of the spectrum. An alternative correction can be made using the non-dispersive Polo-Wilson (PW) correction factor[49] (which is based on Onsager's model[20])

$$9n_{\alpha}/(n_{\alpha}^2+2)^2 \qquad .....I.41$$

where n_{α} is the refractive index associated with e_{α}. Sum rule analysis will be presented in which the KKV, NZ correction factor is also used for comparison with the results obtained using the PW factor.

I.7 Kramers-Krönig Relations

The measured quantity in both the microwave and far-infrared experiments was the power absorption coefficient $\alpha(\omega)$ which is the decrease in energy of the radiation along its propagation direction. The field at frequency ω at point x is given by[17,40,48]

$$E=E_i\exp[i\omega(t-n^{*}x/c)] \qquad .....I.42$$

where c=velocity of light,and

$$n^{*}=(n-i\kappa) \qquad .....I.43$$

the frequency dependent refractive index. Rewriting

$$E=E_i\exp[i\omega(t-nx/c)]\exp(-\kappa\omega x/c) \qquad .....I.44$$

hence the absorption coefficient is given by

$$\alpha(\omega)=2\kappa(\omega)\omega/c \qquad .....I.45$$

The Maxwell identity $\epsilon=(n^{*})^2$ then gives

$$\epsilon''(\omega)=cn(\omega)\alpha(\omega)/\omega \qquad \text{.....I.46}$$

and

$$n(\omega)=[(\epsilon'(\omega)^2+\epsilon''(\omega)^2)^{1/2}+\epsilon'(\omega)]^{1/2}/\sqrt{2} \qquad \text{.....I.47}$$

with

$$\epsilon'(\omega)=n(\omega)^2-\kappa(\omega)^2 \qquad \text{.....I.48}$$

and

$$\epsilon''(\omega)=2n(\omega)\kappa(\omega) \qquad \text{.....I.49}$$

Therefore in order to calculate $\epsilon''(\omega)$ (to be used in the correlation function analysis in chapter V) from $\alpha(\omega)$ one requires $n(\omega)$. This is achieved in this thesis by using the Kramers-Kronig relations[50] which are general equations that express the link between the real and imaginary parts of a complex number. When applied to equation I.43 they are

$$n(\omega)-n_{\infty}=2/\pi P\int_0^{\infty}\kappa(\omega')\omega'd\omega'/\omega'^2-\omega^2 \qquad \text{.....I.50}$$

$$\kappa(\omega)=2/\pi P\int_0^{\infty}n(\omega')\omega d\omega'/\omega'^2-\omega^2 \qquad \text{.....I.51}$$

where P means take the principal value. The relations between ϵ' and ϵ'' are exactly analogous. Equation I.50 can also be written[5]

$$n(\omega)-n_{\infty}=1/\pi P\int_{-\infty}^{+\infty}\kappa(\omega')d\omega'/\omega'-\omega \qquad \text{.....I.52}$$

which is equivalent to the Hilbert equation[51] that is

$$n(\omega)-n_{\infty}=H[\kappa(\omega)] \qquad \text{.....I.53}$$

thus n and κ and ϵ' and ϵ'' are Hilbert transforms of each other. The following method for obtaining the Hilbert transform of $\kappa(\omega)$ using Fourier transform methods was worked out by Khuen[52].

According to Chamberlain[53]

$$F(H[f(y)])=isgn(y)\hat{F}(y') \qquad .....I.54$$

where sgn is the signum function, F is the Fourier transform, H is the Hilbert transform and

$$\hat{F}(y')=F[f(y')] \qquad .....I.55$$

Equation I.54 expresses the fact that the Hilbert transform can be considered as a convolution of the function f(y) with 1/y'

$$H[f(y')]=-1/y\pi \ *f(y') \qquad .....I.56$$

Back transformation gives

$$H[f(y)]=F^{-1}(isgn(y').F[f(y)]) \qquad .....I.57$$

Equation I.57 states `take the function f(y) calculate the Fourier transform and multiply by i which means consider the real part of F[f(y)] as the imaginary part and the imaginary part as the negative real part. Sgn(y) means now multiply all values of y<0 by -1. then backtransformation gives the Hilbert transform of f(y'). In this work $\kappa(\omega)$ is the function to be Hilbert transformed. It is an odd function; therefore to obtain the function from -infinity to +infinity we need to make

$$\kappa(\omega)=-\kappa(-\omega) \qquad .....I.58$$

See Fig.I.3

Fig.I.3.

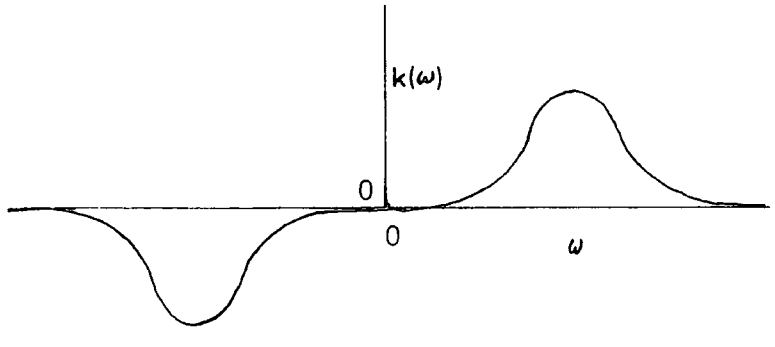

Equation I.50 shows that to obtain $n(\omega)$ n_{ω} is required, which for the

microwave/far-infrared rotation band lies around 300 cm^{-1}. It was not possible to measure this using either the apparatus in Durham or Aberystwyth. However ϵ_0 values for all the solutions were measured at Aberystwyth so that the value of n_∞ was simply adjusted until $n(0)=\sqrt{(\epsilon_0)}$. A computer program was written to do the Hilbert transformation by Khuen[52] using a fast fourier transform technique and implemented in Durham as the program HTRAN. The program was tested on CCl_4 data obtained by O'Neill[54] on a dispersive interferometer at the National Physical Laboratory (NPL). This instrument can be used to measure both $\kappa(\omega)$ and $n(\omega)$. The microwave data of Whiffin[55] $(\epsilon''(\omega)/\epsilon'(\omega))$ was used to calculate $\kappa(\omega)$ using equations I.45 to I.49. The two sets of data were combined and Hilbert transformed using the method outlined above. The calculated refractive index is shown compared with the measured curve in Fig.I.4. As can be seen the agreement is very close i.e. within 1% of each other.

Fig.I.4. Calculated and observed $n(\bar{\nu})$ curves for CCl_4

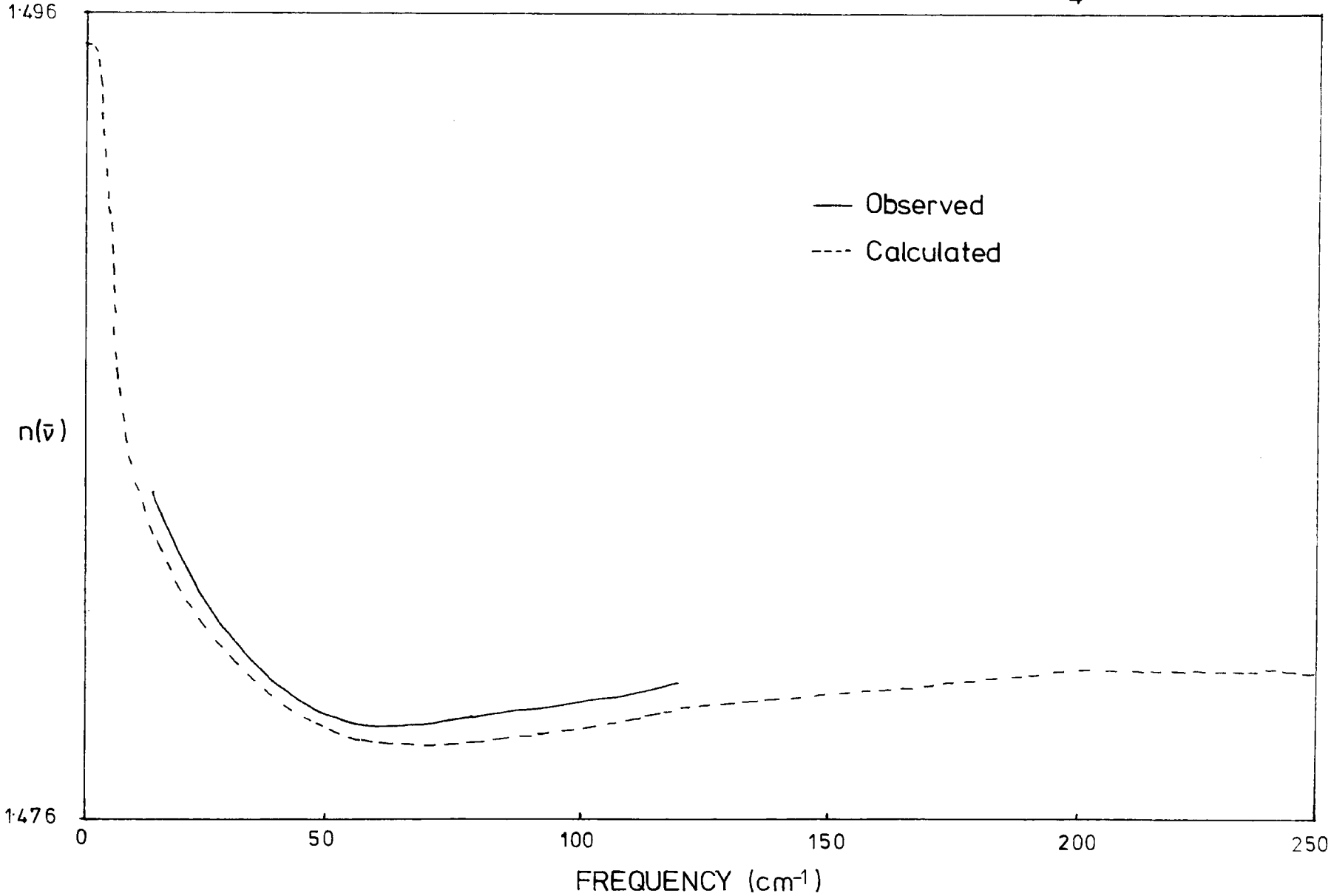

Chapter II.

Brief Discussion on some of the Mathematical Models for Rotational Motion in Liquids.

II.1 Rotational Diffusion

Debye[9] suggested that the rotation of a dipole in an applied field is constantly interrupted by interactions with neighbouring molecules due to their thermal or 'Brownian' motion. In this way the angular motion is restricted to very small (infinitessimally small in the theory) angular displacements. This physical picture enables diffusional equations to be used. The torque applied to a molecule by a field of force F, where $F=F_m \exp(i\omega t)$, at an angle θ to the field is

$$M=-\mu F \sin\theta \qquad \text{.....II.1}$$

which is opposed by the microscopic friction due to the neighbouring molecules

$$M=\zeta \, d\theta/dt \qquad \text{.....II.2}$$

where ζ is the frequency independent friction coefficient. The rotational Langevin equation of motion per unit moment of inertia is

$$\dot{\theta}(t)-\zeta\,\theta(t)=\Gamma(t) \qquad \text{.....II.3}$$

Γ is the random torque imposed on a molecule by the motion of its neighbours. Debye[9] then used the Lorentz field (see Chapter 1 section 4) to calculate F. He derived

$$\tau_{sp.} = \tau \, (\epsilon_\infty+2)/(\epsilon_o+2) \qquad \text{.....II.4}$$

where τ is the macroscopic relaxation time.

Rocard[15] and Powles[16] modified this theory to take into account the inertia of the molecules, which is expected to be important at high field frequencies. Powles suggested that M should include a second order term in θ i.e.

$$M=\zeta \, d\theta/dt + I_b d^2\theta/dt^2 \qquad \text{.....II.5}$$

I_b is the moment of inertia perpendicular to the C_3 axis. For dilute solutions of polar molecules in non-polar solvents for which the Lorentz

field is thought to be suitable. Powles[16] did obtain small deviations from the Debye predictions for $\epsilon''(\omega)$, in the microwave region in the form of a slight flattening.

It is, however, in the regime of absorption per cm ($\alpha(\omega)$) at high frequencies that the Debye model fails to predict the experimental detail in the most pronounced manner. The Debye model predicts that $\alpha(\omega)$ is proportional to $\omega^2(1+\omega^2)^{-1}$ which leads to a high frequency plateau and no return to transparency (see Fig.II.1), whereas the observed $\alpha(\omega)$ rises above the level of the plateau (excess absorption) and returns to transparency between 100 and 200 cm^{-1} forming the so-called Poley[56] band. The band is often named after Poley because he predicted the presence of 'whole molecule' absorptions other than the Debye type absorption. This he did on the basis that ($\epsilon_\infty - n_d^2$) (n_d is the refractive index at the sodium D lines and ϵ_∞ was that predicted by the Debye equations[1,7]) was too large to be accounted for by the infrared intra-molecular vibration absorptions. The Powles inertia corrected model predicts a small excess absorption with an earlier than observed return to transparency[57]. It is known however, that dipoles induced by intermolecular collisions also contribute to the far-infrared absorption[58]. The induced absorption has been evaluated by Rothschild[48] for some simple systems (e.g. HF in cyclohexane) from calculations of the intermolecular potential (Lennard-Jones potential); he found that the induced absorption contributed about 5% to the total far-infrared band, largely at the high frequency end of the band. It is this mechanism that causes the far-infrared absorption of non-polar liquids such as carbon tetrachloride and benzene[58]. Davies[58] has obtained evidence from intensity measurements that the absorption arises from bi-

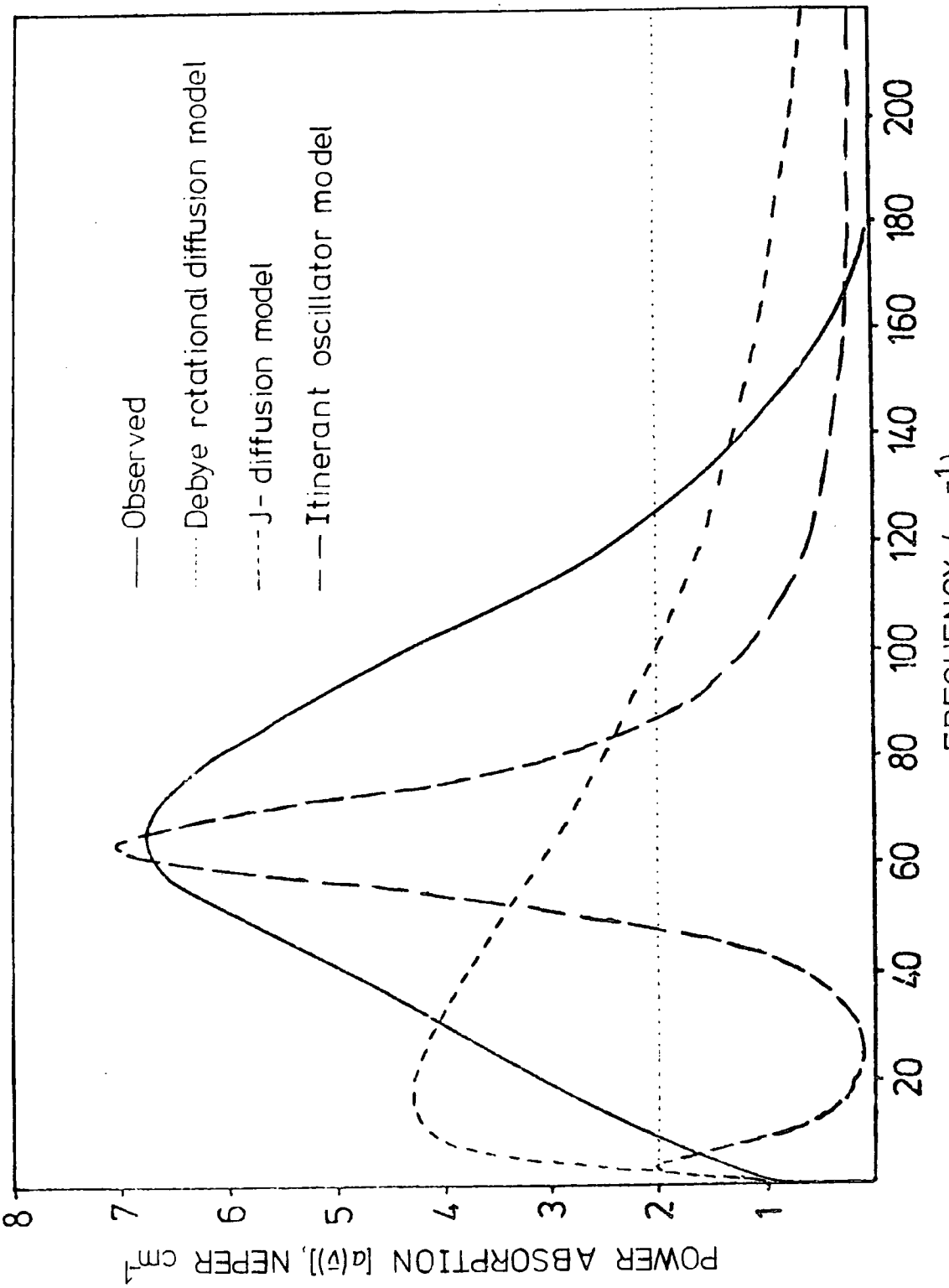

Fig.II.1. Observed and calculated far-infrared absorption spectra for 0.018 M.F. CH_3CN/CCl_4 solution[39]

molecular collisions. The application of Gordon's[59] sum rule for integrated absorption (see chapter V) will be used to estimate the extent of the induced dipolar absorption present in the far-infrared bands.

II.2 Gordon's M and J Diffusion Models

The Debye model restricts angular motion to small angle steps which Gordon[60] assesses to be more plausible for large molecules than small ones. In his M and J diffusion models angular steps of arbitrary large size are allowed. The physical picture is of collisionally interrupted free rotation and the models are characterised by a time between collisions (τ_j).

a) M-diffusion

This is a result of Gordon's diffusion theory which has free rotation terminated by instantaneous collisions that randomise the angular momentum of the molecule in direction only.

b) J-diffusion

This is the same as the M-diffusion except that both the magnitude and direction of the angular momentum vector are randomised on collision. This is essentially an inertia corrected Debye model[32] and expected to be the more realistic of Gordon's derivations[17]. This model again fits the low frequency (long time) part of the $\alpha(\omega)$ curve but has a slow return to transparency in the far-infrared. The peak in $\alpha(\omega)$ occurs at the maximum in the gas phase rotational envelope (see Fig.II.1).

II.3 Memory Function Formalism

This is not a physical theory but a formal scheme for introducing variables needed to describe the observed phenomena. It requires no

underlying model but can be adapted to reproduce the results of any of the models[32].

In the memory function approach[51,61] applied by Evans and co-workers[47,62,63] to the problem the following restrictions of the Debye rotational diffusion model are removed in order to obtain a more physically realistic picture:

a) Molecular collisions have a finite time and the torque acting at collision is finite.

b) The friction tensor be time dependent.

The formalism is used in order to solve the more general form of the Langevin equation proposed by Kubo[64]:

$$\dot{\omega}(t)+\int_0^t K_\omega(t-\tau)\omega(\tau')d\tau'=\Gamma(t) \qquad \text{.....II.6}$$

$K_\omega(t)$ is the time dependent friction tensor called the memory function.In terms of the dipole-dipole autocorrelation function,

$$g(t)=\langle \mu_l(0).\mu_l(t)\rangle \qquad \text{.....II.7}$$

$$dg(t)/dt = - K_o(t-\tau')g(\tau')d\tau' \qquad \text{.....II.8}$$

The Fourier transform of $K_o(t-\tau')$ is the frequency dependent friction coefficient. The set of memory functions $K_o(t)....K_n(t)$ obey the set of coupled Volterra equations such that

$$\delta K_{n-1}(t)/\delta t = - K_n(t-\tau')K_{n-1}(\tau')d\tau' \qquad \text{.....II.9}$$

The Laplace transforms then yield Mori's[65] continued fraction representation of the correlation function

$$g(p)= \frac{g(0)}{p+K_o(p)} = \frac{g(0)}{p+K_o(0)} \cfrac{}{p+K_1(p)} =----- \qquad \text{.....II.10}$$

where p is the Laplace variable($i\omega$). Truncation of the series requires a suitable form of $K_n(t)$. The various forms used for the truncation which

lead to all the various models of reorientational motion are described by Rowlinson and Evans[32]. Evans truncates at the second order using the form

$$K_1(t)=K_1(0)\exp.(-\gamma t) \qquad \text{.....II.11}$$

which then yields, for the spectral density

$$\alpha(\omega)= \frac{A\omega^2 K_0(0)K_1(0)\gamma}{\gamma^2[K_0(0)-\omega^2]^2+\omega^2\{\omega^2-[K_0(0)+K_1(0)]\}^2} \qquad \text{.....II.12}$$

where $A=(\epsilon_0-\epsilon_\infty)D/n(\omega)c$. D is an internal field correction factor. For linear and symmetric top molecules $K_0(o)=2kT/I_b$, where I_b is the moment of inertia perpendicular to the dipole axis i.e. it is the rotational second moment (see chap. I.6), a purely single molecule property. $n(\omega)$ does not need to be known as it can be obtained in terms of $\epsilon''(\omega)$ and $\epsilon'(\omega)$ using:

$$\epsilon''(\omega) = \alpha(\omega)n(\omega)c/\omega \qquad \text{.....II.13}$$

and

$$n(\omega)=\{[\epsilon''(\omega)^2+\epsilon'(\omega)^2]^{1/2}+\epsilon'(\omega)\}^{1/2}/\sqrt{2} \qquad \text{..II.14}$$

where $\epsilon''(\omega)$ and $\epsilon'(\omega)$ are given by

$$\epsilon''(\omega)= \frac{(\epsilon_0-\epsilon_\infty)K_0(0)K_1(0)\gamma\omega}{\gamma^2[K_0(0)-\omega^2]^2+\omega^2[\omega^2-K_0(0)+K_1(0)]^2} \qquad \text{....II.15}$$

and

$$\epsilon'(\omega)=\epsilon_0- \frac{(\epsilon_o-\epsilon_\infty)\omega^2\{[\omega^2-(K_0(0)+K_1(0))]+\gamma^2[\omega^2-K_0(0)]\}}{\gamma^2[K_0(0)-\omega^2]^2+\omega^2[\omega^2-K_0(0)+K_1(0)]^2} \qquad \text{.....II.16}$$

The parameter $1/\gamma$ is said to be a correlation time for the intermolecular torques and $K_1(0)$ is related to the mean square intermolecular torque $\langle O(v)^2\rangle$ via[61]

$$K_1(0)=([8(kT/I_b)^2(1+I_a/4I_b+\langle O(v)^2\rangle/(kT)^2]/K_o(0)) - K_o(0)$$

.....II.17

where I_b and I_a are as defined in chapter I.6.

The measured and calculated (using the Mori formalism) velocity-velocty (angular velocity) autocorrelation functions[32,47] show a short time oscillation suggesting that some form of molecular libration (rotatory oscillation) is responsible for the Poley absorption. Chantry[86] and the NPL workers who first observed the far-infrared absorption of dipolar liquids did in fact propose a form of librational motion occuring in a liquid 'pseudo lattice' as being the source of this band. This approach to the explanation of Poley band was also developed by Hill[66] and extended by Coffey[67] and Wyllie[68] in the form of an itinerant oscillator model. Here a non-spherical molecule performs libration inside a cage of neighbouring molecules, while the cage performs rotatory diffusion. In this model the frequency at $\alpha(\omega)_{max.}$ is taken to be the librator frequency. A fit to the experimental curve using this model is shown in Fig.II.1[39]. This model puts a clear separation between the microwave and far-infrared peaks which is not seen in practice. The librator model of Brot[69] is different in that a molecule may librate about any one of many stable orientations; then random collisions cause it to jump from one potential well to another.

Good experimental evidence for the presence of resonant energy transfer to an oscillating molecule comes from the fact that the refractive index ($0-250cm^{-1}$) shows a shallow minimum[39,57,70] in the region of $\alpha(\omega)_{max}$. It is well established[40] that the refractive index of a system of damped oscillators under resonance has a minimum slightly displaced to the high frequency side of the frequency of oscillation.

Fig.II.2 shows the form of the $n(\omega)$ curve in the region of a)pure relaxation band. b)a resonance absorption band and c)a measured cuvre for CH_3CN in CCl_4 (0.02 mole fraction). It appears that curve c is then a combination of predominantly a but with some b present.

II.4 Use of Three Parameter Mori Model

Yarwood and James[39,70,71] have applied this model to a series of solutions of acetonitrile in CCl_4. The work presented in chapter V will solely be concerned with the neat liquid.

The parameter $K_1(0)$ can be obtained by differentiating equation II.12 giving $\alpha(\omega)_{max}$ in terms of $K_o(0)$ and ω_{max}, i.e.

$$K_1(0)= \frac{4\omega^4_m(\omega^2_m-K_o(0))}{\pi(K_o(0)-\omega^2_m)(K_o(0)+\omega^2_m)+4\omega^4_m} \quad .....II.18$$

The molecular relaxation time (τ_{sp}) is then obtained from

$$K_1(0)=[2kT\tau_{sp}/I_b]^2\pi/2 \quad .....II.19$$

The parameters γ+$K_1(0)$ can also be varied until the calculated $\alpha(\omega)$ (using equation II.12) curve fits the measured one. This was done using the program NEWFITF which employs a National Algorithms Group(NAG) non linear least squares fitting routine E04FAF. At low frequencies the model gives Debye behaviour enabling τ_{sp} to be calculated using the fitted parameters from

$$\tau_{sp}^2=([K_o(0)+K_1(0)]^2-2K_o(0)\gamma^2)/(K_o\gamma)^2 \quad ...II.20$$

Results obtained from both ways of using the two variable model are presented in chapter 5.

Fig.II.2. Three types of refractive index curve

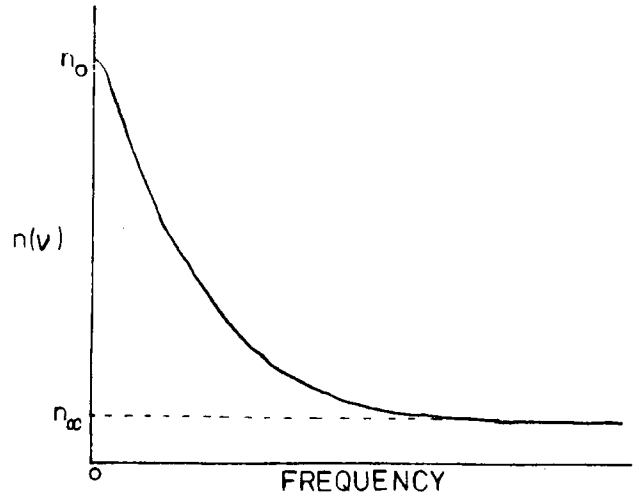

a) Diagram of n(ν) for an exponential relaxation

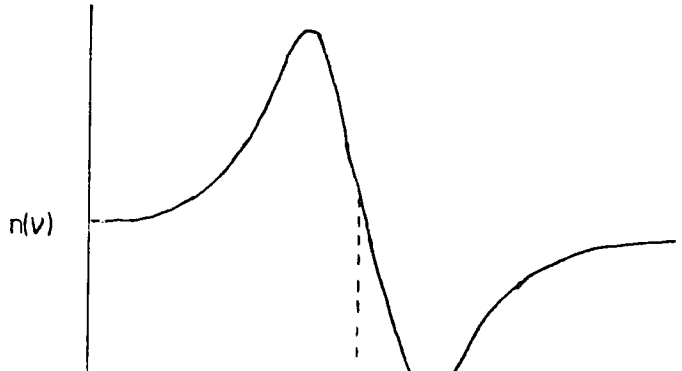

b) Diagram of n(ν) through a resonance absorption band[40]

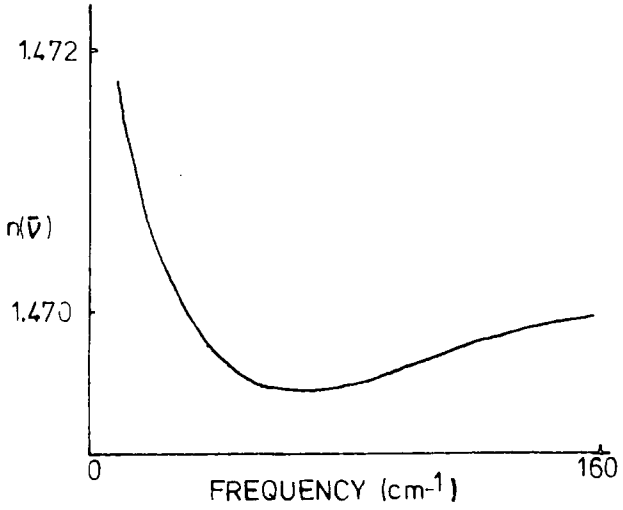

c) Measured n(ν̄) curve for CH_3CN/CCl_4 0.02 M.F. 45°C[70]

Chapter III.

Microwave Measurements.

III.1 Introduction

The dielectric loss of the liquids studied for this thesis is important over a range of frequencies from 4 to 3000GHz. For the low frequencies, the sample size is of the same order as that of the wavelength of the electric field; this means that the waves must be confined within metal waveguides which contain the sample[1]. The upper frequency limit is determined by the difficulty in manufacturing very small waveguides of precise geometry. The upper limit is about 75GHz=2.5cm^{-1}. For higher frequencies optical or free space techniques have to be used. In this regime the sample (usually a rectangular slab perpendicular to the incident beam) has to be large compared with the wavelength of radiation so that diffraction effects can be neglected.

The frequency range 4-18GHz was covered using a sweep frequency technique and the higher microwave frequencies were sampled at the spot frequencies of 34 and 66GHz. The basis of both types of microwave experiment was to measure the attenuation of the radiation at different liquid depths. The Kramer[72] relation is then used to derive the absorption coefficient

$$E_o/E_i=K\exp(-\alpha d)=t \qquad \text{.....III.1}$$

E_o and E_i are the output and input wave amplitudes, d is the sample depth in cm, α the attenuation coefficient in cm^{-1} and K a function of the reflection coefficient at various interfaces. The effects of reflection were reduced in both types of experiment by having the base of the sample cell at an angle of about 15 degrees to the incident radiation[73]. The attenuation is measured in decibel units

$$\text{Amplitude ratio}=\log_e t=2.303dB/20 \qquad \text{.....III.2}$$

$$\text{Power ratio}=\log_e t^2=2.303dB/10 \qquad \text{.....III.3}$$

α is derived directly from

$$\log_e t = \log_e K - \alpha d = 2.303 dB/20 \quad \text{.....III.4}$$

thus plotting dB against d gives a slope of

$$-\alpha 20/2.303 = dB/d \quad \text{.....III.5}$$

therefore

$$\alpha = (2.303/20)\ (dB/d)\ cm^{-1} \quad \text{.....III.6}$$

The CH_3CN used was Eastman Kodak spectro grade while all the solvents (CCl_4, benzene and n-heptane) were manufactured by the BDH company and were spectroscopic grade. All the microwave measurements were performed at room temperature which did not vary by more than 2° from 295K.

III.2 Experimental Sweep Frequency Measurements 4-18GHz

This equipment was manufactured by 'Systron and Donner' and set up to measure the attenuation of liquids by Dr. A.H. Price at U.C.W. Edward Davies Chemical Laboratories, Aberystwyth. The layout of the apparatus is shown in Fig.III.1. The attenuation can be measured over a continuous spread of frequencies from 0.01 to 4.2GHz and 4 to 18GHz, only the latter was used for the liquids studied here. The source module(s) contains a varactor[74] diode which can have its characteristic frequency varied over a large range by varying the applied voltage. From the source the radiation is transmitted along a co-axial line through the sample cell which forms part of the co-axial line and then into a detector which forms part of the power meter. The source output is not flat so the signal from the initial depth of liquid is stored in a 400 bit data normaliser. The signal from different liquid depths is compared with the reference signal and the difference displayed on a flatbed plotter and simultaneously on a cathode ray oscilloscope. The data

Fig.III.1. Diagram of sweep frequency apparatus

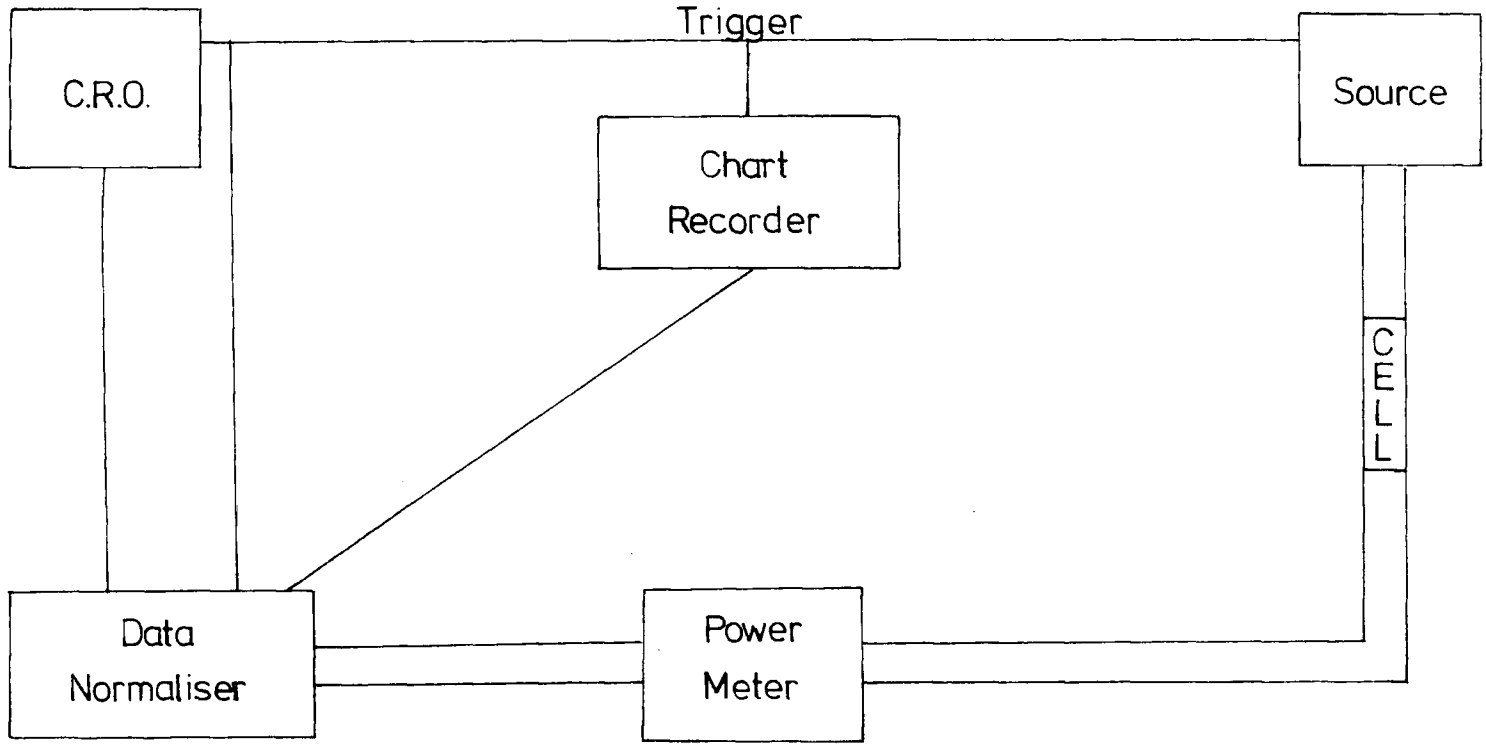

normaliser .CRO and plotter are all triggered simultaneosly by the source. The traces of attenuation versus frequency at different liquid depths were calibrated using standard Hewlett Packard attenuators inserted between the sample cell and detector. The experimentally variable parameters were the sensitivity of the power meter, sensitivity of the plotter and the speed of the sweep (usually about 20 seconds). Each was varied until smooth trace was obtained. Each solution was usually measured at between 5 and 10 different depths. A typical set of traces is shown in Fig.III.2.

The cross sectional area of the space inside the co-axial cell was 0.307 cm^2 thus 1ml. of liquid forms a liquid depth of 3.26 cm. The known volumes of liquid were introduced from a burette or micro-syringe. The limiting liquid depths are determined by the attenuation of the liquid, if very high the radiation becomes completely attenuated by one thin liquid layer on the base of the cell and if very low the cell becomes full before a noise-free trace can be obtained. For CH_3CN solutions the range of concentrations found to be convenient were 0.1 to 10 moles per litre (0.01 to 0.7 mole fraction in CCl_4).

Measurements of attenuation were taken at various frequencies at convenient portions of the traces. The effects of reflection at the various interfaces is to put a slight sinusoidal variation in the plot of attenuation against depth[73]. A straight line was put through the points by using a linear least squares regression treatment on them. Typical plots are shown in Fig.III.3. The data obtained from these measurements for all solutions is shown in table III.1

III.3 Spot Frequency Measurements. 33.9775 and 69.66GHz.

A 36GHz klystron oscillator in conjunction with a Q-band 8mm

Fig.III.2. Output traces from the sweep frequency apparatus. CH_3CN/CCl_4 0.16M.F.

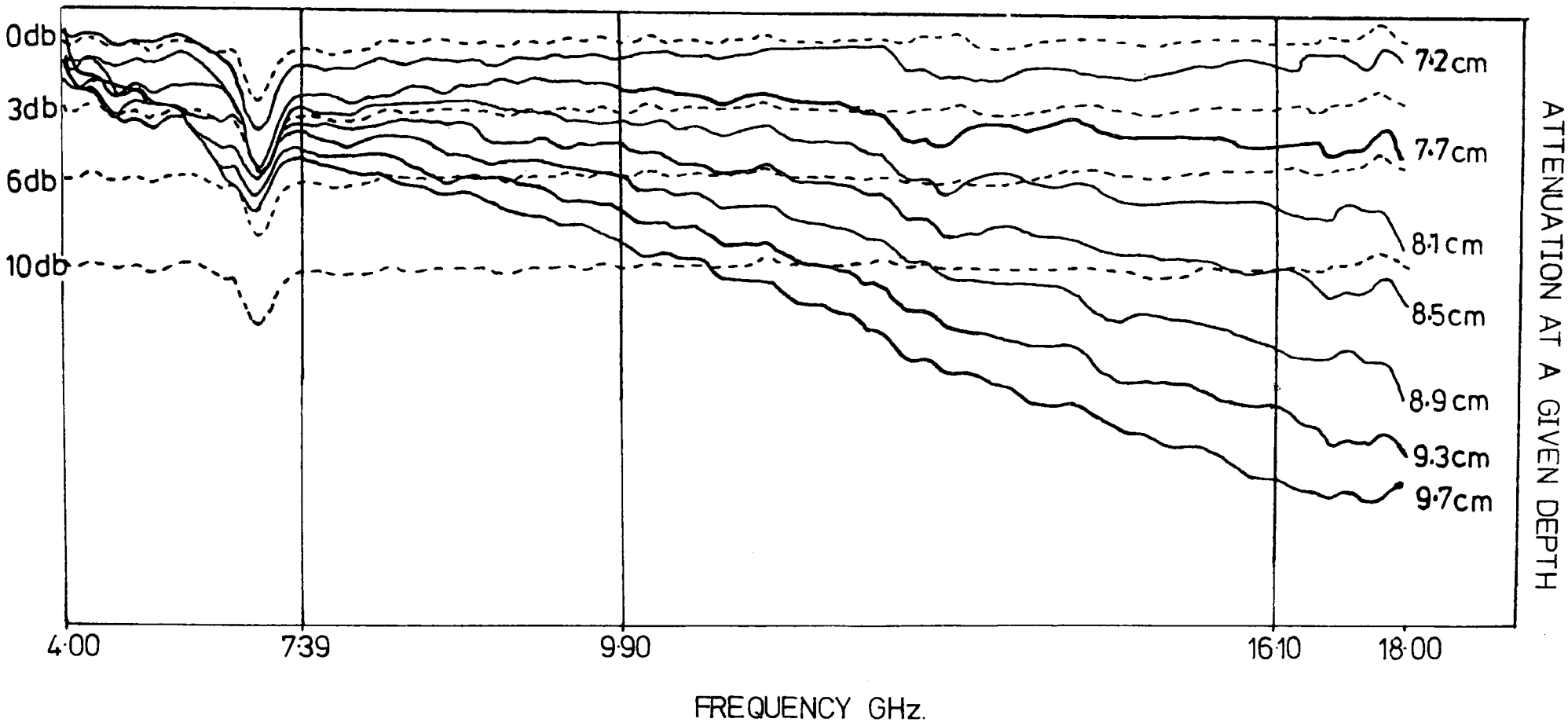

Fig.III.3. Plots of attenuation against depth at different frequencies. CH_3CN/CCl_4

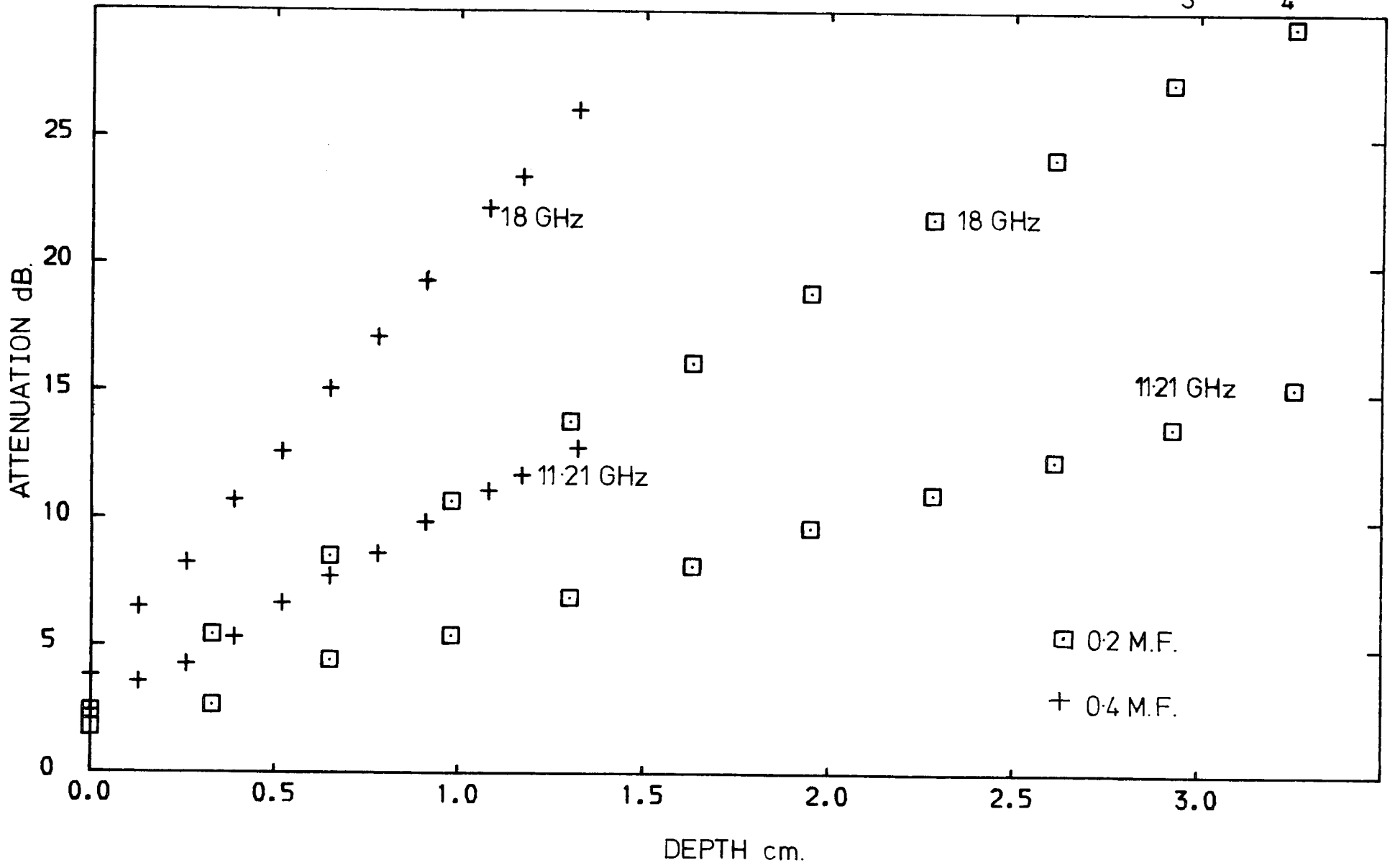

Table III.1 Absorbancies from Sweep Frequency Measurements

All absorbancies are in cm^{-1} and in amplitude ratio. Frequencies are in GHz. Estimated errors in α are ±5%

CH_3CN/CCl_4-

M.F. \ Freq.		11.21	12.92	14.63	16.01	17.53	18.00
0.01	a	0.024	0.033	0.039	0.046	0.054	0.056
0.10	a	0.241	0.294	0.359	0.412	0.468	0.481
0.20	a	0.479	0.590	0.713	0.812	0.932	0.954
0.30	a	0.701	0.869	1.048	1.199	1.379	1.418
0.40	a	0.907	1.139	1.364	1.548	1.797	1.882
0.50	a	1.050	1.310	1.619	1.882	2.167	2.244
0.60	a	1.132	1.451	1.823	2.108	2.480	2.615
0.70	a	1.287	1.609	2.021	2.254	2.661	2.899

0.016 M.F.

Freq.	8.14	11.31	15.51	18.00
a	0.027	0.042	0.080	0.094

0.06 M.F.

Freq.	6.46	9.72	16.57	18.00
a	0.057	0.112	0.273	0.317

0.16 M.F.

Freq.	7.39	9.90	16.10	18.00
a	0.217	0.330	0.683	0.794

CH_3CN/Benzene

0.016 M.F.

Freq.	7.48	10.97	17.39	18.00
a	0.028	0.045	0.106	0.116

Table III.1 Continued

		0.06 M.F.		
Freq.	6.88	10.45	16.97	18.00
a	0.070	0.128	0.293	0.336
		0.16 M.F.		
Freq.	6.97	11.72	16.48	18.00
a	0.189	0.412	0.728	0.833

CH_3CN/n-heptane

	0.027 M.F.		
Freq.	12.05	15.40	18.00
a	0.029	0.051	0.056

(0.28x0.14 inches) rectangular waveguide together with a 72GHz klystron with an E-band 4mm (0.122x0.061 inches) waveguide were used for these experiments. The system for the 36GHz set-up is shown in Fig.III.4. The frequency meter measures the actual frequency particular to the waveguide by adjusting the dimensions of a cavity until a resonance condition is reached. When this occurs energy is stored in the cavity and a sharp drop in power is observed. The frequency at which this occurs can be read directly from the wave meter on the E-band system but in the Q-band case the micrometer reading is converted to frequency using (Elliott) tables.

Measurements of attenuation were made on a power meter connected to a crystal detector. The attenuation of the sample was balanced against an adjustable, calibrated attenuator so as to maintain a constant reading on the power meter, this is to overcome any non-lineararity which may be present in the detection system. The attenuator in the E-band system reads directly in decibels while the readings on the attenuator in the Q-band line were converted to decibels using (Elliott) tables. Care had to be taken to ensure that the first liquid layer completely covered the bottom of the cell otherwise non-linear attenuation plots are obtained. The maximum concentration of CH_3CN that could be measured on both systems was 3.6 moles per litre. Plots of attenuation against different liquid depths were very reproduceable (see Fig.III.5.) This shows two runs done on different days. Price[73] estimates that each value of attenuation has an error of +or- 5%. Results are shown in table III.2. The neat solvents showed no detectable attenuation of the radiation at any of the microwave frequencies.

Fig.III.4. Diagram of 33·98 GHz. apparatus

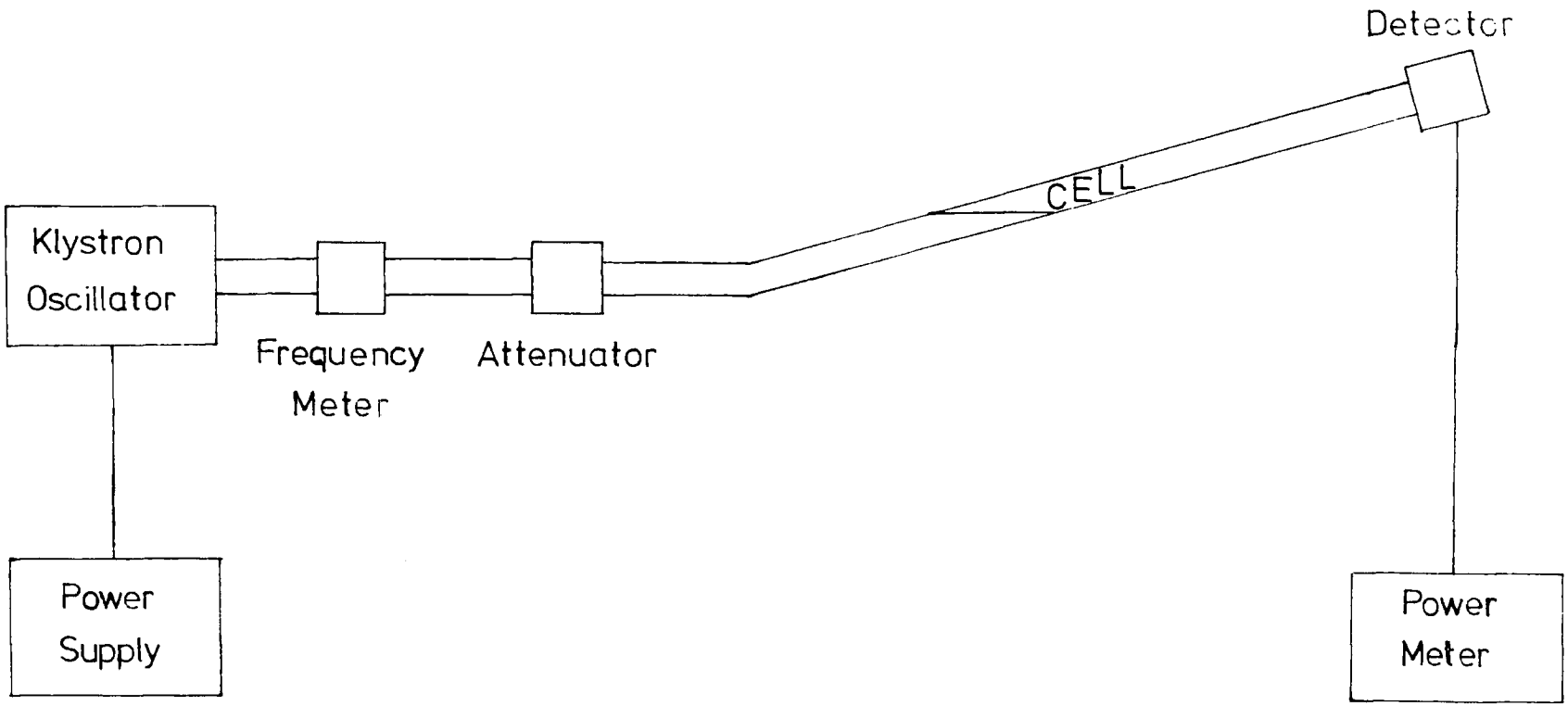

Fig.III.5. Plots of attenuation against depth, for two runs. CH_3CN/CCl_4 0·016 M.F., 33·98 GHz.

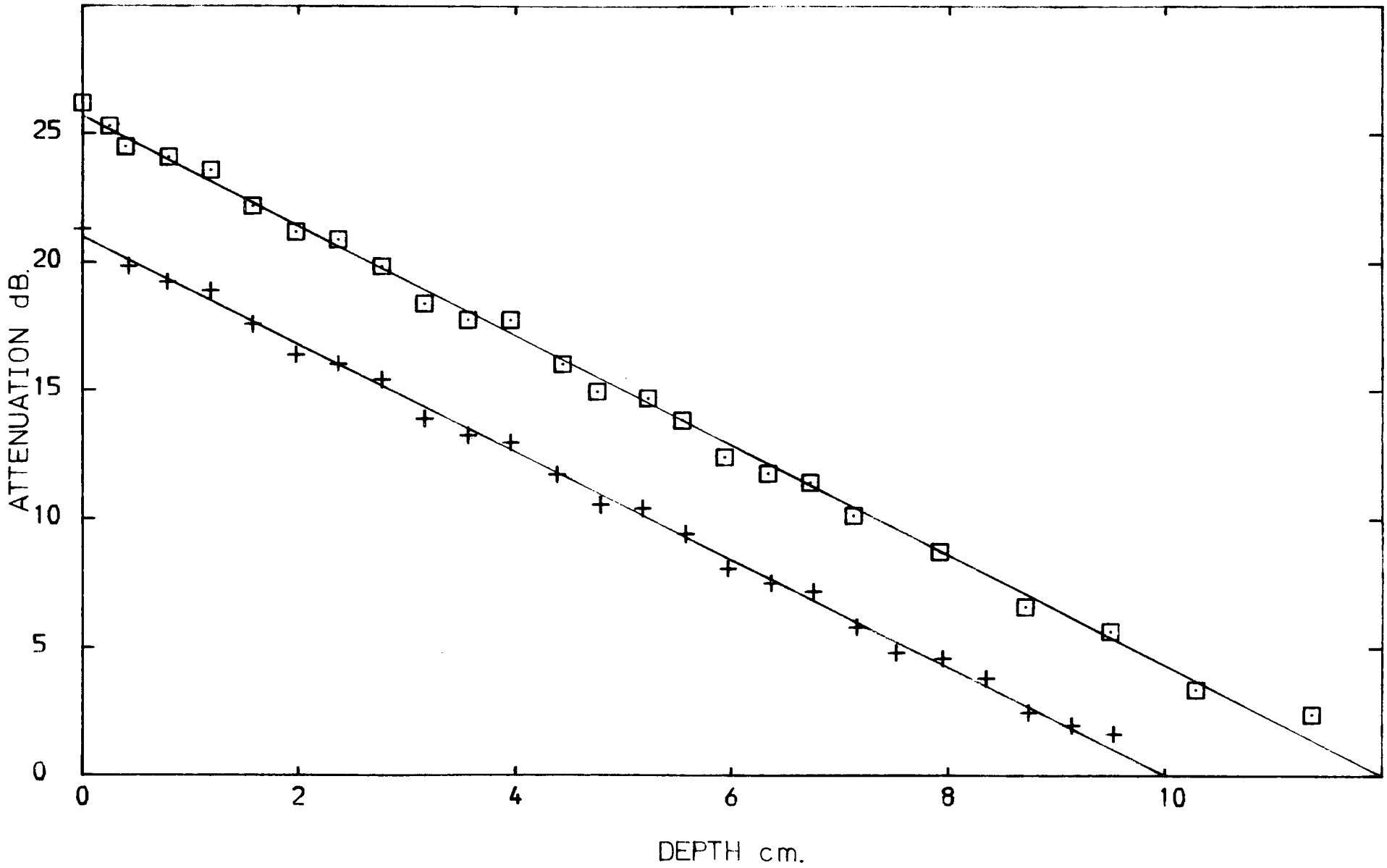

Table III.2 Absorbancies from Spot Frequency Measurements

All absorbancies are in cm^{-1} in amplitude ratio. All frequencies are in GHz. All α values are ±5%

CH_3CN/CCl_4-

M.F. \ Freq		33.9775 GHz.	69.66 GHz.
0.01	α	0.160	0.283
0.016	α	0.244	0.432
0.06	α	0.753	1.309
0.10	α	1.126	1.792
0.16	α	1.757	2.700
0.20	α	1.988	3.741

CH_3CN/benzene

0.016	α	0.299	0.519
0.06	α	0.843	1.464
0.16		2.105	3.807

CH_3CN/n-heptane

0.027	α	0.176	0.478

III.4 Measurments of ϵ_o

Measurements of ϵ_o were made on all of the solutions. These were performed at Aberystwyth using a Wayne-Kerr B201 bridge instrument which measures the liquid's capacitance at 100KHz. Since capacitance is directly proportional to permittivity[1], the permittivity was obtained from calibration graphs of known liquid capacitance against permittivity. The results are presented in table III.3. Also shown in tableIII.3 are calulated ϵ_o values for the CH_3CN/CCL_4 solutions using equation III.7.[1]

$$\epsilon_{12}-1/\epsilon_{12}+2=\Phi_1(\epsilon_1-1/\epsilon_1+2)+\Phi_2(\epsilon_2-1/\epsilon_2+2) \qquad .....III.7$$

Where 12, 1, and 2 refer to the solution, solvent and solute respectively. Φ_1 and Φ_2 are the volume fractions of the respective components in the solution. This equation is based on Debye's equation (equation I.11) and so is only expected to be applicable to dilute solutions of non-interacting polar solutes in non-polar solvents[1]. However table III.3 shows that even at very low concentrations this equation is not obeyed indicating that there are quite strong interactions between CH_3CN and CCL_4 molecules.

III.5 Data Analysis and Results

In order to obtain τ from the absorption data a modified Fouss-Kirkwood[73] equation was employed. τ is obtained from

$$\nu_{max}=[(3\epsilon_o+\epsilon_\infty)/(\epsilon_o+3\epsilon_\infty)]^{1/2}/\ 2\pi\tau_m \qquad ....III.8$$

where ν_{max} is obtained using

$$\cosh^{-1}\frac{(\alpha(\nu)/\nu)_{max}}{(\alpha(\nu)/\nu)} = \beta\log_e(\nu_{max}/\nu) \qquad ....III.9$$

where α is the absorption coefficient in amplitude ratio, ν is the frequency in Hertz and β an empirical parameter ($0<\beta<1$). A plot of the

Table III.3 ϵ_o values

Mole Fraction	ϵ_o	ϵ_{12}(calc)[$]
CH_3CN/CCl_4-		
0.01	2.388±2%	2.406
0.016	2.450	2.529
0.06	3.050	3.370
0.10	3.652	4.124
0.16	4.670	5.415
0.20	5.188	6.233
0.30	7.382	8.534
0.40	9.576	11.706
0.50	12.412	13.948
0.60	15.753	17.081
0.70	19.636	20.859
1.00	36.500	
CH_3CN/benzene		
0.016	2.600	--
0.06	3.220	--
0.16	5.120	--
CH_3CN/n-heptane		
0.027	2.224	--

Literature values, ϵ_o for pure CH_3CN 36.23[11]

37.4[10]

Solution data[12]	M.F.	ϵ_o
CH_3CN/CCl_4	0·1	3.60
	0·15	4.38
	0·2	5.20

[$] Calculated using equation III.7 with ϵ_o (CCL_4)=2.234[1] (20C)

left hand side of equation III.9 against $\ln(\nu)$ for a series of α's (usually between 4 and 6) is a linear plot with a slope of β and an X-axis intercept of $\ln(\nu)_{max}$. The modification of the original Fuoss-Kirkwood equation[14] is in using α/ν instead of ϵ'' (see equation I.46), so to correct for this the square rooted factor in equation III.8 was introduced[73]. This factor was derived using the Debye equations (I.5 and I.6), and since it is known that these equations do not predict $\alpha(\omega)$ very well above $\epsilon''(\omega)_{max}$ (see chapter II) this equation will only be used on α/ν data below $(\alpha/\nu)_{max}$. The analysis technique was tested using $\alpha(\omega)$ data generated using equations I.5,I.6,I.46 and I.47 with ϵ_o = 37.5, ϵ_∞=2.25 and τ=6.0x10^{12} seconds (see footnote I.1). The analysis yielded τ=7.0p.s., that is 17% too high, and β=1.0. Then using ϵ_o=5.0, ϵ_∞=2.25 and τ=6.0p.s. the equations III.8 and III.9 gave τ=6.2ps. i.e 3% too high, and β=0.96. These results must be borne in mind when the method is applied to the experimental data. The values for ϵ_∞ for these solutions were obtained from the Kramers-Krönig analysis shown in chapter V (see table V.1). The frequency at which the ϵ_∞ values were measured was 250cm^{-1}.

Some typical plots of α/ν against $\log_e(\nu)$ and corresponding Fuoss-Kirkwood plots are shown in Figs.III.6,7 and 8. The solutions above 0.2 mole fraction CH_3CN in CCl_4 were too highly absorbing to be measured at 34 and 70GHz so that $(\alpha(\nu)/\nu)_m$ could not directly be observed. In order to estimate the value of $(\alpha(\nu)/\nu)_m$ of the remaining solutions my data at 34GHz was plotted along with that of 0.25 mole fraction data of Eloranta[75] and pure liquid data of Mansingh[11] at the same frequency (see Fig.III.9) ,from which an estimate of the α(34GHz) value of the solutions 0.3 to 0.7 mole fraction was read off. It was expected from

Fig.III.6. a/ν curve and resulting Fuoss-Kirkwood plot. CH_3CN/CCl_4 0·01 M.F.

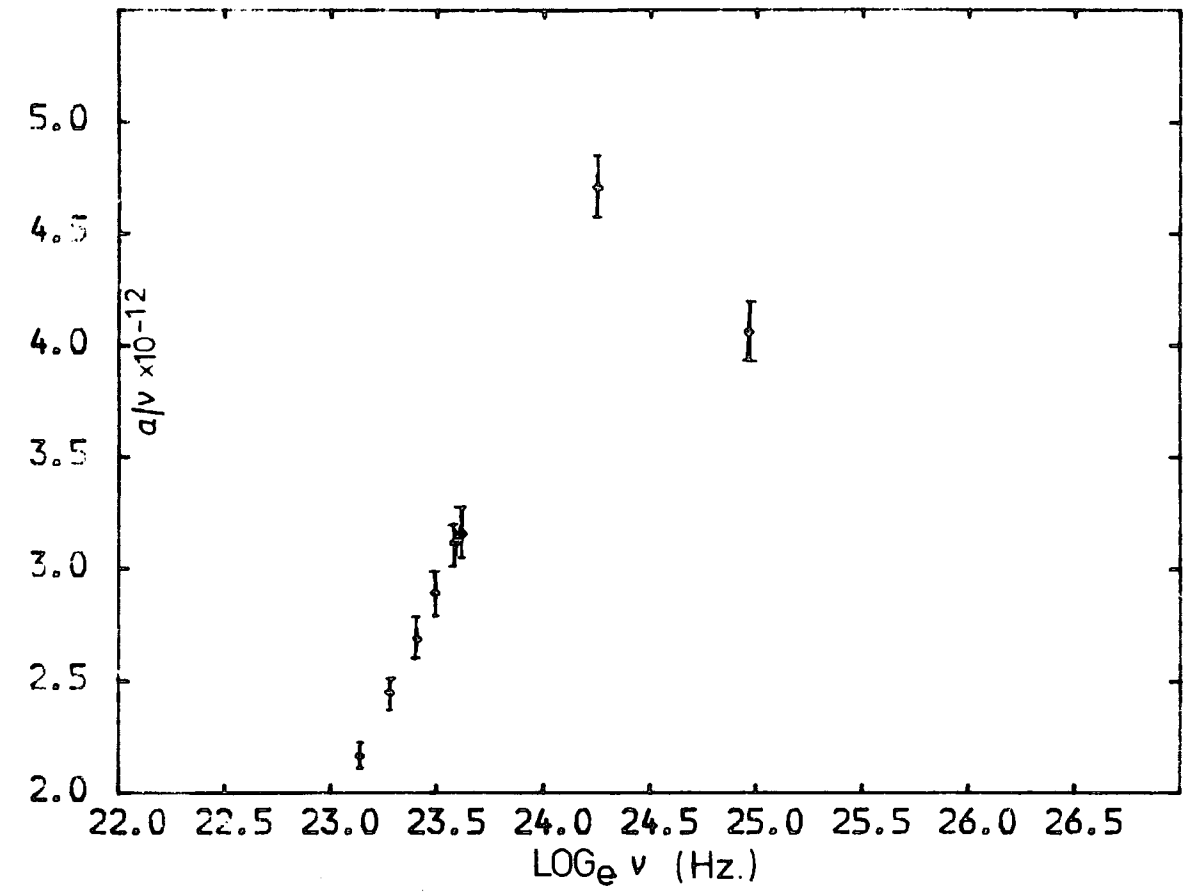

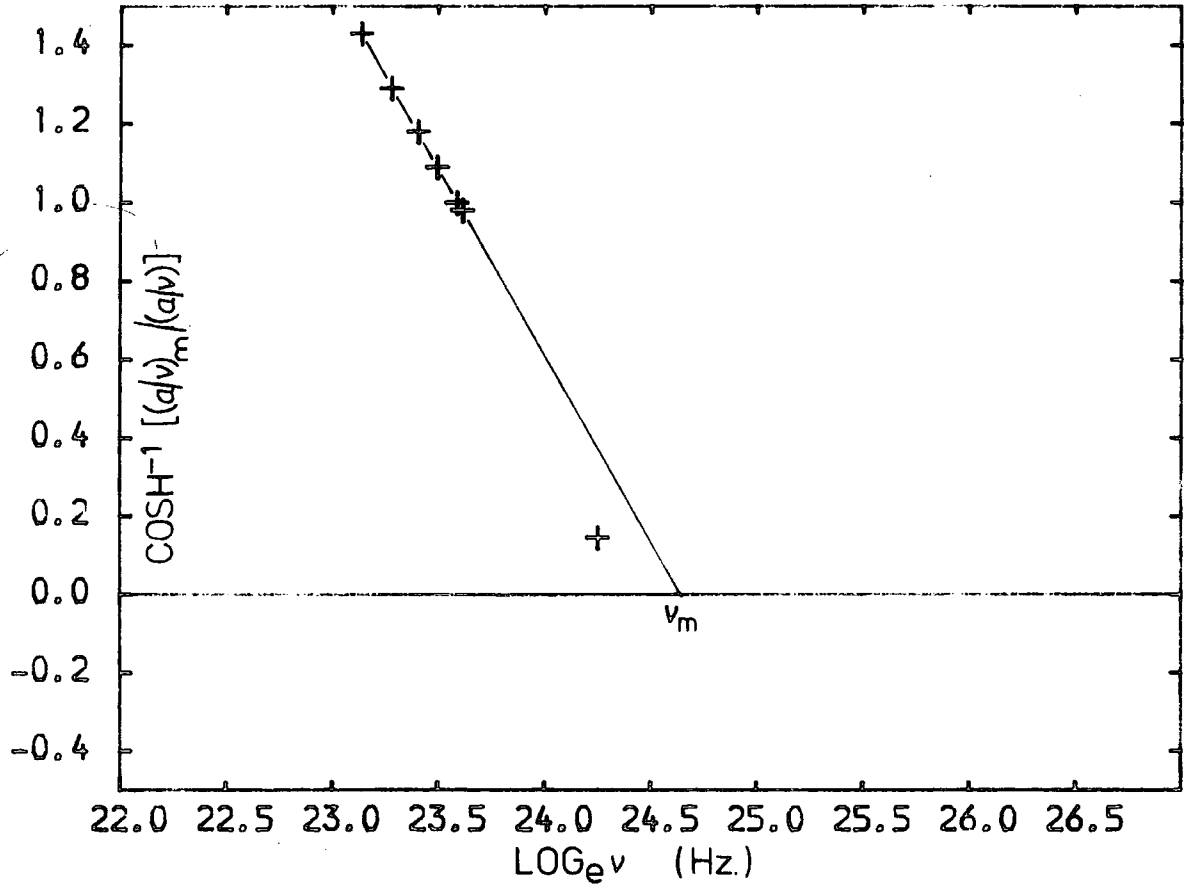

Fig.III.7. a/ν curve and resulting Fuoss-Kirkwood plot. CH_3CN/CCl_4 0·2 M.F.

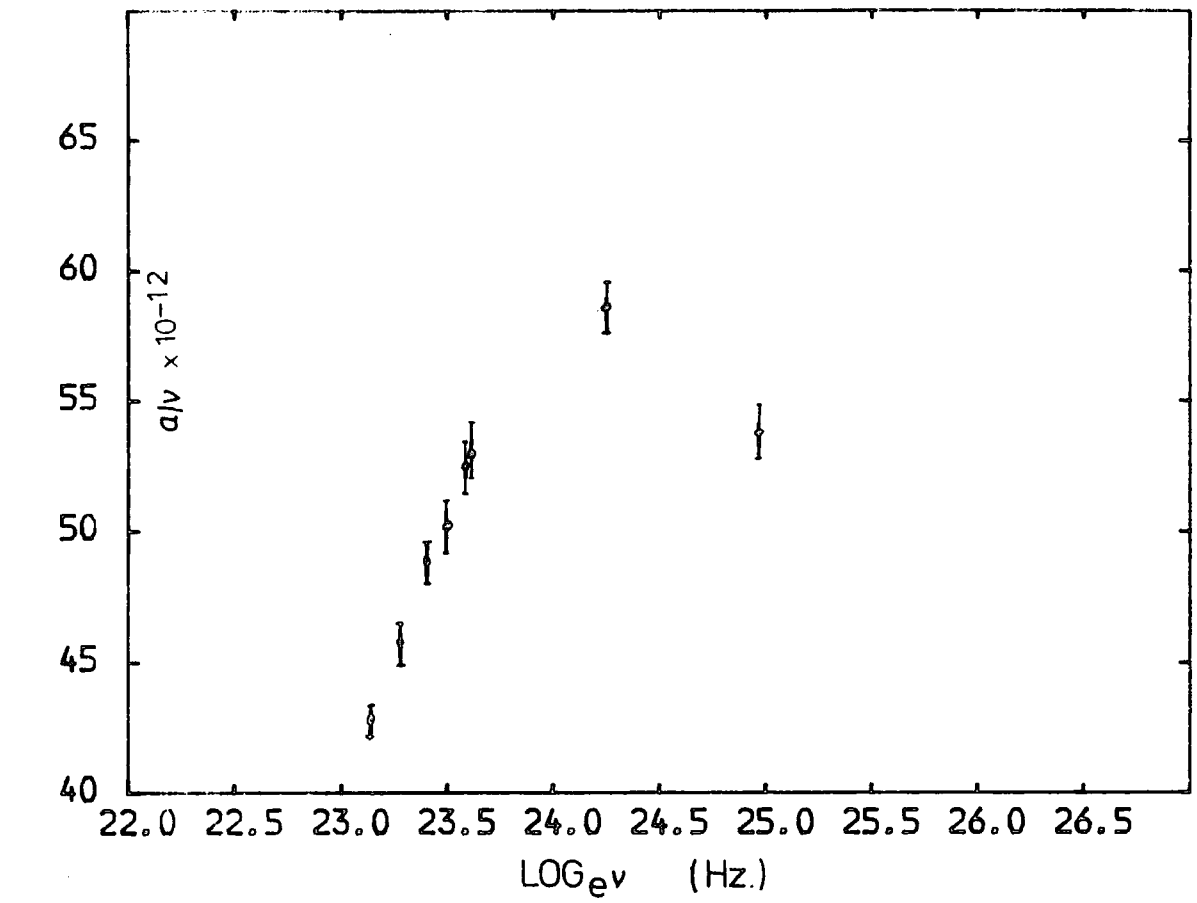

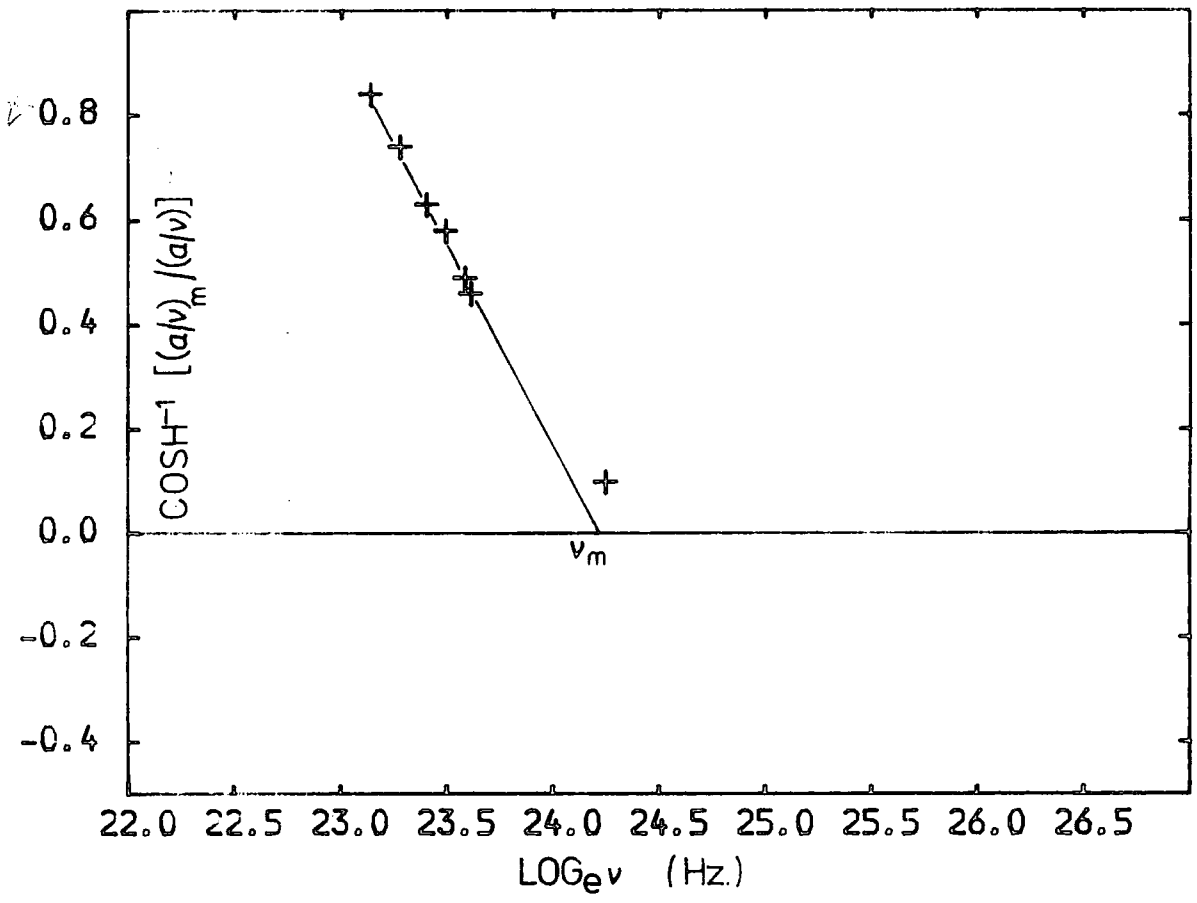

Fig.III.8. a/ν curve and resulting Fuoss-Kirkwood plot. CH_3CN/n-hept. 0·027M.F.

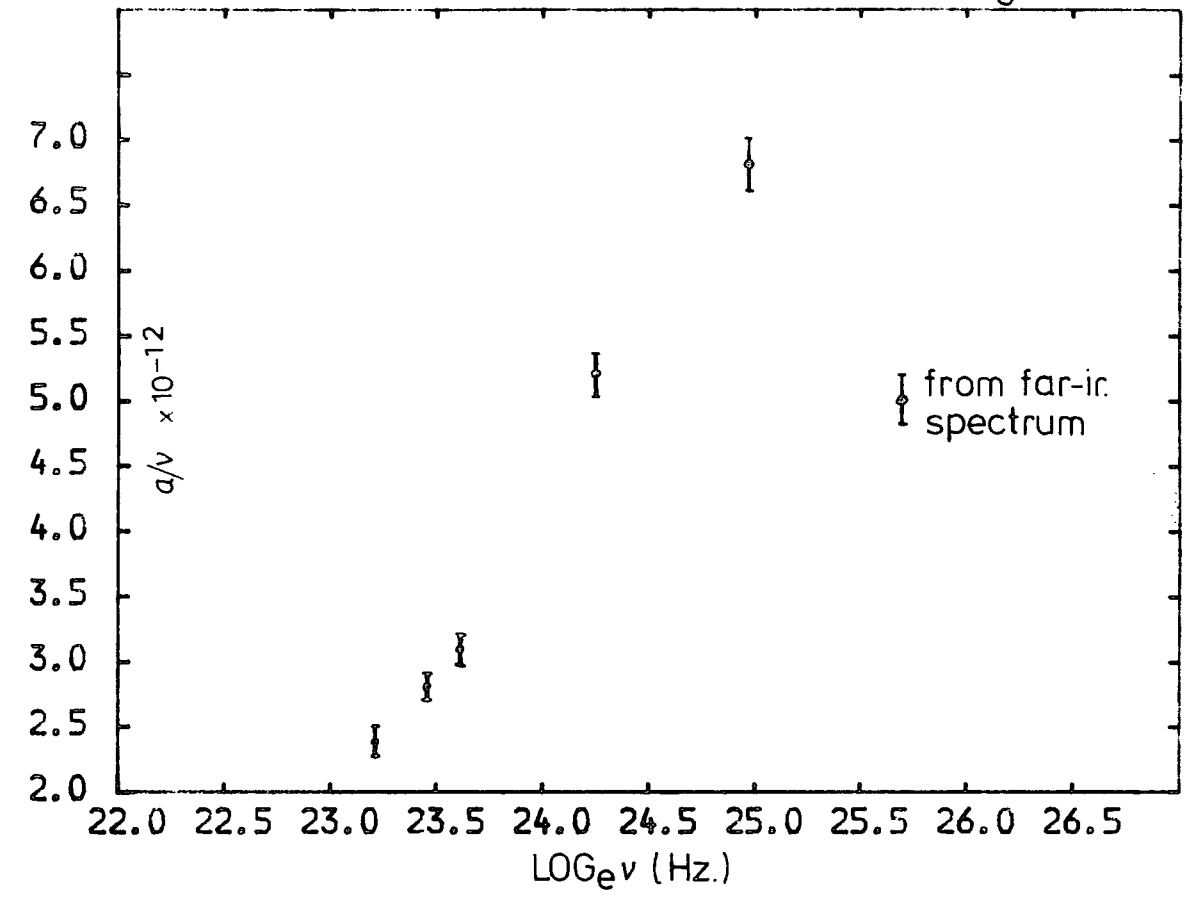

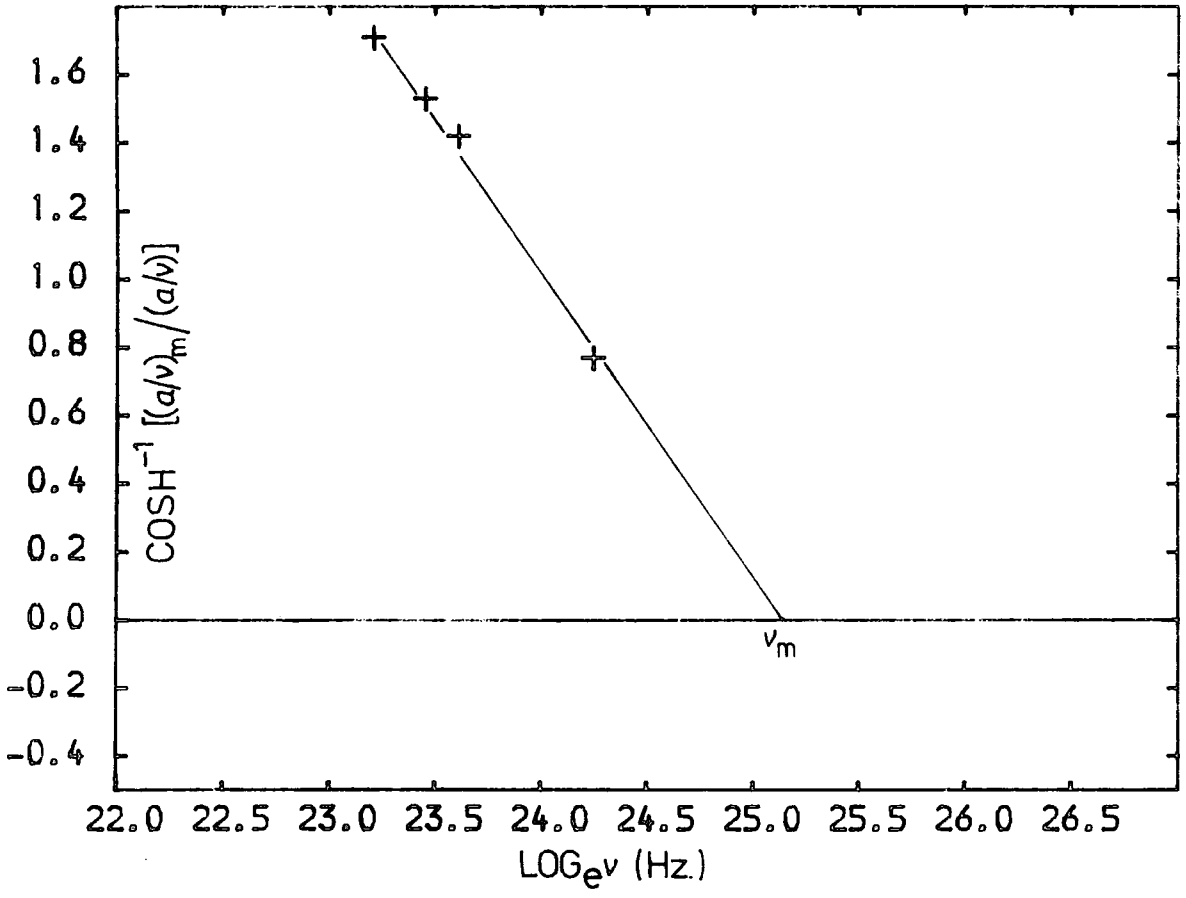

Fig.III.9. $a(\nu)$ mole^{-1}. CH_3CN/CCl_4 data at 33·97 and 11·21 GHz.

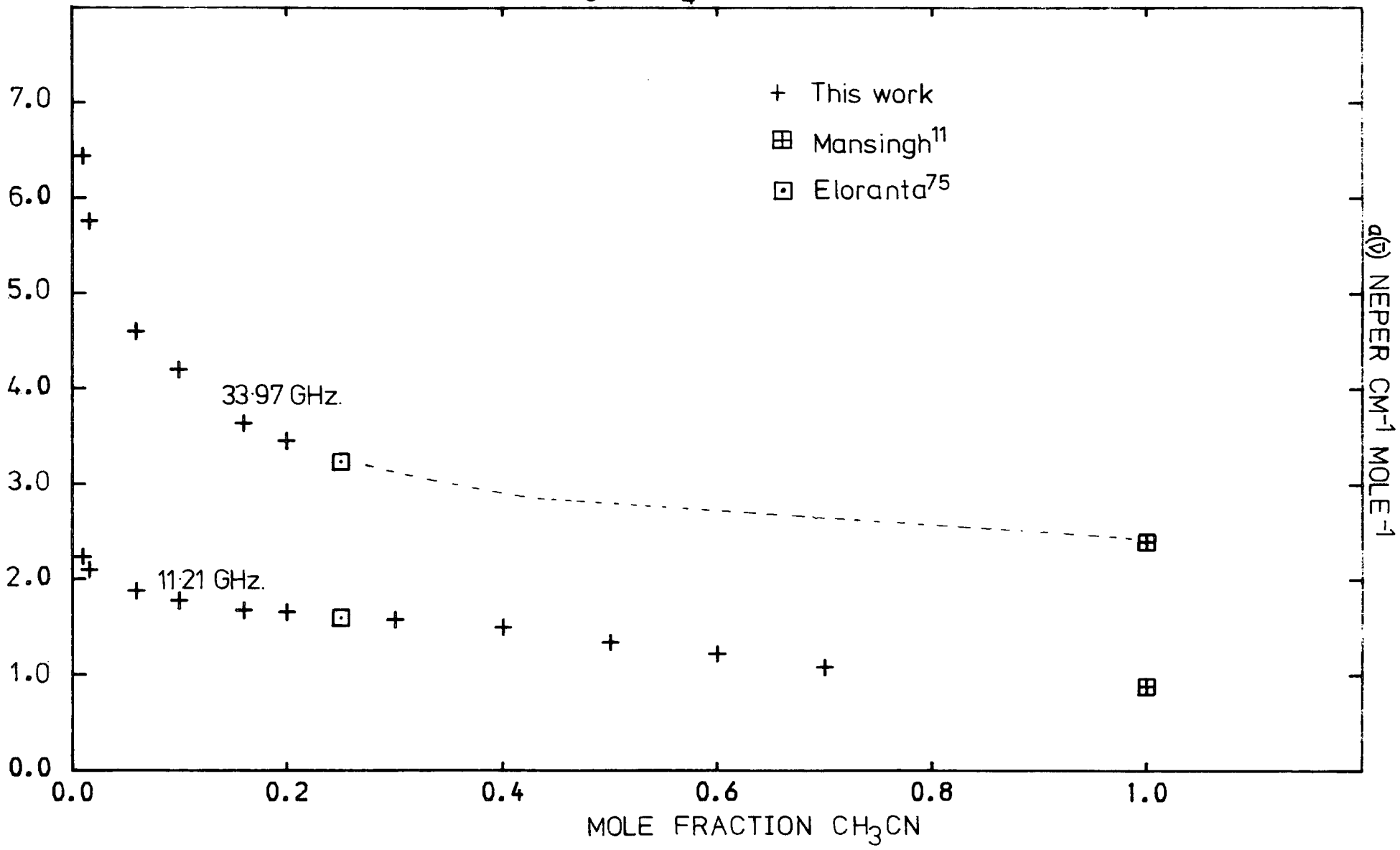

the previous analysis that the value of $\alpha(\nu)/\nu$ at this frequency would be close to its maximum value. The justification for using the literature data was that the data of Eloranta[75] and Mansingh[11] fitted in very well with my data at the frequency of 18GHz see Fig.III.9. Fig.III.10 shows this point plotted for the 0.5 mole fraction data together with the corresponding Fuoss-Kirkwood plot. The estimated accuracy in the τ values obtained is +or- 0.5ps. for the 0.01 to 0.2 mole fraction solutions and +1.5 or -1.0 for the 0.3 to 0.7 mole fraction liquids. The value of τ for the pure liquid was calculated from the combined data of Janik[12], Vaughan[10] and Mansingh[11]. Table III.4 shows the computed τ values together with the Powles[24], Glarum[22] and Cole[23] (CGP) (chapter I equation I.14) modified values. Fig.III.11 is a plot of the unmodified τ values against mole fraction. Table III.4. also shows the computed values of β. These are a measure of the deviation from the Debye equations in terms of the width of the $\epsilon''(\omega)$ curve[1]. They are all less than one which means that the band is broader than the Debye prediction. They do not show any trend and so the spread in their values is probably an indication of the accuracy of the experimental points.

Fig.III.10. a/ν curve and resulting Fuoss-Kirkwood plot. CH_3CN/CCl_4 0·5M.F.

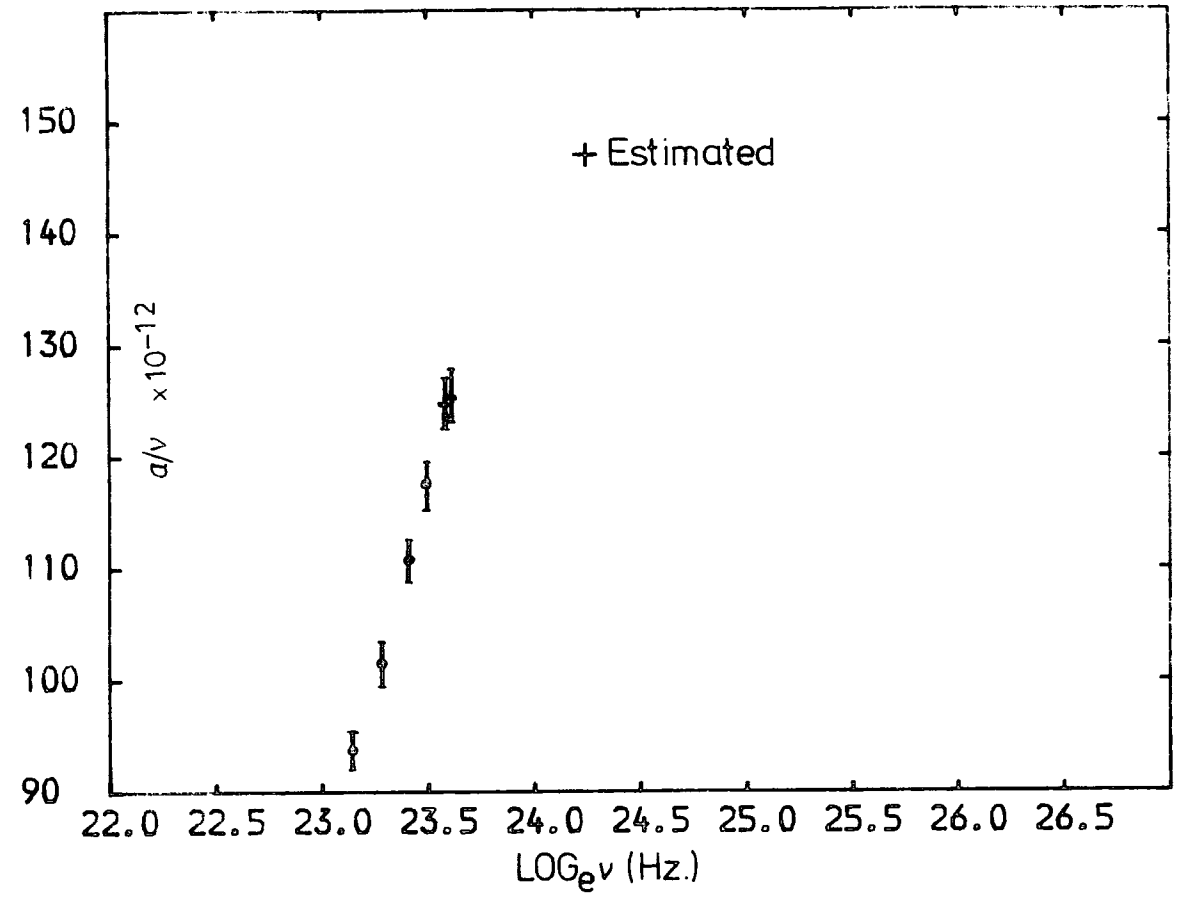

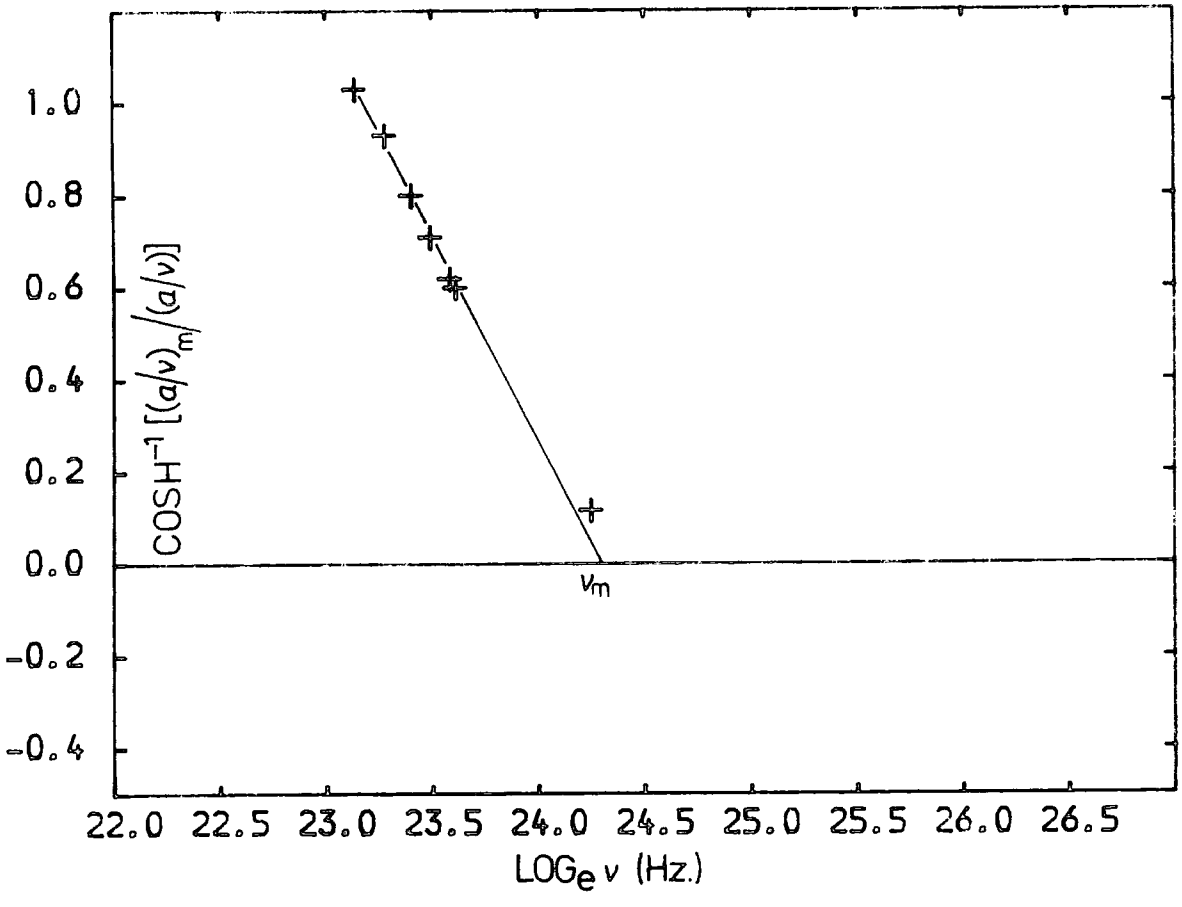

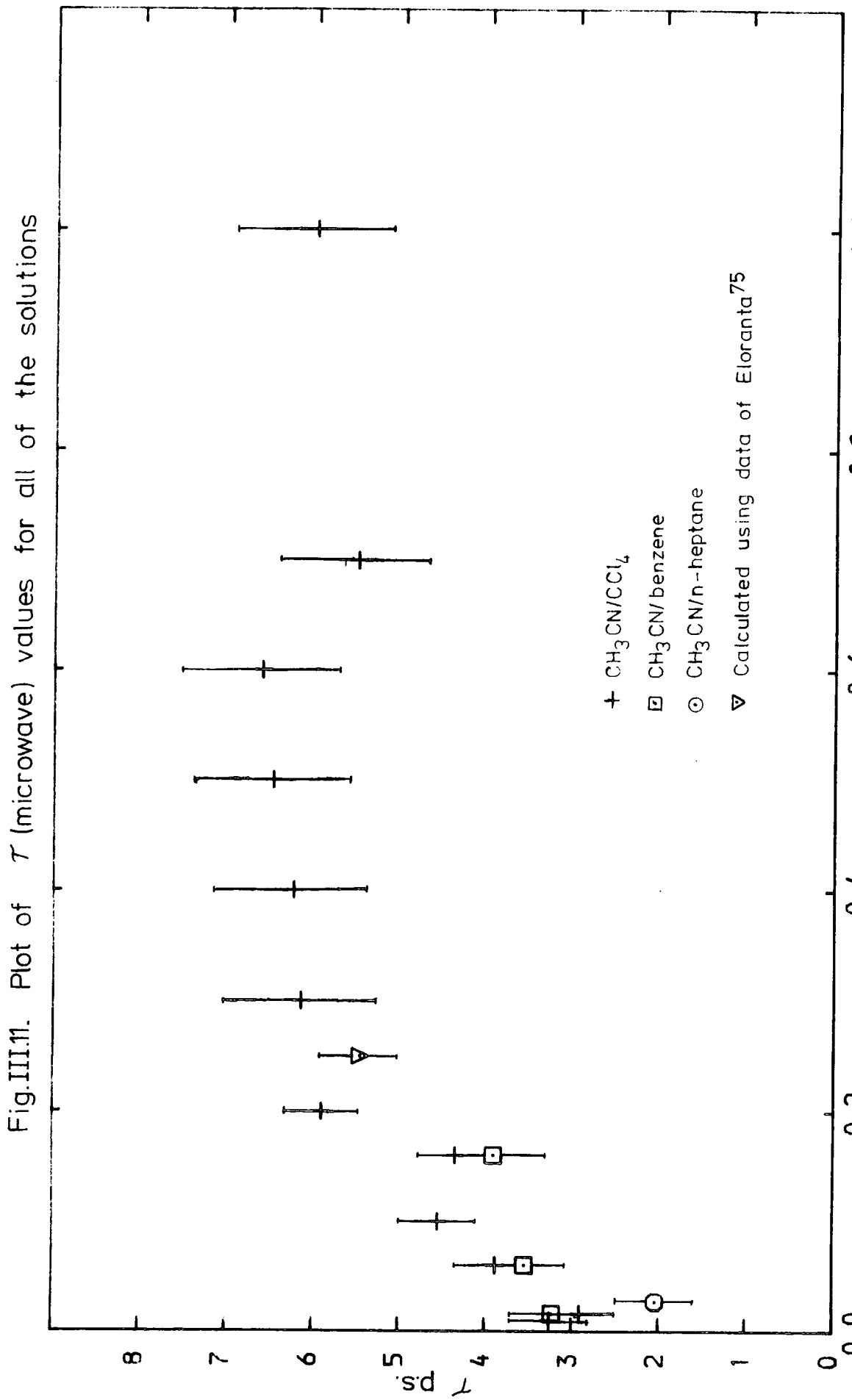
Fig.III.11. Plot of τ (microwave) values for all of the solutions
τ p.s.
0
1
2
3
4
5
6
7
8
0.0
0.2
0.4
0.6
0.8
1.0
MOLE FRACTION CH_3CN
+ CH_3CN/CCl_4
⊡ CH_3CN/benzene
⊙ CH_3CN/n-heptane
▽ Calculated using data of Eloranta[75]

Table III.4 Microwave τ values from theFuoss-Kirkwood Analysis.

All τ values are in picoseconds.

CH_3CN/CCl_4 solutions

M.F.	τ	τ(C-G-P)	β
0.01	3.26 ±0.5	3.20	0.96
0.016	2.91	2.83	0.76
0.06	3.88	3.54	0.83
0.10	4.55	3.97	0.82
0.16	4.35	3.60	0.70
0.20	5.90	4.79	0.79
0.25[¤]	5.46	4.33	0.87
0.30	6.14 ±1.0	4.72	0.82
0.40	6.23	4.64	0.92
0.50	6.47	4.70	0.93
0.60	6.60	4.71	1.00
0.70	5.50	3.88	0.85
1.00[$]	6.00	4.12	0.90
CH_3CN/benzene			
0.016	3.23 ±0.5	3.09	0.81
0.06	3.55	3.19	0.79
0.16	3.91	3.17	0.75
CH_3CN/n-heptane			
0.027	2.04	1.98	0.92

[¤] This value was calculated by the Fuoss-Kirkwood method on the data of Eloranta[75].

[$] This value was calculated using the Fuoss-Kirkwood method on the combined data of Mansingh[11], Vaughan[10] and Janik[12].

Chapter IV.

Far-Infrared Measurements.

IV.1 Basic Principles of Interferometry

For very good detailed accounts of the principles of interferometric spectroscopy see the books of Bell[76] and Chamberlain[53]. This account will only point out the important experimental considerations in the use of an interferometer. A diagram of a conventional Michelson interferometer is shown in Fig. IV.1a. The Beckman RIIC FS-720 instrument in Durham has this basic layout.

The source is a mercury vapour lamp which emits radiation in a continuous form from the far-infrared to the ultraviolet although it is relatively weak in the far-infrared region. The radiation is amplitude modulated by a mechanical rotating blade chopper operating at 12Hz. This is coupled with a phase sensitive detection system to enable only radiation modulated at the chopper frequency to be detected. This reduces the amount of background noise in the interferogram. The beam is then split into two parts at the dielectric ('Melinex') beamsplitter. One half is reflected onto the moving mirror and the other half is transmitted onto the stationary mirror. The two beams are then recombined at the beamsplitter with some of the radiation then being focused onto the sample, after which it is refocused onto the Golay detector window. The essential feature of an interferometer is the introduction of a phase difference between the two beams. In this interferometer it is done by moving a moving mirror so as to create a path difference between the two beams. The recombined beams then form an interference pattern of intensity against path difference which then has to be Fourier transformed into the frequency domain. For a single sided symmetric interferogram we have

Fig.IV.1.

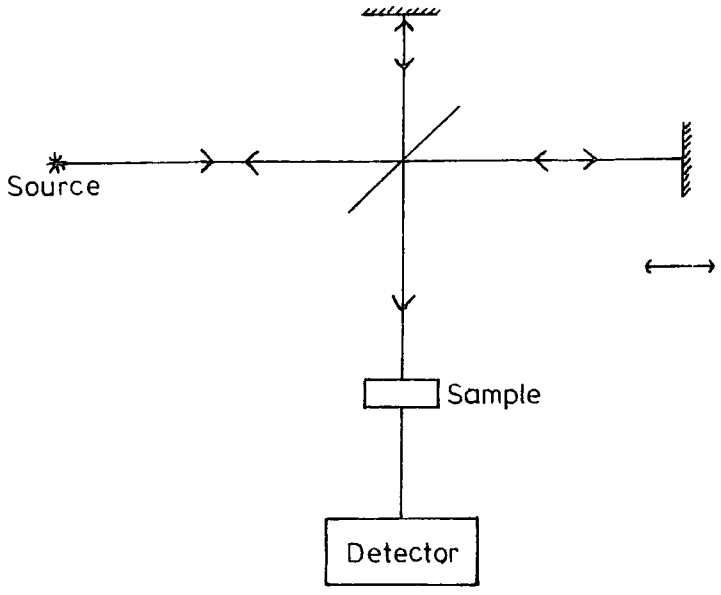

a). Diagram of Michelson interferometer

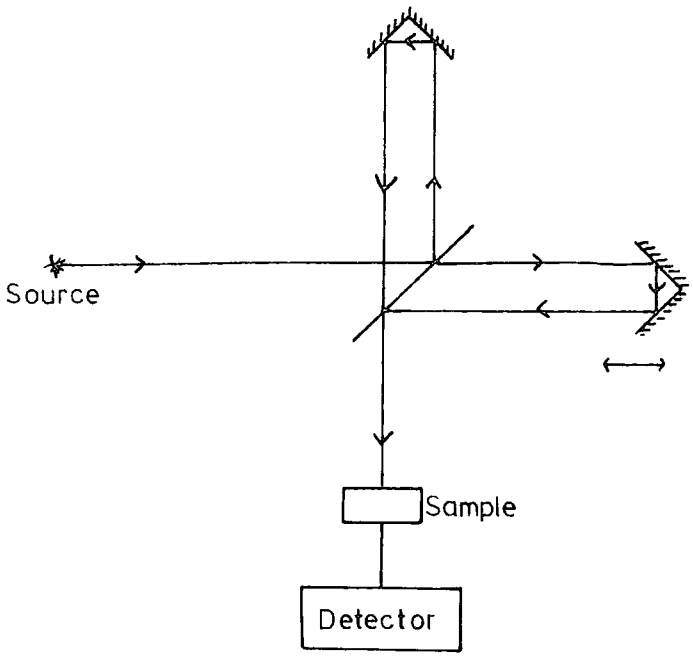

b). Diagram of Martin and Puplett polarising interferometer

$$I(x) - I_o = \int_0^\infty 2S(\nu)\cos(2\pi\nu x)\, d\nu \qquad \text{.....IV.1}$$

I(x) is the intensity in the interferogram, I_o a constant offset (mean level) in the interferogram and $S(\nu)$ the spectral intensity in the frequency domain. If x is measured in cm. then ν is in $cm.^{-1}$. The main advantages of this technique for far-infrared spectroscopy (where the output from source is relatively low) over conventional grating spectrometers such as a grating mid-infrared spectrometer are:

a) Fellget or multiplex advantage.

This arises because all of the spectral range is observed for the duration of the experiment, whereas in grating spectrometers the spectral elements are observed individually through a slit for short periods. This means that each spectral element in the case of the interferometer will be subject to less noise (from external sources) than in the sequential spectrometer. This leads to several possible gains in sensitivity over a grating spectrometer[76]. This only applies if the spectrometer is detector noise limited (i.e. most of the noise is due to the detector) where the noise is frequency independent, and this is expected to be the case with far-infrared radiation detectors[76].

b) Jacquinot advantage.

This is otherwise known as the throughput advantage, which means that an interferometer has high energy throughput compared to that allowed through the narrow slit of a grating spectrometer, enabling high signal to noise ratios to be achieved. The radius of the beam is limited by the first mirror in the instrument after the source which is about 4 inches in diameter in the FS-720.

The major disadvantage is that a computer is required to Fourier transform the interferogram into the frequency spectrum which means that

it cannot be seen in real time. However, on the Durham instrument there is now a microcomputer into which the interferogram is fed directly and then Fourier transformed. This reduces the lag to a minimum.

IV.2 Experimental Considerations

a)Beamsplitter

Fig.IV.2 shows the relative efficiency of the various gauge beamsplitters which can be used in an experiment. The spectral range of interest in these studies was 0 to 300 cm^{-1} so the type most often used was 25 or 50 gauge (6 and 12.5 microns in thickness). The sinsoidal variation in the efficiency curves is due to interference within the thin film its self.

b) Spectral Resolution

The resolution of the spectrum in the frequency domain is determined by the total path difference between the two beams

$$\Delta\nu = 1/x_{max} \qquad \text{.....IV.2}$$

where $\Delta\nu$ is the resolution in the frequency spectrum and x_{max} is the total path difference between the two beams.

c)Aliasing

The interferograms are sampled digitally at pre-controlled intervals of mirror movement. This means that the interferogram function has to be evaluated as a summation rather than an integral.

$$S(\nu) = \Delta x \sum_{n=(-n.max/1)}^{n=(n.max/2-1)} I(n\Delta x) \cos 2\pi\nu n\Delta x \qquad \text{.....IV.3}$$

This means that in the evaluation of the summation the computed spectrum will be repeated along the frequency axis every $(2\Delta x)^{-1}$, where only one is required. Each repeated spectrum is called an alias. In addition, there are alternating negative aliases along the axis which may overlap with the positive ones to give a distorted spectral profile. Alias

Fig.IV.2. Relative efficiencies of 'Melinex' dielectric beamsplitters

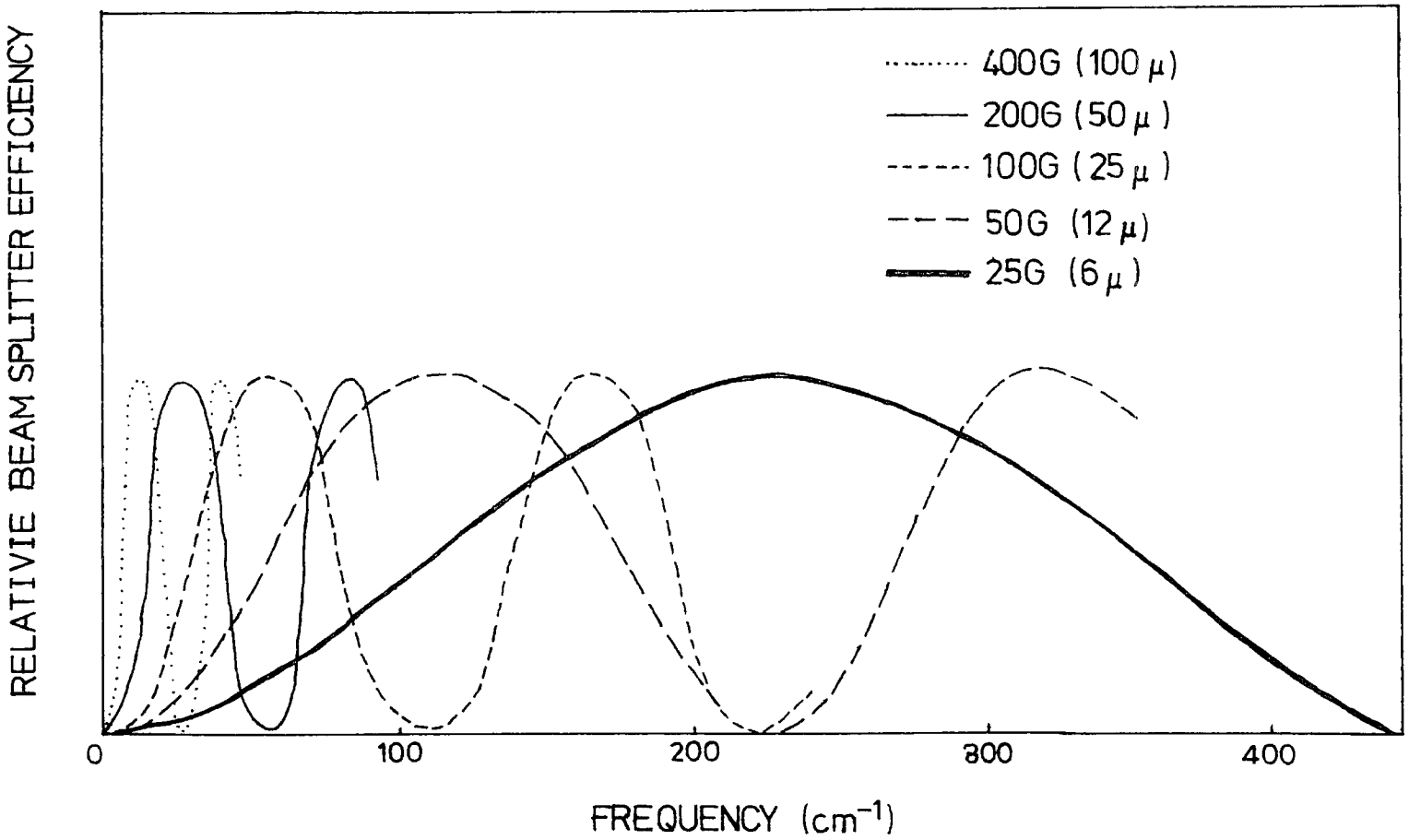

overlap is prevented by using filters to cut off radiation at frequncies above $(2\Delta x)^{-1}$ from forming part of the interferogram. A convenient sampling interval to use is 8 microns which has an aliasing frequency of $625cm^{-1}$ for which a convenient filter is black polythene.

d) Dynamic Range

Filtering of high frequencies not required in the spectral range of interest is also desirable in order to fill the dynamic range of the analog to digital converter with only those frequencies in which the spectral feature is observed. This is particularly relevant since the intensity of the source output increases with increasing frequency.

e) Mirror speed, sampling interval, amplifier time constant and amplifier sensitivity

These four parameters have to be adjusted in order to obtain the maximum signal to noise ratio in the interferogram while ensuring that the interferogram function is correctly sampled.

IV.3 Computation of an Interferogram

A typical digitised interferogram is shown in FigIV.3. To begin with, the average value of the interferogram is removed so that only modulation above and below the mean level is present. Then four main procedures have to be applied to the data in order to obtain the spectrum.

a) Sampling Error Correction

When the interferogram is digitised it is unlikely that the grand maximum at zero path difference will be sampled precisely at its peak. This will result in an asymmetric interferogram being recorded. Other asymmetries may be introduced by misalignments within the instrument, although these are reduced to an absolute minimum by fine adjustments to

Fig.IV.3. Typical single sided interferogram. 8 micron sampling interval

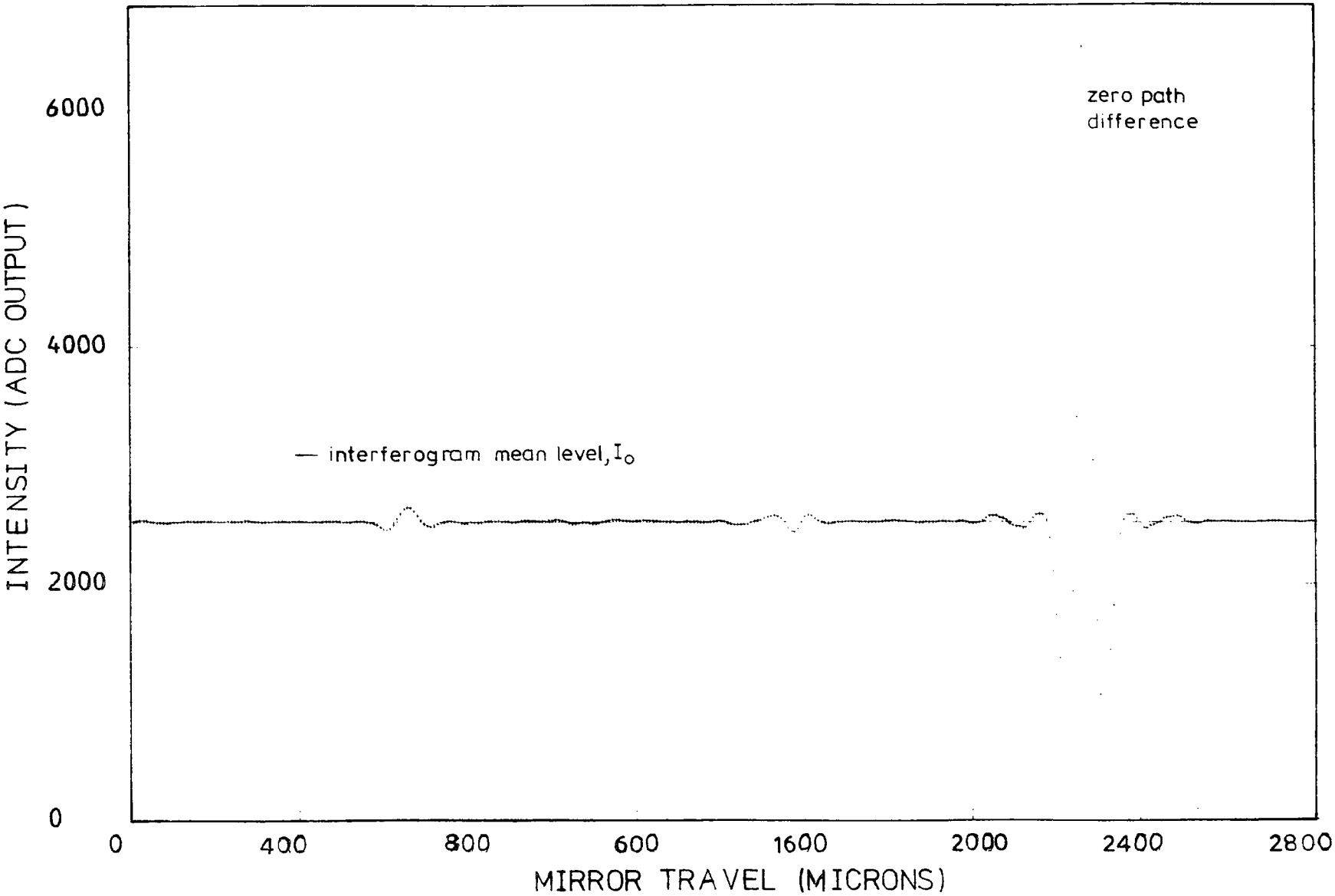

the moving and stationary mirrors.

An interferogram function can be substantially symmetrised by autocorrelating a double sided interferogram. A double sided interferogram is a complex function consisting of a real symmetric cosine part and an assymmetric imaginary sine function. If the interferogram is unsymmetric we have[53]

$$I_u(x)=\int_{-\infty}^{+\infty} S(\nu)\exp(2\pi\nu x)d\nu \qquad \text{.....IV.4}$$

where $S(\nu)$ is the complex spectral intensity. Fourier transformation gives

$$S(\nu)=\int_{-\infty}^{+\infty} I_e(x)\cos(2\pi\nu x)dx - i\int_{-\infty}^{+\infty} I_o(x)\sin(2\pi\nu x)dx \quad \text{....IV.5}$$

If the interferogram is symmetric the sine part is zero. However, if a complex interferogram is autocorrelated

$$f(k)*f(k)=\int_{-\infty}^{+\infty} f(h+k)f(h)dh \qquad \text{.....IV.6}$$

according to the Wiener-Khinchin[53] theorem the Fourier transform is the modulus squared of the Fourier transform of the function

$$\int_{-\infty}^{+\infty}[f(k)*f(k)]\exp.(2\pi ikx)dk = |F(x)|^2 \quad \text{.....IV.7}$$

As the interferogram is made virtually symmetric by autocorrelation the exponential can be replaced by the cosine function. This method was used in a program called FTRAN6.

An alternative approach which only involves the collection of a single sided interferogram, is called phase correction[82]. This method involves the computation of both the sine and cosine transforms in order to obtain the phase function of the spectrum $\Phi(\nu)$ which is the sine

transform divided by the cosine transform. This is evaluated from just a few points around the central maximum as only very low spectral resolution is required[53]. The Fourier transform of this function ($\chi(x)$) is then convolved with the interferogram to produce a symmetric function.

$$I_e(x)=\int_{-\infty}^{+\infty} S_e(\nu)\exp(-2\pi\nu x)dx \qquad \text{.....IV.8}$$

$$=\int_{-\infty}^{+\infty}[S_e(\nu)\exp(-i\Phi(\nu))]\exp(+i\Phi(\nu))\exp(2\pi\nu ix)d\nu \qquad \text{..IV.9}$$

$$=I_u(x)*\chi(x) \qquad \text{.....IV.10}$$

The subscripts o and e refer to odd (asymmetric) and even (symmetric) functions. It is found that this convolution puts a small non-zero mean level back into the interferogram which has to be removed. This method was used in the program called HIBRD which had been supplied by Q.M.C.

b) Apodisation

Because the interferogram cannot be collected to infinite path difference there will be truncations at each end of the interferogram. These truncations would then lead to distortion of the spectrum obtained. The ends of the interferogram are reduced smoothly to zero by a process of mathematical filtering called apodisation. In this process an apodising function (in the programs used by the Durham group a cosine function) is convolved with the interferogram. The function used is

$$APOD=\cos^2(\theta) \qquad \text{.....IV.11}$$

where θ goes from 0 to $\pi/2$ as the interferogram goes from the central maximum to the far wing. The effect of apodisation is to reduce the resolution by a factor of approximately two.

c) Fourier Transformation

Both programs, FTRAN6 and HIBRD, use the Cooly Tukey[77] fast Fourier transform method on a single sided symmetric interferogram to calculate the cosine transform. Fig.IV.4 shows transmission spectra obtained using both programs on the same interferogram. As can be seen they are virtually indistinguishable.

IV. Cooled Detector and Polarising Optics

The low frequency limit of the Golay detector is 15 to 20cm^{-1}, so, in order to measure down to 4cm^{-1}, a special liquid helium cooled Indium/Antimony photoelectric detector (made by QMC Industries Ltd.) was used. Together with this the instrument was converted to operate in the Martin and Puplett[78] polarising mode, in which the energy throughput at low frequencies (<100cm^{-1}) is greater than that of the standard mode of operation.

a) Martin and Puplett Polarising Mode

FigIV.1b shows the basic layout of the polarising system. A detailed description of the Beckman instrument converted to operate in this mode can be found in the MSc. thesis of James[79]. In this system the wire grid chopper modulates the radiation into alternating mutually perpendicular polarisations. The wire grid beam splitter arranged at such an angle will only transmit radiation of the correct polarisation which, when combined with the reversal in polarisation produced by the roof mirrors, means that no radiation is reflected back to the source when the beams are recombined at the beamsplitter. The polarisation produced by the chopper means that the mean level of the interferogram is removed. This has the practical advantage that the full dynamic range of the analog to digital converter can be more fully utilised i.e.

Fig.IV.4. Fourier transforms (cosine) of the same interferogram using two methods of symmetrisation

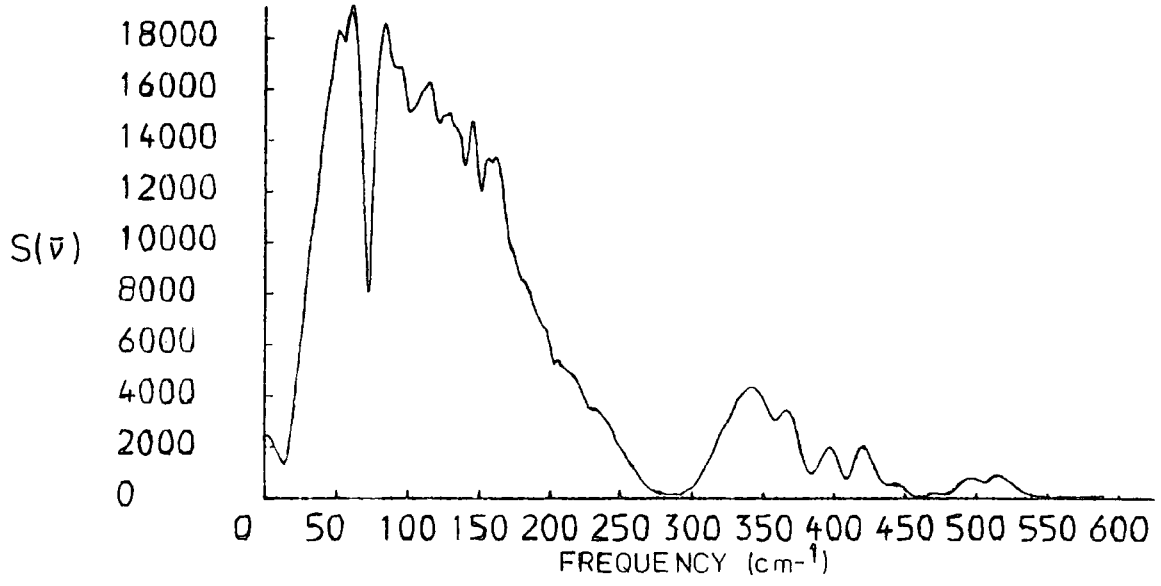

a). Obtained using autocorrelation method (FTRAN6)

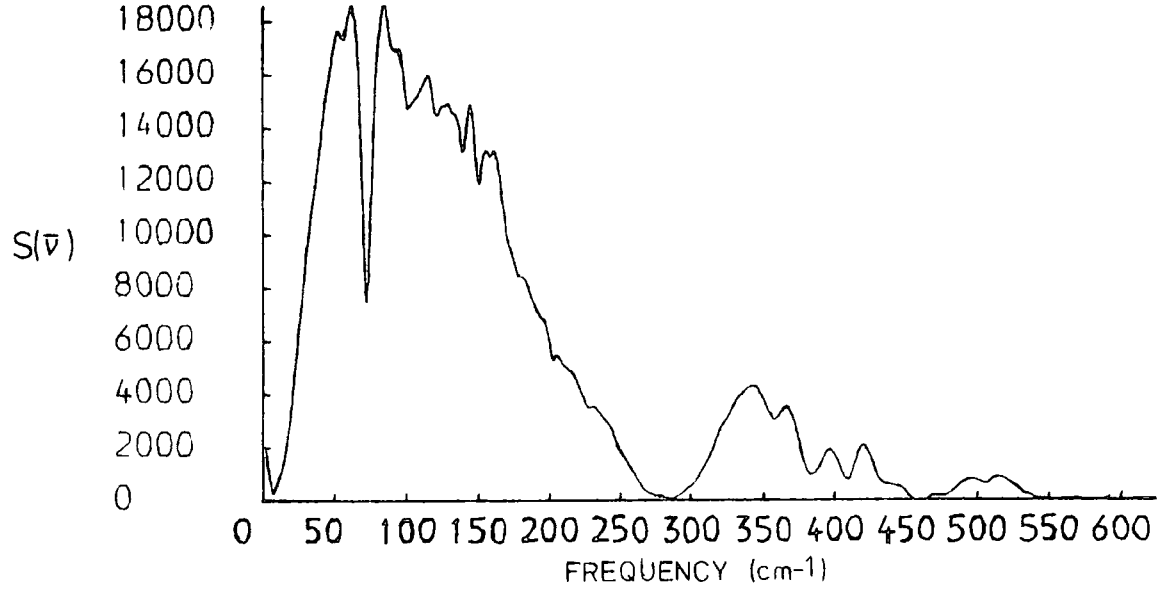

b). Obtained using phase correction method (HIBRD)

increasing sensitivity of the amplifier does not shift the mean level of the interferogram. The spacing of the wires in the wire grids controls the upper frequency limit which, for the Durham instrument, is about $120cm^{-1}$. Fig.IV.5 is the ratio of an instrument background collected in polarising mode to one collected in convential mode. Both were collected using the Golay detector.

The frequency range 3 to $40cm^{-1}$ was covered using the photoelectric detector. For this range a 32 micron sampling interval was used with a $67cm^{-1}$ Cambridge filter.

IV.4 Collection Of Spectra

a) Sample Handling

The instrument was evacuated to a pressure of 0.001 Torr except for the sample compartment which was purged with dry nitrogen gas. The interferometer is a single beam instrument which means that spectra with all the background instrumental features removed have to be obtained by ratioing a sample spectrum against an instrument background spectrum collected immediately after the sample one. This quotient is the transmission spectrum of the sample. It is given by

$$T(\nu)=S(\nu)_{sample}/S(\nu)_{background} \qquad .....IV.12$$

The absorption coefficient is then

$$(\alpha(\nu))=\log_e[1/T(\nu)] \qquad .....IV.13$$

The samples were held in a standard demountable Beckman FH-01 liquid cell mounted in a Beckman VLT-2 variable temperature cell holder which was maintained at 20°C + or - 1°C by a thermostatted water supply from a TECAM TU-14 temperature controller and water circulator.

For the solution spectra the cell windows were made from high density polyethylene with PTFE spacers ranging in thickness between 100 microns

Fig.IV.5. Ratio of instrument efficiencies. Polarising mode/normal mode (25G. beamsplitter)

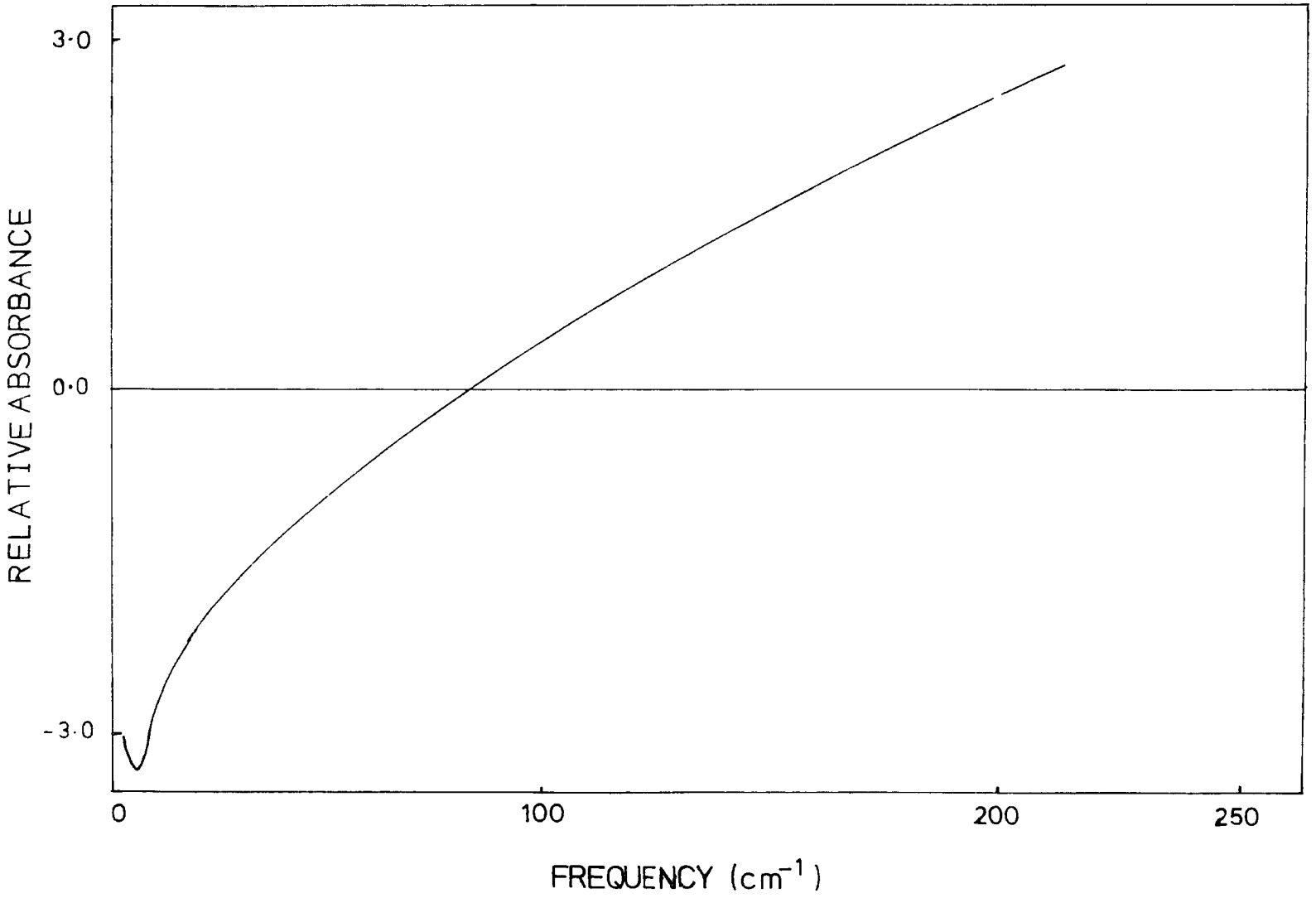

and 3mm depending on solution concentration. All the solution spectra were obtained with the cell containing the pure solvent as the background. The pure solvent spectra of O'Neill[54] were used to calculate the error introduced into the absorption coefficient of the solute by this method of removing the absorbence of the solvent. The error was found not to be greater than 0.4% in any of the solutions.

The spectrum of pure CH_3CN was very difficult to obtain because of its very high absorbence. Very thin spacers had to be used. These were 25,50 and 75 microns in thickness at which errors caused by spacer or window compression become important. For this reason the more rigid window material 'TPX' (poly-4-methyl-pent-1-ene) was used. This material is also transparent to light so that any cell leakage can be easily observed. Leakage did indeed occur with CH_3CN which was overcome by attaching a constant supply of liquid to the cell from a syringe. To check that the spectra were reliable several experiments were made at time intervals of two or three months with new cell windows used each time. The reproducibility was found to be + or - 20%. The sample and background spectra were made using liquid samples of different thicknesses.

The high frequency spectra (20 - 300 cm^{-1}) were collected using the instrument in its conventional mode. An 8 micron sampling interval was used and a mirror drive of 5mm for a double sided interferogram gave a spectral resolution of 2.4cm^{-1}. The high frequency spectra were always collected as a double sided interferogram because in the computation of a double sided interferogram the autocorrelation process smoothes and averages the function to reduce the noise in the interferogram and averages out fluctuations in the intensity from the lamp[53]. The spectra

were computed using FTRAN6.

The low frequency spectra (4-40cm^{-1}) were collected using the cooled detector and the instrument in the polarising mode. A total mirror drive of 1.5 microns for a single sided interferogram gave a spectral resolution of 0.6 cm^{-1}. The length of time the cooled detector can be operated for is determined by the cryostat's hold time for the (expensive) Helium. So in order to get the maximum use of the Helium only single sided interferograms were collected. These were then transformed using the program HIBRD.

b) Assessment of errors

The thickness of the windows was measured before and after an experiment to check on any compression. This was found to be less than 5 microns. To check on possible contraction of the spacers particularly the thinnest ones a spacer was held between wedge shaped silicon windows and scanned through the mid-infrared region on a Perkin-Elmer 580Z spectrometer. The resulting interference fringes caused by reflections due to the large difference in refractive index between air and the silicon (n=3 to 4 in the mid-infrared region) enables the space between the windows to be calculated from

$$b=n\lambda_l\lambda_s/2(\lambda_l-\lambda_s) \qquad \text{.....IV.14}$$

where λ_l is a convenient long wavelength, λ_s is a convenient short wavelength, n is the number of complete cycles of transmission maximum or minimum between λ_l and λ_s and b the cell thickness. Using a cell tightened to the same amount as one used in an experiment no contraction of the spacer was detected.

The transmitted radiation is reduced not only by absorption due to the sample but by reflection at the various interfaces due to differences in refractive indices. See Fig.IV.6.

Fig.IV.6

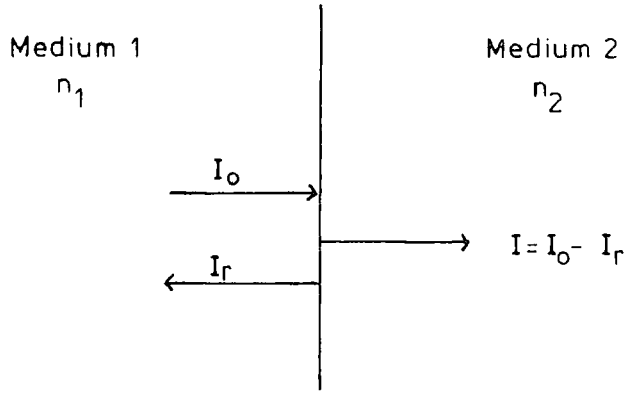

According to one form of Fresnel's[80] equations

$$I_r/I_o=[(n_2-n_1)/(n_2+n_1)]^2 \qquad \text{.....IV.15}$$

where n for the liquids is about 1.5[54,71] between 20 and 200cm^{-1} and that of the windows is about 1.4[81]. This gives the ratio in equation IV.15 of about 1.0x10^{-3} i.e. provided the refractive indices of the two media are similar then reflection losses are very small. However, n rises appreciably obove 1.5 in the low frequency regions (below 25 cm^{-1}) for the pure liquid and high concentration solutions. For n_2 =2.0 the ratio in equation IV.15 becomes 0.02.

Taking all these factors together the estimated maximum errors in the absorption coefficients are + or - 10% for the solutions up to 0.4 mole fraction and + or - 20% for the remaining liquids.

IV.4 Results

Fig.IV.7 shows the very close overlap between the low and high frequency data collected on the two types of detection systems. Table IV.1 gives the far-infrared absorbance data for all the solutions. The table shows that the absorption per mole remains constant within the

Fig.IV.7. Comparison of spectra obtained using a) instrument in polarising mode with photoelectric detector and b) conventional instrument with a Golay detector. CH_3CN/CCl_4 0·1 M.F.

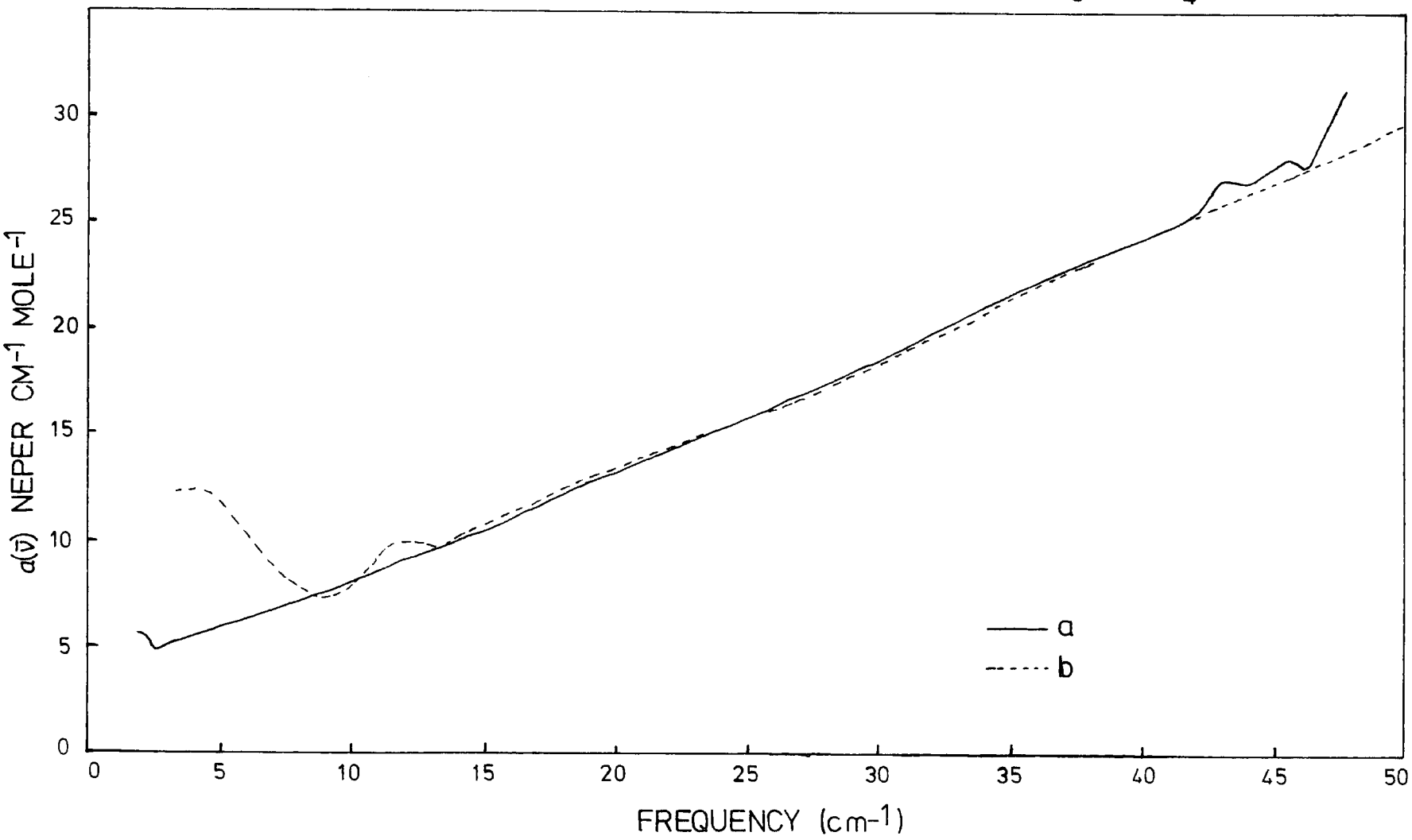

experimental error accros the concentration range in CCl_4 i.e. Beer's law is obeyed by these solutions. The table shows how the slight decrease in peak height is offset by a slight increase in band width accross the concentration range to maintain the fairly constant (within the experimental error) absorption per mole. In addition, the values for the CCl_4 solutions are very similar to those of the benzene solutions but markedly different to the n-heptane solution. Fig.IV.8 shows complete far-infrared spectra of some examples of low concentration solutions in CCl_4, benzene and n-heptane together with a medium concentration in CCl_4 and the pure CH_3CN. It can be seen from this and table IV.1 that the peak positions of the Benzene and CCl_4 solutions are the same wheras that of the n-Heptane solution is $30cm^{-1}$ lower. The peak position of the pure liquid is $20cm^{-1}$ higher than the CCl_4 and Benzene dilute solutions. All the $\nu_{max.}$ data is shown plotted in Fig.IV.9. The value for the band height at $\alpha(\nu)_{max}$ of the pure liquid is 670 nepers per cm. (one neper is an e-fold decrease of the density of energy) This compares with a value of 456 Bulkin[83] 103 by Hindle[84], about 225 by Vaughan[10] but is much closer to that of Knözinger[85] which is 800. I suggest that the discrepencies are due to the problem of accurately determining the cell path length.

Fig.IV.10 shows the interpolation which has to be made between the microwave and far-infrared spectra for a typical solution, 0.1 mole fraction in CCl_4. Clearly in terms of a frequency scale of cm^{-1} the interpolation can be readily performed. Fig.IV.11 shows the interpolation required when there was no microwave data at 34 and 70GHz. This is a much more serious problem and does lead to relatively large uncertainties in the correlation functions obtained from this sort of spectrum (see chapter V.).

Table IV.1 Far-Infrared Data

M.F.	Conc.	$(\bar{\nu})_{max.}$	$\Delta\bar{\nu}1/2^{+}$	A_1^{*}	$(\alpha)_{max}$
	mole.dm-3	cm-1	cm-1		neper cm-1. mole-1
CH_3CN/CCl_4-					
0.01	0.099	71.8 ±3.0	87.72 ±10%	3413.77 ±10%	37.1 ±10%
0.016	0.170	72.4	95.39	3962.48	37.5
0.06	0.652	73.5	93.20	3662.26	36.6
0.10	1.085	74.6	91.01	3413.92	36.5
0.16	1.825	80.0	93.2	3558.5	36.0
0.20	2.294	80.0	93.20	3610.17	36.6
0.30	3.608	82.2	93.20	3723.5	35.7
0.40	5.072	85.5	96.49	3939.6	36.8
0.50	6.718	86.6	99.78 ±20%	3929.6 ±20%	36.4 ±20%
0.70	10.682	88.8	107.46	4363.37	37.3
1.00	19.137	93.3	100.88	3712.7	35.1
CH_3CN/Benzene					
0.016	0.182	72.4 ±3.0	95.4±10%	3727.9±10%	35.7±10%
0.06	0.704	74.6	100.88	3725.8	35.0
0.16	1.955	80.0	97.58	3597.6	35.1
CH_3CN/n-Heptane					
0.027	0.189	44.76 ±3.0	81.88±10%	2691.48±10%	33.0±10%

* A_1 is the integrated absortion per mole in nepers per cm. Measured from 0.0 to 250cm^{-1}.

+ $\Delta\bar{\nu}$ is the band width at half height.

Fig.IV.8. Complete microwave/far-infrared spectra for five of the solutions studied

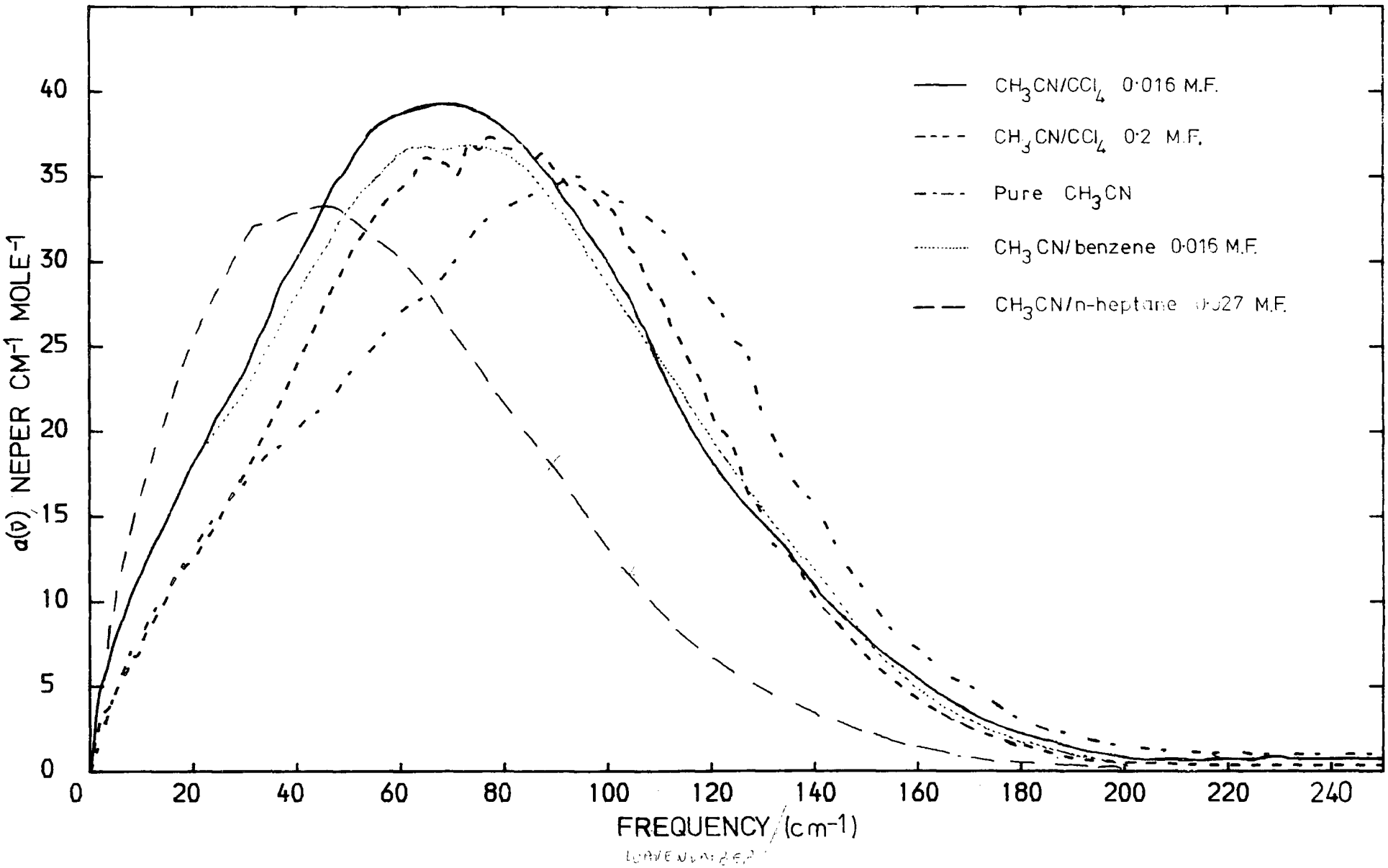

Fig.IV.9. $\bar{\nu}$.max. data for all of the solutions studied

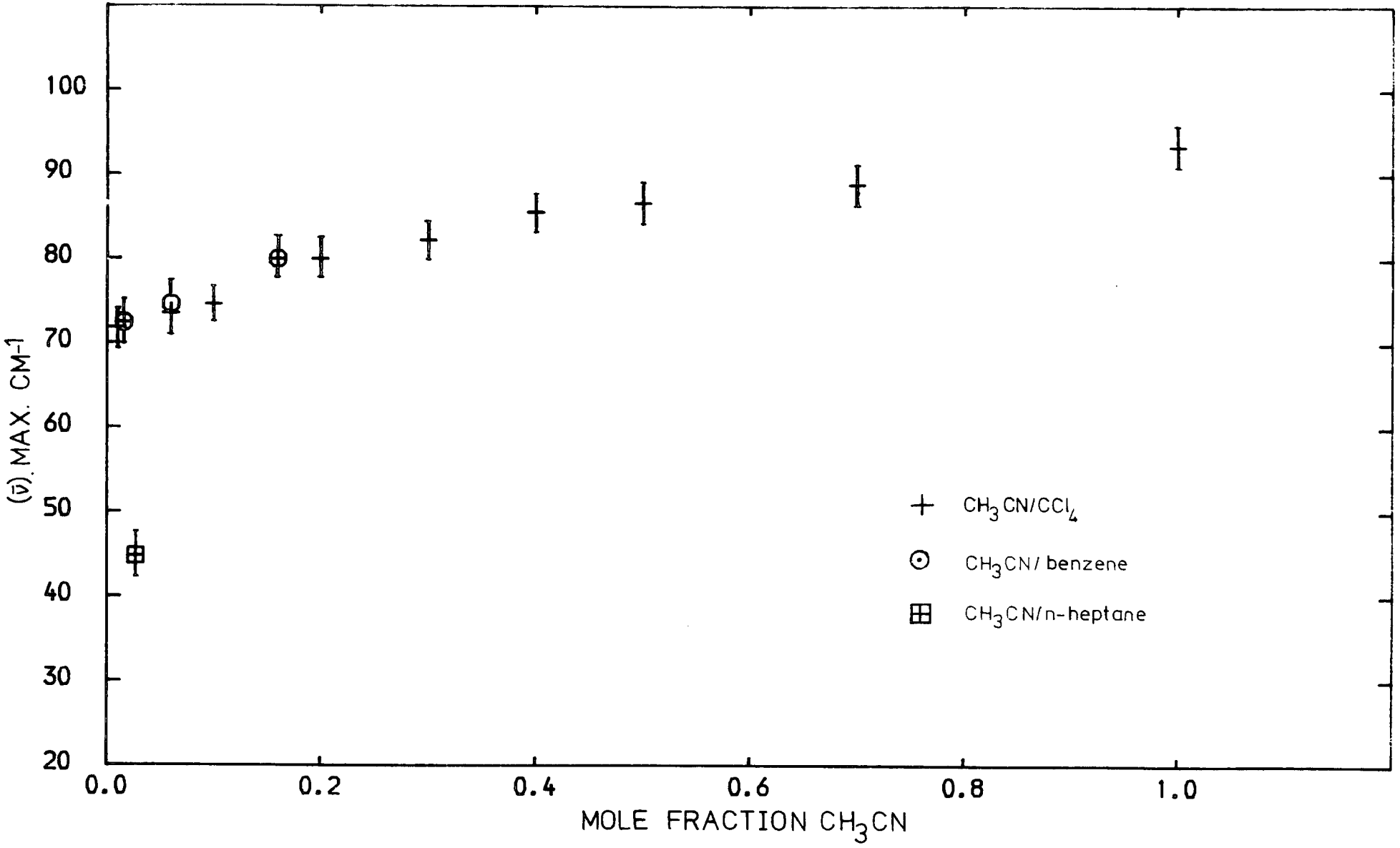

Fig.IV.10. Interpolation required between microwave and far-ir data. CH_3CN/CCl_4 0·1M.F.

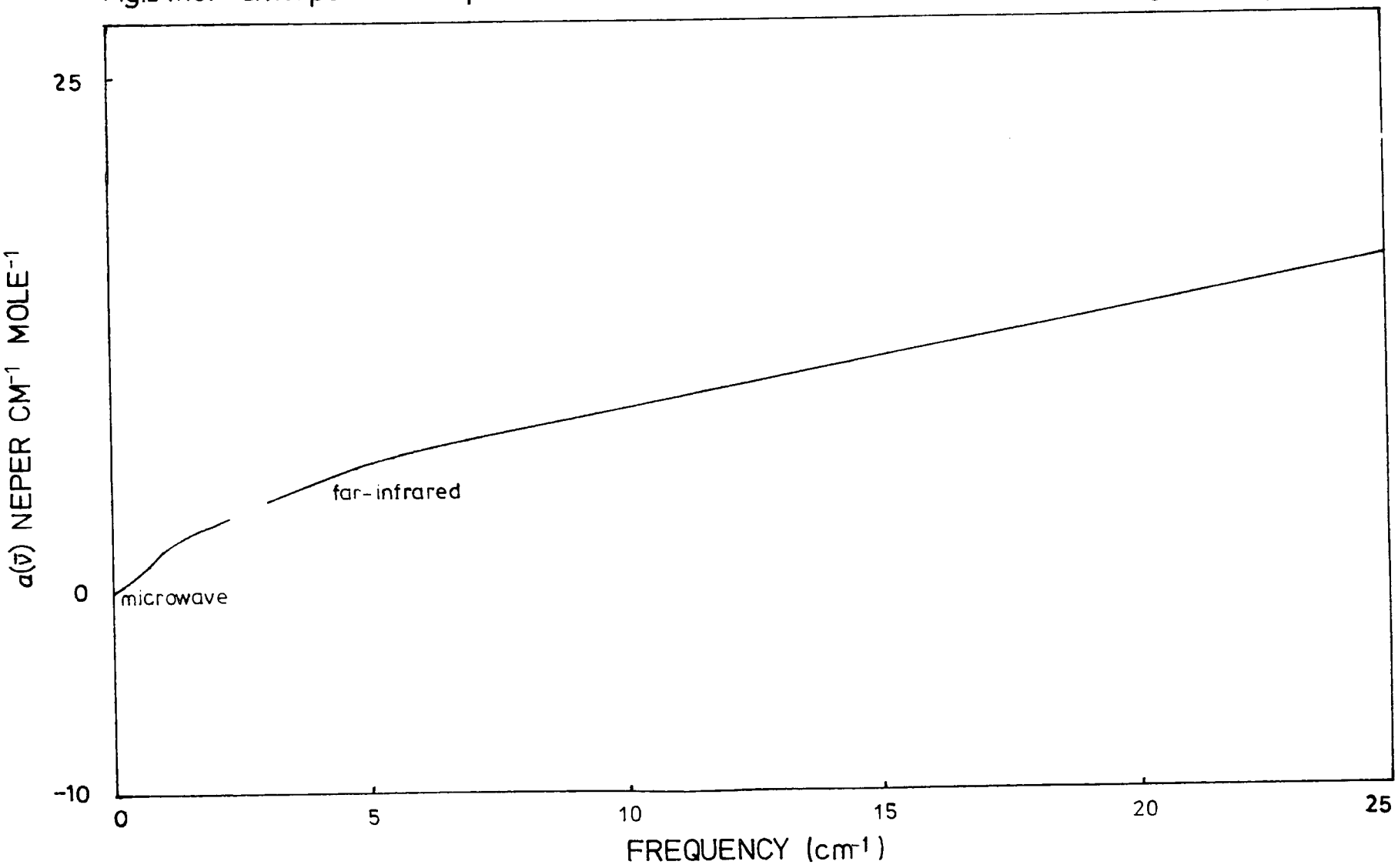

Fig.IV.11. Interpolation required between microwave and far-ir data. CH_3CN/CCl_4 0·3 M.F.

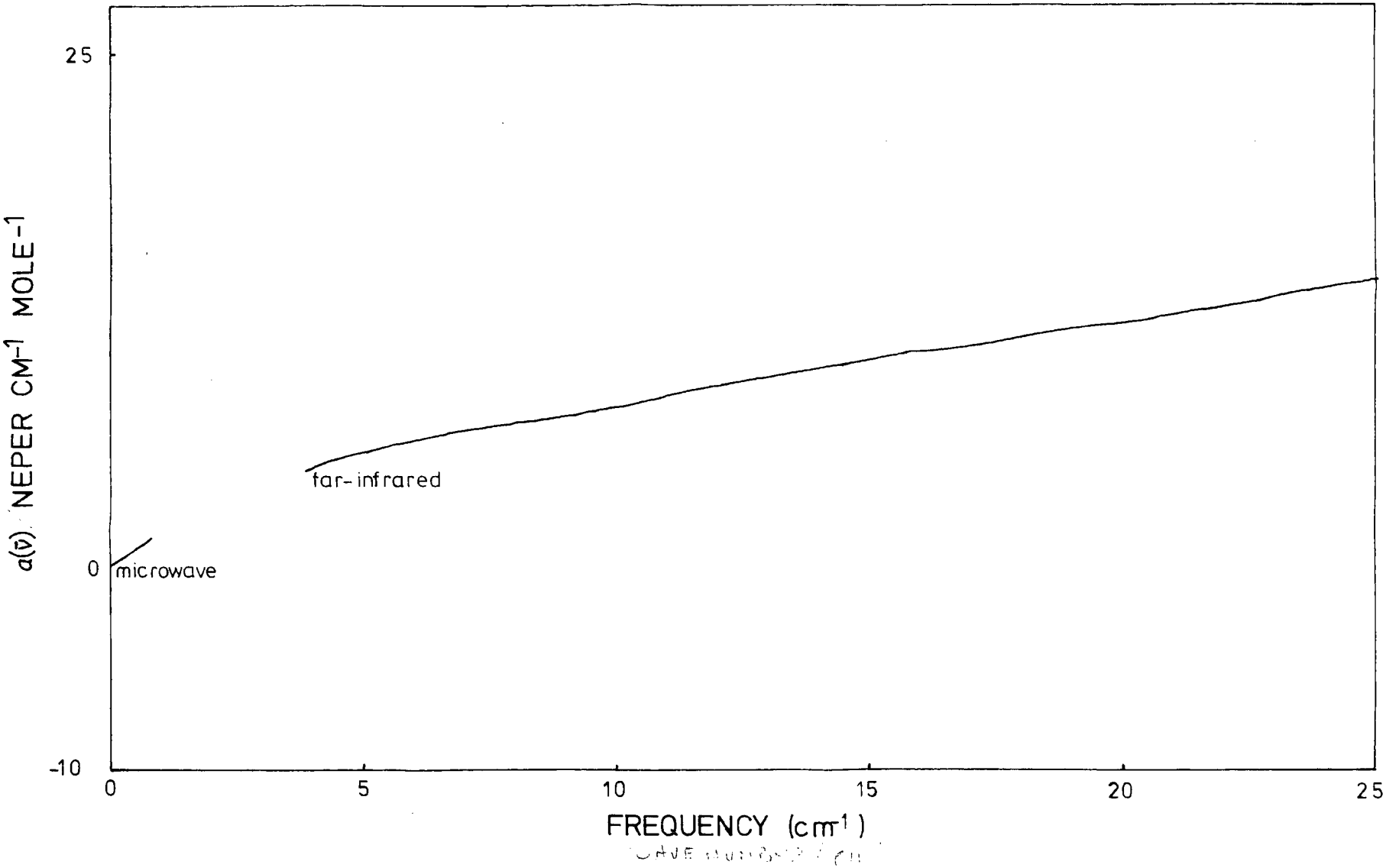

Chapter V.

Analysis of Combined Microwave and Far-Infrared Data.

V.1 Kramers-Krönig Analysis

This section presents the results from the Kramers-Kronig (see chapter I.7) analysis on the microwave/far-infrared spectra. Fig.V.1 shows the $\kappa(\bar{\nu})$ function for the 0.016 mole fraction CH_3CN in CCl_4 solution. This function was Hilbert transformed (chapter I.7) to give the $n(\bar{\nu})$ curve shown in Fig.V.2. This was then used to give (equation I.49) the $\epsilon''(\nu)$ curve shown in Fig.V.3. This figure also shows the calculated Debye curve for this solution. This clearly shows that the deviations from the Debye curve in the observed spectra are in the high frequency bulge and lower $\epsilon''(\nu)_{max}$. It can also be seen that the integrated intensities of both curves are about the same, indicating that both arise from fluctuations of the same dipolar quantity.

Figs.V.4,5 and 6 show $n(\bar{\nu})$ curves obtained for 0.016 mole fraction solutions of CH_3CN in CCl_4 and benzene and 0.027 mole fraction in n-heptane, all of which have approximately the same concentration of CH_3CN molecules per unit volume (about 0.18 moles per litre). Fig.V.4 also has plotted the measured refractive index data of James[70] obtained on a dispersive interferometer at NPL for a 0.018 mole fraction solution at 14°C. The agreement between the two curves is within 1% at any point. Even this small difference can probably be accounted for by the fact that the measured curve is for a solution whereas the calculated curve was computed from a solute spectrum. Fig.V.7 is the calculated $n(\bar{\nu})$ curve for the pure liquid. All the $n(\bar{\nu})$ curves clearly show a shallow minimum displaced by several cm^{-1} to the high frequency side of $(\bar{\nu})$ max, which, as already stated, must be due to resonance energy transfer to oscillating dipoles in the liquid. Chantry[86] first attributed the far-infrared absorption to lattice type vibrations of the dipoles in a pseudo cage within the liquid. Chantry[86] found for measurements on

Fig.V.1. $k(\bar{\nu})$ curve for CH_3CN/CCl_4 0·016 M.F.

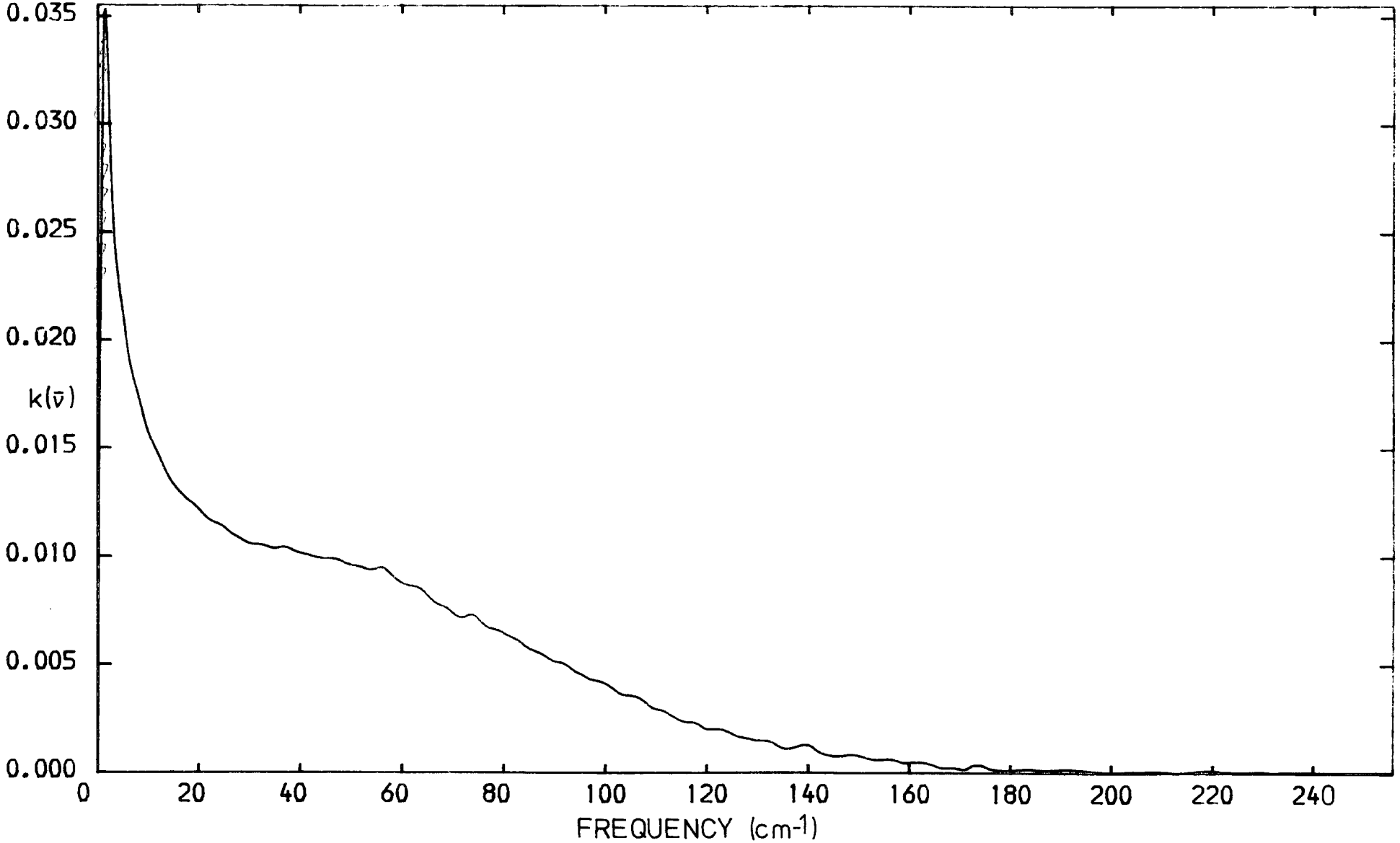

Fig.V.2. Calculated $n(\bar{\nu})$ curve for CH_3CN/CCl_4 0·016 M.F.

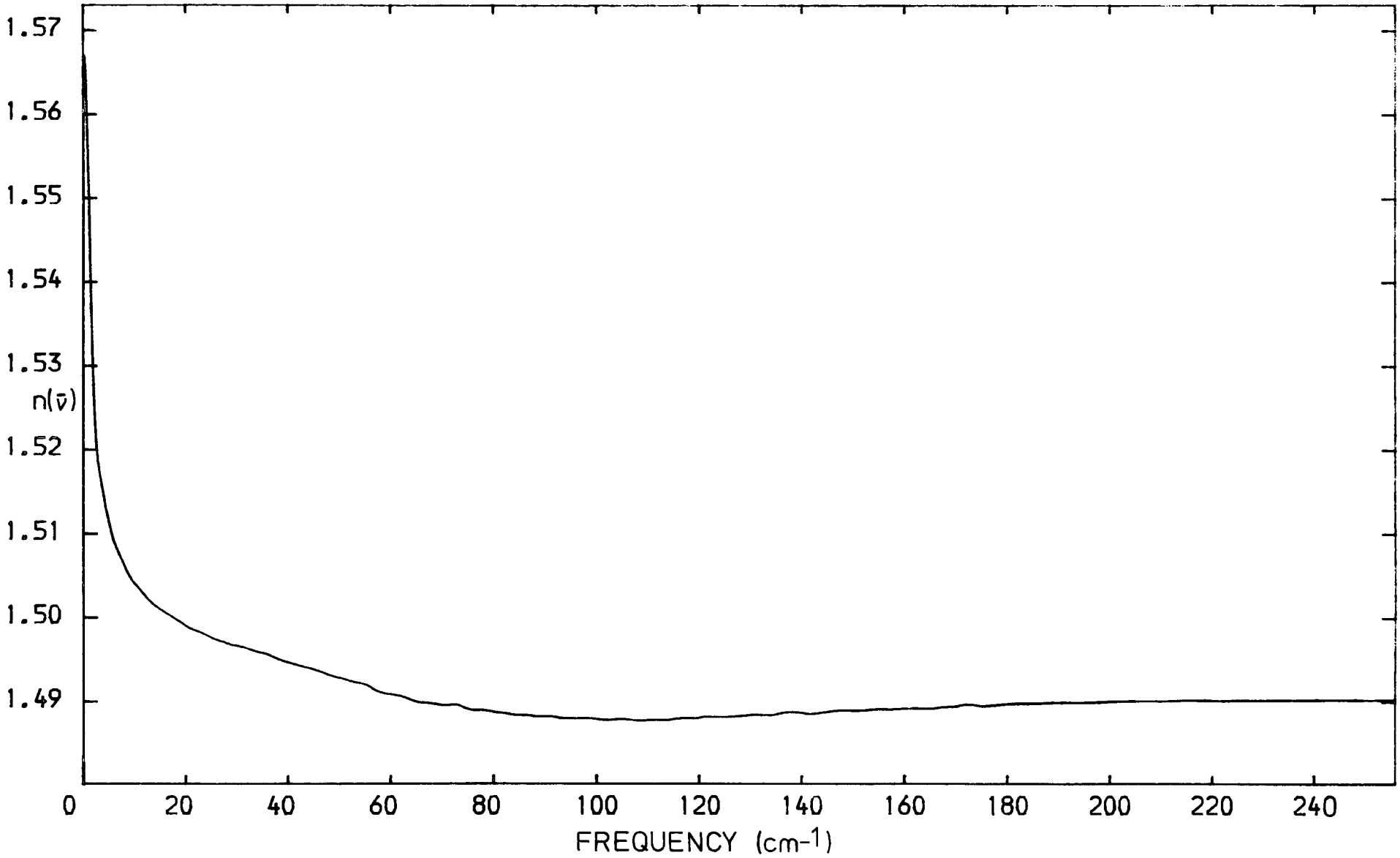

Fig. V.3. $\varepsilon''(\nu)$ curves obtained from a) this work and b) the Debye model. CH_3CN/CCl_4 0·016 M.F.

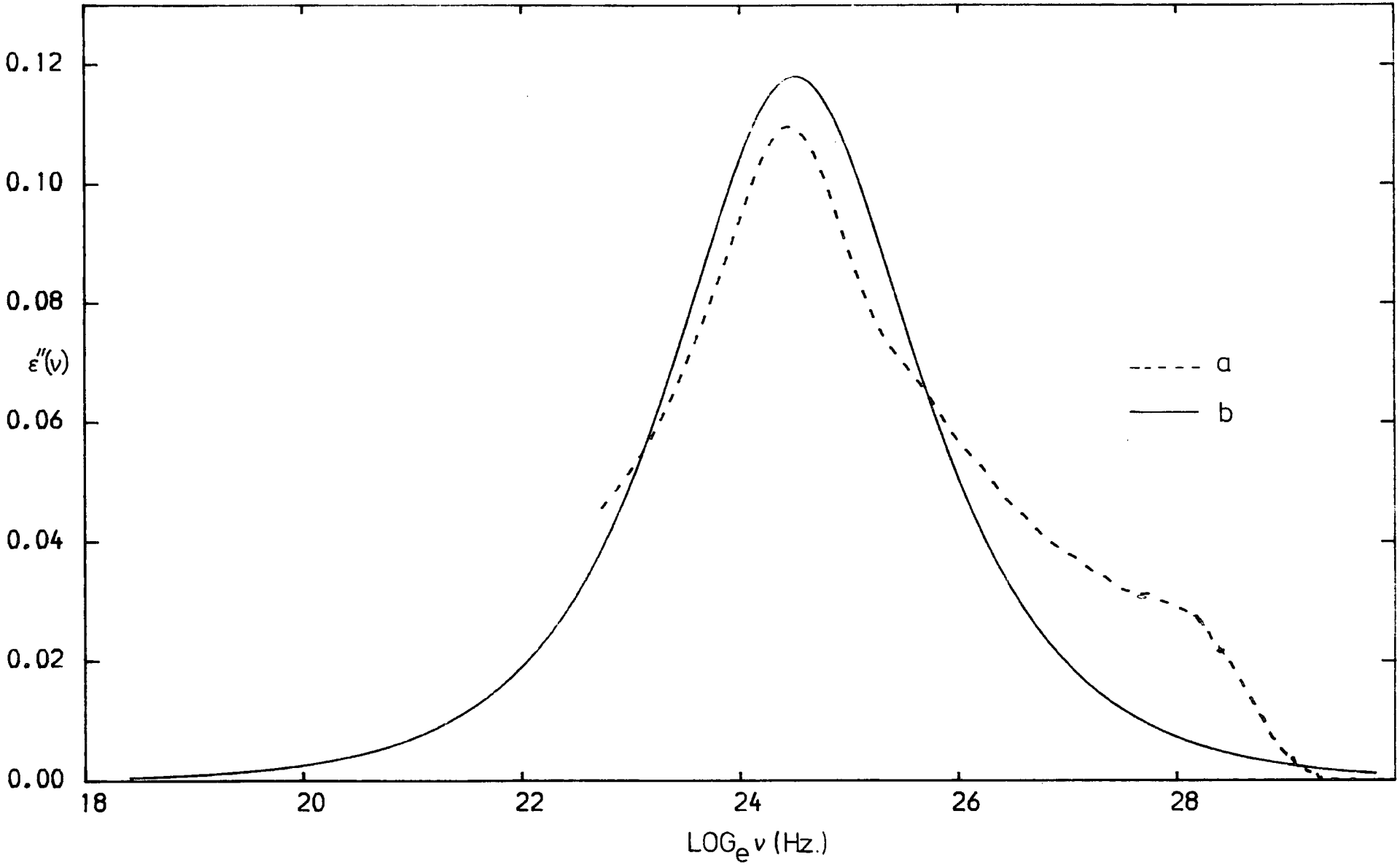

Fig.V.4. Calculated and observed $n(\bar{\nu})$ curves for CH_3CN/CCl_4 0·016 M.F.

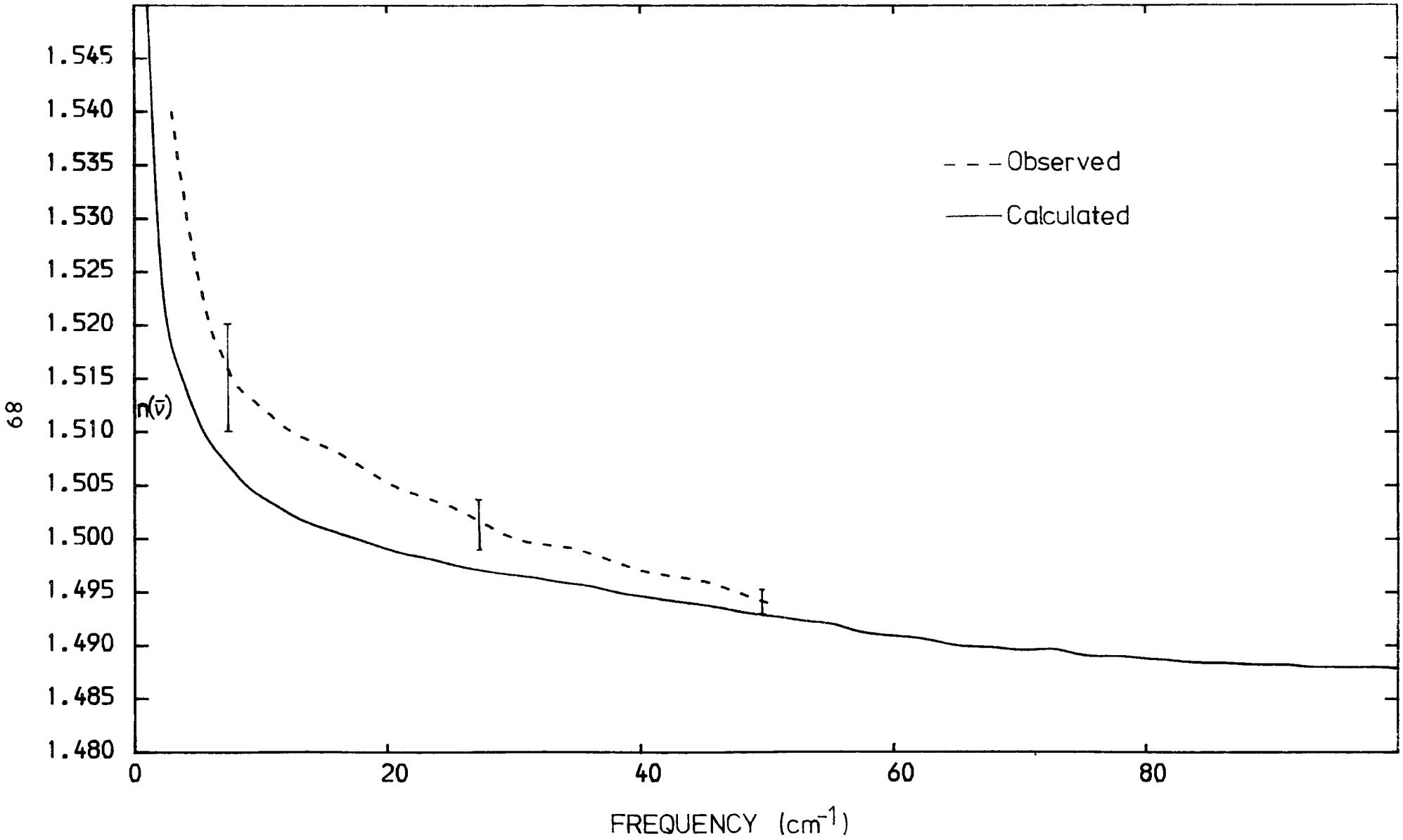

Fig.V.5. Calculated $n(\bar{\nu})$ curve for CH_3CN/benzene 0·016 M.F.

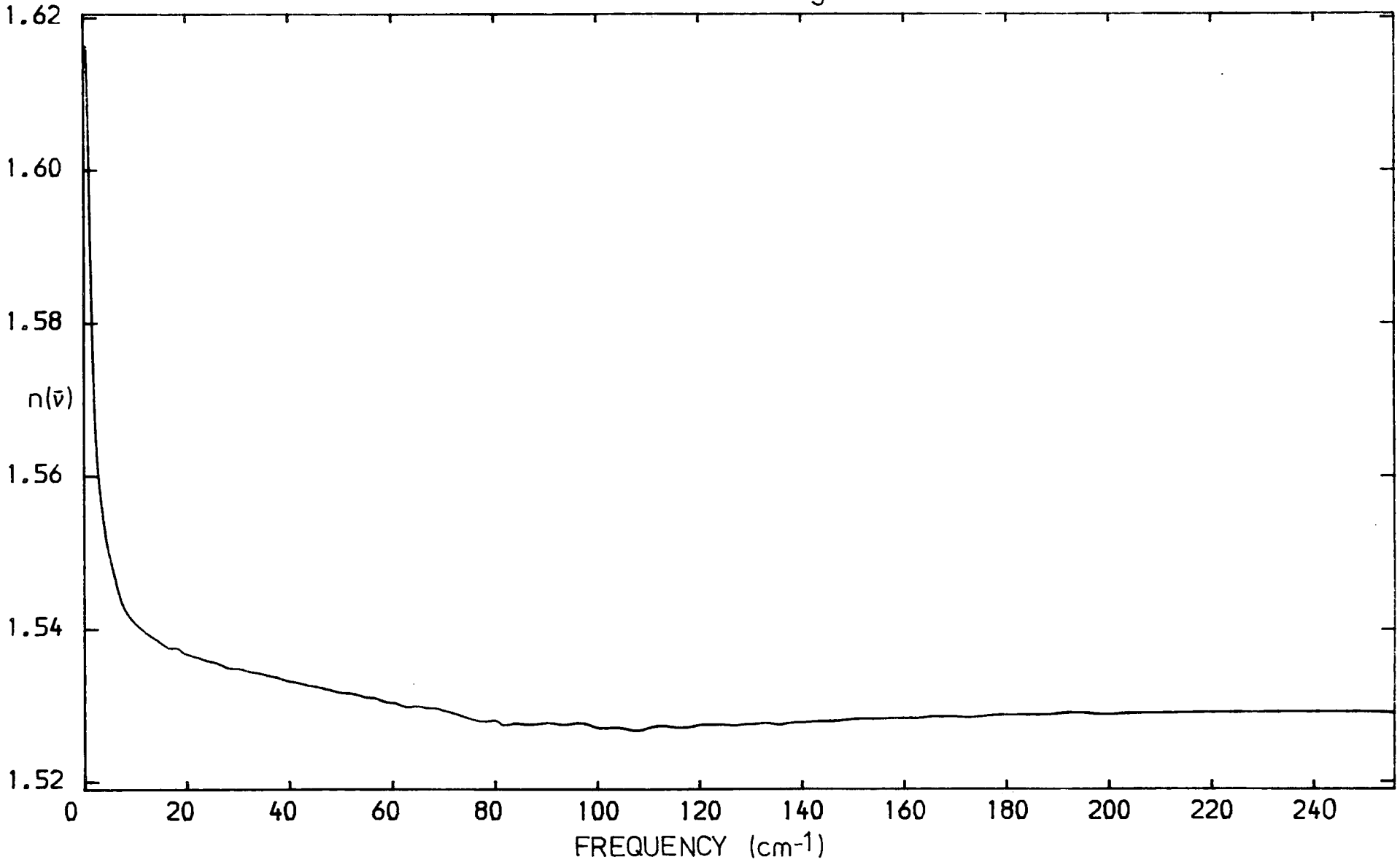

Fig.V.6. Calculated $n(\bar{\nu})$ curve for CH_3CN/n-heptane 0·027 M.F.

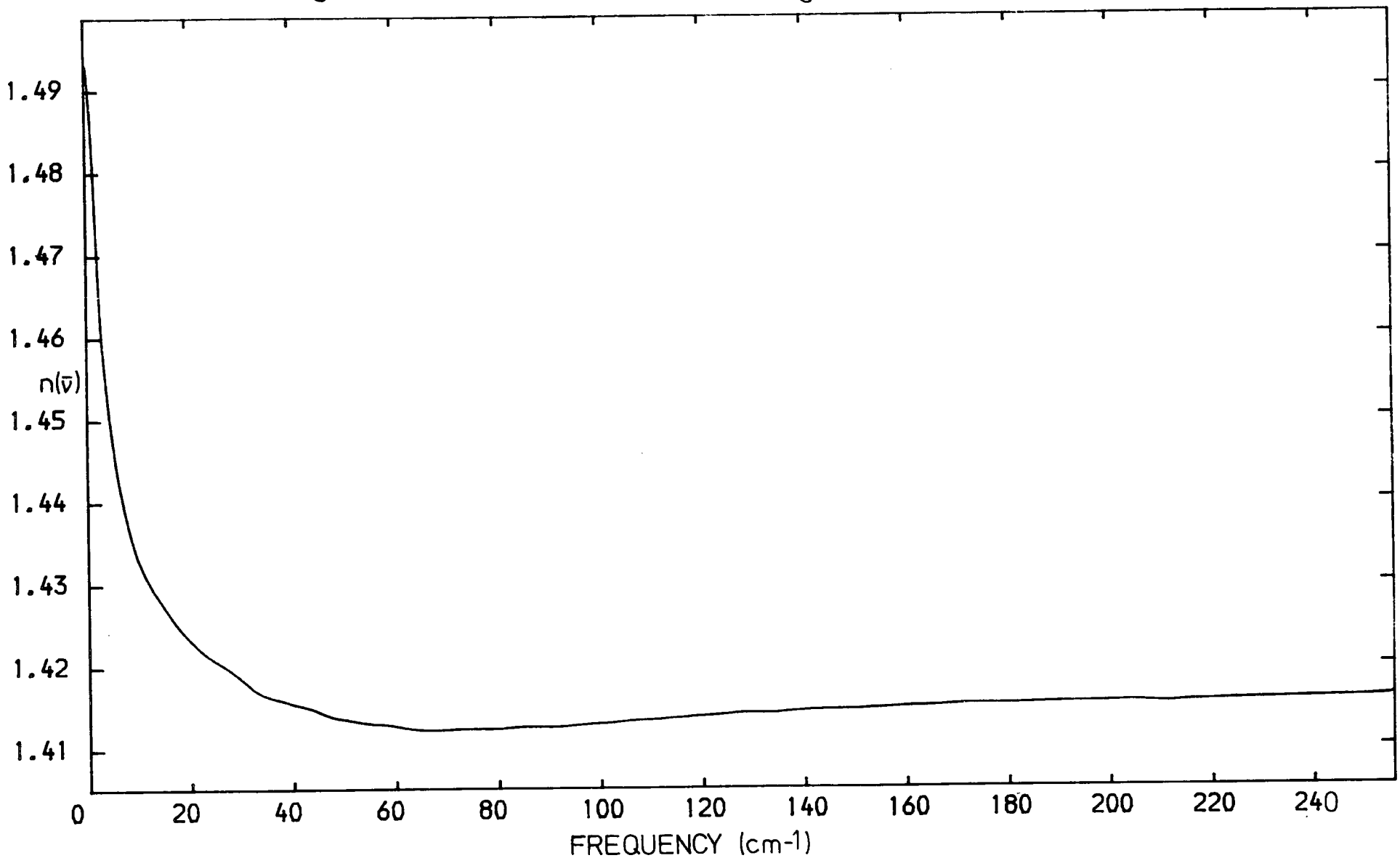

Fig.V.6. Calculated $n(\bar{\nu})$ curve for CH_3CN/n-heptane 0·027 M.F.

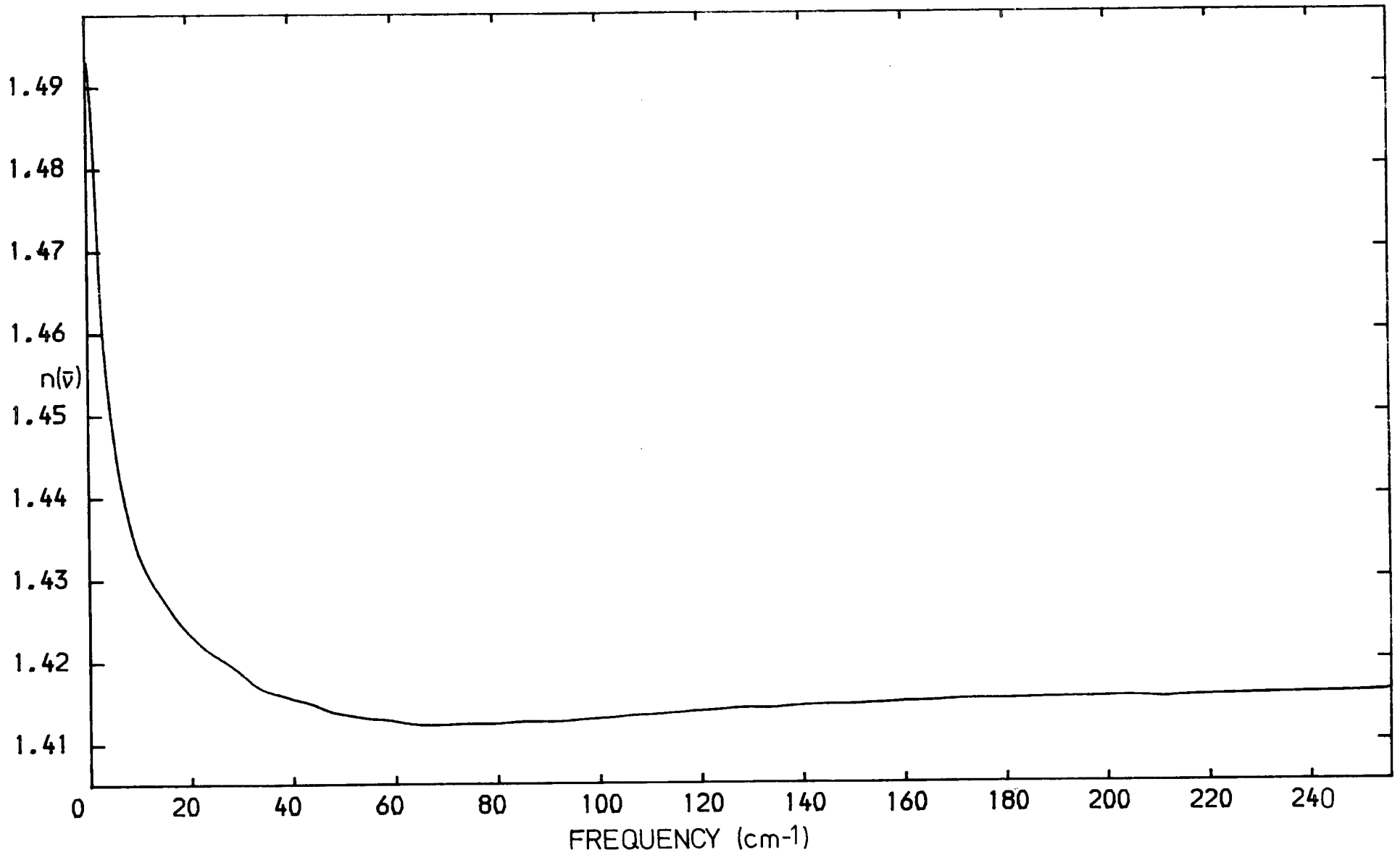

Fig.V.7. Calculated $n(\bar{\nu})$ curve for pure CH_3CN

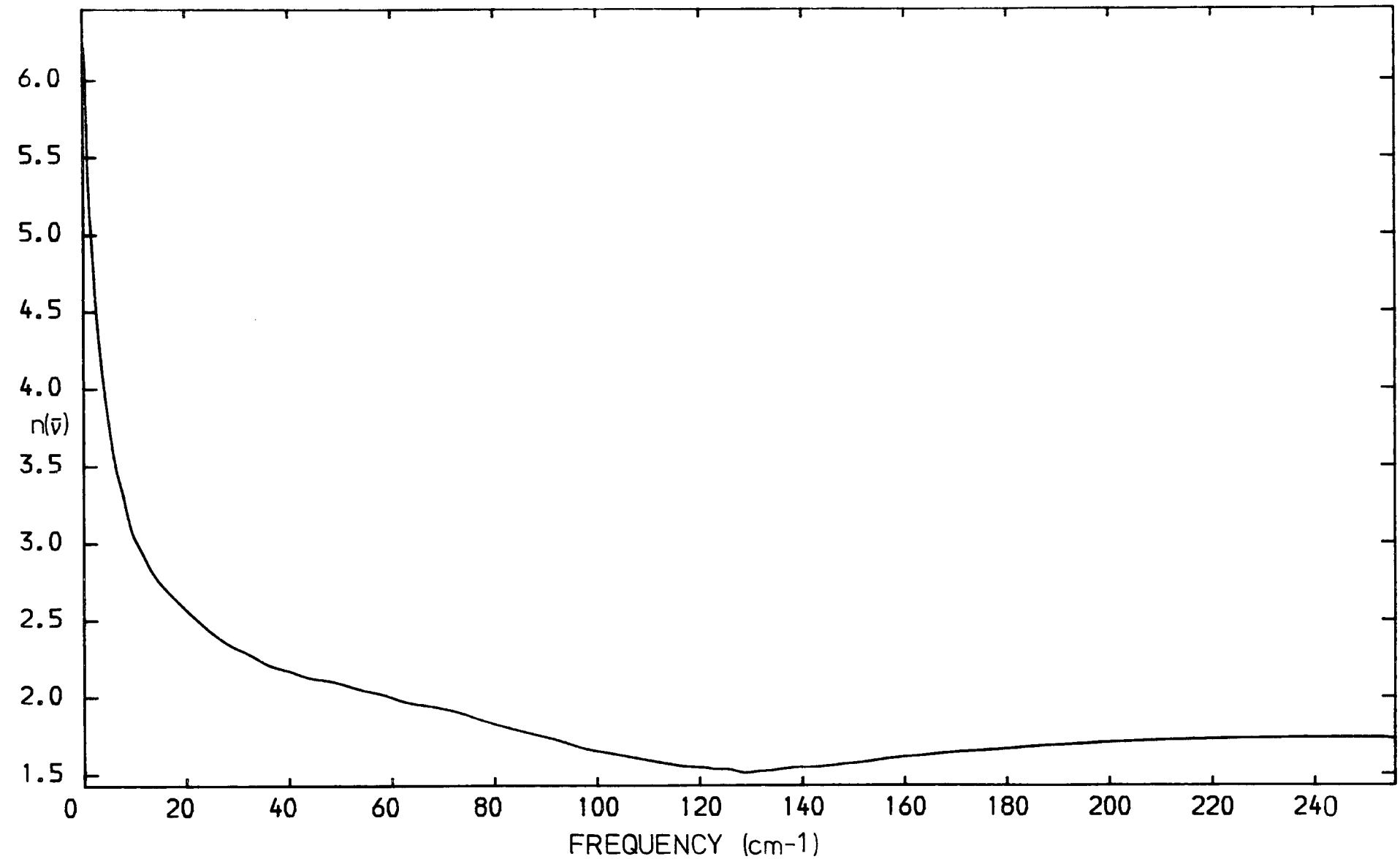

chlorobenzene that the integrated intensity of the liquid phase far-infrared band was very similar to that of the solid phase lattice vibrations occuring in the far-infrared. The very large width of the minimum in the $n(\nu)$ and indeed of the far-infrared band itself is understood in terms of the 'cage' of near neighbours which form a potential energy well in the pseudo lattice[66]. The local order will be asymmetric and will only extend for a very short distance away from the probe molecule. This is as opposed to the solid phase where the order is symmetric and the order extends throughout the whole crystal. The order has only a short lifetime because of the motions of the molecules. All these factors lead to a very broad spread of resonance frequencies[66]. One of the problems still to be decided in the work on the far-infrared 'resonance' absorption is whether the resonance is regarded as a separate molecular motion to the relaxation of the molecule as in the liquid lattice vibration approach[86] or simply the short time part of the same relaxational motion (see chapter II.7). More theoretical work is required to resolve this problem.

The Kramers-Krönig relation between $\epsilon'(\omega)$ and $\epsilon''(\omega)$:

$$\epsilon'(\omega)-\epsilon_{\infty}=2/\pi\int_{o}^{\infty}\epsilon''(\omega)\,d\omega'/\omega'-\omega \qquad .....V.1$$

at $\omega=0$

$$\epsilon_{o}-\epsilon_{\infty}=2/\pi\int_{o}^{\infty}\epsilon''(\omega)\,d\omega'/\omega' \qquad .....V.2$$

was also used to provide an internal check on the data. Table V.1 shows $(\epsilon_{o}-\epsilon_{\infty})$ where ϵ_{∞}(a) is from equation I.50. ϵ_{∞}(b)=2.25 (see Chapter I) and ϵ_{∞}(c) is from equation V.2. The results for ϵ_{∞}(c) are 10% greater than those from the other two methods. This may be due to the large

Table V.1 Kramers-Krönig Analysis

M.F.	ϵ_∞(a)	$(\epsilon_o-\epsilon_\infty)$(a)	$(\epsilon_o-2.25)$(b)	$(\epsilon_o-\epsilon_\infty)$(c)
CH_3CN/CCl_4-				
0.01	2.26	0.128	0.138	0.145
0.016	2.22	0.23	0.200	0.258
0.06	2.28	0.77	0.800	0.873
0.10	2.10	1.552	1.402	1.774
0.16	2.52	2.150	2.420	2.503
0.20	2.47	2.718	2.938	3.156
0.30	2.32	5.062	5.132	5.896
0.40	2.46	7.116	7.326	8.265
0.50	3.25	9.162	10.162	10.445
0.70	2.28	17.356	17.386	19.949
1.00	2.49	34.010	34.250	38.170
CH_3CN/benzene				
0.016	2.34	0.260	--	0.292
0.060	2.32	0.900	--	1.002
0.160	2.56	2.650	--	3.009
CH_3CN/n-heptane				
0.027	2.00	0.224	--	0.241

(a), (b), (c) see text.

limits of the integration. If the limit is reduced to 200cm^{-1} the agreement is much better.

V.2 Gordon's Sum Rule

As already stated in chapter I.6 the second moment of the spectral intensity and to a close approximation the integrated $\alpha(\bar{\nu})$ intensity are independent of molecular interactions and therefore single molecule properties. A formula linking the integrated intensity of the far-infrared absorption with the permanent dipole moment and molecular moment of inertia has been proposed by Gordon[59] and Brot[17], where for a symmetric top molecule

$$A_i = 2\pi\mu_{calc}^2(1/I_b)/3c^2 \qquad \text{.....V.3}$$

where A_i is the integrated absorption intensity per molecule, evaluated in this work from 0 to 250cm^{-1}, c is the velocity of light and all other symbols are as defined previously. The absorption intensity is corrected using the Polo-Wilson[49] internal field correction factor. If μ_{calc} is greater than μ_{gas} (=3.92 Debyes[87]) the difference might then be attributed to the formation of interaction induced dipoles which have not had time to average out. Measurements of μ at microwave frequencies probably do not contain contributions from collision induced dipoles because at low frequencies (long time) the molecules have had time to return to their equilibrium configurations. In the Onsager[20] model the dipole moment of the molecule is enhanced by the reaction field of the polarised (by the central molecule) surrounding sphere of molecules on the central molecule[7]. The enhanced dipole moment is given by

$$\mu^{*} = (2\epsilon_o + 1)(\epsilon_\infty + 2)\mu_{gas}/3(2\epsilon_o + \epsilon_\infty) \qquad \text{.....V.4}$$

where ϵ_∞ is that of the pure solute. The values of μ calc. and μ^{*} are shown in Table V.2. The results agree very well with those of Sato et

Table V.2 Gordon's Sum Rule

μ_{gas}=3.92 Debyes[87], all μ values given below are in Debyes.

M.F.	μ^{*}	μ_{calc}	μ_{calc} P-W corr.
CH_3CN/CCl_4-			
0.01	4.57	4.71	4.07
0.016	4.56	5.07	4.39
0.06	4.72	4.88	4.22
0.10	4.83	4.71	4.07
0.16	4.95	4.81	4.16
0.20	5.00	4.84	4.19
0.30	5.14	4.92	4.26
0.40	5.23	5.06	4.37
0.50	5.30	5.05	4.37
0.70	5.38	5.32	4.60
1.00	5.46	4.91	4.25
CH_3CN/benzene			
0.016	4.62	4.92	4.25
0.06	4.75	4.92	4.25
0.16	5.01	4.84	4.18
CH_3CN/n-heptane			
0.027	4.52	4.18	3.73

For solutions from 0.03 to 0.16 moles per litre Sato et al[88] obtain the following results using the Polo-Wilson correction factor:

CH_3CN/CCl_4 $\mu_{calc.}$=4.4 D

CH_3CN/benzene $\mu_{calc.}$=4.6 D

CH_3CN/n-hexane $\mu_{calc.}$=4.3 D

al[88] (also shown in Table V.2). It is seen that μ calc. agrees best with μ^* when the Polo-Wilson (PW) factor is not used to correct A_I. This may again point to the inadequacy of this correction factor. The reaction field corrections may also be incorrect since the cavity is unlikely to be spherical nor will the CH_3CN molecules have the same polarisabilities along all three mutually perpendicular axes of the molecule. These problems also affect the Polo-Wilson factor since it is based on the Onsager model (See chapter I.4).

There is an additional problem in the use of the sum rule as pointed out by Ried[89]. This concerns the fact that at short times random orientations caused by the librational motion of the molecules will not be averaged out. These errors depend on the size of the angle through which libration occurs. Ried[89] calculates that for a swept angle during libration of 6° the error in μ would be 4%.

As far as one can suggest from this analysis, the presence of collision induced dipolar absorption in the far-infrared band of these solutions and pure liquid is small compared with the absorption due to the permanent moment. This means that the solute-solute and solute-solvent interactions in these solutions are not large enough to distort the solute molecules enough to produce any observable effects in the intensity of the solute spectra. This may be due in part to the very large permanent moment that CH_3CN possesses 'swamping' the effects of induced dipoles. However, sum rule studies on less polar molecules such as CH_3I and $CHCl_3$ by Sato[88] does not indicate the presence of any notable amount of collision induced dipolar far-infrared absorption.

V.3 Band Moment Analysis

Figs.V.8,9,10 and 11 show plots of equation I.39 for the n=2 (second moment) and n=4 (fourth moment) functions for 0.01 mole fraction CH_3CN in CCl_4 and the pure liquid. These show how the band moments are weighted by the high frequency part of the spectrum and how they are modified by the KKV[34],NZ[35] and Hill[33] correction factors. It can be seen that these factors reduce the intensity by more than 50%. This cannot be taken as very reliable since these factors are based on models which predict a Debye type plateau for the far-infrared absorption intensity[90]

Calculated second and fourth moments are listed in Table V.3. These have been corrected for internal fields using both the Polo-Wilson[49] and KKV[34] correction factors (which gave the same results as the Hill factor). The classical value of M_2 - the rotational second moment - independent of interactions is given by $2kT/I_b=8.95x10^{24}$ sec.$^{-2}$ at 293K. It is purely a measure of the rotational kinetic energy of the CH_3CN molecule. The moments of inertia might, however, differ between molecules in dense media and in the gas phase[91]

The best agreement with this value comes from the use of the KKV factor, where the values show an average positive deviation from 2kT/I of 12% although the value from the n-heptane solution is smaller than the classical value. When the P-W factor is used the M_2 is about 50% greater and shows a slight general increasing trend as the concentration of CH_3CN increases. This trend is not present in the integrated $\alpha(\omega)$ data so must be due to the P-W correction factor itself. All of the second moments are higher than the theoretical value by an amount that is greater than the experimental error. As discussed in section V.2 this probably cannot be attributed to the presence of induced dipolar absorption but rather to the inadequacies of the correction factors and

Fig.V.8. Second moment (M_2) curves for CH_3CN/CCl_4 0.01 M.F.

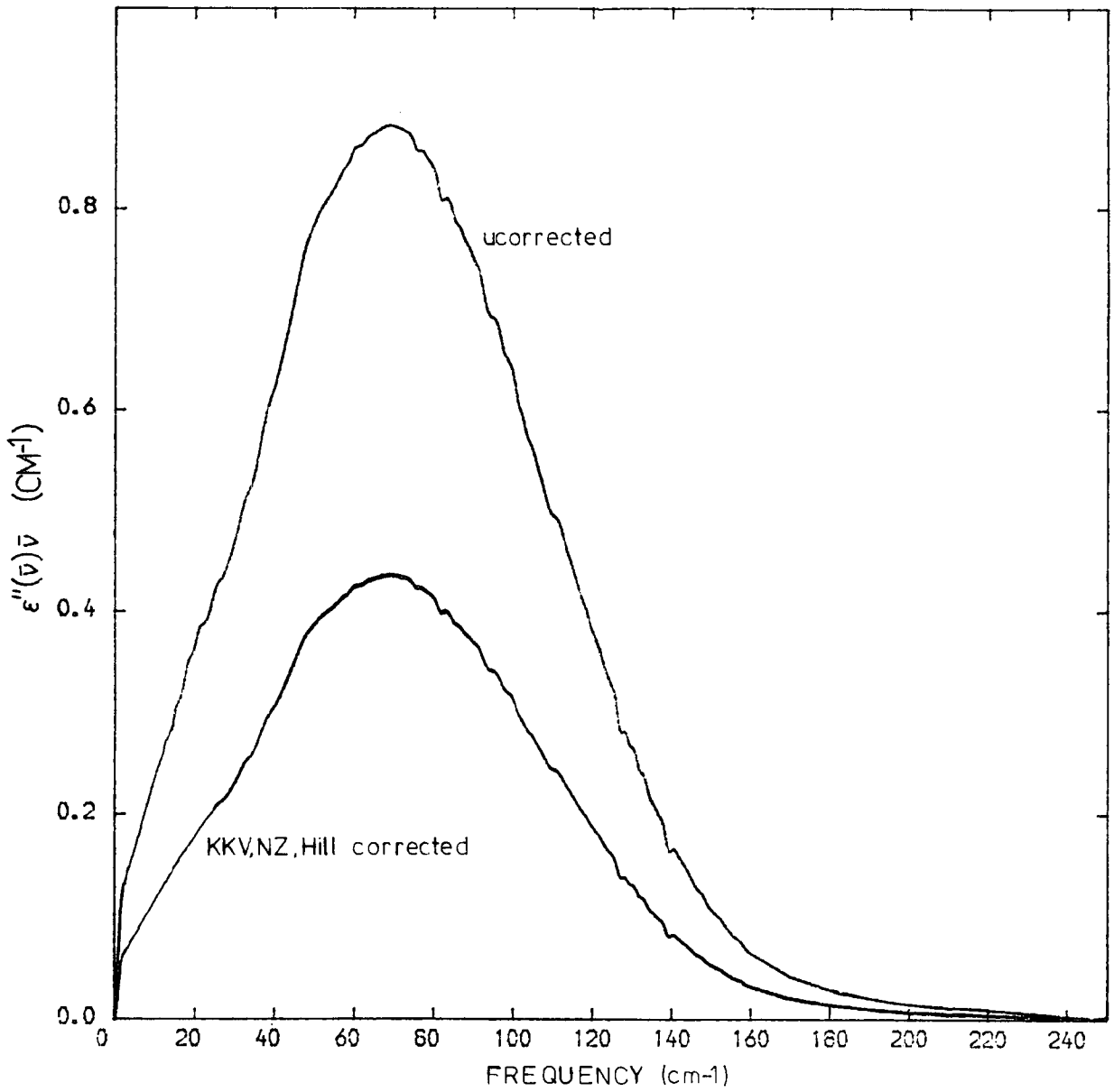

Fig.V.9. Fourth moment (M_4) curves for CH_3CN/CCl_4 0.01 M.F.

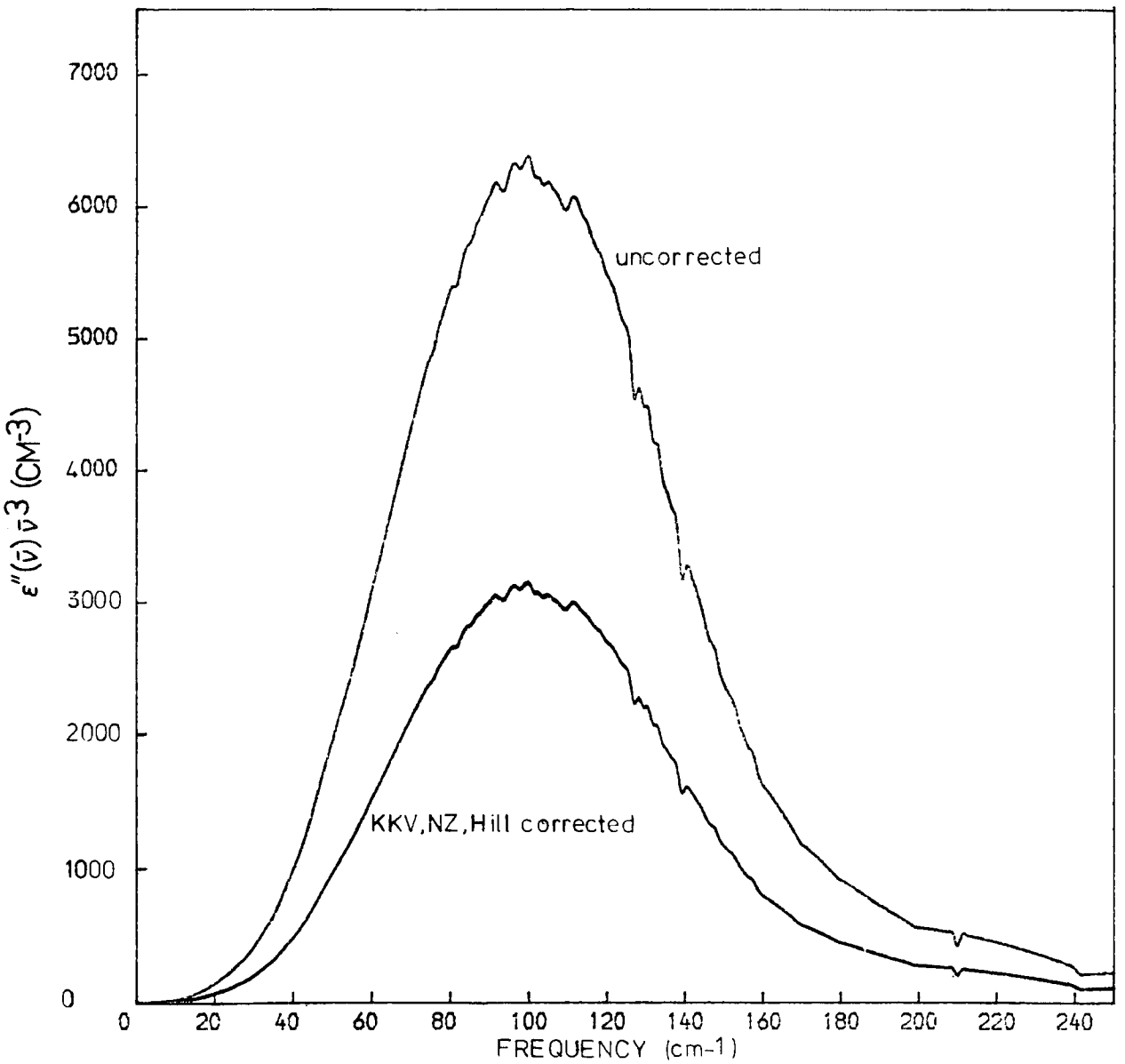

Fig.V.10. Second moment (M_4) curves for pure CH_3CN

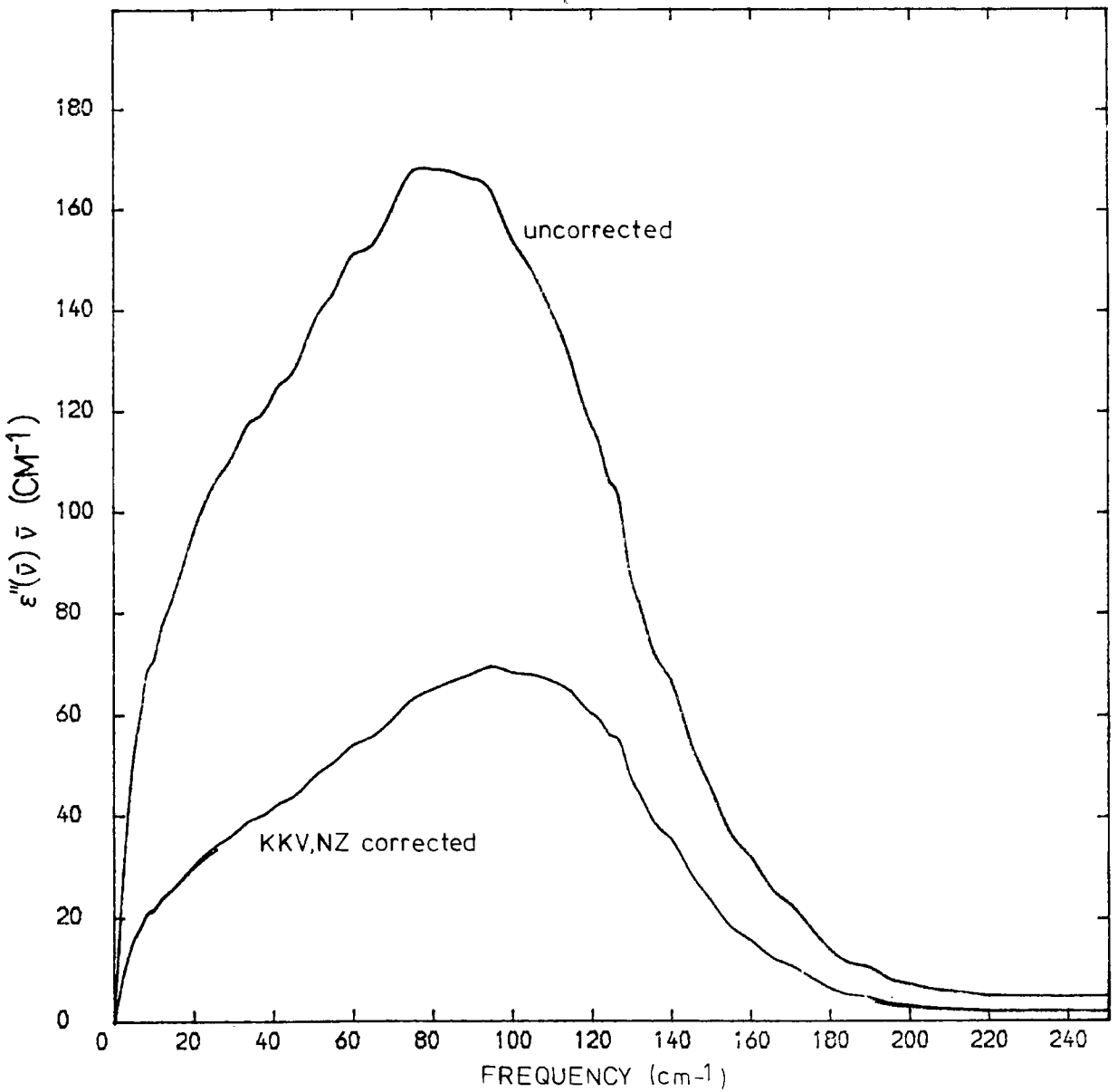

Fig.V.11. Fourth moment (M_4) curves for pure CH_3CN

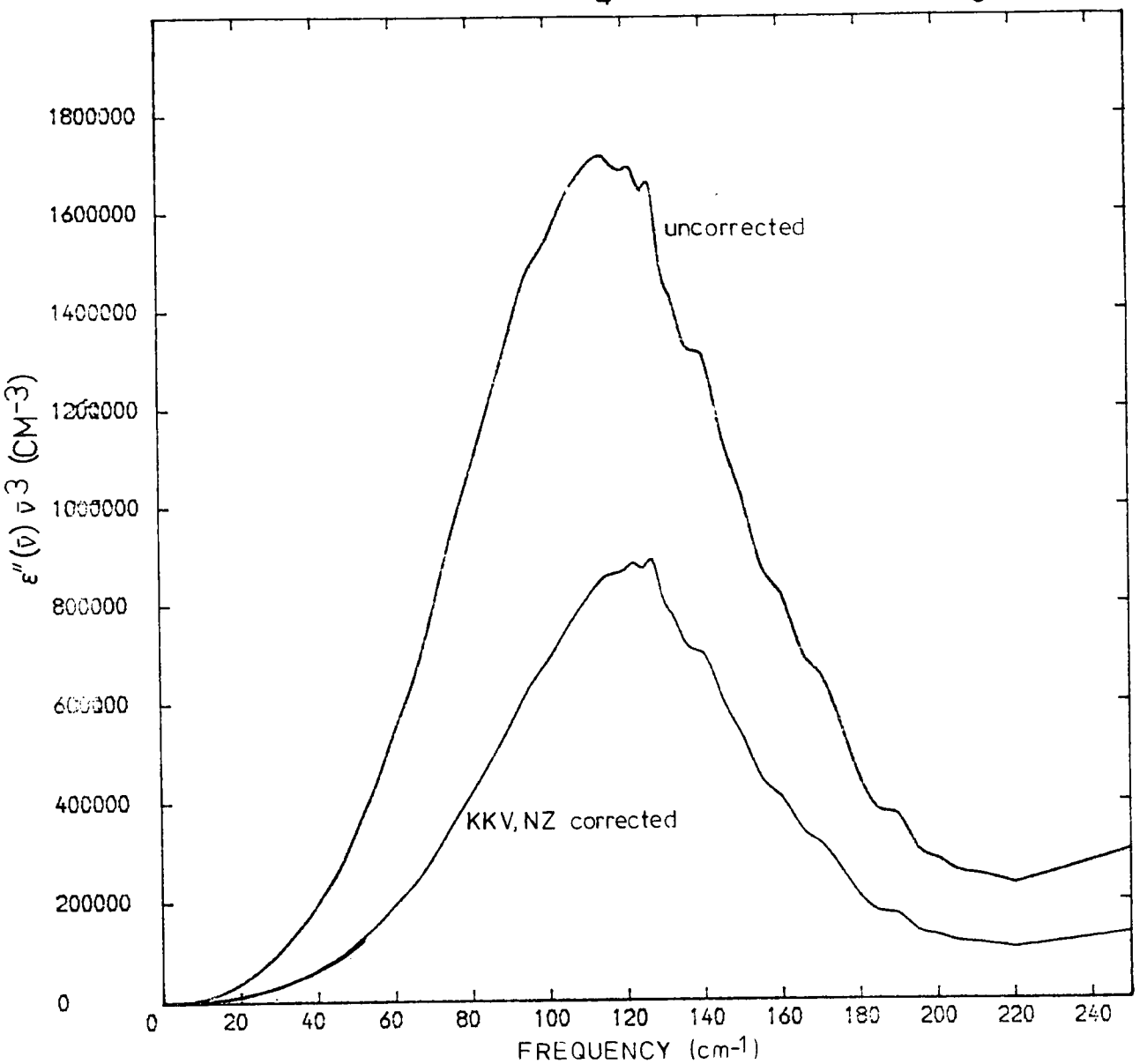

the inherent problems in making intensity measurements in the far-infrared as mentioned in V.2.

The fourth moments are presented in table V.3. Again there is very good agreement with the results of Sato et al[92]. It is expected that the fourth moments will be more affected by the presence of induced dipolar absorption as this is thought to be more important at short times[48] which is where the fourth moment functions have most of their spectral weighting. The fourth moments again do not show any trend when the KKV factor is used but do show a pronounced increase when the P-W factor is applied. This latter behaviour agrees with the predictions of the Mori model (Chapter II. Eq. 18) in which $(\bar{\nu})_{max.}$ is proportional to the fourth moment which is in turn proportional to the intermolecular torques (see equation I.40) and as Fig.IV.9 shows the $(\nu)_{max.}$ does increase on increasing concentration. The fourth moments of the benzene solutions are similar to those in the CCl_4 solutions while that in the n-heptane solution is very much smaller. It can be seen that the intermolecular torques are greater in the pure CH_3CN solution than in dilute CCl_4 and benzene which are about the same while they are about a third as large in the alkane solvent. Thus the intermolecular (of which the intermolecular torques are a measure) interactions between solute and solvent molecules are probably smaller in n-heptane than in CCl_4 and benzene. This is probably due to greater induced and dispersion forces in the latter two solvents than in n-heptane due to their larger polarisabilities as indicated by their larger ϵ_∞ values (see table V.1). The greater interactions in CCl_4 and benzene is illustrated by the complete miscibility of CH_3CN with them whereas it is only sparingly soluble in n-heptane.

Table V.3 Band Moments

2nd moments are $\times 10^{24}$ sec.$^{-2}$ and 4th moments are $\times 10^{50}$ sec.$^{-4}$

M.F.	M2 P-W corr.	M4 P-W corr.	M2 KKV corr.	M4 KKV corr.
CH_3CN/CCL_4-				
0.01	14.38±10%	36.06±10%	9.54±10%	23.95±10%
0.016	16.56	46.45	11.18	31.42
0.06	15.53	48.68	10.18	32.12
0.10	13.90	34.56	9.93	24.99
0.16	15.93	49.68	9.30	29.47
0.20	16.07	44.97	9.56	27.46
0.30	16.17	56.06	10.23	36.53
0.40	17.70	64.51	10.41	39.48
0.50	20.35±20%	76.39±20%	8.61±20%	33.88±20%
0.70	19.48	76.73	11.99	51.04
1.00	17.61	55.01	9.66	34.31
CH_3CN/benzene				
0.016	15.93±10%	53.39±10%	10.21±10%	34.18±10%
0.06	15.95	49.26	10.24	31.85
0.16	16.25	52.53	9.31	30.61
CH_3CN/n-heptane				
0.027	11.37	13.04	8.01	9.22

The following results were obtained by Sato et al[92] for solutions between 0.03 and 0.16 moles litre^{-1} and employing the Polo-Wilson correction factor.

CH_3CN/CCl_4 M4=32.35x10^{50} sec.$^{-4}$

CH_3CN/n-hexane M4=19.19x10^{50} sec.$^{-4}$

V.4 Reorientational Correlation Times

Fig.V.12 shows the absorption cross section (chapter I equation 23) for the 0.2 mole fraction solution in CCl_4 and Fig.V.13 the absorption cross section of the pure liquid. Figs.V.12 and 13 also show how the correction factors modify their shapes. It is seen that the intensity is reduced but the width of the bands at half height remains very similar.

The interpolation between the microwave and far-infrared data occurs at a critical region in the spectrum corresponding to the region around $\epsilon''(\omega)_{max}$. The interpolation required for the spectra of the solutions up tp 0.2 mole fraction required an interpolation of only about $1cm^{-1}$ which was quite straightforward. The microwave data for the pure liquid was taken from the combined results of Vaughan[10], Mansingh[11] and Janik[12]. The high frequency limit of this data was $1.07cm^{-1}$ from the Mansingh paper. The errors in the τ values calculated from the resulting correlation functions I estimate to be + or - 0.5p.s. As shown in chapter IV the interpolation required for the higher concentration solution spectra is much more difficult. For these spectra a gap of about $3cm^{-1}$ had to be interpolated. Using trial interpolations by eye I assess the errors in the calculated τ values to be + or - 1.0p.s.

In order to calculate the correlation functions the spectra had to be interpolated to a constant frequency interval. This was done to $0.25cm^{-1}$ using a NAG routine (E01AAF) in the program INTERPOL. The resulting spectra were found to be identical to the originals. The correlation functions were calculated using a 'slow' Fourier transform program called FIRFT.

A frequency interval of $0.25cm^{-1}$ gives a theoretical long time

Fig. V.12. $\varepsilon''(\bar{\nu})/\bar{\nu}$ curves for CH_3CN/CCl_4 0.2 M.F.

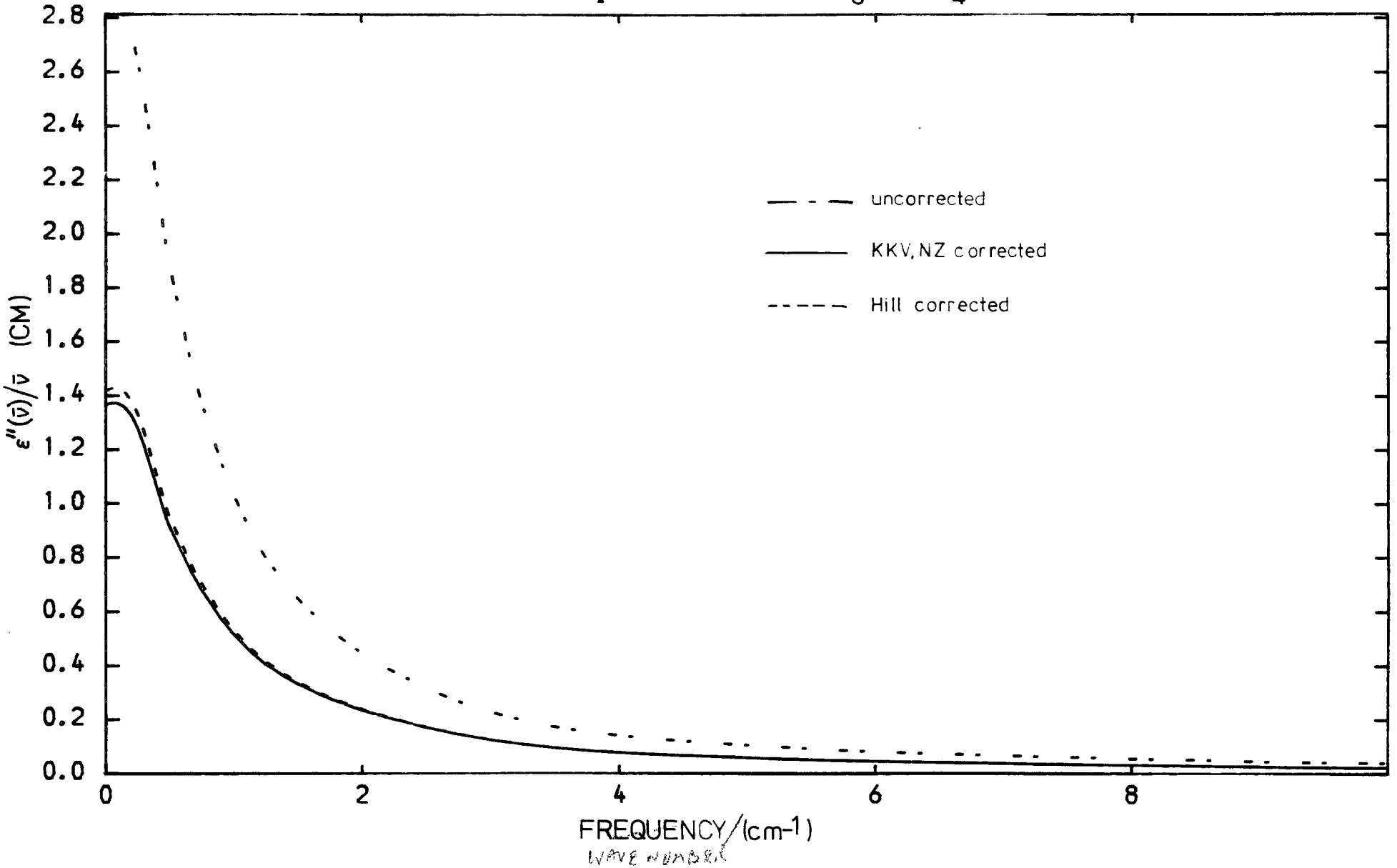

Fig.V.13. $\varepsilon''(\bar{\nu})/\bar{\nu}$ curves for pure CH_3CN

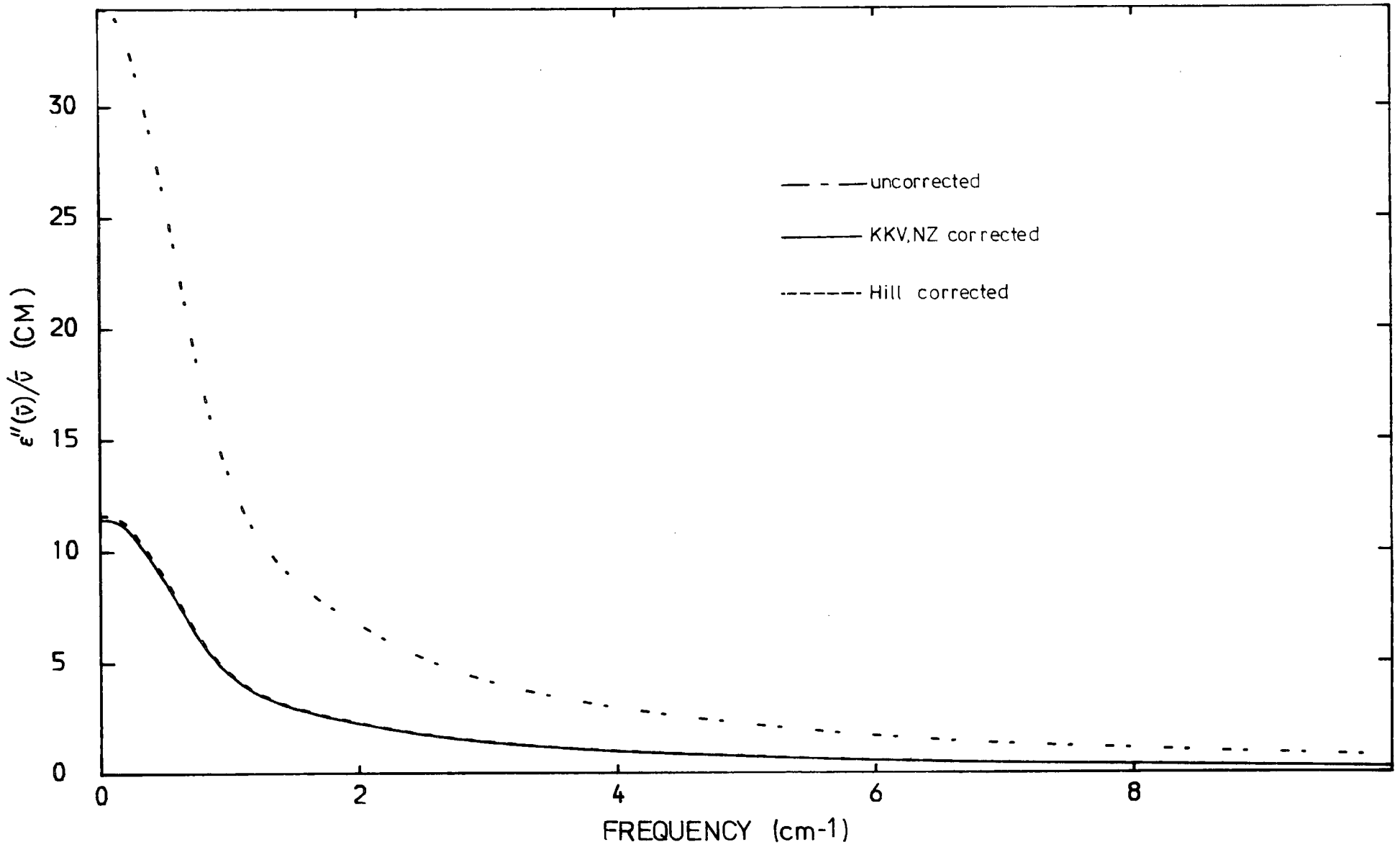

reliability limit in the correlation functions of[91] $t_{max}=\pi/\Delta\omega=12$p.s. However, because of the interpolation required (see above) this limit was reduced to an estimated 7 or 8p.s. this is not large enough to permit the integration of the area under the function in order to obtain the correlation time. The relaxation time was calculated from the slope of the $\log_e$ of the long time part of the functions τ_s. This is the time domain which is well described by Debye type relaxation processes[1,7] (see chapter II). In addition the $\tau_{1/e}$ was also calculated. This was then compared with τ_s in order to show how much the correlation functions deviated from pure Lorentzians. The frequency range over which the correlation functions were calculated was $250cm^{-1}$ which means a theoretical resolution limit in the correlation functions of[91] $\Delta\omega=\pi/\omega_{max.}=0.06$ p.s.

An example of a normalised correlation function is shown in Fig.V.14. The functions were normalised so that their value at t=0.0 is 1. Figs.V.15,16 and 17 show the natural logarithms of the correlation functions for the 0.016, 0.2 and 1.0 mole fraction solutions in CCl_4. These show that the correction factors have little effect on the value of τ obtained from the slope of the log plot. The relative amount of their effect is small at low mole fraction. It increases with increasing CH_3CN concentration until approximately 0.3 mole fraction and then decreases towards the pure liquid. Fig.V.18 shows the uncorrected $\log_e$ functions for the 0.016, 0.2 and 1.0 mole fraction solutions in CCl_4 together with the 0.016 M.F. benzene solution and the 0.027 M.F. in n-heptane.

Fig.V.19. shows the $\log_e$ of a pure Lorentzian function ($g(t)=\exp(-t/\tau)$

Fig.V.14. Normalised correlalation functions for CH_3CN/CCl_4 0.016 M.F.

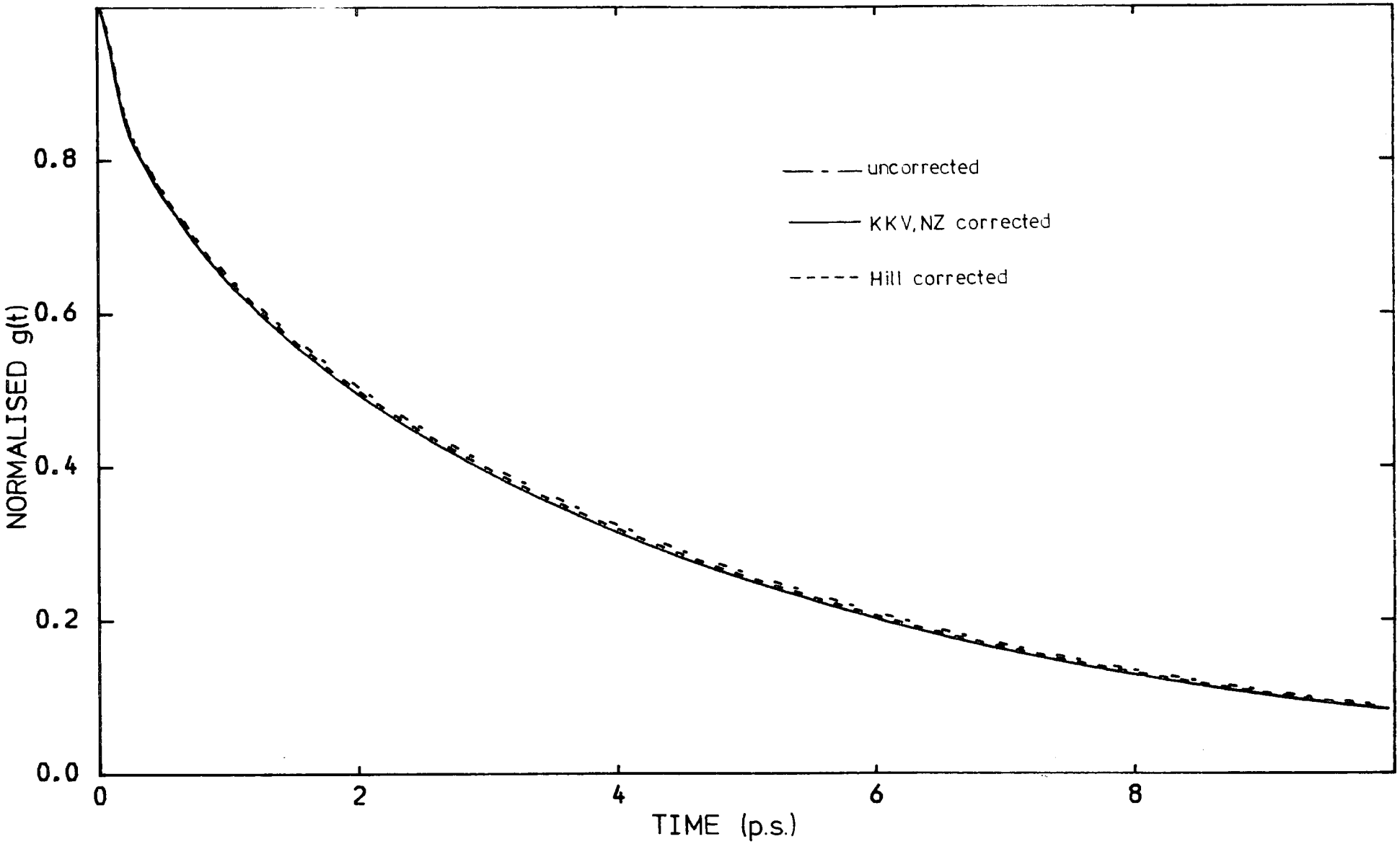

Fig.V.15. LOG_e. of the normalised g(t) functions for CH_3CN/CCl_4 0.016 M.F.

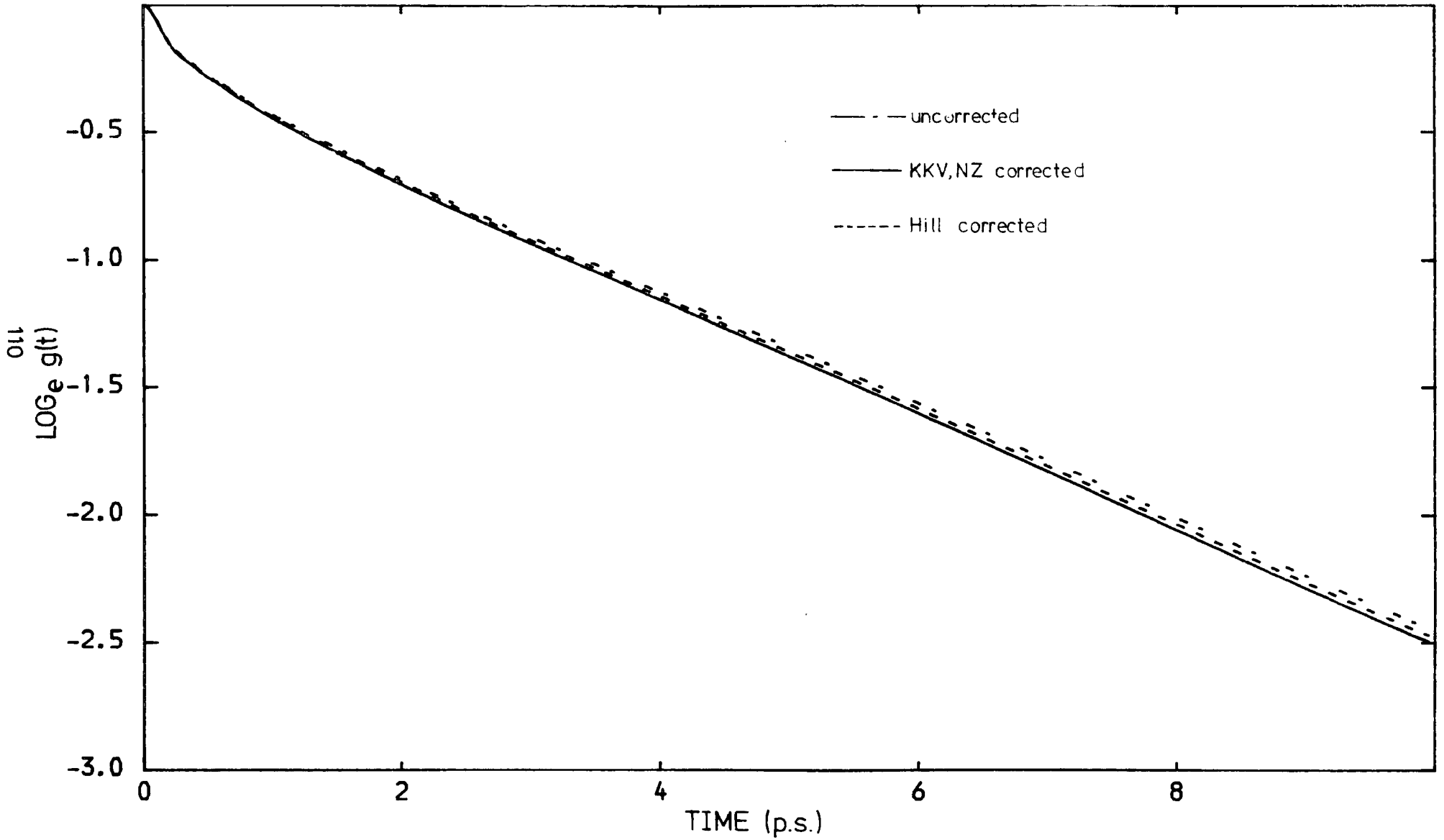

Fig.V.16. LOG_e. of the normalised g(t) functions for CH_3CN/CCl_4 0.2 M.F.

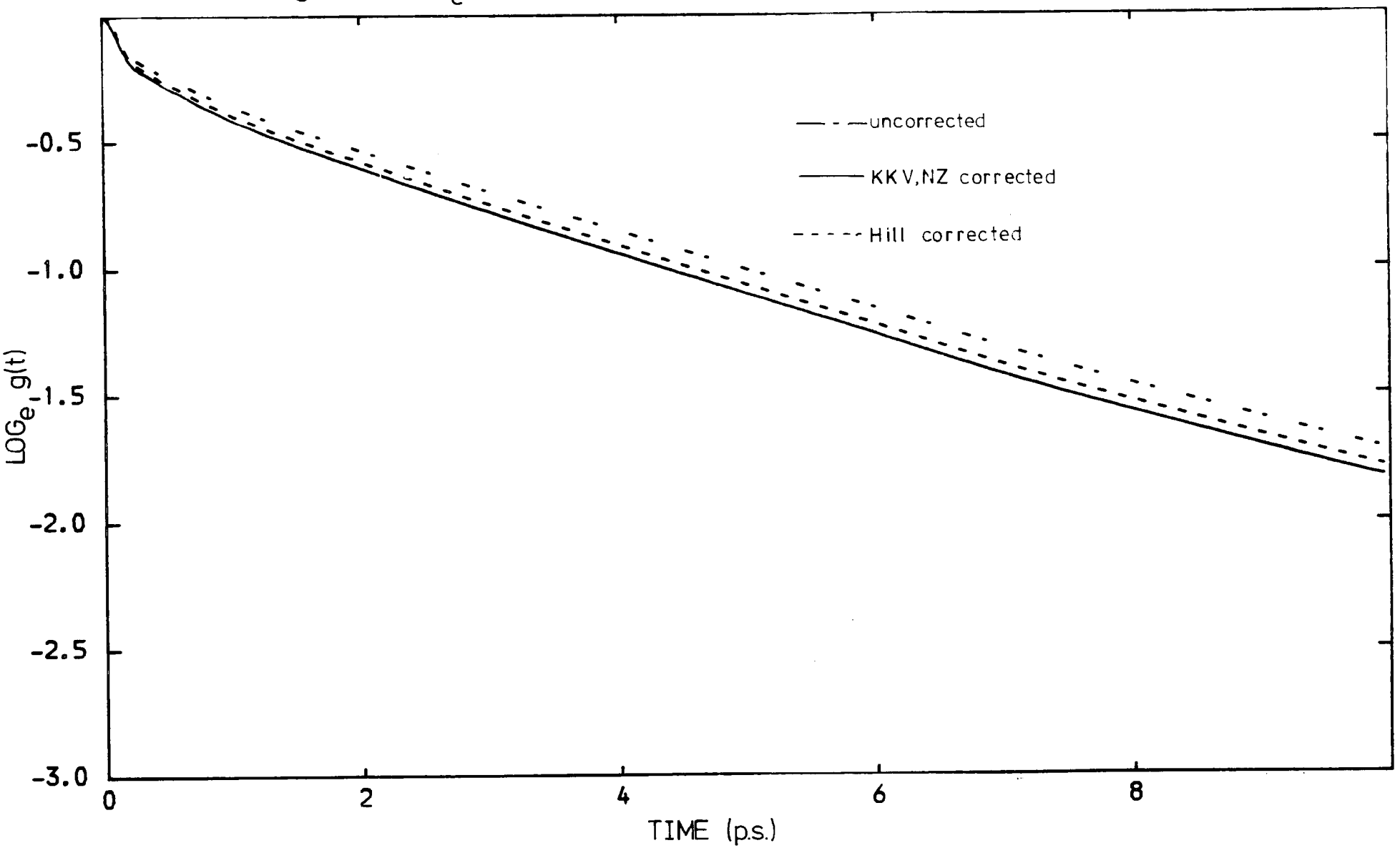

Fig.V.17. LOG_e of the normalised g(t) functions for pure CH_3CN

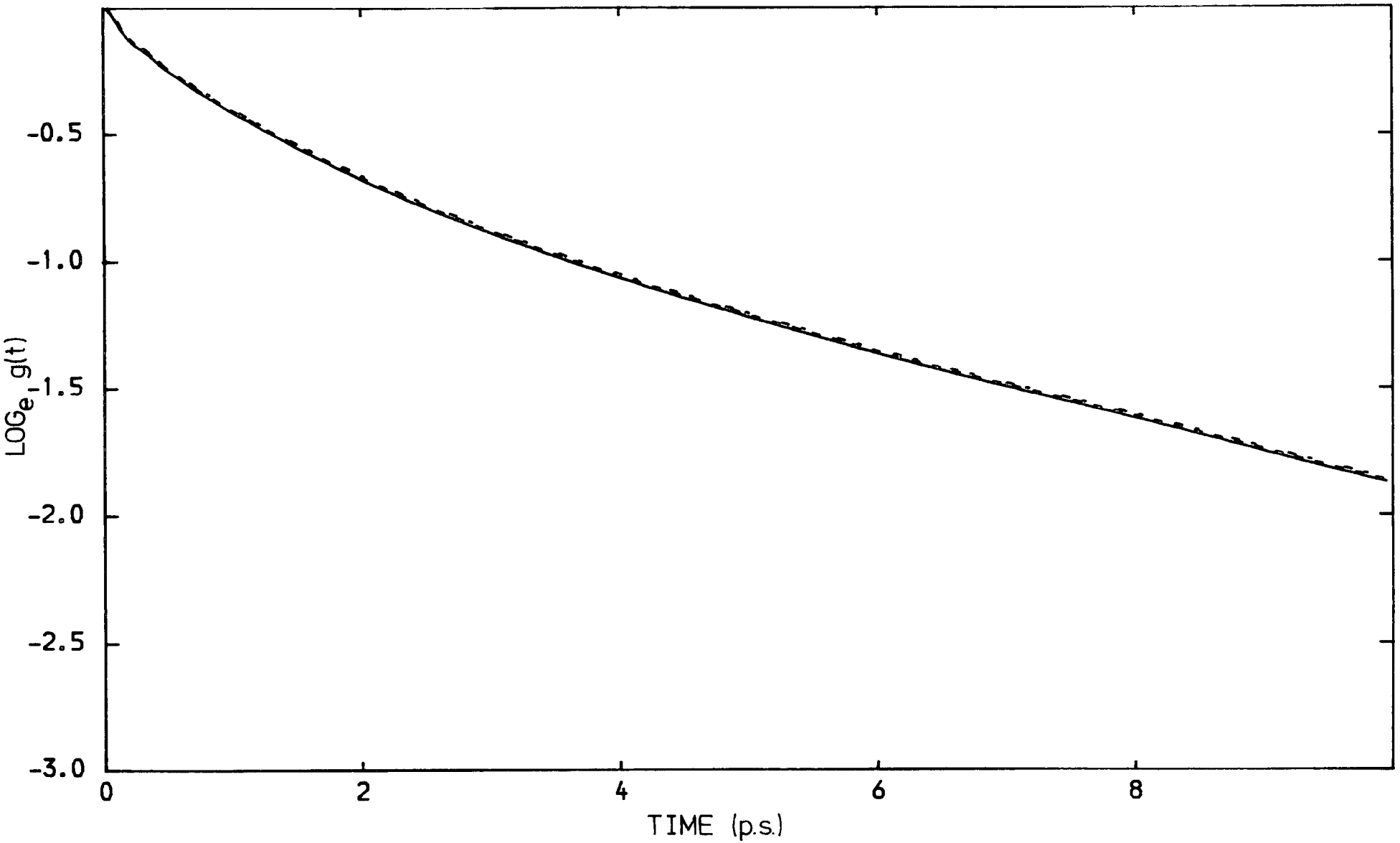

Fig.V.18. Uncorrected $\log_e$s. of the normalised g(t) functions for five of the solutions studied

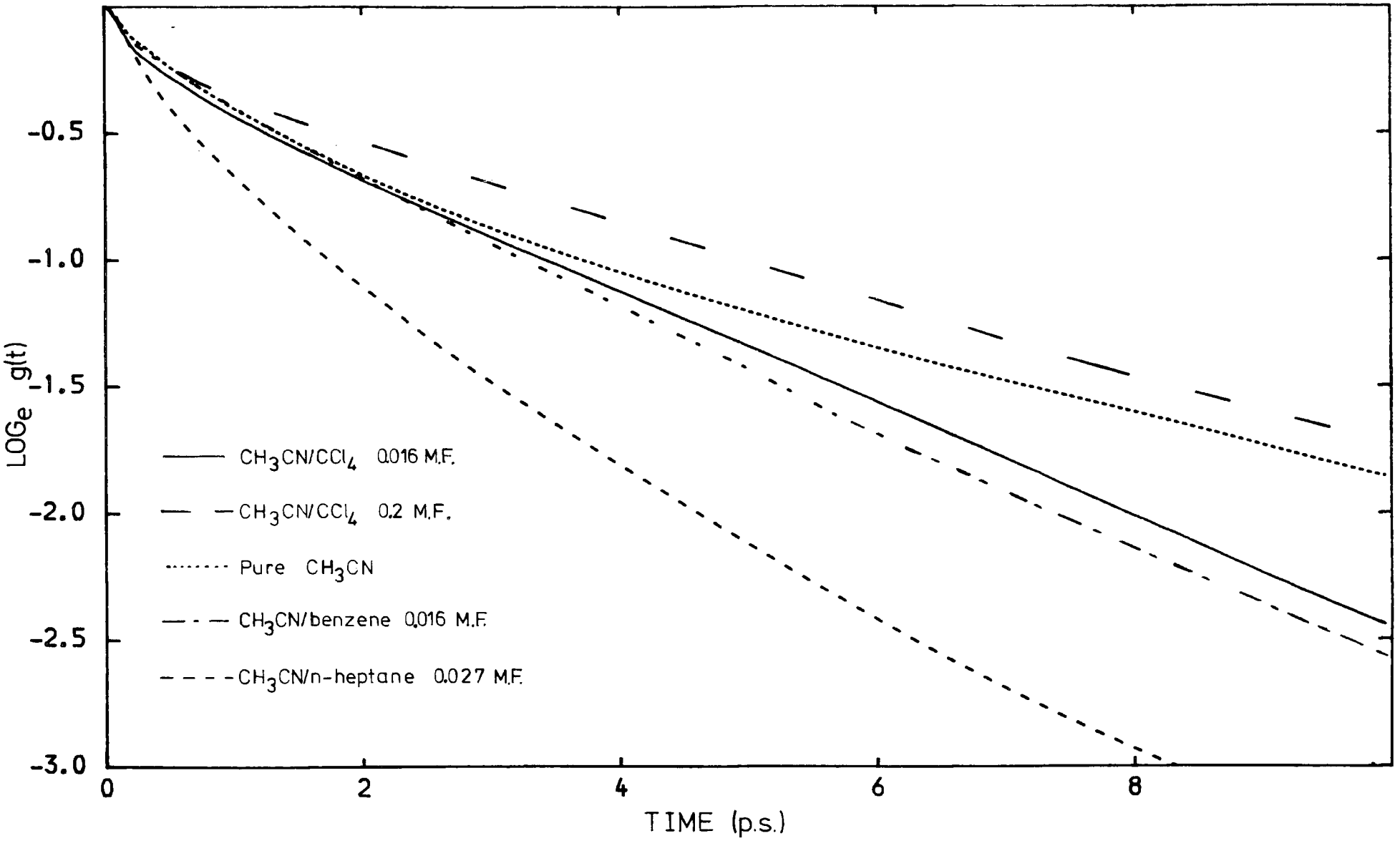

Fig.V.19. Observed, pure Lorentzian and free rotor C.F.s

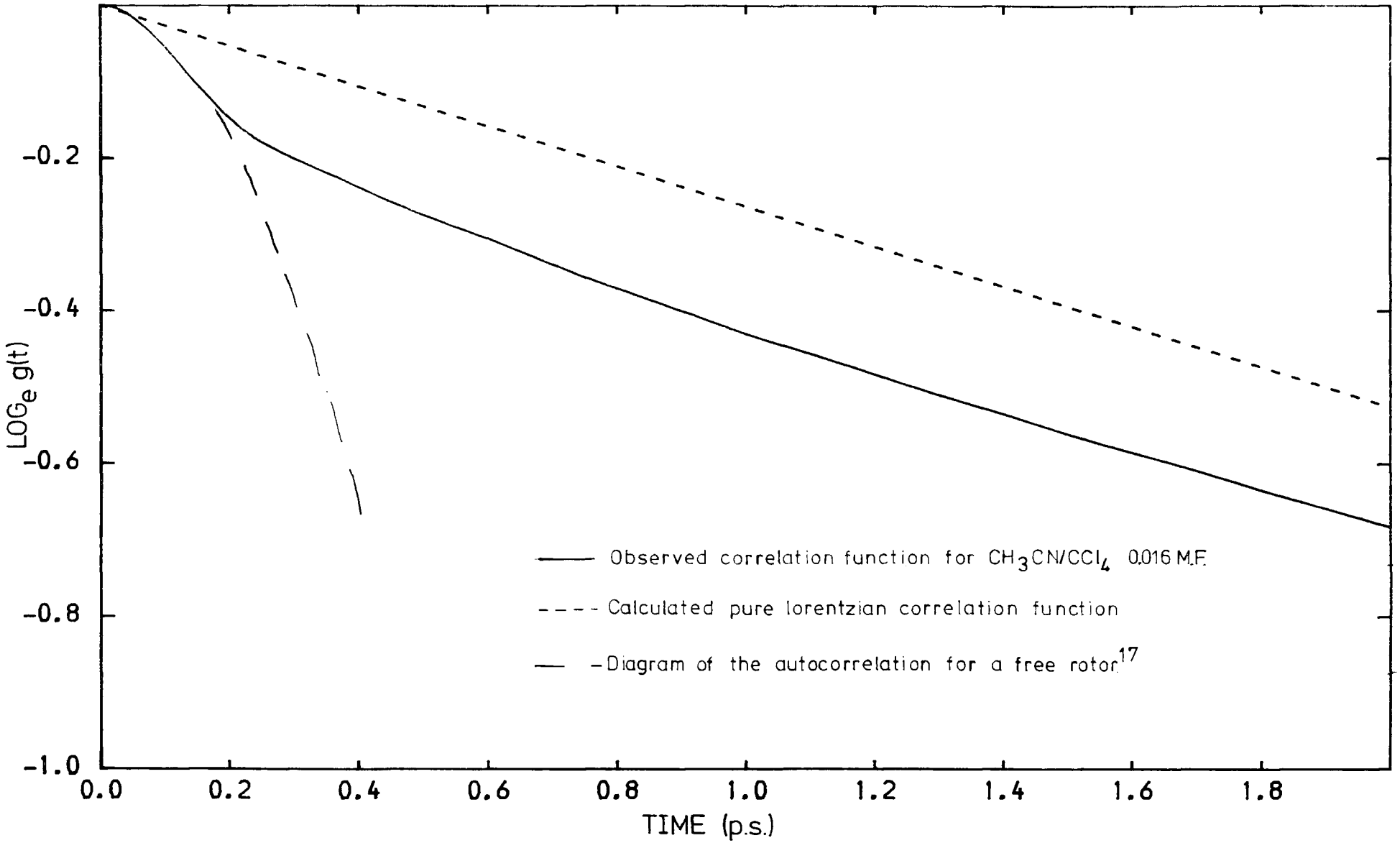

t/τ) compared with the experimental curve. It clearly shows the non-exponential short time part of the motion. Some of the non-exponential part of the function will be due to the truncation of the cross section function (see Fig.V.12) before infinite frequency. However, since the band was Fourier transformed out to 250cm^{-1} the truncation errors are expected to be unimportant. Also on Fig.V.19 is the correlation function for free-rotor behaviour[17]. The closeness of this function to the short time part of the measured function implies that the short time part of the motion does consist of relatively unhindered rotatory motion which contributes only a small amount to the loss of orientational permittivity but which leads to a very intense absorption per unit length[38].

The full list of τ far-infrared values is shown in table V.4. The corrected values using the Klug, Kranbuehl and Vaughan[34] (KKV), Nee-Zwanzig[35] and Hill[33] correction factors (see chapter I.4) are also shown. Table V.5 shows the calculated g(0) and g-factor values for all the solutions. The static correlation factors for the solutions are not expected to have very much physical meaning since the internal field correction factors are not defined for solution data (see chapter I.4). However the pure liquid factors do show a reasonable average of about 0.66 which suggests some static orientational ordering in the pure liquid (see later discussion).

The $\tau(s)$ values shown in table V.4 compare closely with the relaxation times from the microwave analysis (see table III.4 and Fig.III.11; the latter is also reproduced in this chapter). The differences are about 1p.s. at low concentrations. This difference does lie within the experimental error; it is difficult to account for but

Table V.4 Far-Infrared Correlation Times

All τ values are quoted in picoseconds.

M.F.	$\tau_{1/e}$	τ_s	τ_s(KKV,NZ)	τ_s(HIII)
CH_3CN/CCl_4 -				
0.01	3.74±0.5	3.92	3.92	3.92
0.016	3.45	4.41	4.41	4.41
0.06	3.84	4.73	4.46	4.63
0.10	4.13	4.31	4.02	4.22
0.16	5.02	6.52	6.18	6.37
0.20	4.88	6.42	5.98	6.13
0.30	4.79±1.0	5.93	5.65	5.78
0.40	4.63	6.27	6.26	6.23
0.50	4.29	6.27	6.18	6.23
0.70	4.40	4.90	4.90	4.90
1.00	4.00	5.88	5.88	5.88
CH_3CN/benzene				
0.016	3.35±0.5	3.92	3.77	3.82
0.06	3.35	4.26	4.02	4.17
0.16	4.00	6.00	4.75	4.85
CH_3CN/n-heptane				
0.027	1.88	2.35	2.35	2.35

Table V.5 Static Correlation factors

M.F.	g(0)	g(0)KKV corrected	Kirkwood g-factor
CH_3CN/CCl_4-			
0.01	1.52	0.74	0.66
0.016	1.59	0.77	0.69
0.06	1.40	0.62	0.55
0.10	1.71	0.77	0.68
0.16	1.43	0.52	0.45
0.20	1.44	0.52	0.46
0.30	1.70	0.62	0.54
0.40	1.70	0.56	0.49
0.50	1.62	0.39	0.35
0.70	1.95	0.66	0.58
1.00	2.08	0.63	0.55
Kirkwood g-factor with ϵ_∞=2.25, = 0.66			
CH_3CN/benzene			
0.016	1.67	0.76	0.69
0.06	1.48	0.64	0.58
0.16	1.61	0.56	0.50
CH_3CN/n-heptane			
0.027	1.33	0.71	0.65

may be due to the failure of linear response theory as applied to the embedded sphere. I.e. the two values are made on different physical quantities, the relaxation time is an inverse frequency and the correlation time is measured from a correlation function. As the corrections to the correlation times do not lie within the experimental errors only the uncorrected ones will be discussed further. The relaxation times calculated from the microwave data as modified by the Cole[23], Glarum[22] and Powles[24] correction factor (equation I.14) are all smaller than the uncorrected ones but do show a similar trend with concentration. However, this correction factor was not thought to be as physically realistic by Deutch[26] (see chapter I.4) as the Fatuzzo-Mason[25] approach which does not have a correction to the relaxation time (in the first approximation). This is reflected in the 'corrections' to far-infrared correlation times which are based on the Fatuzzo-Mason result and are quite small. Consequently only the uncorrected data will be disussed further. The uncorrected far-infrared τ_s values are plotted in Fig.V.20. Both sets of unmodified data for CCl_4 solution show the same general trend of increasing τ up to about 0.2 m.f.. Then a plateau is reached. This is a very similar trend to that shown by the peak in the far-infrared absorption $(\bar{\nu})_{max.}$ (see Fig.IV.9).

Table V.4 also shows the $\tau_{1/e}$. These are smaller than the corresponding τ_s values and do not show the same trend, in fact they display a rise to a peak value at 0.2 mole fraction in CCl_4 followed by a fall to the pure liquid. Rather than being a reflection of the behaviour of the relaxation times this probably shows just how much the short time non-lorentzian part of the correlation function affects the longer time parts by 'pulling' the function down. This might suggest

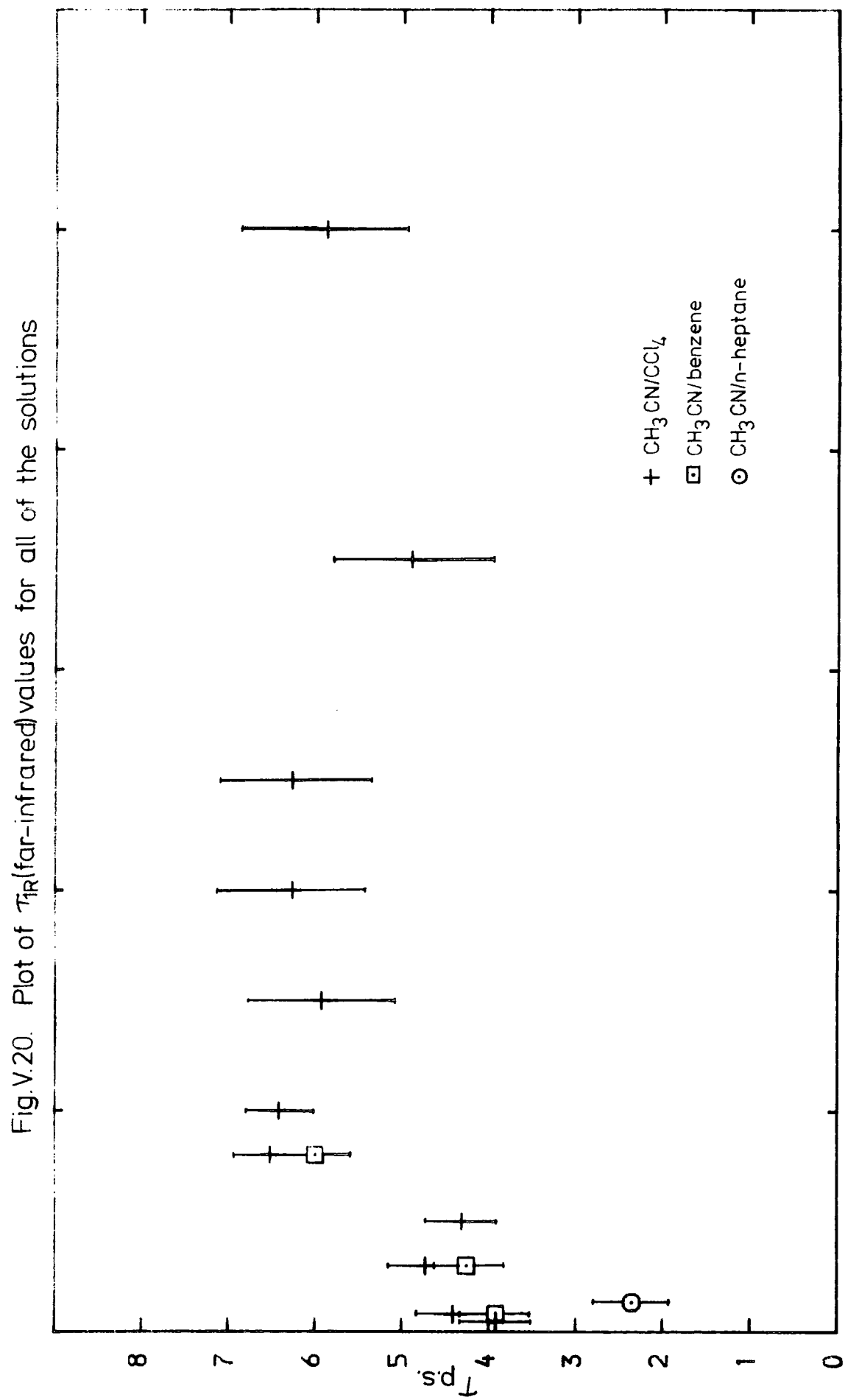
Fig. V.20. Plot of τ_{IR} (far-infrared) values for all of the solutions
τ p.s.
0
1
2
3
4
5
6
7
8
0.0
0.2
0.4
0.6
0.8
1.0
MOLE FRACTION CH_3CN
+ CH_3CN/CCl_4
⊡ CH_3CN/benzene
⊙ CH_3CN/n-heptane

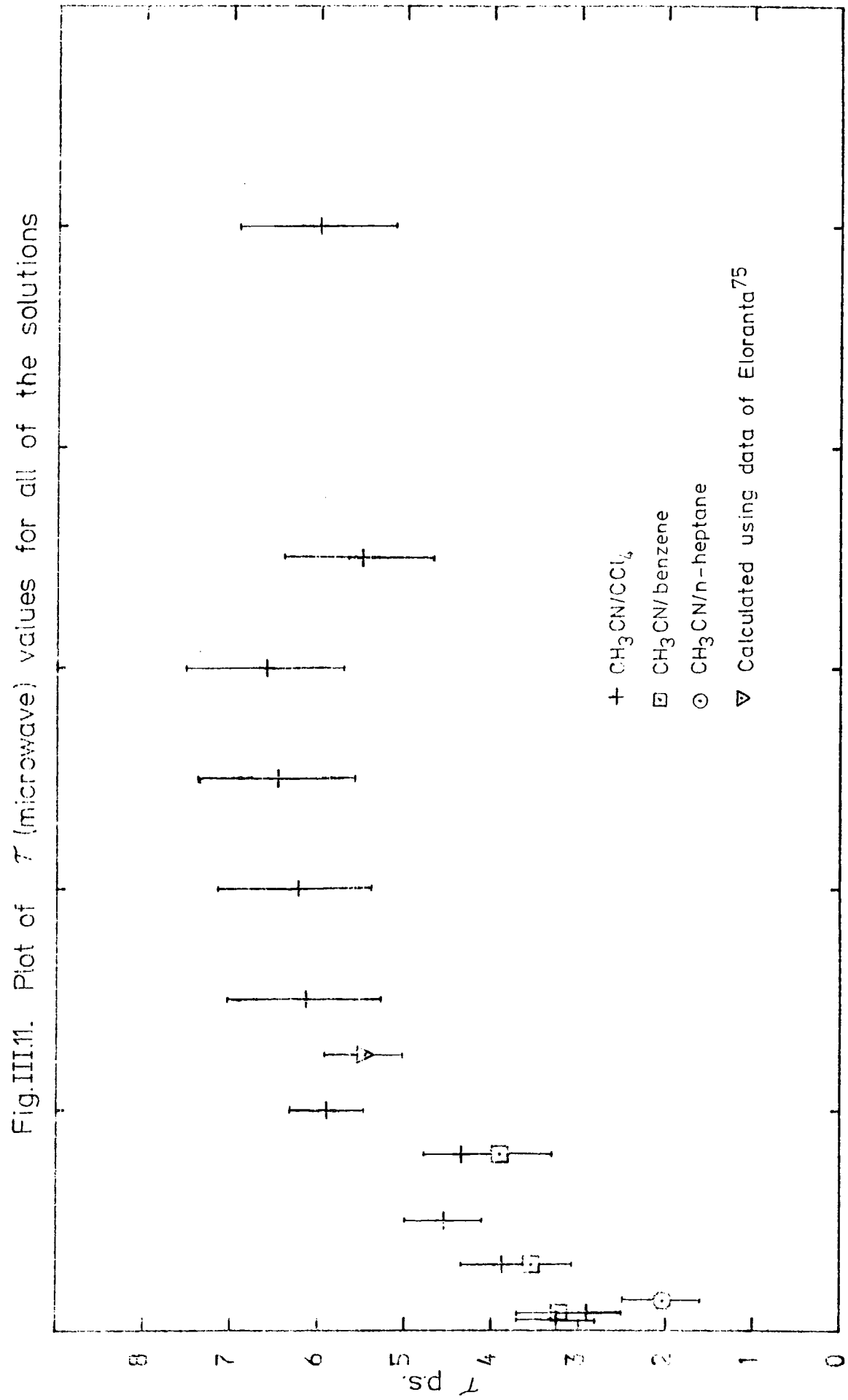
Fig.III.11. Plot of τ (microwave) values for all of the solutions
τ p.s.
MOLE FRACTION CH_3CN
+ CH_3CN/CCl_4
⊡ CH_3CN/benzene
⊙ CH_3CN/n-heptane
▽ Calculated using data of Eloranta[75]

that as $(\bar{\nu})_{max.}$ moves to higher frequencies (Fig.IV.4) the librational frequency of the molecule is higher and consequently orientational autocorrelation will decay faster.

The rotation of CH_3CN molecules in benzene appears to be very similar to that in CCl_4 while in n-heptane it is much faster. This must be due to greater interactions between the solute and solvent molecules in CCl_4 and benzene than in n-heptane. The interactions in these very dilute solutions in which dipole-dipole interactions will have been largely removed can be separated into short range rapidly varying repulsive interactions (r^{-12} dependence) or longer range more slowly varying (r^{-6}) attractive interactions such as induced dipole and dispersive forces[93]. As for the repulsive hard sphere interactions the relatively bulky chlorine atoms in CCl_4 might hinder the rotation CH_3CN molecules by providing channels and barriers over which the CH_3CN molecules must move. Benzene and n-heptane do not have such bulky groups. The magnitude of the inductive and dispersive forces is largely determined by the polarisabilities of the solvent molecules[93] of which ϵ_{∞} is a measure[1,7]. Table V.1 shows that CCl_4 and benzene both have higher ϵ_{∞} values than n-heptane. Therefore, it might be suggested that the inductive and dispersive (attractive) forces are the controlling forces for the rate of reorientation in these solutions. It must also be mentioned that other multipole forces are also present but these have much lower orders of magnitude than the inductive and dispersive forces[93] and are thus thought to be less important. There is also a correlation of relaxation times with the number density of the solvent. CCL_4 and benzene have similar concentrations at 10.36 and 11.25 moles per litre respectively. N-heptane has a relatively low molecular density

at 6.8 moles per litre. This means that there are less pairwise interactions between CH_3CN and n-heptane per unit volume than there are in the other solvents. Therefore, not only are the interactions expected to be less strong in the n-heptane solution there will also be less of them per CH_3CN molecule. As mentioned earlier the attractive forces between CH_3CN molecules and n-heptane molecules are low enough to permit only sparing miscibility of the two liquids. It was found that the dilute solution used in these experiments (0.2 molar) was about the maximum concentration possible at room temperature.

Applying similar reasoning to the concentration range in CCl_4 one can suggest that, as the solutions become more concentrated, the amount of dipole-dipole interactions increases and the reorientation of the CH_3CN molecules becomes more difficult. This interpretation is complicated by the possible presence of molecular intercorrelations between CH_3CN molecules. This is discussed more fully later. It must also be mentioned that CH_3CN has a high molecular density at 19.13 moles per litre which means that the central or probe molecule is subject to many more interactions in the neat liquid than in dilute CCl_4 solutions.

The trends shown by the τ values are also seen in the fourth moments and hence intermolecular torques (equation I.40). I.e. as the torques increase the relaxation becomes slower. This is as expected since the torques between molecules are one measure of the intermolecular forces. This also means that as the torques increase the frequency of the librations increases indicating the greater difficulty for the molecules to undergo larger angle reorientational motion. The intermolecular torques are directly proportional to the peak in far-infrared curve according to the 3 parameter Mori model of Evans et al[106] (see chapter

II.4).

$$I_r \bar{\nu}^2_{max} = T_q 10^{38} \qquad \text{.....V.5}$$

where I_r is the reduced inertia of the molecule and T_q is the torque product. From the positions of $(\bar{\nu})_{max}$ it is seen that the intermolecular torques in n-heptane solution are only 65% of those and those in dilute CCl_4 solution are 75% of the pure liquid. In addition, if the peak in this band is a librational frequency as it is in the itinerant oscillator models[67,68,69] then as the peak moves to higher frequencies the angle through which libration occurs and hence the volume swept during a libration is smaller i.e.

$$\theta \propto 1/\bar{\nu}_{max} \qquad \text{.....V.6}$$

θ is the angle swept during libration which will be directly proportional to the volume swept. This means that as the mean square intermolecular torques increase the librating molecules have less room to oscillate and rotate within. This might suggest that the free volume of the liquids was varying between the different solutions. Experiments performed at high pressures would be able to illuminate this aspect of the rotational motion.

The plateau in the plot of τ as a function of mole fraction might suggest the formation of relatively stable long-lived clusters of CH_3CN molecules which then reorient together. There is however, no reason why the contribution of CH_3CN to the intermolecular potential should be linear with concentration. There is evidence[94] for the formation of dimers in the gas phase which give rise to a very weak band at $78cm^{-1}$ due to intermolecular vibrational modes. Knozinger[94] obtained an equilibrium constant for the dimerisation of 42 + or - 26 litre per mole. Then there is the possibility that some of the far-infrared band

of the liquid is due to the same intermolecular vibrations. The sum rule analysis presented above does not indicate the presence of any other intensity than that due to dipolar rotational motion in the liquid. The presence of dimers in the gas phase does suggest that short range dipolar interactions in the liquid phase would be sufficiently stong to form dimers or clusters. Even if 'stable' long lived dimers are not present in the solutions and liquid their presence in the gas phase clearly indicates that attractive forces in acetonitrile are indeed strong over short intermolecular distances.

The increase in τ on increasing concentration in CCl_4 is the opposite trend to that found by Versmold[44] for the light scattering multimolecular correlation times. Versmold also quotes in this paper the τ_{2r} single particle correlation times obtained from N.M.R. data by Bopp95 which also show the same decreasing trend with increasing CH_3CN concentration. Versmold points out that this follows the bulk viscosity of these solutions with CH_3CN (0.345c.p.)[101] being less viscous than CCl_4 (0.951 c.p.)[101]. He found that the gradient of the viscosity curve was the same as that for the τ_{2r} single particle with concentration. The Stokes[93] relation for rotational diffusion can be applied to relate relaxation time with macroscopic viscosity of these solutions

$$\tau = 4\pi\eta a^3/kT \qquad \text{.....V.7}$$

where η is the bulk viscosity and a is the radius of the 'spherical' molecule. It is the value taken for this quantity which will decide whether the relation above is completely obeyed. The viscosity can be discussed in terms of the shapes of the molecules as defined by the hard sphere dimensions. The cylindrical shaped and relatively smooth CH_3CN molecules (see Fig.I.1) can move around each other more easily than they

can in CCl_4 where the bulky chlorine atoms provide channels which hinder the rotation of the CH_3CN molecules.

If τ_{1r} single particle does follow the viscosity and decrease on increasing CH_3CN concentration then it is the cross terms in the total correlation function which increase with increasing dielectric strength. This implies that the long range electrostatic forces (r^{-6}) do not show up in the light scattering data. This is probably because the $g^{(2)}$ is more sensitive to short range forces than it is for long range dipolar, inductive and dispersive interactions. A value for τ_{1r} single particle has been obtained from the mid-infrared vibration band ν_2 for the pure liquid by Breuillard-Alliot[96] using the Rakov[97] method to remove the vibrational line width. In this approach the liquid is solidified in order to remove rotational motion to leave only the vibrational line width. This can then be separated from the liquid phase vibration-rotation band. However, there is no reason why the vibrational line width should remain constant with temperature (see chapter VI). In addition, this band is also disturbed by a small hot band in its low frequency wing. The value they obtained was 3.2p.s. at 298K. This is close to the τ single particle obtained from the microwave far-infrared dilute solutions of CH_3CN in CCl_4 and benzene. Therefore, taking a value of $\tau 1r$ single particle of 3p.s. for the pure liquid and an average $\tau 2r$ single particle for the pure liquid of 1.1[95,98,99,100,101,102] (which is an average obtained from various techniques, Raman, NMR and Rayleigh experiments which vary between 0.9 and 1.4p.s. for similar temperatures) the ratio of $\tau_{1r}/\tau_{2r} \approx 3$ agrees with that predicted for rotational diffusion by Hubbard[103]. This may be just coincidence when one considers the difficulties in determining τ_{1r}. It is also known that Debye type

rotational diffusion is not an accurate model for the rotational motion of the molecules especially at short times (see chapter II).

Applying the Keyes-Kivelson equation[28] (equation I.16) assuming no dynamic correlation see (chapter I).

$$g=\tau\text{total}/\tau\text{single particle} \qquad \text{.....V.8}$$

with τ total 6.0p.s and g=0.70 gives τsingle particle of 9.0p.s. This means that because of the strong static correlations implied in the value of g less than one CH_3CN reorientation is much slower in the pure liquid than in any of the non-polar solutions, i.e. dipolar and inductive interactions dominate over short range repulsive interactions. This high value of τ single particle compared with the value of 3.1p.s. might suggest that there are dynamic angular correlations present in the pure liquid and F is not zero. Versmold[44] applied this equation again assuming F=0

$$g^{(2)}=\tau\text{Is(total)}/\tau 2r\text{(single particle)} \qquad \text{...V.9}$$

which yielded a value of 1.6 for $g^{(2)}$. Fig.21 shows a plot of functions P_1 and P_2 from which it can be seen that the g of 0.7 and $g^{(2)}$ of 1.6 agree fairly well to suggest an average preferential static mutual orientations between 90 and 180°. This is an antiparallel arrangement between adjacent molecules. This might suggest that the dipoles are aligned along side each other so as to have opposite charges of the dipole next to each other. However, a head to head arrangement of the molecules also constitutes an antiparallel configuration. The agreement between the far-infrared and light scattering static correlation factors implies that the light scattering correlation times contain no dynamic correlations. This again suggests that the dynamic correlations are due to slowly varying dipolar and inductive interactions which the light

Fig.V.21. First and second Legendre polynomials (P_1 and P_2)

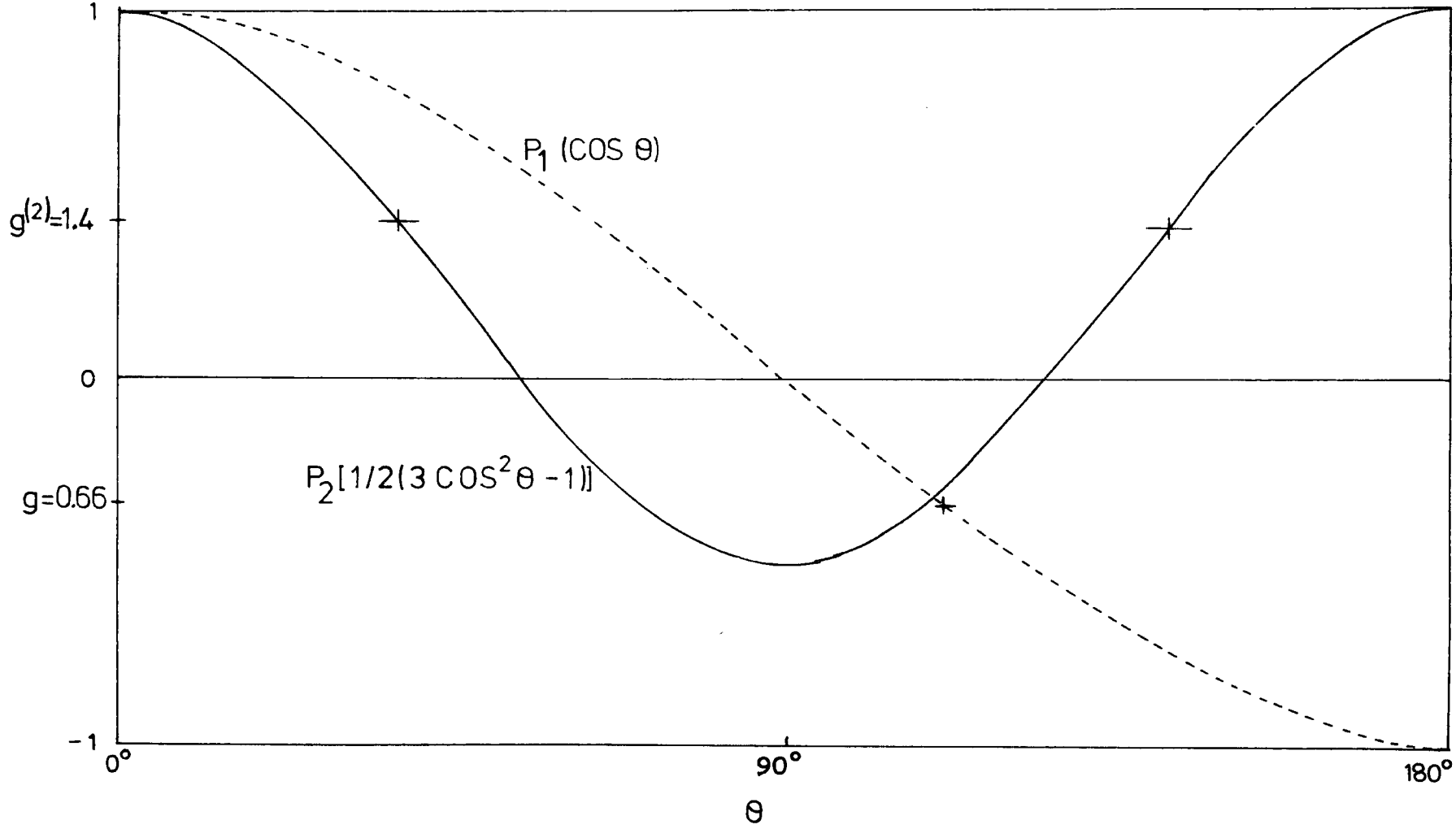

scattering experiment is not sensitive to. The Keyes-Kivelson[28] theory can also be used to calculate the relaxation time for the distinct correlation function for rotational diffusion. Again, this is thought to apply fairly well to the long time part (relaxational) of the reorientational motion (see chapter II)

$$1/\tau_{distinct} = 1/\tau_{single\ particle} - 1/g\tau_{total} \quad .....V.9$$

where g is the static correlation factor taken as 0.66, if $\tau_{sp.}$ is taken as 3.0p.s. and τ_{tot} as 6.0p.s. then $\tau_{dis.}$ is 0.12p.s. This is faster than either the total or single particle relaxation times. According to Keyes and Kivelson it should be greater than either of them because it isolates the reorientation of many particles. This result reinforces the proposition that dynamic correlations between the angular momenta of adjacent molecules cannot be neglected as it appears they can be in the second rank tensor, light scattering experiments[18].

Chandler[104] has applied his RISM (Rough Hard Sphere Theory) calculations to CH_3CN. This model includes only short range rapidly varying repulsive forces acting between the molecules. He found that there was strong static preference for antiparallel angular correlations in the pure liquid. These correlations were due to the shapes of the molecules and not dipolar interactions. The model does fit the experimental X-ray and neutron scattering structure factors in all but the region that corresponds to long range interactions. Chandler does concede that dipole-dipole potentials do contribute to the static order of liquids. However, he also points out that the structure factors of CS_2 which has a very similar shape but no dipole moment to CH_3CN are qualitatively similar. The experimental x-ray and neutron site-site structure factors are difficult to interpret in terms of angular

correlations for light molecules[105] because of the approximations involved in calculating, for instance, the nitrogen-nitrogen structure factor.

V.5 Results of 2nd. Order Mori Model Analysis

a. Calculation of τ using eqns.II.18 and II.19

The calculated τ was 3.35p.s. This is close to the τ for the dilute solutions in CCl_4 and benzene solutions. This value is also similar to the value predicted for the τ_{1r} single particle by the Hubbard[103] equation from the τ_{2r} single particle data (see V.4) of about 3.0p.s. The model was in fact formulated to calculate single particle functions and since the far-infrared band should not have any contributions from molecular intercorrelations (see Chapter I.6) the agreement with the predicted single particle correlation time is very good.

The calculated 4th. moment (equation II.17) was $125 \times 10^{50} s^{-4}$. This is much higher than the measured values (section V.2). The value of the $1/\gamma$ parameter was 2.2×10^{-14} seconds. This data is an indication of the intrinsic quality of the model without any fitting to the observed data.

b) Fitting of the Two Parameters $K_1(0)$ and γ Using Equation II.12

Two fits to the experimental curves were made. Fit 1 had the Polo-Wilson correction factor[49] used to correct the intensity and fit 2 had no correction done. The fitted curves are shown in Figs.V.22 and 23, the results of the fits in table V.6. As can be seen the best fit was obtained when the correction factor was used. Both fitted curves have a shoulder at about $15cm^{-1}$ which is not present in the experimental curve. This implies that the second order truncation Mori model has a separation beween the microwave (Debye) relaxation behaviour and the far-infrared librational behaviour which is not present in reality. The

Table V.6 Results of 3 Parameter Mori Model Analysis

a) Calculated values

	$M4 \times 10^{50} s^{-4}$	$1/\gamma \times 10^{-14}$ s.
	125.0	2.17

b) Fitted values

Fit 1.	39.3	5.90
Fit 2.	34.8	5.00

Fig.V.22. Observed and fitted (eqn.II.12) $\alpha(\bar{\nu})$ spectrum for CH_3CN. 20°C. Fit 1

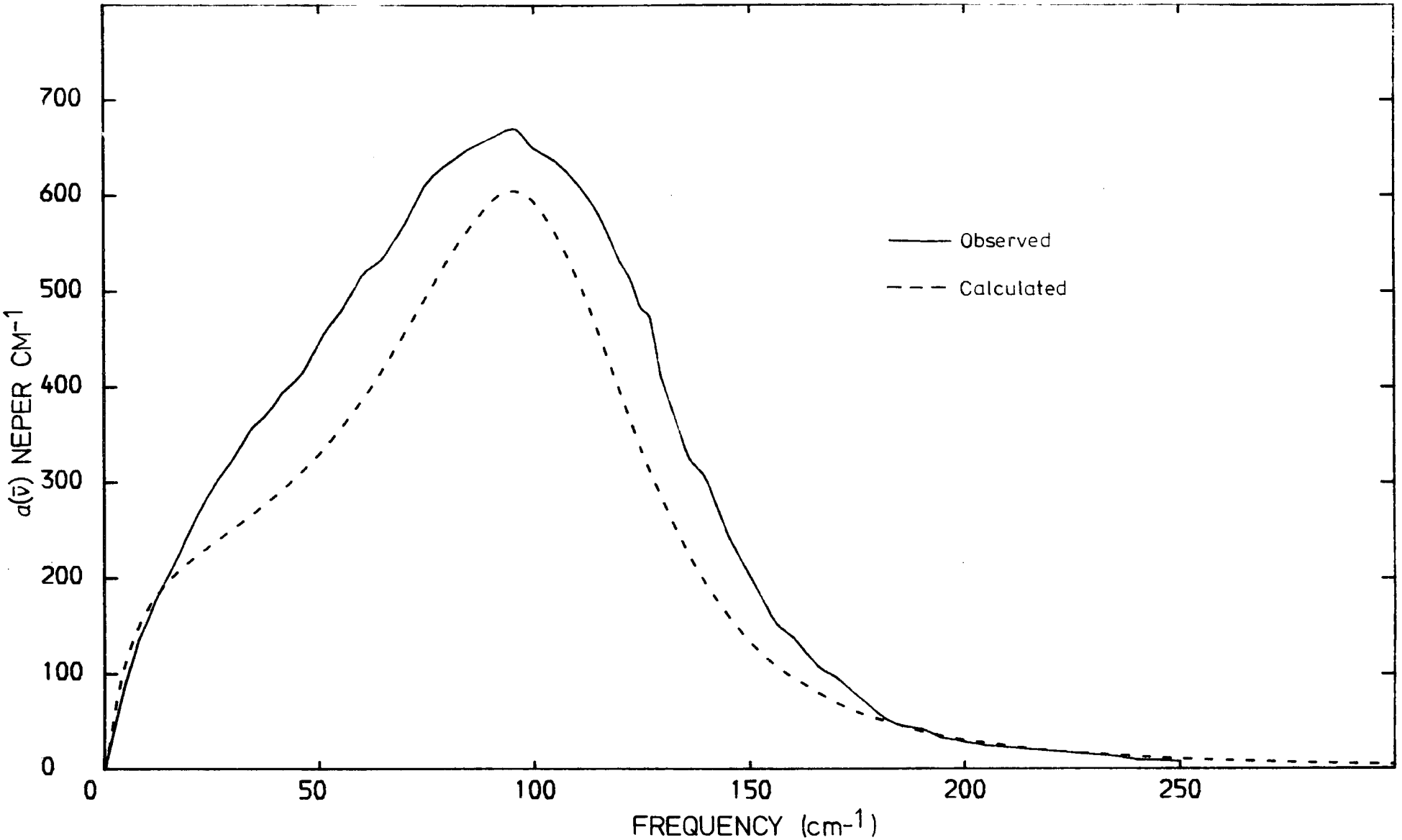

Fig.V.23. Observed and fitted $a(\bar{\nu})$ spectrum for pure CH_3CN. Fit 2

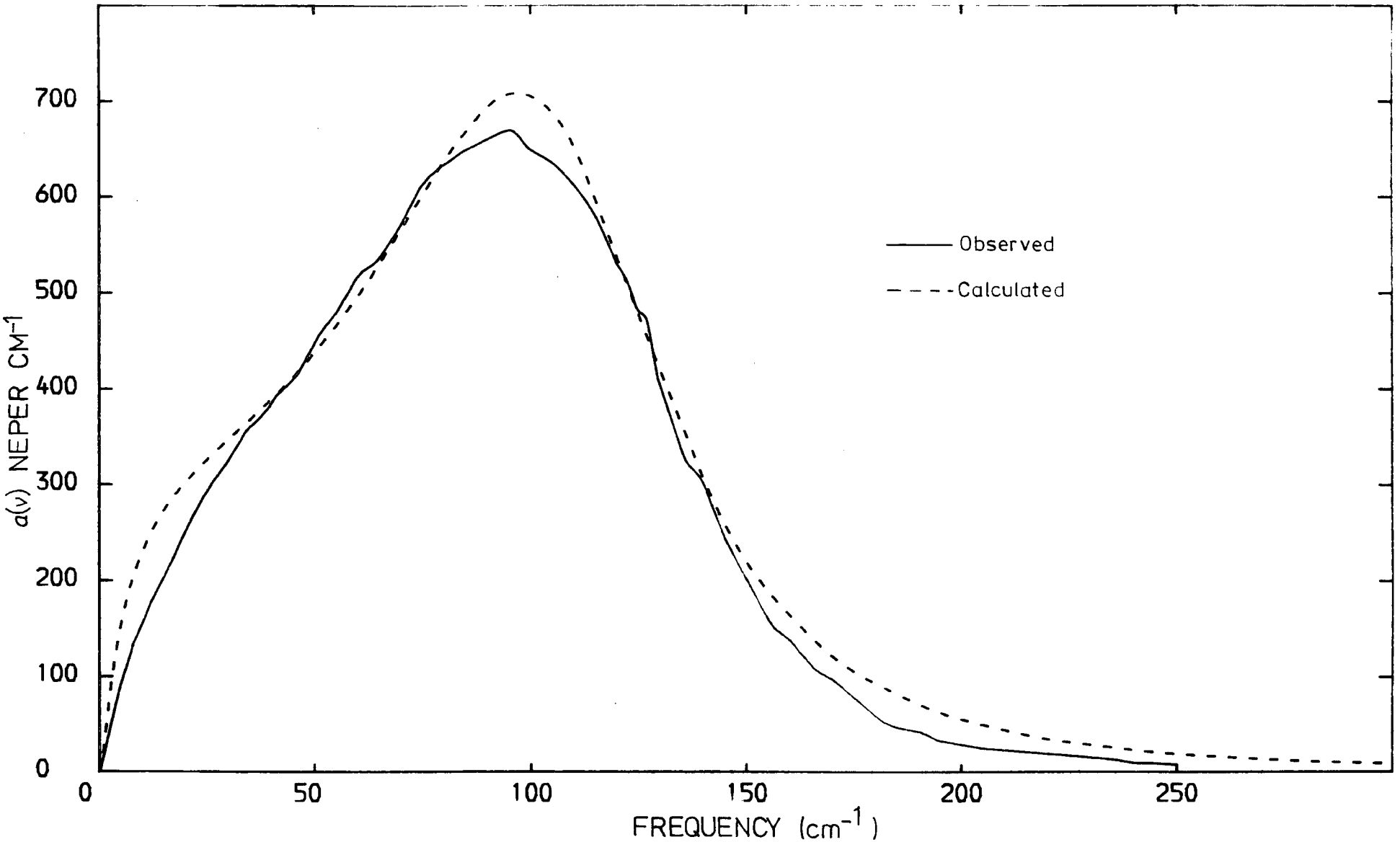

recalculated τ values have an average of about 2.5p.s. which is smaller but still quite similar to those discussed in section V.5.a.

The calculated 4th moments are very similar to the measured ones. The model is therefore (unless this agreement is only coincidence) correctly simulating the far-infrared absorption in terms of the intermolecular mean square torques. The torque correlation time parameter $1/\gamma$ values are longer than those from the one in section V.5.a. This value being greater than nought reflects the move away from the rotational diffusion picture which has zero time duration of torques.

Equation II.12 has the property that as the peak in $\alpha(\nu)$ moves to high frequency the peak in $\epsilon''(\nu)$ moves in the opposite way[47]. I.e. as the intermolecular torques increase molecular relaxation is slower which is just what is found experimentally (section V.4). In addition, as γ is proportional to $K_1(0)$ II.19 this means that as the torque increases the duration of the torque is reduced. This again reflects the differences with the rotational diffusion picture in which the peak in $\alpha(\nu)$ is at infinite frequency and infinite torques act instantly.

The recalculated $\epsilon''(\nu)$ and $\epsilon'(\nu)$ are shown in FigV.24. The curves do reproduce the bulge on the high frequency side of the $\epsilon''(\nu)$ function and the minimum in the $\epsilon'(\nu)$ which are observed in practice See Fig.I.2 and Fig.V.2.

More recent work on the Mori[106] formalism has shown that, in molecules where the centre of volume is located at some distance from the centre of mass such as in bromobenzene then the librational motion is strongly coupled to the translation of the molecule. In this situation a libration about the centre of volume which is the most

Fig.V.24. Calculated $\varepsilon'(\nu)$ and $\varepsilon''(\nu)$ curves from fitted $K_1(0)$ and γ parameters. CH_3CN Fit 2

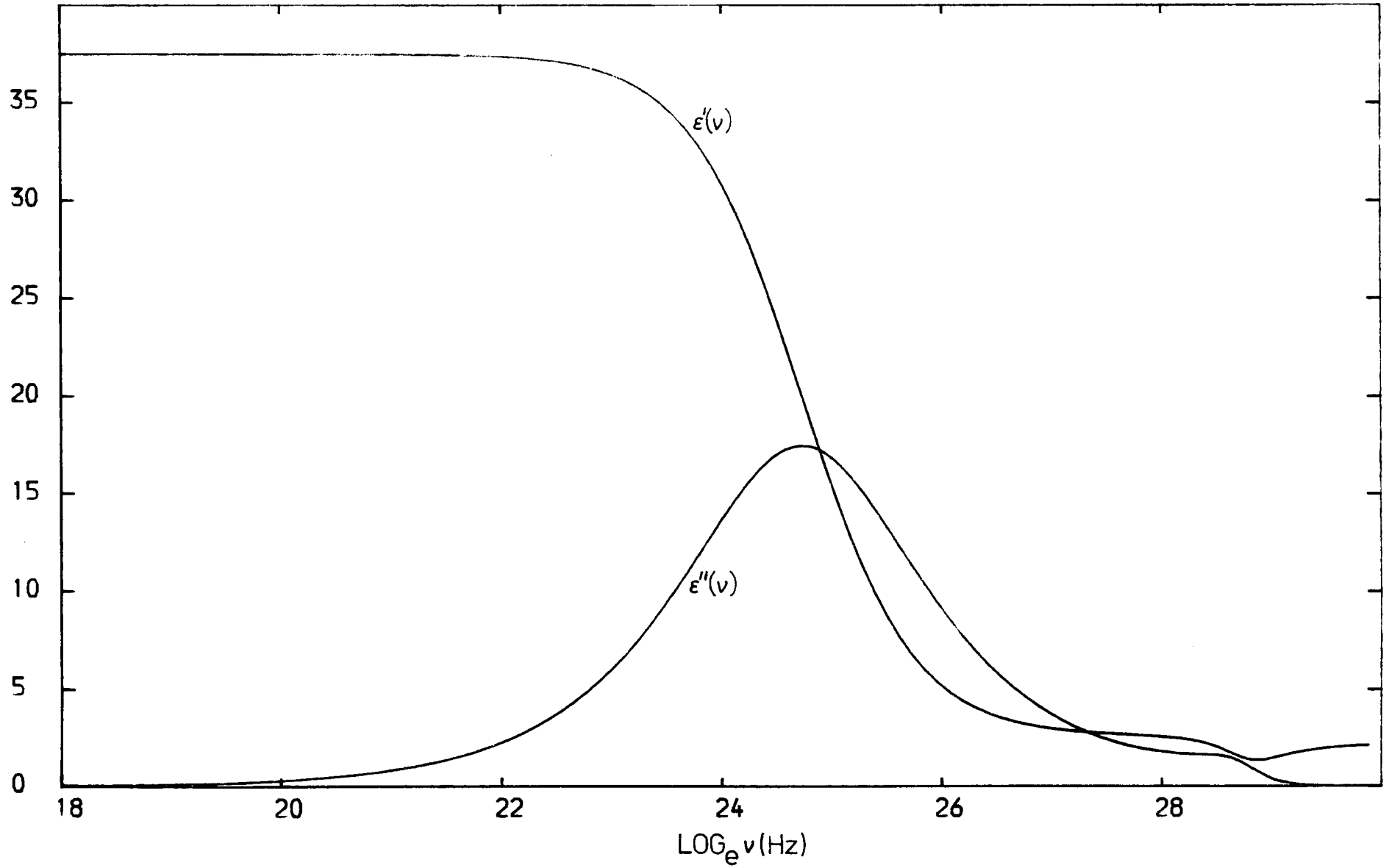

likely event in a condensed phase[107] is made up of a libration about the centre of mass and a translational oscillation of the centre of mass. This separation is unlikely in CH_3CN as the centre of mass and centre of volume are probably very close.

V.6 *Further Discussion*

Computer simulations of dynamic assemblies of molecules can be made on computers of high central processing power. This method consists of solving the equations of motion for hundreds or thousands of interacting particles. After a certain time the desired correlation functions can be extracted from the recoded motions of the particles. Computer simulations provide a means whereby experimental data can be reconstructed using an adopted intermolecular potential. There are problems in including long range forces in the intermolecular potential because only limited numbers of molecules (of the order of hundreds of molecules) can be simulated in one 'experiment'[17]. Adams[108] has simulated cylindrical molecules with a central point dipole and found some correlation between rotational and translational motion. It was found that orientational correlation was reduced more rapidly when the molecule was translating perpendicular to its main axis than along this direction. This is because in this direction the molecule presents more cross sectional area for collision than when it moves in the direction of the major axis. In addition the molecule is more likely to move in this direction since it meets fewer obstacles to motion. On these terms there is some correlation between translational and rotational motion. These 'experiments' are not completely trustworthy because they involve the use of an assumed intermolecular potential which may not be correct[17]. It is expected that computer simulation techniques will lead

to new generations of models of motion in the future because they afford more accurate 'experimental' tests of the models than by fitting to observed data[17,109].

Chapter VI.

Raman Study on the ν_1 vibration band of CH_3CN in Methanol Solutions

VI.1 Introduction

This study is on the ν_1 (C-H symmetric stretch) vibration band of CH_3CN by Raman spectroscopy. The shape of a vibrational band is affected by the intermolecular interactions in the liquid[3]. It is hoped that a band shape analysis of the ν_1 band when the nitrogen atom of CH_3CN is 'hydrogen bonded' to the hydrogen atom of the alcohol group of methanol will enable some of the mechanisms which cause the band broadening to be understood. In the solutions of CH_3CN with CD_3OD the biggest additional contribution to the interaction potential above that in the pure liquid will be the hydrogen bonding interactions, the complex has an equilibrium constant[125] of 2.6dm^3 mol^{-1}. The ν_1 band is the most intense band in the Raman spectrum of CH_3CN enabling very dilute solutions to be studied at high signal to noise ratio. Its vibrational frequency in the liquid is at about 2940 cm^{-1}. In addition, the band is relatively undisturbed by other vibrations. It does have some intensity from ν_5 at 3003 cm^{-1} but this is overcome by using only the low frequency half of the band which is not thought to contain any intensity from the ν_5 band. Raman band shapes were analysed by the correlation function method (see chapter I. equations I.27 to I.31) the Raman scattering correlation functions are obtained from the Fourier transform of the polarised and depolarised spectra.

$$I_{iso}(\omega)=I_{VV}(\omega)-4/3I_{VH}(\omega) \qquad \text{.....VI.1}$$

$$I_{aniso}(\omega)=I_{VH}(\omega) \qquad \text{.....VI.2}$$

$$\Phi_v(t)=\int_{band} I_{iso}(\omega)\ \cos\omega t\ d\omega \qquad \text{.....VI.3}$$

$$\Phi_v(t)\Phi_{2r}(t)=\int_{band} I_{aniso}(\omega)\ \cos\omega t\ d\omega \qquad \text{.....VI.4}$$

The depolarisation ratio[43] ($\rho=I_{VH}/I_{VV}$) of the ν_1 band of CH_3CN is extremely small $\rho=0.009$[110], which is too small to allow the rotational (Φ_{2r}) correlation function to be obtained from the spectra using equation I.34.

Several workers[110-114] have attempted to elucidate the non-reorientational mechanisms by which the ν_1 band is broadened in the liquid. There are two basic subdivisions into which vibrational broadening can be divided[115-118].

a) Energy relaxation. These processes are transfer of vibration energy to the surrounding molecules via rotational and translational degrees of freedom; also vibrational energy redistribution to other vibrational modes. This may be possible with ν_1 because of the presence of other bands of similar frequency (e.g. ν_5 3003, $\nu_1+\nu_4$ 3000, $2\nu_6$ 2800 and $2\nu_8+\nu_2$ 2990cm^{-1})[110].

b) Phase coherence is lost through intermolecular interactions. The frequency of vibration of a molecule is changed because the interaction energy of the excited molecule with its surroundings is different to that of the molecule in its ground state. This is due to electrical and mechanical anharmonicity of the vibration. In the second cause of phase relaxation the vibrational frequency of the excited molecule is shifted because of vibrational coupling with surrounding molecules. In this situation vibrational energy is not confined to a single molecule. In both these cases one gets a distribution of frequencies caused by random mutual orientations and separations between molecules.

If the frequencies of energy fluctations in the probe molecule's surroundings do not match the vibrational frequencies, then phase relaxation will be much faster than energy relaxation and will therefore, determine the band width[118]. For the ν_1 vibration $h\omega$ is about ten times kT so it is expected that phase relaxation will control the band broadening.

The interactions change as a function of time according to the motions of the molecules. The short time part of the vibrational correlation function exhibits the static structure of the liquid. The band is said to be inhomogeneously broadened[117]. At longer times the static structure is averaged out by the molecular motions of the surrounding molecules and the band is said to be motionally narrowed[110]. Now only pure phase relaxation remains and the band is said to de homogeneously broadened.

Previous studies on ν_1 of the pure liquid by Yarwood[110] and Schroeder[112] found no additional motional narrowing on increasing the temperature. This implies that as the attractive forces which may contribute to the band width are thermally averaged out and the band is not narrowed these interactions are probably not be a major factor in determining the width if this particular band. This in turn might suggest that repulsive interactions play a mojor role in determining the width of this band. Dilution studies in CCl_4 by Yarwood[110] et al showed quite a sharp decrease in τ_v on increasing the concentration of CH_3CN, going to a much less steep curve at 0.2m.f. This a similar but reverse trend to that shown by τ_{1r} far-infrared multimolecular correlation time. (see chapter V). One might suggest that this is due to the presence of 'clusters' of CH_3CN which only break up when the dilution of CH_3CN

molecules falls to 0.2 mole fraction. However, as pointed out by Yarwood[110] there is no reason why the contribution of CH_3CN molecules to the intermolecular potential should be linear. On going from the pure liquid to a very dilute solution τ_v increased from 1.5p.s. to 2.8p.s. This shows that as the slowly varying (r^{-6} dependence) dipolar interactions are removed and replaced by interactions with the CCl_4 solvent the vibrational relaxation gets slower. The remaining interactions which cause the band broadening may be due to dispersive (r^{-6} dependence), inductive, (r^{-6}) octopolar (less than r^{-8}) or repulsive interactions (r^{-12})[110]. In another paper by Yarwood, work on CH_3CN diluted in both polar and non-polar solvents was reported[119]. Here it was found that the band was $1cm^{-1}$ wider in the polar solvent CD_3NO_2 than in the pure liquid and between 1 and $2cm^{-1}$ narrower in other non-polar solvents (CS_2, C_6D_6, (CH_2Br_2). This suggests that assuming additional forces present in these solvents above those in the pure liquid are not tco great about $5cm^{-1}$ of the band broadening is caused by other interactions than dipole-diploe interactions. The additional interactions would be due to greater inductive, dispersive and repulsive forces. However, the theory developed by Döge[116] suggests that the dipole-dipole interactions are strongly dependent on the lengths of the interacting dipoles and these are difficult to estimate. Therefore, it is difficult to monitor what effects are expected if ground state dipolar interactions are important in vibrational band broadening. Transition dipole interactions (leading to resonant energy transfer between adjacent vibrating molecules) were not thought to contribute very much to broadening of the ν_1 band since there was very little effect when CH_3CN was diluted in CD_3CN in which the transition dipole is

much different to that in the pure liquid because of its different normal coordinate for the ν_1 vibration.

VI.2Kubo Line Shape Theory.

According to Rothschild[117], since the vibrational correlation functions have a short time Gaussian part and a long time Lorentzian tail and there is no inflexion between them, then the average spread of transition frequencies at zero time $\langle\omega^2\rangle$ can be identified by the normalised vibrational second moment of the band

$$\langle\omega^2\rangle = M_2 = \frac{\int_{\omega_o}^{\infty} I_{iso}(\omega-\omega_o)\ (\omega-\omega_o)^2\ d\omega}{\int_{\omega_o}^{\infty} I_{iso}(\omega-\omega_o)\ d\omega} \qquad \text{.....VI.5}$$

where ω_o is the band centre. If vibrational energy relaxation is slow compared with dephasing then it can be ignored as determining the band width. The binary collision model of Fischer and Laubereau[121] has The energy relaxation 10^{-6} to 10^{-8} slower than phase relaxation. However, energy relaxation or the intrinsic line width of the band can be measured using picosecond pulse laser techniques[126]. In this experiment a pump pulse from the laser increases the population of molecules in the excited vibrational state. This gives rise to enhanced anti-Stokes Raman scattering of a second pulse of different frequency. Varying the delay time between the pump and probe pulse, the rise and decay of the excess density of molecules in the excited state is observed. The decay of the scattering signal is a direct measure of the energy relaxation time. Using this method Harris[122] has obtained a value for the intrinsic relaxation time of ν_1 of CH_3CN of 5.3p.s. Thus if these measurements are accurate energy relaxation is not slow enough to be neglected[122].

Assuming only phase relaxation, then Kubo[123] has shown that for each process that contributes to[116] Φ_{pp}

$$\Phi_{pp}(t)=\exp(-\langle\omega^2\rangle[t\tau_c+\tau_c^2\ \exp(-t/\tau_c)-1])\text{..VI.6}$$

where τ_c is the correlation time for the fluctuations in the intermolecular potentials. It is a measure of the rate at which the band is 'motionally' narrowed. If the potentials are slowly varying - slow modulation - i.e. $\langle\omega^2\rangle 1/2\tau_c \gg 1$, then

$$\Phi_{pp}(t)=\exp(-1/2\langle\omega^2\rangle t^2) \qquad \text{.....VI.7}$$

τ_c is not involved. This is a Gaussian function. This equation also applies to the short time part of the fast modulation case. For long times in the slow modulation limit

$$\Phi_{pp}(t)=\exp(-\langle\omega^2\rangle t\tau_c+\langle\omega^2\rangle\tau_c^2) \qquad \text{.....VI.8}$$

In the fast modulation limit $\langle\omega^2\rangle 1/2\tau_c \ll 1$ then

$$\Phi_{pp}(t)=\exp(-\langle\omega^2\rangle\tau_c t) \qquad \text{.....VI.9}$$

This is a Lorentzian correlation function. As already stated observed correlation functions have a small Gaussian short time part $t \ll \tau_c$ which in the model[117] corresponds to oscillators vibrating with random phase in different molecular environments which have not yet had time to rearrange through fluctuations (and the initial phase is rapidly lost since each perturbation remains significant for a long time) as time increases and $t \gg \tau_c$. M_2 and τ_c determine the phase loss in the rapid modulation limit where there is slower loss of phase as the effect of rapid perturbations decreases rapidly and a Lorentzian profile is observed. The slope of $\log_e\Phi_{pp}(t)$ versus t is $-\langle\omega^2\rangle\tau_c$ so if τ_v vibrational relaxation = τ_{pp} phase relaxation and the vibrational correlation function is Lorentzian then

$$\Phi_{pp}(t)=\exp(-t/\tau_{pp})=\exp(-\langle\omega^2\rangle t\tau_c) \qquad \text{.....VI.10}$$

and

$$1/\tau_{pp} = \langle\omega^2\rangle \tau_c \qquad \text{.....VI.11}$$

$\langle\omega^2\rangle$ can be measured for the ν_1 band since the high frequency side of the band is undisturbed for $50cm^{-1}$ from the band centre. In this work τ_v and τ_c have been evaluated for a series of solutions in which CH_3CN is subject to long-range slowly varying (with distance) interactions with methanol. In fact CD_3OD was used in order to avoid interference from the ν_1 band of the H compound.

VI.3 Experimental

All the spectra were recorded at the Institut fur Physikalische Chemie der Technischen Universitat, Braunschweig, West Germany, in collaboration with Professor G. Doge and his research team.

The spectra were recorded on a Coderg LRT80 Laser Raman Spectrometer connected to a Spectra Physics 171-06 Argon Ion Laser operating on the green line (514.5nm). The power was adjusted depending on the concentration of CH_3CN in the sample but was between 1 and 4 Watts at the sample.

The laser light was polarised before entering the sample and after the sample a rotating analyser allowed the polarised (I_{VV}) and depolarised (I_{VH}) components of the scattered light to be separated. The analyser was placed at 90° to the incident beam with the polarised light being scrambled before it entered the photomultiplier to avoid any difference in sensitivity the photomultiplier might have to the polarisation of the radiation. The scattered radiation was scanned through a spectral slit of width no greater than $1.3cm^{-1}$. The width depended on the concentration of CH_3CN in the solution. This is varied to give a high signal to noise ratio in the spectrum without putting too

much slit function in the measured band. A slit of 1.3cm^{-1} is 28% of the band width which is low enough to avoid band distortion[110]. The resolution from a slit of this size puts a theoretical long-time reliable limit in the correlation function of[91] $t_{max}=\pi/\Delta\omega$ = 12p.s. The time constant of the detection system was also adjusted to give a smoother signal but was not made too slow as to interfere with the speed at which the spectra were digitised. The time constant was usually 0.1secs. and the spectra sampled for 5secs. at every 0.25cm^{-1}. This was achieved by use of a stepping motor to drive the monochromater and a photon count integrator attached to the photomultiplier. The total number of counts at each frequency interval was punched on paper tape by a Facit 4070 punch. The spectrum was also displayed on a Servoscribe chart recorder.

The samples were contained in a glass 1cm section ultra-violet cell. All the liquids were spectroscopic grade. The CD_3OD was supplied by CIBA-Geigy. The liquids were distilled before use in order to remove dust particles which can scatter light and put noise in the spectrum. The temperature of the sample was maintained at 15°C by circulating water from a Hacke F.S. temperature controller.

VI.4 Computation

The spectra were analysed in Durham on program NEW1. The program performs several manipulations on the data. First the points were linearly interpolated to 0.125cm^{-1} intervals in order to permit more accurate location of the band centre. The band centre was taken as the average of the centre of the band at 70, 80 and 90% of the band height. The accuracy in the peak positions is estimated to be + or - 0.5cm^{-1}. A Gaussian slit function of width equal to the slit width used was then

deconvoluted from the band. The normalised second moments were then calculated. Next the isotropic function was calculated, the band was normalised and the Fourier transform of the centre outwards to about $50cm^{-1}$ away from the band centre was performed using a 'slow' Fourier transform method to calculate the cosine transform. The $50cm^{-1}$ scanned frequency limit yields a time resolution in the correlation function of[91] $\Delta t=\pi/\omega max.=0.3p.s.$ τ_v was obtained by integration, 1/e drop and from the slope of $\log_e$ of the correlation function.

The errors in the calculation of τ produced by random noise in the spectra are not thought to lead to errors of more than + or - 0.1p.s. Errors in the calculation of the vibrational second moments are much greater. It is now thought that their computation up to 50 cm^{-1} from the band centre is about half as far as is necessary to properly obtain M2(vib.) (see ref. 112). This means that the M2 values are all smaller by an inestimable amount (it might be as much as 50%) than they should be. Discussion involving M2 can thus only be on a qualitative level.

VI.5 Description of Solutions

A series of three experiments was performed.

a) The ratio of CD_3OD to CH_3CN was kept constant at 4:1 while the relative amount of CCl_4 was increased from 0.0 to 0.8 mole fraction.

b) The concentration range of CH_3CN in CD_3OD was studied from 0.07 to 0.9 mole fraction.

In both a and b, the band was measured from 2900 to $2950cm^{-1}$ i.e. approximately $6cm^{-1}$ beyond the band maximum.

c) A short concentration range of CD_3CN in CH_3OH of 0.07 to 0.2 mole fraction. The peak frequency in the deuterated compound is at approximately $2115cm^{-1}$. This band has some structure in its low

frequency wing and so the high frequency half of the band was used. The spectra were recorded from 2110 to 2160cm^{-1}.

Examples of spectra are shown in Figs.VI.1,2 and 3.

VI.5 Results and discussion

a) $CH_3CN/CD_3OD/CCl_4$ System

Table VI.1 shows all the data for the $CH_3CN/CD_3OD/CCl_4$ solutions. Fig.VI.4 shows a typical correlation function and Fig.VI.5 is the natural log. of this function.

The variation in the peak frequency of vibration on increasing concentration of CCl_4 is seen as a steady decrease from 2943.375 to 2941.125 cm^{-1}. This is tending towards the value in a dilute solution of CH_3CN in CCl_4 which is 2940.5[110] cm^{-1}. This suggests that the CCl_4 molecules have little difficulty in 'penetrating' the 4 CD_3OD molecules surrounding the central CH_3CN molecule and affecting the C-H stretching vibration. Frequency shifts from the gas phase value of the central Q-branch line are thought to be caused by distortion of the molecule by the reaction field on the central molecule by the field induced in the surrounding molecules[124]. The magnitude of the shift is determined by the dielectric properties of the surrounding molecules. The magnitude of the shift can be obtained from the following expression by Buckingham[124]

$$\Delta\omega/\omega = C + C_1(\epsilon_o - 1/2\epsilon_o + 1) + C_2(\epsilon_\infty - 1/2\epsilon_\infty + 1) \qquad \text{.....VI.12}$$

where the C constants depend only on the vibrating molecule. The greater shift in the presence of CCl_4 molecules suggests that the second term in VI.12 is unimportant i.e. that dipolar forces do not affect the frequency shifts to any large extent. This then implies that the third term in VI.12 is the controlling factor. The greater shift in CCl_4 suggests that this solvent has a higher ϵ_o value than the CH_3CN/CD_3OD

Fig.VI.1 ν_1 band of CH_3CN in $CH_3CN/CD_3OD/CCl_4$. $CH_3CN:CD_3OD$=1:4. Mole fraction of CCl_4 =0.4

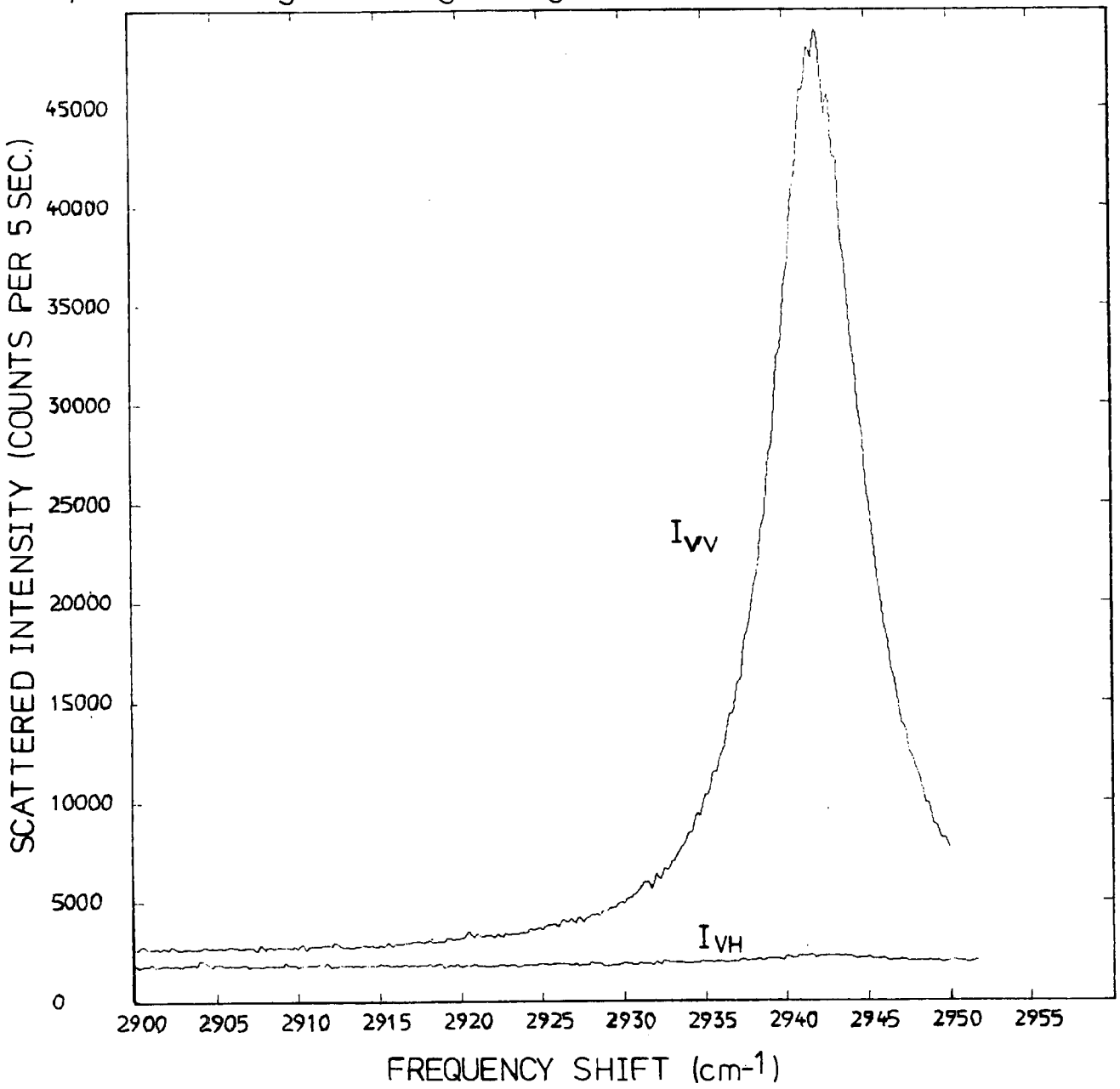

Fig.VI.2. ν_1 of CH_3CN in CH_3C/CD_3OD. Mole fraction of CH_3CN=0.9

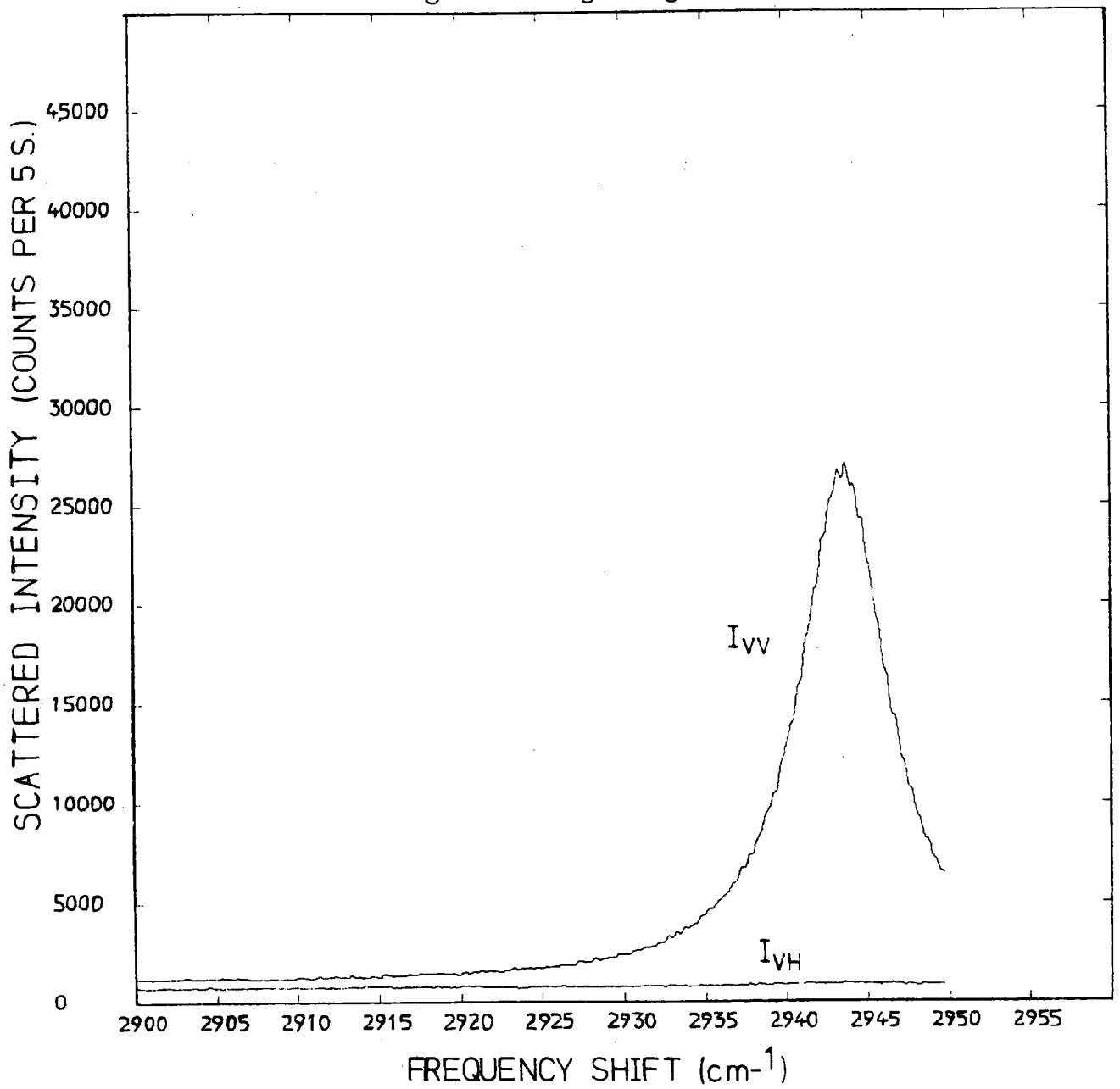

Fig.VI.3. ν_1 of CD_3CN in CD_3CN/CH_3OH. Mole fraction CD_3CN=0·2

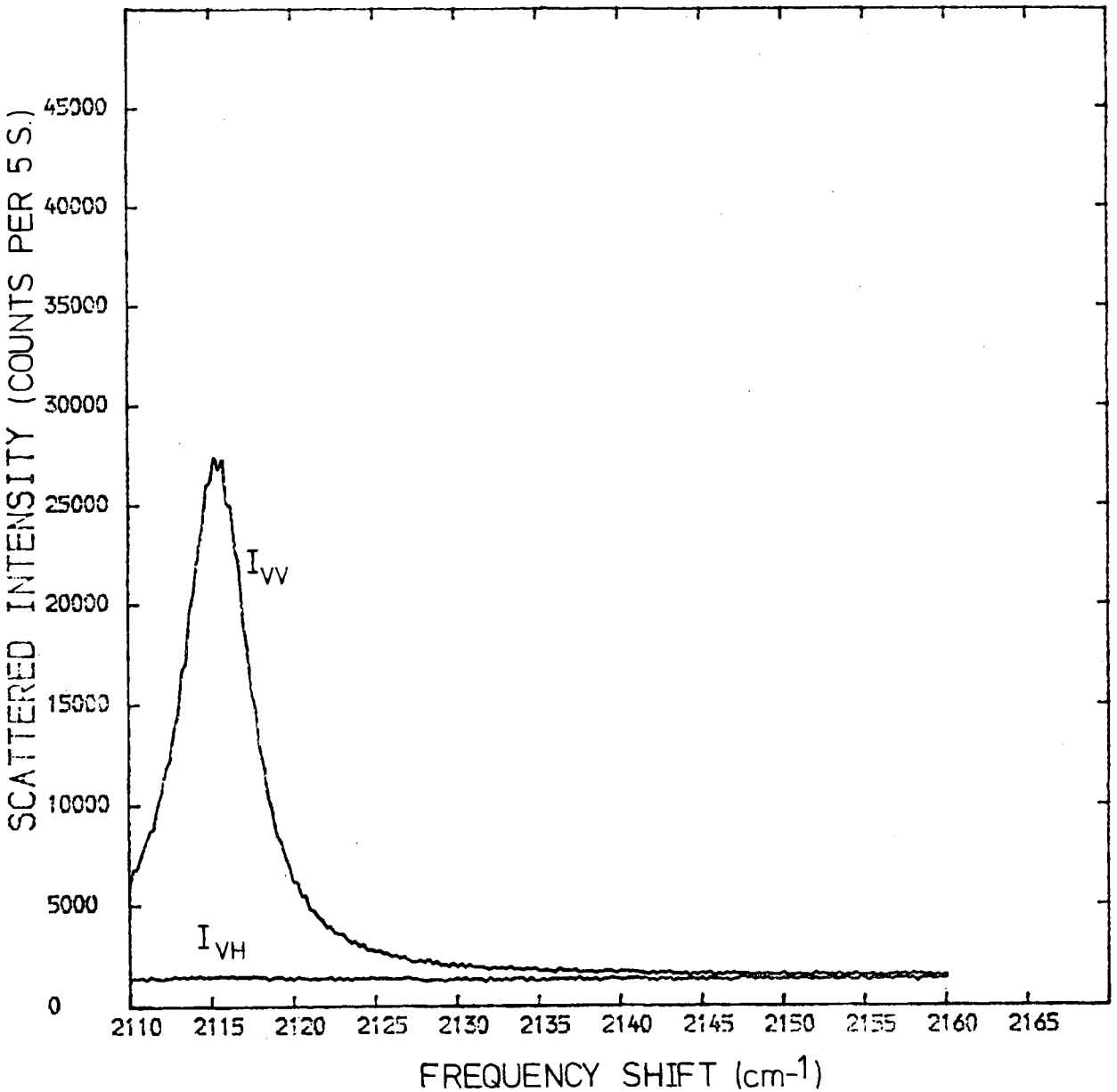

Fig.VI.4. $\Phi_V(t)$ obtained from ν_1 . $CH_3CN/CD_3OD/CCl_4$. Mole fraction of CCl_4 = 0.4

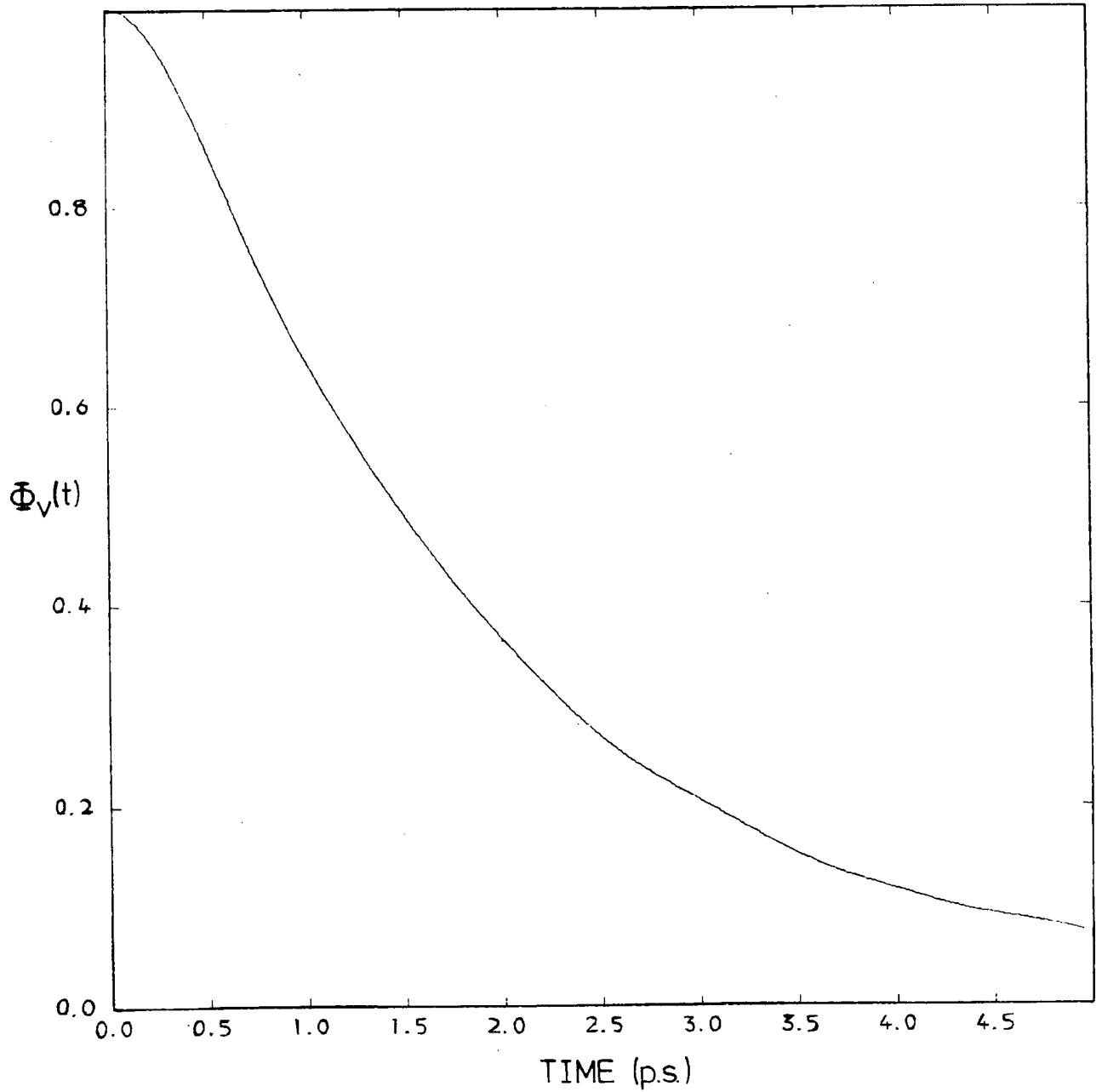

Fig.VI.5. $Log_e \Phi_\nu(t)$ obtained from ν_1. $CH_3CN/CD_3OD/CCl_4$. Mole fraction of CCl_4 = 0.4

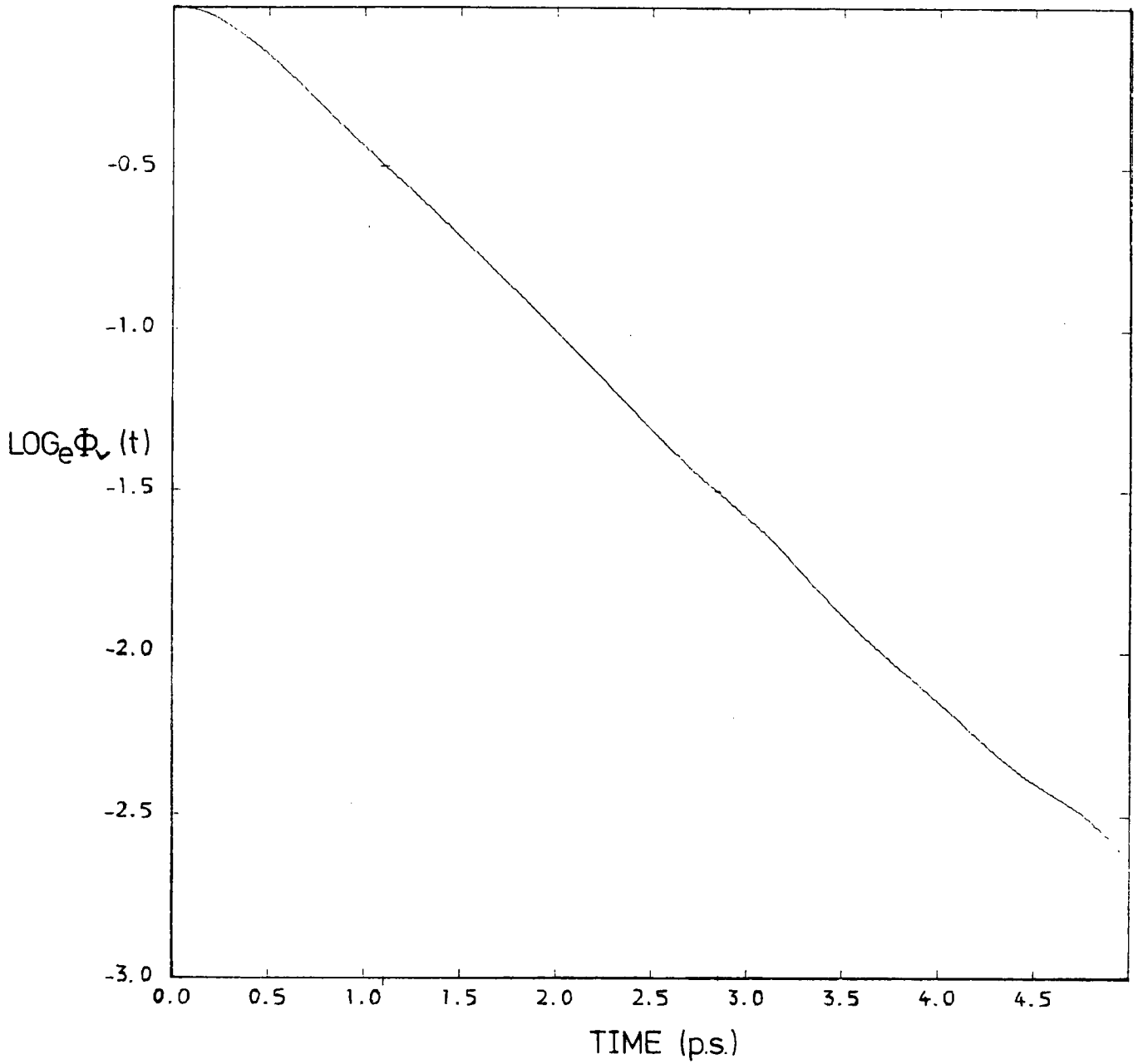

solution and indeed pure CH_3CN[119]. The latter proposition is, however, not borne out by the ϵ_o data obtained by the Kramers-Kronig analysis data presented in chapter V which has CH_3CN and CCl_4 having similar ϵ_o values.

The τ values are shown in table VI.1. First it should be stated that the τ_i values are all smaller than they should be because the correlation function has not decayed to zero at the limit of the integration which was 5p.s. (see Fig.VI.4). It is estimated that the τ_i values are about 5% too small. This means that the τ_i and $\tau_{1/e}$ values are very close to each other both of which are about 10% larger than the τ_s values. Since τ_s measures the relaxation of the long time part (Lorentzian) of the motion this means that the short time Gaussian part of the correlation function adds about 10% to the total relaxation time of the band. Some of the Gaussian contribution will be due to truncation of the band before infinite wavelength i.e. before the band has decayed completely to zero. However, the band was recorded over a range of $40cm^{-1}$ from the band centre at which point the band had become almost completely level (see Fig.VI.1). Therefore, it is thought that most of the Gaussian part is a real reflection of the short time part of the relaxation of the ν_1 vibration. All three sets of correlation times show a steady increasing trend (about 0.5p.s. accross the concentration range) as the concentration of CCl_4 is increased. As with the peak frequencies this is a trend towards the value in a dilute CCl_4 solution (1.66p.s. for a 0.06 mole fraction solution[110]). The M_2 and τ_c data do not show any trend within the experimental error. This means that in the rapid modulation limit (equation VI.9) assumed in this calculation the structure around the probe molecule in all of these solutions decays at

Table VI.1 $CH_3CN/CD_3OD/CCl_4$ Solutions

All τ values are in 10^{-12} seconds. M_2 is in 10^{24} $secs^2$

CCl_4 M.F.	τ_v^l	τ_v^s	$\tau_v^{1/e}$	$\langle\omega^2\rangle$	τ_c^s	$\bar{\nu}$(max)cm^{-1}
0.00	1.70	1.50	1.72	1.31	0.45	2943.375
0.10	1.72	1.55	1.77	1.58	0.37	2942.750
0.218	1.74	1.65	1.85	1.49	0.39	2942.375
0.399	1.87	1.75	2.00	1.34	0.43	2941.875
0.501	1.89	1.70	1.94	1.37	0.39	2941.750
0.596	2.00	1.90	2.14	1.01	0.51	2941.375
0.800	2.21	2.22	2.46	1.02	0.44	2941.125

$CH_3CN:CD_3OD = 1:4$

the same rate. The trends shown by $\bar{\nu}_{max}$ and τ_v indicate that the interactions in the CH_3CN/CD_3OD system are strong enough to cause greater perturbation of the frequency of vibration and faster dephasing of the ν_1 vibration than when CCl_4 molecules are present. These interactions are readily replaced by what is thought to be weaker interactions with CCl_4 molecules leading to slower dephasing. This can be rationalised by the fact that the dipolar and 'hydrogen bonding' interactions affect the CN end of the CH_3CN molecule which is at the opposite end of the molecule to the C-H stretch. The results also suggest that the ratio of 4 CD^3OD molecules to 1 CH_3CN is not maintained in a 'stable' cluster around the CH_3CN since the CCl_4 molecules can get close enough to interact with the CH_3CN molecules. The interactions with CCL_4 molecules will be less in number of pairwise interactions because of its much lower number density than CH_3CN and CD_3OD (10.4 moles per litre compared with 19.1 and 21.9 respectively). This means that each pairwise interaction with CCl_4 molecules in these liquids which leads to the dephasing of the ν_1 band is probably as strong as it is with the other two liquids. These results imply that attractive interactions do not greatly affect the width of the ν_1 vibrational band in these solutions. One might again suggest that repulsive interactions and/or energy relaxation play a major role in determining the width of this band.

b) CH_3CN/CD_3OD and CD_3CN/CH_3OH solutions

Typical correlation functions for these solutions are shown in Figs.VI 6-10. Results from analysis of the bands are shown in table VI.2. The peak frequency data does not show any trend in the CH_3CN/CD_3OD system. This suggests that whatever interactions affect the peak frequency in these solutions they are essentially the same in all of these solutions. In addition, the vibrational relaxation times show only a slight variation across the concentration range, the relaxation in dilute CD_3OD solution being about 0.1 p.s. faster than in the most concentrated solution. These results show that the mechanisms responsible for relaxation in pure CH_3CN and in these solutions lead to very similar relaxation rates. This might suggest that the interactions which lead to band broadening are also similar. There is little variation in τ_c as well, indicating that the structure around the probe molecule which affects the ν_1 vibration is modulated at the same rate across the concentration range.

The data for the CD_3CN/CH_3OH system shows that the relaxation of the band in the deuterated compound is slower than it is in the H-compound. The same behaviour was found for the pure liquids by Schroeder et al[112]. This observation suggests that (if all other interactions are equal in the hydro and deutero compounds) that frequency dependent interactions which cause band broadening are quite important for the ν_1 band. According to the binary collision model of Kaiser et al[121] for vibrational relaxation τ_{pp} is proportional to $1/\omega^2$. This is the opposite trend to that found for the ν_1 band on going from CH_3CN to CD_3CN in which the vibrational frequency falls from about 2943 to about 2115 cm^{-1}. In addition, this model has τ_{er} decreasing exponentially with increasing ω , which is a trend in the same direction as found for the ν_1 vibration on going from CH_3CN to CD_3CN. However, the difference in mass between D and H also affects the band width.[112,121]

Fig.VI.6. $\Phi_v(t)$ from ν_1. CH_3CN/CD_3OD. Mole fraction of $CH_3CN = 0.9$

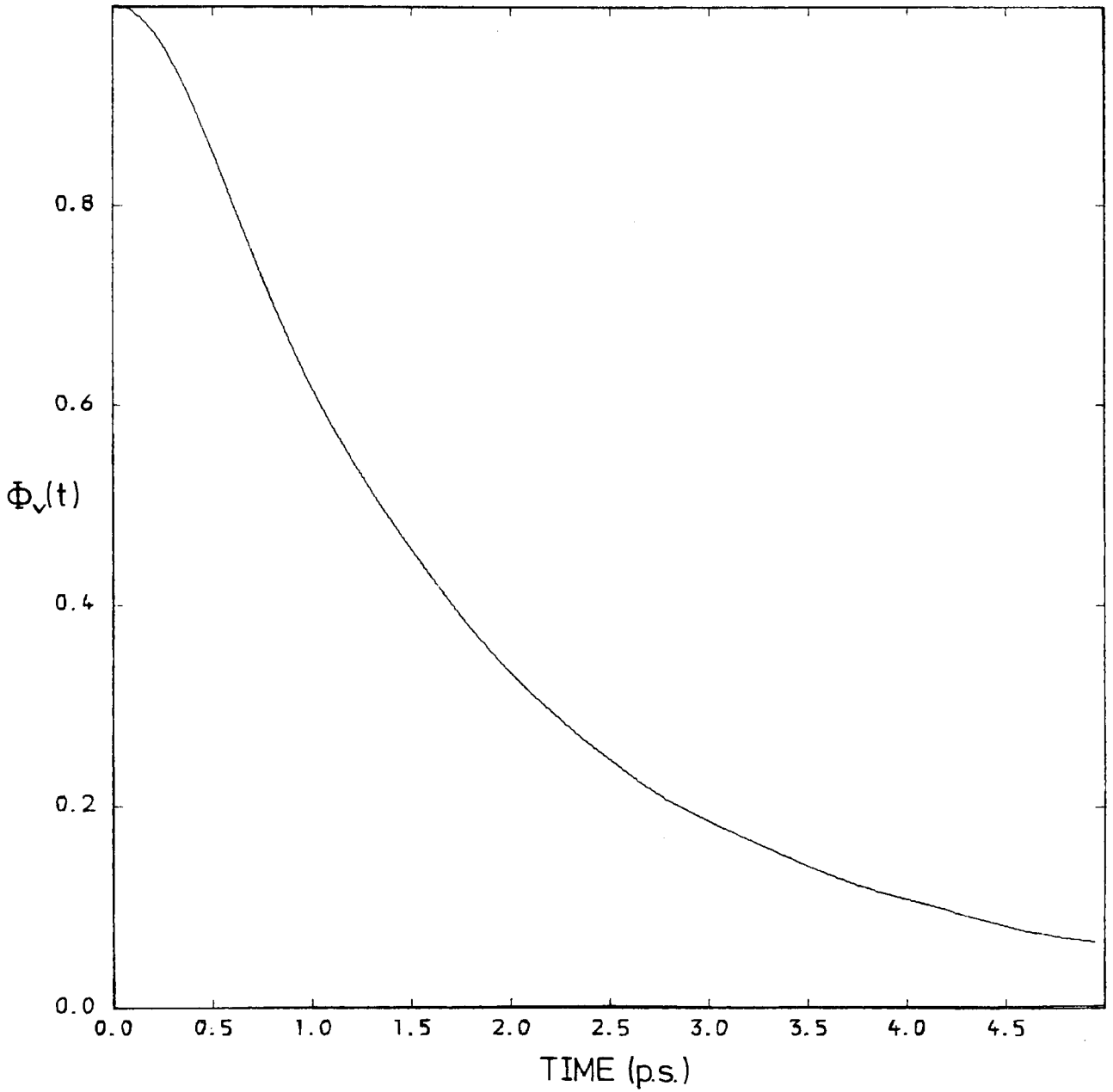

Fig.VI.7. $Log_e \Phi_v(t)$ from ν_1 CH_3CN/CD_3OD. Mole fraction of $CH_3CN = 0.9$

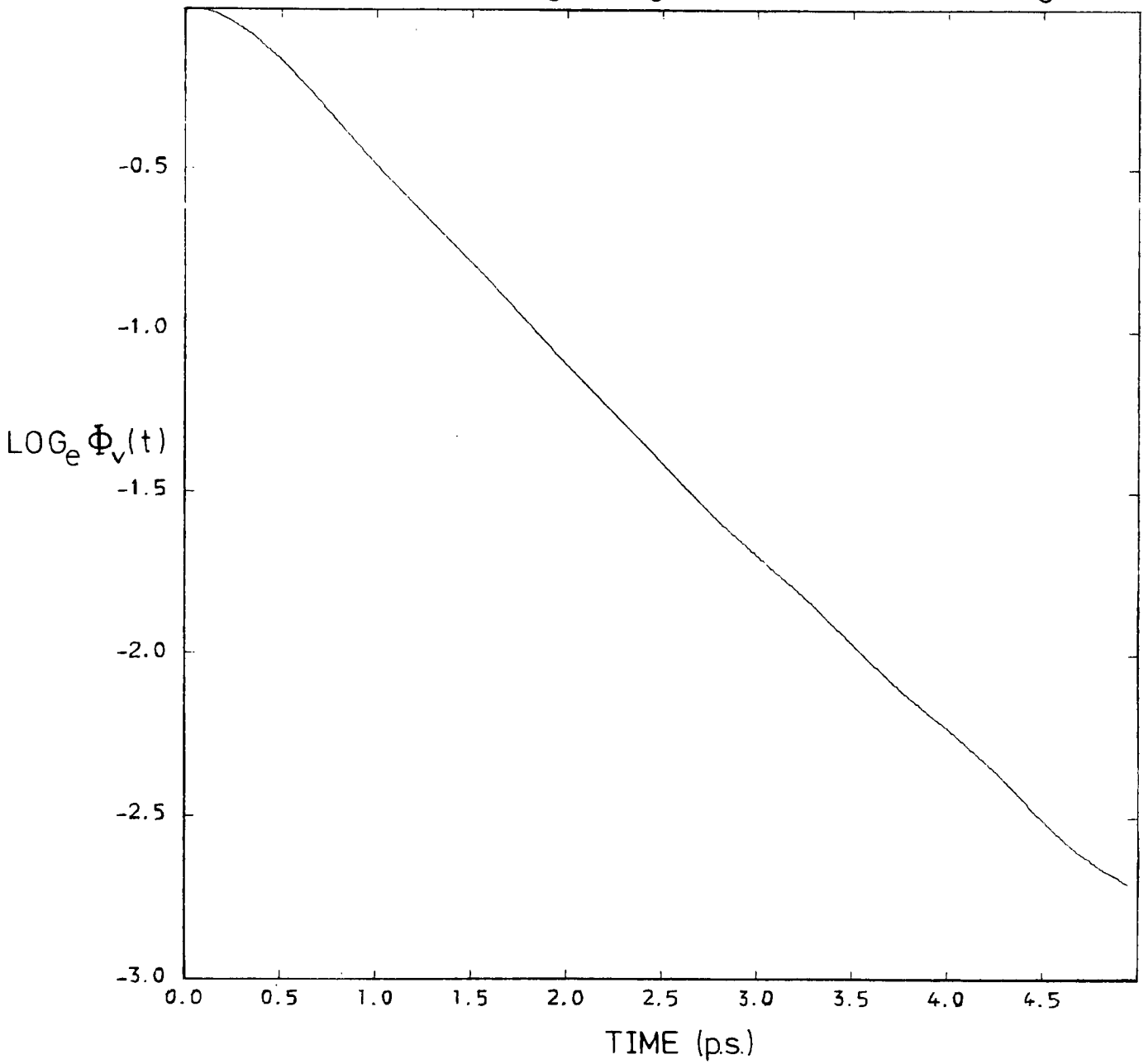

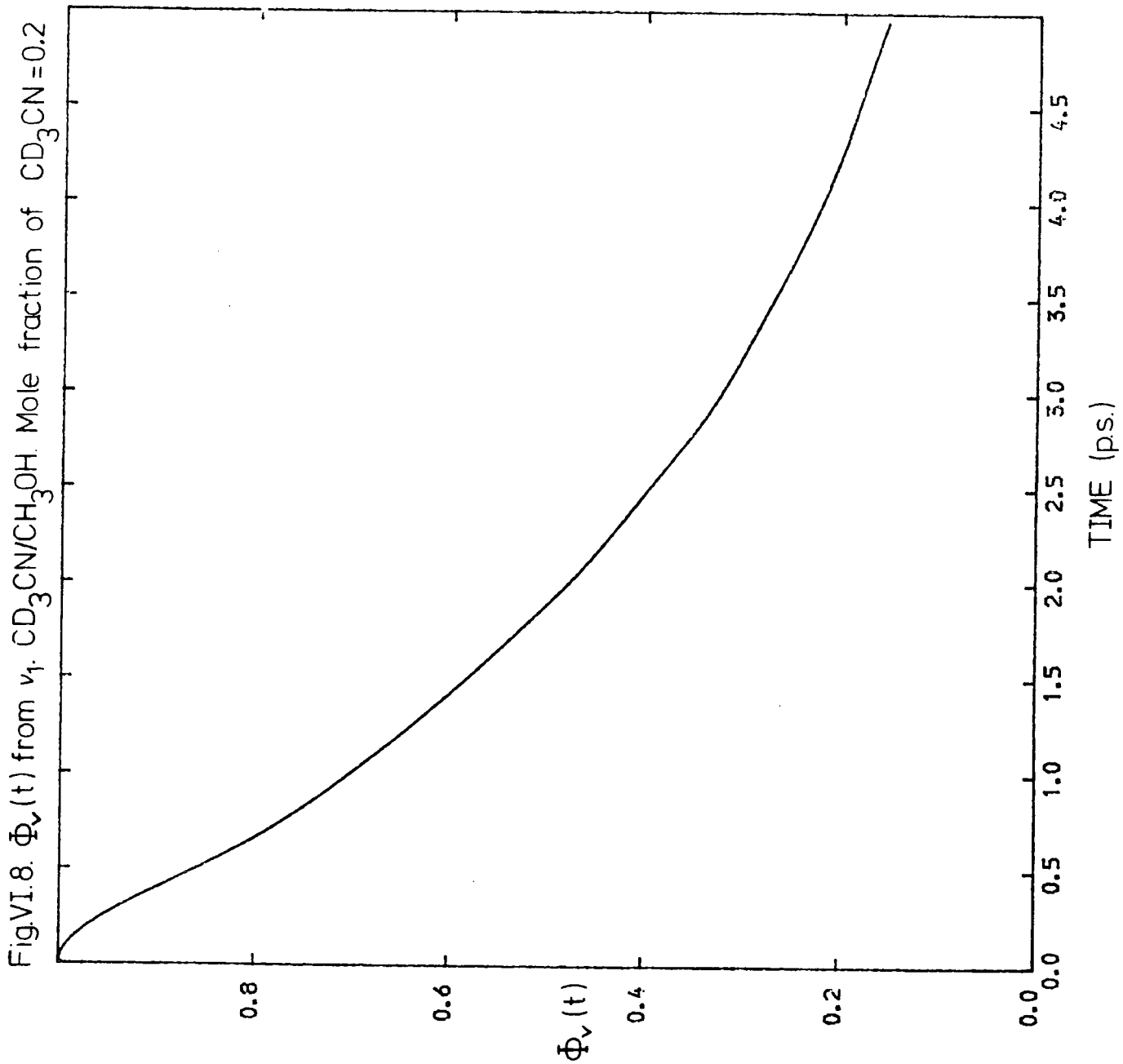
Fig.VI.8. $\Phi_v(t)$ from ν_1. CD_3CN/CH_3OH. Mole fraction of $CD_3CN=0.2$
$\Phi_v(t)$
0.0
0.2
0.4
0.6
0.8
0.0
0.5
1.0
1.5
2.0
2.5
3.0
3.5
4.0
4.5
TIME (p.s.)

Fig.VI.9. $Log_e \Phi_v(t)$ from ν_1. CD_3CN/CH_3OH. Mole fraction of CD_3CN=0.2

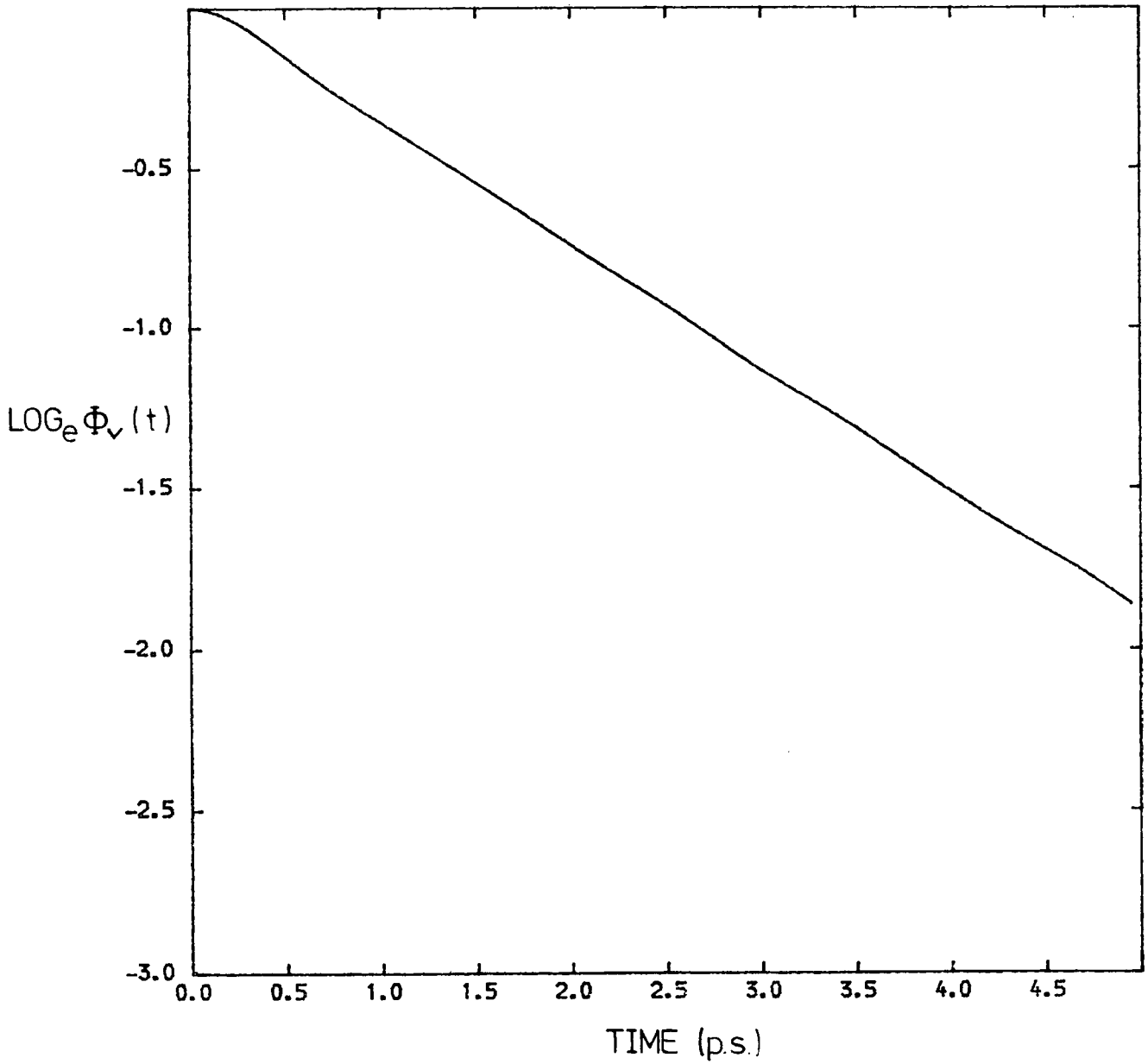

Table VI.2 CH_3CN/CD_3OD and CD_3CN/CH_3OH Solutions

CH_3CN M.F.	τ_v^l	τ_v^s	$\tau_v^{1/e}$	$\langle\omega^2\rangle$	τ_c^l	ν(max)cm^{-1}
0.072	1.61	1.45	1.72	1.73	0.36	2943.00
0.189	1.67	1.52	1.75	1.69	0.35	2943.25
0.318	1.72	1.53	1.80	1.41	0.41	2943.25
0.411	1.73	1.52	1.80	1.56	0.37	2943.25
0.502	1.72	1.53	1.81	1.61	0.36	2943.375
0.608	1.74	1.52	1.82	1.38	0.42	2943.375
0.721	1.75	1.54	1.82	1.35	0.42	2943.00
0.795	1.75	1.54	1.83	1.63	0.35	2943.25
0.894	1.77	1.55	1.84	1.42	0.40	2943.50
CD_3CN/CH_3OH						
CD_3CN M.F.						
0.072	2.27	2.35	2.67	1.45	0.34	2115.0
0.091	2.29	2.72	2.72	1.528	0.29	2115.375
0.189	2.41	2.72	2.79	0.78	0.53	2115.375

All τ values are in picoseconds. The vibrational second moments are in units of 10^{24} $sec.^{-24}$.

VI.6 Conclusions

These results on their own do not enable one to say which of the intermolecular interactions is the dominant cause of dephasing. However, the measurement of the rate of energy relaxation of the ν_1 band in the pure liquid by Harris[122] of 5.3 p.s. means that energy relaxation probably cannot be ignored in these systems. Assuming energy relaxation and phase relaxation are uncorrelated then[3].

$$1/\tau_v = 1/\tau_{er} + 1/\tau_{pp} \qquad \text{.....VI.13}$$

gives values for τ_{er} in the solutions studied here between 2.09 p.s. (solution 1 in the $CH_3CN/CD_3OD/CCl_4$ system) and 5.5p.s. (first solution in the CD_3CN/CH_3OH system). This implies that phase relaxation and energy relaxation contribute broadely similar amounts to the vibrational relaxation time. Clearly measurements of the energy relaxation by the pulsed laser technique[122] would be required on all of the solutions to verify this.

As already mentioned the slower relaxation for ν_1 in CD_3CN than CH_3CN in the solutions studied here agrees with the predictions of the binary collision model of Fischer et al[121] for energy relaxation. This reinforces the proposal that energy relaxation is important for these solutions and that energy levels are depopulated through binary collisions.

References

1. N.Hill, W.E.Vaughn, A.H. Price and M.Davies, 'Dielectric Properties and Molecular Behaviour', Van Nostrand, London (1969).

2. R.T. Bailey,Ir Molecular Spectroscopy Vol.2, eds. R.F. Barrow, D.A. Long and D.J. Mullen, The Chemical Society London (1974).

3. J. Yarwood and R. Arndt in 'Molecular Association Vol 2', ed. R. Foster, Wiley-interscience New York (1978).

4. F. Volino and A.J. Dianoux, Proceedings of meeting on Structure and Dynamics of Organic Liquids, Mittenwald, (1976).

5. S. Abragam, 'The Principles of Nuclear Magnetism', Oxford University Press, London (1961).

6. H. Bertagnolli and M.D. Zeidler, Molecular Physics, 35, 177 (1978).

7. C.F. Bottcher 'Theory of Electric Polarisation', Elsevier, Amsterdam (1952).

8. T. Bien, M. Possiel, G. Doege, J. Yarwood and K.E. Arnold, Chemical Physics, 56,203 (1981).

9. P. Debye, 'Polar Molecules', Reinhold Publishing Corporation, New York, (1929).

10. R.L. Gaither and W.E. Vaughan, Advances in Molecular Relaxation and Interaction Processes, 18, 169 (1980).

11. K. and A. Mansingh, J. Chem. Phys., 41, 827 (1964).

12. B. Janik and E. Kluk, Personal Communication.

13. H. Frolich, 'Theory of Dielectrics', Oxford University Press, London (1949).

14. R.M. Fuoss and J.G. Kirkwood, J. Amer. Chem. Soc., 63, 385 (1941).

15. M.Y. Rocard, J.Phys. Radium Paris, 4, 247 (1933).

16. J.G. Powles, Trans. Faraday Soc., 42a, 802 (1948).

17. C. Brot,In Specialist Periodical Reports, Dielectric and Related Molecular Processes, ed. M. Davies, Vol.2, The Chemical Society, London (1975).

18. D. Kivelson and P. Madden, Mol. Phys., 30, 1749 (1975).

19. H. A. Lorentz, `Theory of Electrons', Leipzig (1909).

20. L. Onsager, J. Amer. Chem. Soc., 58, 1486 (1936).

21. J.G. Kirkwood, J. Chem. Phys., 7, 911 (1939).

22. S.H. Glarum, J. Chem. Phys., 33, 1371 (1960).

23. R.H. Cole, J. Chem. Phys., 42, 637 (1965).

24. J.G. Powles, J. Chem. Phys., 21, 633 (1953).

25. E. Fatuzzo and P.R. Mason, Proc. Phys. Soc., London, 90, 741 (1967).

26. U.M. Titulaer and J.M. Deutch, J. Chem. Phys., 60, 1502 (1974).

27. J.M. Deutch, Faraday Symposium, 11-11/2 (1976).

28. T. Keyes and D. Kivelson, J. Chem. Phys., 56, 1057 (1972).

29. A.K. Burnham, G.R. Alms and W.H. Flygare, J. Chem. phys., 62, 3289 (1975).

30. R. Kubo, J. Phys. Soc. Japan, 7, 911 (1957).

31. R. Zwanzig, Am. Rev. Phys. Chem, 16, 67 (1965).

32. J.S. Rowlinson and M. Evans, Ann. Rep. Chem. Soc., A, 5 (1975).

33. N.E. Hill, J. Phys., C5, 415 (1972).

34. D.D. Klug, D.E. Kranbuehl and W.E. Vaughan, J. Chem. Phys., 50, 3904 (1969).

35. T.W. Nee and R. Zwanzig, J. Chem. Phys., 53, 6352 (1970).

36. L.C. Rosenthal and H.L. Strauss, J. Chem. Phys., 64, 282 (1976).

37. R.G. Gordon, J. Chem. Phys., 43, 1307 (1965).

38. W.G. Rothschild, G.J. Roasco and R.C. Livingston, J. Chem. Phys., 62, 1253 (1975).

39. M.W. Evans, G.J. Evans, J. Yarwood, P.L. James and R. Arndt, Mol. Phys., 38,699 (1979).

40. S.G. Lipson and H. Lipson, 'Optical Physics', Cambridge University Press (1981).

41. L.A. Nafie and W.L. Peticolas, J. Chem. Phys., 57, 3145 (1972).

42. R.M. Lynden-Bell, Mol. Phys., 33, 907 (1977).

43. G. Herzberg, 'Molecular Spectra Vol.2', Van Nostrand, Princeton (1945).

44. H. Versmold, Ber. Bunsenges. Phys. Chem., 82, 451 (1978).

45. W. A. Steele, Adv. in Chem. Phys., XXXIV, 1 (1976).

46. A. Ben Reuven and N.D. Gershon, J. Chem. Phys., 51, 893 (1969).

47. G.J. Evans and M.W. Evans J. Chem. Soc., Faraday 2, 72, 1169 (1976).

48. K.D. Moller and W.G. Rothschild, 'Far-Infrared Spectroscopy', Wiley-Interscience, New York (1971).

49. S.R. Polo and M.K. Wilson, J. Chem. Phys., 23, 2576 (1955).

50. H.A. Kramers, Atti. Congr. Int. Fisici, Como, 2, 545 (1927). R. Kronig, J. Opt. Soc. Amer, 12, 547 (1926).

51. B.J. Berne and G.D. Harp, Adv. in Chem. Phys., 17, 100 (1970).

52. A. Khuen, personal communication.

53. Chamberlain, 'Principles of Interferometric Spectroscopy',Wiley-Interscience, New York (1970).

54. G.P. O'Neill personal communication.

55. D.H. Whiffen, Trans. Faraday Soc., 46, 124 (1950).

56. J. Poley, J. Appl. Sci., B4, 337 (1955).

57. M. Davies, G.W.F. Pardoe, J.E. Chamberlain and H.A. Gebbie, Trans. Faraday Soc., 64, 847 (1968).

58. G.J. Davies and J.E. Chamberlain, J. Chem. Soc. Faraday Trans.2 69, 1739 (1973).

59. R.G. Gordon, J. Chem. Phys., 38, 1724 (1963).

60. R.G. Gordon, J. Chem. Phys., 44, 1830 (1966).

61. A. Gerschel, I. Damron and C. Brot, Mol. Phys.m 23, 317 (1972).

62. M.W. Evans,in Specialist Periodical Reports, Dielectric and Related Molecular Processes, ed. M. Davies, Vol.3, The Chemical Society, London, 1 (1977).

63. W.T. Coffey, G.J. Evans, M.W. Evans and G.H. Wedgam, J. Chem. Soc., Faraday 2, 74, 310 (1978).

64. R. Kubo,in Reports on Progress in Physics, Vol.29, ed. A.C. Strickland, Inst. of Physics, London (1966).

65. H. Mori, Prog. Theor. Phys. 33, 423 (1965).

66. N.E. Hill, Proc. Phys. Soc., 82, 723 (1963).

67. J.H. Calderwood and W.T. Coffey, Proc. R. Soc., A356, 269 (1977).

68. G. Wyllie, in Specialist Periodical Reports, Dielectric and Related Molecular Processes, ed. M. Davies, Vol.1, The Chemical Society, London, 21 (1972).

69. B. Lassier and C. Brot, Discussions of the Faraday Society, 48, 39 (1969).

70. J.R. Birch, M.N.Afsar, J. Yarwood and P.L. James, I.R. Phys., 21, 9 (1980).

71. J. Yarwood, P.L. James, G. Doge and R. Arndt, Faraday Disussions of The Chemical Society, 66, 252 (1978).

72. Kramer, Zeit. Phys., 157 134 (1959).

73. A.H. Price and G.H. Wegdam, J. Phys. E, 10, 478 (1977).

74. P. Penfield and P.P. Rafuse, 'Varactor Applications', M.I.T. Press, Cambridge, Mass. (1962).

75. J. Eloranta and P.K. Kadaba, Mat. Sci. Eng., 8, 203 (1971).

76. R.J. Bell, 'Introductory Fourier Transform Spectroscopy', Academic Press, London and New York, (1972).

77. J.W. Cooley and J.W. Tukey, Math. Comput., 19, 297 (1965).

78. D.H. Martin and E. Puplett, Infrared Physics, 10, 105 (1969).

79. P.L. James, M.Sc. thesis, Durham (1976).

80. J.R. Birch and T.J. Parker, in 'Infrared and Millimeter Waves', Vol.2, Ed. K.J. Button, Academic Press, New York, (1979).

81. J.R. Birch, J.D. Dromey and J. Lesurf, NPL Report DES 69 (1981).

82. M.L. Forman, W.H. Steel and G.A. Vanasse, J. Opt. Soc. Amer., 56, 59 (1966).

83. B.J. Bulkin, Helv. Chim. Acta., 52, 1348 (1969).

84. P. Hindle, S Walker and J. Warren, J. Chem. Phys., 62, 3230 (1975).

85. E. Knozinger, D. Leutloff and R. Wittenbeck, J. Molec. Struct., 60, 115 (1980).

86. G.W. Chantry, IEEE Transactions on Microwave Theory and Techniques, Vol.Mtt-25, 6, 496 (1977).

87. 'Handbook of Chemistry and Physics', The Chemical Rubber Co., Cleveland, 60, (1980)

88. K. Sato, Y. Ohkubo, T. Moritsu, S. Ikawa and M. Kimura, Bull. Chem. Soc. Japan, 51, 2493 (1978).

89. C. Ried, Ph.D. Thesis, U.C.W., Aberystwyth, (1979).

90. E. Kestemont, F. Hermans, R.Finsy and R. Van Loon, Infrared Physics, 18, 855 (1978).

91. B. Keller and F. Kneubhuhl, Helv. Phys. Acta., 45, 1127 (1972).

92. S. Ikawa, K. Sato and M. Kimura, Chem. Phys., 47, 65 (1980).

93. P. Kruus, 'Liquids and Solutions Structure and Dynamics', Marcel Dekker, New York, (1977).

94. D. Leutloff and E. Knozinger, Spectrosc. Lett., 12, 815 (1979).

95. T.T. Bopp, J. Chem. Phys., 47, 3621 (1967).

96. C. Breuillard-Alliot and J. Soussen-Jacob, Mol. Phys., 28, 905 (1974).

97. A.V. Rakov, Opt. Spectrosc., 13, 203 (1962).

98. J.E. Griffiths, J. Chem. Phys., 75, 751 (1973).

99. F.J. Bartoli and T.A. Litovitz, J. Chem. Phys., 56, 413 (1972).

100. A.M. Aman da Costa, M.A. Norman and J.H.R. Clarke, Mol. Phys., 29, 191 (1975).

101. S.L. Whitterburg and C.H. Wang, J. Chem. Phys., 66, 4255 (1977).

102. T.E. Bull, J. Chem. Phys., 62, 222 (1975).

103. P.S. Hubbard, Phys. Rev., 131, 1155 (1963).

104. C.S. Hsu and D. Chandler, Mol. Phys., 36, 215 (1978).

105. L. Blum and A.H. Narten, J. Chem. Phys., 64, 2804 (1976).

106. C.J. Ried and M.W. Evans, J. Chem. Soc., Faraday 2, 76, 286 (1980).

107. W. Steele, in 'Advances in Chemical Physics', Wiley-Interscience, New York (1974).

108. D.J. Adams, Meeting of the Royal Society of Chemisty, Faraday Division, Statistical Mechanics and Thermodynamics Group, Cambridge, April (1981).

109. J.P. Hansen and I.R. McDonald, 'Theory of Simple Liquids', Academic press, New York, (1976).

110. J. Yarwood, R. Arndt and G. Doge, Chem. Phys., 25, 387 (1977).

111. J. Yarwood, R. Arndt and G. Doge, Chem. Phys., 42, 331 (1979).

112. J. Schroeder, V.H. Schiemann, P.J. Sharko and J. Jonas, J. Chem. Phys., 66, 3215 (1977).

113. K. Tanabe, Chem. Phys., 38, 125 (1979).

114. J.E. Griffiths, J. Chem. Phys., 59, 751 (1973).

115. S. Bratos and E. Marechal, Phys. Rev. A4, 1078 (1972).

116. G. Doge, Z. Naturforsch, 23a, 1405 (1968); 28a, 919 (1973), in Molecular Motions in Liquids ed. J. Lascombe (Reidel, Dordrecht, 1974) p.225.

117. W.G. Rothschild, J. Chem. Phys., 65, 455 (1976).

118. R. Arndt, G. Doge and A. Khuen, Chem. Phys. Lett., 42, 1 (1977).

119. J. Yarwood, R. Ackroyd, K.E. Arnold, G. Doge and R. Arndt, Chem. Phys. Lett., 77, 239 (1981).

120. T. Yoshino and H.J. Bernstein, J. Mol. Spec., 2, 241 (1958).

121. S.F. Fischer and A. Laubereau, Chem. Phys. Lett., 35, 6 (1975).

122. S.M. George, H. Auweter and C.B. Harris, J. Chem. Phys., 73, 5573 (1980).

123. R. Kubo, In 'Fluctuation, relaxation and resonance in magnetic systems' ed. D. Ter Haar, Oliver and Boyd, Edinburgh, (1962).

124. A. Lovenstein and Y. Margalit, J. Phys. Chem., 69, 4152 (1965).

125. A.D. Buckingham, Proc. Roy. Soc., A248, 169 (1958).

126. A. Laubereau, D. Von Der Linde, and W. Kaiser, Phys. Rev. Lett., 28 1162 (1972).

APPENDIX 1.

a) Lectures and Seminars organised by the Department of Chemistry during the period 1978-1981

(* denotes those attended)

15 September 1978*

Professor W. Siebert (University of Marburg, West Germany), "Boron Heterocycles as Ligands in Transition Metal Chemistry".

22 September 1978

Professor T. Fehlner (University of Notre Dame, USA), "Ferraboranes: Syntheses and Photochemistry".

12 December 1978

Professor C.J.M. Stirling (University of Bangor), "'Parting is such sweet sorrow' - the Leaving Group in Organic Reactions".

14 February 1979*

Professor B. Dunnell (University of British Columbia), "The Application of NMR to the Study of Motions in Molecules".

16 February 1979*

Dr. J. Tomkinson (Institute of Laue-Langevin, Grenoble), "Properties of Adsorbed Species".

14 March 1979

Dr. J.C. Walton (University of St. Andrews), "Pentadienyl Radicals".

20 March 1979

Dr. A. Reiser (Kodak Ltd.), "Polymer Photography and Mechanism of Cross-link Formation in Solid Polymer Matrices".

25 March 1979

Dr. S. Larsson (University of Uppsala), "Some Aspects of Photoionisation

Phenomena in Inorganic Systems".

25 April 1979*

Dr. C.R. Patrick (University of Birmingham), "Chlorofluorocarbons and Stratospheric Ozone: An Appraisal of the Environmental Problem".

1 May 1979*

Dr. G. Wyman (European Research Office, US Army), "Excited State Chemistry in Indigoid Dyes".

2 May 1979

Dr. J.D. Hobson (University of Birmingham), "Nitrogen-centred Reactive Intermediates".

8 May 1979

Professor A. Schmidpeter (Institute of Inorganic Chemistry, University of Munich), "Five-membered Phosphorus Heterocycles Containing Discoordinate Phosphorus".

9 May 1979*

Dr. A.J. Kirby (University of Cambridge), "Structure and Reactivity in Intramolecular and Enzymic Catalysis".

9 May 1979

Professor G. Maier (Lahn-Giessen), "Tetra-tert-butyltetrahedrane".

10 May 1979*

Professor G. Allen, F.R.S. (Science Research Council), "Neutron Scattering Studies of Polymers".

16 May 1979

Dr. J.F. Nixon (University of Sussex), "Spectroscopic Studies on Phosphines and their Coordination Complexes".

23 May 1979

Dr. B. Wakefield (University of Salford), "Electron Transfer in

Reactions of Metals and Organo-metallic Compounds with Polychloropyridine Derivatives".

13 June 1979

Dr. G. Heath (University of Edinburgh), "Putting Electrochemistry into Mothballs (Redox Processes of Metal Porphyrins and Phthalocyanines)".

14 June 1979*

Professor I. Ugi (University of Munich), "Synthetic Uses of Super Nucleophiles".

20 June 1979

Professor J.D. Corbett (Iowa State University, Ames, Iowa, USA), "Zintl Ions: Synthesis and Structure of Homo-polyatomic Anions of the Post-Transition Elements".

27 June 1979

Dr. H. Fuess (University of Frankfurt), "Study of Electron Distribution in Crystalline Solids by X-ray and Neutron Diffraction".

21 November 1979

Dr. J. Muller (University of Bergen), "Photochemical Reactions of Ammonia".

28 November 1979

Dr. B. Cox (University of Stirling), "Macrobicyclic Cryptate Complexes, Dynamics and Selectivity".

5 December 1979

Dr. G.C. Eastmond (University of Liverpool), "Synthesis and Properties of some Multicomponent Polymers".

12 December 1979*

Dr. C.I. Ratcliffe (University of London), "Rotor Motions in Solids".

19 December 1979*

Dr. K.E. Newman (University of Lausanne), "High Pressure Multinuclear NMR in the Elucidation of the Mechanisms of Fast, Simple Reactions".

30 January 1980*

Dr. M.J. Barrow (University of Edinburgh), "The Structures of some Simple Inorganic Compounds of Silicon and Germanium - Pointers to Structural Trends in Group IV".

6 February 1980

Dr. J.M.E. Quirke (University of Durham), "Degradation of Chlorophyll-a in Sediments".

23 April 1980

B. Grievson B.Sc. (University of Durham), "Halogen Radiopharmaceuticals".

14 May 1980

Dr. R. Hutton (Waters Associates, USA), "Recent Developments in Multi-milligram and Multi-gram Scale Preparative High Performance Liquid Chromatography".

21 May 1980

Dr. T.W. Bentley (University of Swansea), "Medium and Structural Effects in Solvolytic Reactions".

10 July 1980

Professor P. des Marteau (University of Heidelburg), "New Developments in Organonitrogen Fluorine Chemistry".

7 October 1980*

Professor T. Felhner (Notre-Dame University, USA), "Metalloboranes - Cages or Coordination Compounds?".

15 October 1980*

Dr. R. Adler (University of Bristol), "Doing Chemistry Inside Cages -

Medium Ring Bicyclic Molecules".

12 November 1980*

Dr. M. Gerloch (University of Cambridge), "Magnetochemistry is about Chemistry".

19 November 1980

Dr. T. Gilchrist (University of Liverpool), "Nitroso Olefins as Synthetic Intermediates".

3 December 1980

Dr. J.A. Connor (University of Manchester), "Thermochemistry of Transition Metal Complexes".

18 December 1980*

Dr. R. Evans (University of Brisbane, Australia), "Some Recent Communications to the Editor of the Australian Journal of Failed Chemistry".

18 February 1981*

Professor S.F.A. Kettle (University of East Anglia), "Variations in the Molecular Dance at the Crystal Ball".

25 February 1981

Dr. K. Rowden (University of Sussex), "The Transmission of Polar Effects of Substituents".

4 March 1981

Dr. S. Craddock (University of Edinburgh), "Pseudo-linear Pseudohalides".

11 March 1981*

Dr. J.F. Stoddart (I.C.I. Ltd./University of Sheffield), "Stereochemical Principles in the Design and Function of Synthetic Molecular Receptors".

17 March 1981*

Professor W. Jencks (Brandeis University, Massachusetts), "When is an Intermediate not an Intermediate?".

18 March 1981*

Dr. P.J. Smith (International Tin Research Institute), "Organotin Compounds - A Versatile Class of Organo-metallic Compounds".

9 April 1981

Dr. W.H. Meyer (RCA Zurich), "Properties of Aligned Polyacetylene".

6 May 1981*

Professor M. Szwarc, F.R.S., "Ions and Ion Pairs".

10 June 1981*

Dr. J. Rose (I.C.I. Plastics Division), "New Engineering Plastics".

17 June 1981

Dr. P. Moreau (University of Montpellier), "Recent Results in Perfluoroorganometallic Chemistry".

Appendix 2.

Conferences attended during the period 1978-1981

1. Spectroscopy Group of Institute of Physics, "Aspects of Submillimetre Spectroscopy", Westfield College, London, December 1978.

2. The Chemical Society, Statistical Mechanics and Thermodynamics Group, "Polar Fluids", Aberystwyth, September 1979.

3. Annual Congress of the Chemical Society and the Royal Institute of Chemistry, Durham University, April 1980.

4. Royal Society of Chemistry, Statistical Mechanics and Thermodynamics Group, "The Structure of Molecular Liquids", Cambridge, April 1981.

5. Spectroscopy Group of Institute of Physics, "Special Techniques for the Submillimetre Region", Westfield College, London, April 1981.

Appendix 3

Chemical Physics 56 (1981) 203–211
North-Holland Publishing Company

STUDIES OF MOLECULAR MOTIONS AND VIBRATIONAL RELAXATION IN ACETONITRILE. VII. USE OF THE ROTATIONAL DIFFUSION MODEL TO INVESTIGATE THE BAND SHAPES OF THE ν_5 AND ν_8 BANDS OF CH_3CN IN THE LIQUID PHASE

T. BIEN, M. POSSIEL, G. DÖGE
Lehrstuhl B für Physikalische Chemie, Technische Universität, Braunschweig, West Germany

and

J. YARWOOD and K.E. ARNOLD
Department of Chemistry, University of Durham, Durham City, DH1 3LE, UK

Received 28 July 1980

Reorientational correlation functions $G^{(l)}_{rot}(t)$ for the degenerate (E) bands of liquid acetonitrile (CH_3CN) have been computed using NMR spin–lattice relaxation data (for CD_3CN) and gas phase Raman band profiles, assuming that the rotational diffusion model is valid. The effects of both anisotropic rotational motion and of Coriolis coupling are included. The predicted correlation functions along with those calculated using the classical "free" rotor equations, have been compared with those obtained from the ν_5 (Raman) and ν_8 (IR and Raman) experimental band profiles. It is shown that, despite the simplicity of the model and obvious (understandable) discrepancies at short times, sensible conclusions may be drawn. This work represents a starting point for the testing of more complicated models for reorientational motion in dense phases.

1. Introduction

The investigation of vibrational relaxation and molecular reorientational processes in (simple) molecular liquids using spontaneous Raman scattering and infrared absorption spectroscopy has recently generated a considerable literature [1–4]. Most publications have described studies on the parallel bands of symmetric top molecules since, in this case, separation of vibrational and rotational contributions to the overall band profile is relatively straightforward [1,2] (although by no means without its difficulties). One of the molecules most extensively studied in this way has been acetonitrile [5–9] (a full list is given in ref. [5]). Despite the interference of overlapping hot bands [9] and the apparent complexity of the molecular dynamics, a great deal of useful information has been obtained and a number of different theoretical approaches [10–13] to the prediction of the dynamic properties have been tested.

The study of depolarised Raman bands of symmetric top molecules (point groups C_{3v}, D_3 or D_{3d}) belonging to symmetry species other than A_1, is considerably more difficult [1,2,9] and relatively little work has been reported [14–28]. The additional difficulties [10,19,23] may be summarised as follows:

(i) The separation of vibrational and rotational contributions to the band contour is impossible using the standard (Raman) technique [28].

(ii) The Raman band profile is the sum of two components (see below) each of which contains a different vibrational and rotational contribution.

(iii) The band shapes are strongly influenced by first order Coriolis coupling.

Nevertheless, it is very important that such bands are studied, not least because the parallel rotational (spinning) motion of the molecule only affects the relaxation of bands for which the transition moment is perpendicular to the symmetry axis [14,24]. In this paper we therefore present the initial results of a

study of the degenerate (E) bands, ν_5 and ν_8 of liquid acetonitrile. We have used the experimental NMR spin–lattice relaxation times [30–33] (which are sensitive to both spinning ($\parallel$) and tumbling ($\perp$) motions) in order to predict (using an anisotropic rotational diffusion model) the rotational contribution to the overall profiles of infrared and Raman bands. The relative intensities of the two components of the Raman bands, determined by the relative magnitudes of the polarisability matrix elements associated with these components [23], have been estimated from vapour phase measurements. Our approach is similar to that of Gilbert et al. [19] (for NF_3) and of Arndt and McClung [23] (for C_6H_{12}).

2. Theoretical

2.1. Vapour phase spectra

The effects of Coriolis coupling on the vapour phase degenerate (E) Raman bands of symmetric top molecules have been discussed in detail elsewhere [19,34,35] so only the essential outline is given here. There are two sets of K transitions with selection rules $\Delta K = \pm 1$ and ± 2 for a given J transition (with $\Delta J = 0, \pm 1, \pm 2$). The relative intensity, $x/(1-x)$, of the two sets of transitions is controlled by the different components of the polarisability tensor [23] and is not known. The rotational fine structure of each degenerate band is therefore controlled by the ratio $x/(1-x)$ and by the Coriolis coupling constant, ξ. In general, it is difficult to determine the two parameters from the band contour alone although this has been attempted previously [29,37]. In the case of ν_5 and ν_8 of acetonitrile the ξ constants are known from infrared [38] and microwave [39] measurements so only the intensity ratio needs to be determined. This is achieved (see section 5.1) by fitting to the observed spectrum. The Q branches are sometimes resolved, expressions for their spacings being given in a first order approximation by [34]

$$(\mathrm{PR})_{Q_K} = 2[A(1-\xi) - B], \quad \text{for} \quad \Delta K = \pm 1, \qquad (1)$$

$$(\mathrm{OS})_{Q_K} = 4[A(1+\xi/2) - B], \quad \text{for} \quad \Delta K = \pm 2. \qquad (2)$$

Theoretical band contours were, in fact, calculated using a programme similar to that of Masri and Williams [40]. Use is then made of the expected identity of the $x/(1-x)$ ratio in vapour and liquid states [19,36].

2.2. Liquid phase spectra

For the degenerate bands of a C_{3v} molecule, in the (Debye) rotational diffusion limit, the rotational correlation functions [10,19] are given by,

$$G^{(1)}_{\mathrm{rot}}(t) = \exp\{-[\bar{\omega}_\perp^2 \tau_\omega^\perp + (1-\xi)^2 \bar{\omega}_\parallel^2 \tau_\omega^\parallel]t\}, \qquad (3)$$

for the infrared spectrum ($l = 1$), and by

$$G^{(2)}_{\mathrm{rot}}(t) = x \exp\{-[5\bar{\omega}_\perp^2 \tau_\omega^\perp + (1-\xi)^2 \bar{\omega}_\parallel^2 \tau_\omega^\parallel]t\} + (1-x)\exp\{-[2\bar{\omega}_\perp^2 \tau_\omega^\perp + 4(1+\xi/2)^2 \bar{\omega}_\parallel^2 \tau_\omega^\parallel]t\}, \qquad (4)$$

for the Raman spectrum ($l = 2$).

The parallel and perpendicular components of the angular frequency are given by [19]

$$\bar{\omega}_\parallel^2 = kT/I_z, \quad \bar{\omega}_\perp^2 = kT/I_x. \qquad (5)$$

These frequencies are also used to define the relevant (classical) rotational second moments, $M_{2R}^{(l,k)}$, given by

$$M_{1R}^{(1,1)} = kT/I_x + (1-\xi)^2\, kT/I_z, \qquad (6)$$

$$M_{2R}^{(2,1)} = 5kT/I_x + (1-\xi)^2\, kT/I_z, \qquad (7)$$

$$M_{2R}^{(2,2)} = 2kT/I_x + (1+\xi/2)^2\, 4kT/I_z. \qquad (8)$$

The angular momentum correlation times $\tau_\omega^\perp$ and $\tau_\omega^\parallel$ are related to the times between collisions assuming that tumbling and spinning motions are controlled by different dynamic parameters (for anisotropic probe molecule rotation). I_x and I_z are the moments of inertia perpendicular and parallel to the symmetry axis (these values [41] are given for acetonitrile in table 1). In the small angle diffusion limit [10] it is usual to define separate diffusion coefficients for the

Table 1
Moments of inertia for CH_3CN and CD_3CN (g cm^2)

	I_x	I_z
CH_3CN	91.2×10^{-40}	5.4×10^{-40}
CD_3CN	106.8×10^{-40}	10.9×10^{-40}

two rotations. These are given by

$$D_\perp = (kT/I_x)\tau_\omega^\perp \tag{9}$$

and

$$D_\parallel = (kT/I_z)\tau_\omega^\parallel \tag{10}$$

and numerical values may be obtained from NMR electric quadrupole induced spin–lattice relaxation times using expressions of the form [30–32],

$$\tau_{\text{eff}}^{(2)} = \frac{\frac{1}{4}(3\cos^2\theta - 1)}{6D_\perp} + \frac{3\sin^2\theta\cos^2\theta}{5D_\perp + D_\parallel} + \frac{\frac{3}{4}\sin^2\theta}{2D_\perp + 4D_\parallel} \tag{11a}$$

$$= \tfrac{1}{4}(3\cos^2\theta - 1)\tau^{(2,0)} + 3\sin^2\theta\cos^2\theta\tau^{(2,1)} + \tfrac{3}{4}\sin^2\theta\tau^{(2,2)}, \tag{11b}$$

where θ is the angle between the molecular symmetry axis and the electric field gradient tensor. It is probably best, however, to compare values of $\tau_\omega^\perp$ and $\tau_\omega^\parallel$ (rather than $D_\perp + D_\parallel$) since the latter will be different anyway if $I_z \neq I_x$ [eqs. (9) and (10)].

In order to calculate the correlation functions of eqs. (3) and (4) we need the values of x, ξ, $\tau_\omega^\perp$ and $\tau_\omega^\parallel$. As already pointed out the x and ξ values may be extracted from vapour phase measurements. $\tau_\omega^\perp$ (or $D_\perp$) is related via the Hubbard relation [42] to the tumbling motion of the molecule which controls the rotational part of the Raman (depolarised) band shape of a totally symmetric (A_1) vibration [10]:

$$\tau_\omega^\perp = I_x/6kT\tau^{(2,0)}. \tag{12}$$

$\tau_\omega^\parallel$ (or $D_\parallel$) can then obviously be calculated by combining $\tau_\omega^\perp$ (or $D_\perp$) with NMR values of $\tau_{\text{eff}}^{(2)}$ according to eq. (11). This procedure is well established [30,43, 44] and will not be repeated here. It should be noted, however, that in using spin–lattice relaxation measurements for CD_3CN in order to interpret the infrared and Raman spectra of CH_3CN one has to make an assumption about the relationship between the dynamic parameters of the normal and deuterated molecule. We have chosen here to assume that the angular momentum correlation times are independent of isotropic substitution ($\tau_\omega(CD) = \tau_\omega(CH)$) and use

$$D^{CD} = (I_x^{CH}/I_x^{CD})D^{CH} \tag{13}$$

This seems to us preferable to the alternative assumption that τ_ω is isotope dependent (but that D is not). The τ_ω values might be expected to reflect the differing intermolecular potentials (for example, for tumbling or spinning motion) acting on the molecule. We can see no reason why they should depend on isotope nor indeed why D should *not* change when the moment of inertia changes (in the case of $D_\parallel$ by a factor of two).

In order to make a first qualitative assessment of the possible breakdown of eqs. (3) and (4) due to inertial effects (not included in the rotational diffusion model) we have calculated the expected "free rotational" correlation function obtained, for example, by

$$G_{FR}^{(2)}(t) = x\exp[-M_{2R}^{(2,1)}/t^2] + (1-x)\exp[-M_{2R}^{(2,2)}/t^2]. \tag{14}$$

The results of these computations are shown in figs. 6–8 and they show that, except at rather short times (<0.1 ps), the observed correlation functions show little sign of inertial effects and do indeed decay exponentially as expected from eqs. (3) and (4). We note that the model [45] describing inertial corrections to the rotational diffusion equations requires that the log $G_{IR}(t)$ curve gives a zero time intercept >1. Our Raman data for these bands do not, however, show this behaviour.

3. Experimental

Detailed descriptions of the Raman spectrometer and the data evaluation procedures appear elsewhere [5,6,46]. The spectral slit width used for the ν_5 and the ν_8 band were 2.3 cm^{-1} and 1.5 cm^{-1} respectively. To avoid truncation effects, digitized scattering intensities were collected at 0.5 cm^{-1} (ν_5) and 0.25 cm^{-1} (ν_8) intervals over a frequency range of 15 half-widths on the high frequency side of the band maximum.

Vapour phase measurements were made at 80°C under atmospheric pressure without special equipment. The slit width was 5 cm^{-1} and the laser output power was 11 W.

Infrared measurements on ν_8 were made using a Perkin–Elmer model 580B spectrometer equipped with digital readout of transmittance data. Variable temperature measurements were made with a standard CsI heated infrared cell and a Beckman RIIC Ltd. (TEM-1C) temperature controller. All the data

were collected between 430 and 300 cm^{-1} in integrated scan mode 6b which (at 380 cm^{-1}) provides a spectral slit width of 3 cm^{-1}. The parameters quoted here are for data collected over a frequency range of about 10 half-widths on the high frequency side of the band.

Spectral grade acetonitrile was purchased from Merck or Eastman. It was dried and distilled (to remove dust) prior to use.

4. Data analysis

Computation of the correlation functions was carried out using numerical "fast Fourier transformation" (the routine in the Nottingham Algorithmic Group library) using either the ICL 1906S (Braunschweig) or the IBM 370 (Durham, NUMAC) computer. Deconvolution (for liquid phase spectra) and convolution (for the generated vapour phase spectra) of the instrument (slit) function were achieved using a gaussian "slit" profile.

5. Results and discussion

5.1. Vapour

The experimental vapour phase spectrum of ν_5 is shown in fig. 1, with a band centre observed at 3000 cm^{-1}. The highly polarized fundamental ν_1 appears as a sharp line at 2942 cm^{-1}. The Coriolis coupling constant ξ_5 has a value of 0.062 [38]. It follows from eqs. (1) and (2) that the spacing of the Q branches is 9.3 cm^{-1} for the transitions in J with $\Delta K = \pm 1$ and 20.6 cm^{-1} for those with $\Delta K = \pm 2$, and so they should be resolved. Both spacings are observed in the spectrum, and indeed the best fit is obtained with $x = 0.5 \pm 0.15$ given by the smoothed line shown in fig. 1. The experimental spectrum of ν_8 is shown in fig. 2. With a Coriolis constant of 0.878 [39], the spacings of the Q branches are 0.7 cm^{-1} (for $\Delta K = \pm 1$) and 31.6 cm^{-1} (for $\Delta K = \pm 2$), so only the latter should be resolved. However, no Q-branch spacing can be observed in the spectrum and it must be concluded that only the polarizability matrix elements associated with the $\Delta K = \pm 1$ transitions give rise to scattering. So the best fit is obtained with $x = 1$ (the error in x is about 0.15) and given by the smoothed line of fig. 2. The results for ν_8 of acetonitrile are in good agreement with those for ν_8 of the CF_3CN analogue in the work of Masri [37]. In this case it was also shown that intensity arises only from polarizability matrix elements connected with the $\Delta K = \pm 1$ transitions, the ν_8 bending vibration having a similar large positive value of the Coriolis coupling constant (0.53).

5.2. Liquid

The Raman correlation functions for ν_5 and the Raman and infrared correlation functions for ν_8 are shown in figs. 3–5, respectively. The correlation times obtained by numerical integration are given in table 2. As expected, in all cases the correlation functions decay more quickly as the temperature rises. Table 3 gives our values of $\tau_\omega^\perp$ and $\tau_\omega^\parallel$ computed from the correlation times for tumbling motion $\tau^{(2,0)}$ [eq. (12)] given by Yarwood et al. [5] and the effective correlation times $\tau_{eff}^{(2)}$ extracted from the work of Bopp [30]. These values are subject to errors, not least because often several different nuclear quadrupole coupling constants (NQC) have been reported. At least two values are available [30] for both the ^2H (160 kHz or 172.5 kHz) and ^{14}N (3740 kHz or 4400 kHz) nuclei. This inevitably leads to some ambiguity in the values of $\tau_{eff}^{(2)}$ and hence in $\tau_\omega^\parallel$ and $\tau_\omega^\perp$. Fortunately, since $\tau^{(2,0)}$ may be obtained independently [5] from Raman data [eq. (12)], we are able to conclusively deduce that, for the ^{14}N nucleus, a value of NQC of 4400 kHz is to be preferred since this leads to $\tau^{(2,0)}$ values which agree well with the Raman values (table 3). The uncertainty in the value of $\tau^{(2,0)}$ is then about ±0.2 ps. Uncertainty is also introduced due to the different possible values of the ^2H coupling constant (see table 3) and the final possible rotational correlation functions are incorporated in figs. 6–8. It is noted that the values of $\tau_{eff}^{(2)}$ (and $\tau_\omega^\parallel$) have been obtained from NMR data [30] for the deuterated (CD_3CN) species. Isotope effects on $\tau_\omega^\parallel$ are expected [43] to be small, although there is evidence [33] that there may be some such dependence. Since, however, τ_ω values are related to the times between "collisional" events (and hence, as mentioned above, to the intermolecular potentials), it does not seem reasonable to anticipate gross changes on deuteration. As expected, $\tau_\omega^\parallel > \tau_\omega^\perp$, reflecting the fact that the

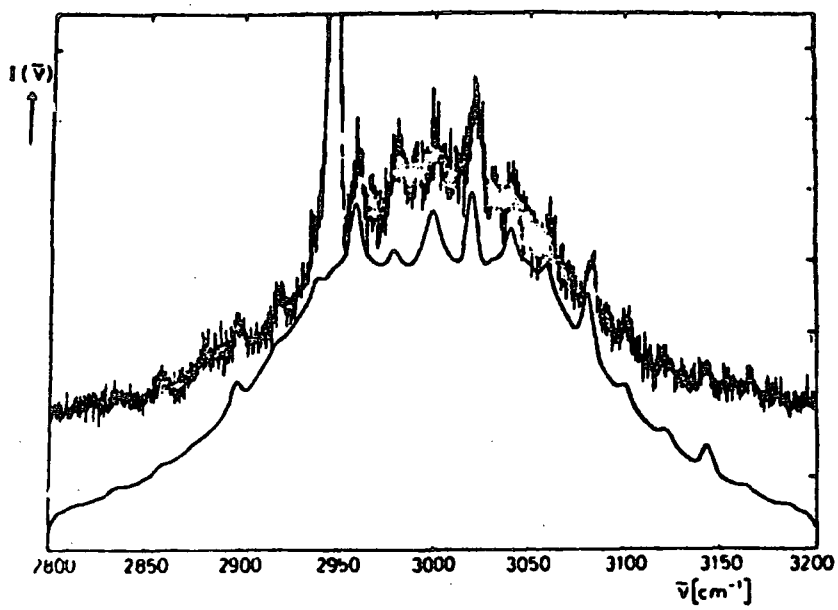

Fig. 1. Vapour phase spectrum of ν_5 and generated spectrum (smoothed line) at 80°C.

"spinning" motion is considerably less hindered than that of "tumbling". This result is in contradiction to the results of Bull [31] who used an isotropic J-diffusion model [10] and concluded that anisotropic reorientation in liquid acetonitrile may be explained simply by the different moments of inertia. Notice, however, that the degree of anisotropy depends very much on the value of the NQC used (table 3).

The two vibrations will now be discussed separately. It is easily shown from eqs. (7) and (8) that for

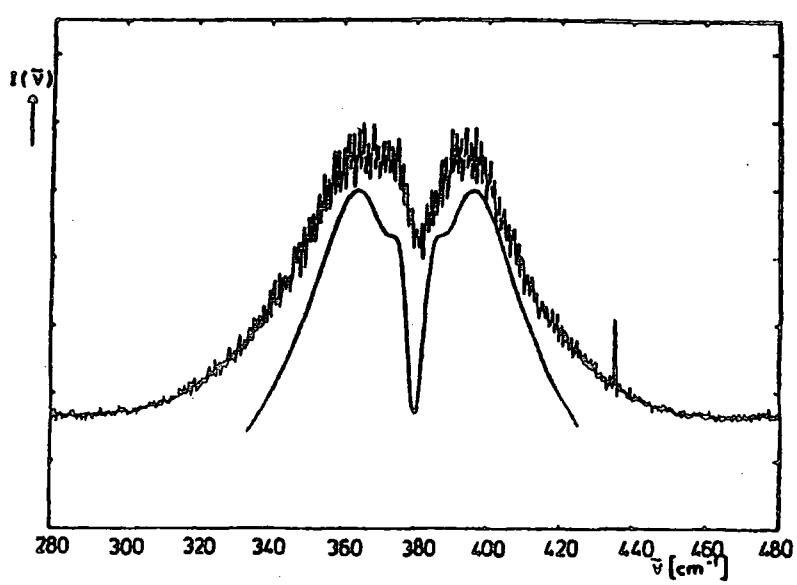

Fig. 2. Vapour phase spectrum of ν_8 and generated spectrum (smoothed line) at 80°C.

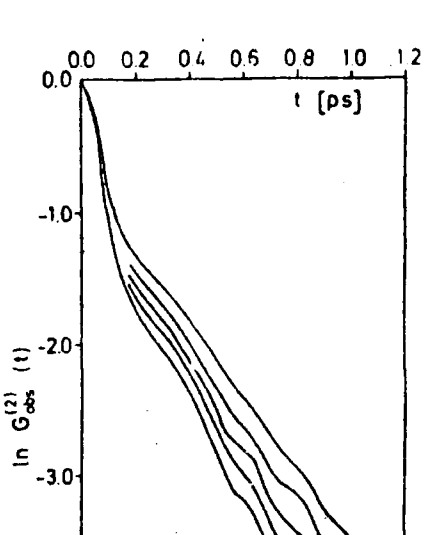

Fig. 3. Raman correlation functions of ν_5 at different temperatures. From top to bottom: 249, 270, 297, 314 and 338 K.

ν_5 ($\xi = 0.062$) the rotational second moment $M_{2R}^{(2,2)}$ is about 3.5 times larger than $M_{2R}^{(2,1)}$. As a consequence the second term in the rotational correlation

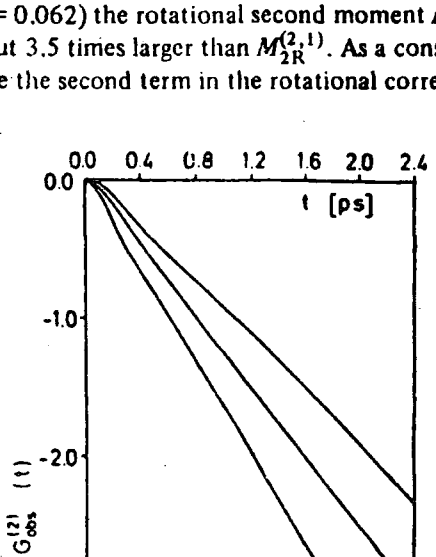

Fig. 4. Raman correlation functions of ν_8 at different temperatures. From top to bottom: 249, 297 and 338 K.

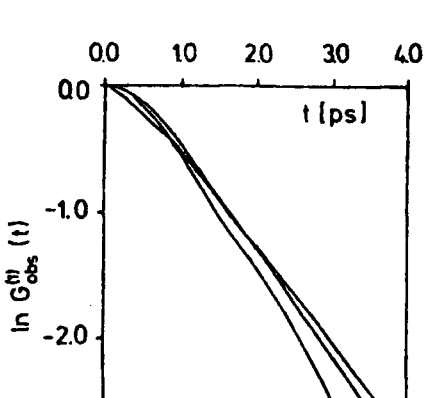

Fig. 5. Infrared correlation functions of ν_8 at different temperatures. From top to bottom 288, 318 and 343 K.

function [eq. (4)] decays considerably faster than the first term. Since both terms have equal weighting factors ($x = 0.5$) the overall $G_{tot}^{(2)}(t)$ is expected to show an overall non-exponential decay and the rotational band shape is the sum of two lorentzians of different half-widths. This means that the correlation function shows a "turning point" which can be observed at $t = 0.2$ ps (figs. 3 and 6). Fig. 6 compares calculated rotational correlation functions (with associated uncertainties discussed above) with the

Table 2
Temperature dependence of the (full) width at half height and the observed correlation times for ν_5 and ν_8

Vibration	T (K)	fwhh (cm^{-1})	τ_{obs} (ps)
Raman			
ν_5	249	35	0.21
ν_5	270	41	0.19
ν_5	297	47	0.17
ν_5	314	51	0.16
ν_5	338	57	0.15
ν_8	249	12.0	1.05
ν_8	297	15.0	0.79
ν_8	338	19.5	0.61
infrared			
ν_8	288	8.5	1.70
ν_8	318	9.3	1.65
ν_8	343	11.7	1.40

Table 3
Temperature dependence of the angular momentum correlation times $\tau^{\perp}_{\omega}$ and $\tau^{\parallel}_{\omega}$

T (K)	$\tau^{(2,0)}$ (ps) [a]	$\tau^{(2)}_{eff}$ (ps) [b]	$\tau^{(2)}_{eff}$ (ps) [c]	$\tau^{\perp}_{\omega}$ (ps)	$\tau^{\parallel}_{\omega}$ (ps) [b]	$\tau^{\parallel}_{\omega}$ (ps) [c]
249	2.2	0.53	0.62	0.020	0.051	0.035
270	1.9	0.44	0.51	0.021	0.060	0.042
297	1.5	0.36	0.42	0.025	0.063	0.044
314	1.3	0.32	0.38	0.027	0.065	0.044
338	1.1	0.28	0.33	0.030	0.066	0.045

[a] Data from ref. [5].
[b] Calculated using data from ref. [30] with NQC = 172.5 kHz.
[c] Calculated using data from ref. [30] with NQC = 160.0 kHz.

observed data for ν_5. The curves based on NQC = 160 kHz come close to the experimental one while a value of 172 kHz gives a function which decays too quickly. (The results for other temperatures are similar.) However, the uncertainty in x should not be forgotten and the results should not be over-interpreted. Two firm conclusions can, however, be formulated.

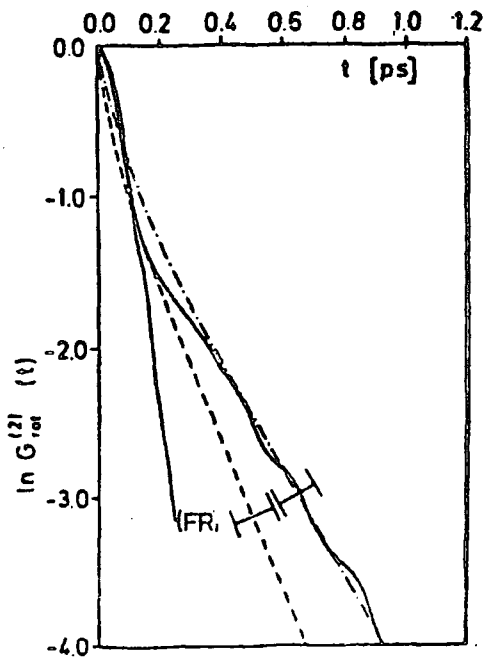

Fig. 6. Raman correlation function of ν_5 at 298 K (solid line). Calculated rotational correlation functions according to eq. (4) based on a ^{2}H NQC of 160.0 kHz (– · – · –) and 172.5 kHz (– – – –). (The error bars represent the uncertainty in the value of $\tau^{(2,0)}$ and the curve marked "FR" is the free rotor correlation function.)

Firstly, the diffusion model appears to produce a correlation function of the correct overall shape. The agreement at low t is not too good but this is expected since it is known [2,9,10] that the model is inadequate in this time regime (reorientation about the symmetry axis, in particular, is probably not diffusional). Indeed, the J-diffusion model (extended to symmetric top molecules [47]) would provide a more realistic approximation for the description of large angle molecular rotations in liquids. But its usefulness is severely restricted by the assumption of an isotropic reorientation ($\tau^{\parallel}_J = \tau^{\perp}_J$). Secondly, it is clear that vibrational relaxation contributes only a small amount to band broadening – at least in the Raman spectrum. This is not unexpected since the largest (Raman) vibrational band width measured [5] for CH_3CN is about 8 cm^{-1} (for the ν_3 band). Even this is small compared with the ≈50 cm^{-1} observed for ν_5 (table 2). The ν_5 (Raman) band shape is thus determined mainly by the effects of rapid rotation about the C_3 axis. Since the infrared band width [48], is at least as large (and since the rotational correlation function, $G^{(1)}_{rot}(t)$, decays more slowly [1,2] – eq. (3)), it seems likely that the infrared and Raman vibrational parts may once again differ [49]. (This will be the subject of more detailed investigation in the future.)

In the case of the ν_8 band both IR and Raman bands have only one contribution ($x \approx 1$) and the effects of rapid spinning motion are reduced by a high Coriolis coupling constant [39] ($\xi = 0.88$) – eqs. (3) and (4). Consequently the band shapes are both nearly lorentzian, the correlation functions decay exponentially (figs. 4, 7 and 8), and the half-widths are much smaller (table 2). Figs. 7 and 8 compare

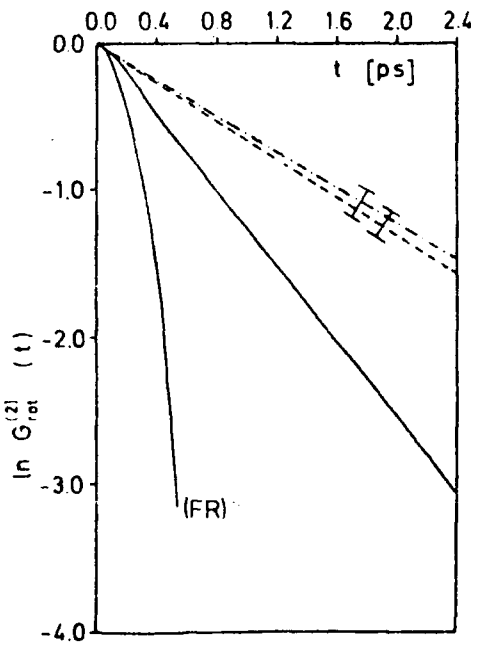

Fig. 7. Raman correlation function of ν_8 at 298 K (solid line). Calculated rotational correlation functions according to eq. (4) based on a NQC of 160.0 kHz (– · – · –) and 172.5 kHz (– – – –). (The error bars represent the uncertainty in the values of $\tau^{(2,0)}$ and the curve marked "FR" is the free rotor correlation function.)

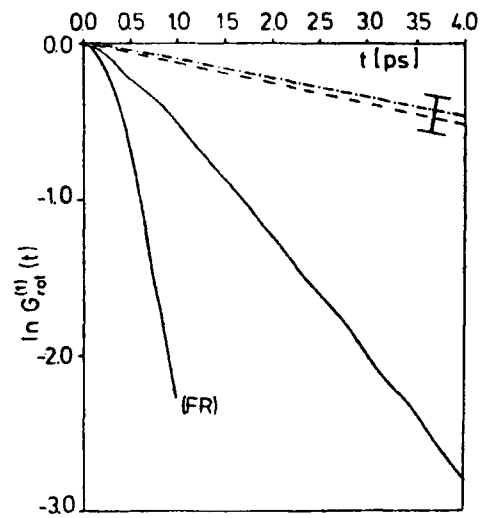

Fig. 8. Infrared correlation functions of ν_8 at 288 K (solid line). Calculated rotational correlation functions according to eq. (3) based on a NQC of 160 kHz (– · – · –) and 172.5 kHz (– · · – · · –). (The error bars represent the uncertainty in the value of $\tau^{(2,0)}$ and the curve marked "FR" is the free rotor correlation function.)

calculated and observed correlation functions, and it is clear that, since spinning motion gives only a minor contribution to the band shape, the choice of NQC (or $\tau^{\parallel}_{\omega}$) has little influence. The calculated $G^{(l)}_{rot}(t)$ decay much more slowly than the observed functions and clearly vibrational relaxation is much more significant than for ν_5. Extraction of the $\phi_{vib}(t)$ functions by division shows that the vibrational relation rate increases with increasing temperature. This may give some insight into the mode of vibrational relaxation [3] but one also has to remember the approximate nature of the calculation of $G^{(l)}_{rot}(t)$ via eqs. (3) and (4). What is clear, however, is that for ν_8 the vibrational part of the band shape seems to be very similar in both Raman and infrared spectra. ($\tau^{(1)}_{vib}$ = 1.9 ps; $\tau^{(2)}_{vib}$ = 1.6 ps at 297 K.) This emphasises that each individual mode *must* be investigated separately when such differences are sought.

Obviously further investigation of the viability of models for molecular rotation in dense fluids is needed. In particular, one needs to examine the validity of our assumption of negligible "cross" terms [13b,c] in rotational correlation functions of degenerate bands. Furthermore, it is not clear that our assumption of $\tau_{\omega}(CH_3CN) = \tau_{\omega}(CD_3CN)$ is absolutely correct [33]. Nevertheless, we feel that the simplest model is where one should start. The results present here represent a step forward, in that we have recognised the anisotropic nature of the rotation of molecules like acetonitrile. The differences in observed band shape between the ν_5 and ν_8 bands are adequately explained, while the comparisons of infrared and Raman band shapes of ν_8 lead to perfectly reasonable conclusions. Furthermore, both the vibrational correlation times and their temperature dependence are very similar to those obtained previously for acetonitrile. We now plan to investigate the (relative) validity of alternative models which have been suggested [11,12,50] with particular emphasis on the short time part of the motion.

Acknowledgement

Valuable discussions with Dr. R. Lynden-Bell are gratefully acknowledged. Thanks are also due to the DFG, the Royal Society and the SRC for equipment grants. One of us (K.A.) also thanks the SRC for a studentship.

References

[1] R.T. Bailey, Specialist Periodical Report, Molecular spectroscopy, Vol. 2, eds. R.F. Barrow, D.A. Long and D.J. Millen (The Chemical Society, London, 1974) p. 198.

[2] J.H.R. Clarke, in: Advances in infrared and Raman spectroscopy, Vol. 4, eds. R.E. Hester and R.J.H. Clark (Heyden, London, 1978) ch. 4, and references therein.

[3] J. Yarwood and R. Arndt, in: Molecular association, Vol. 2, ed. R. Foster (Wiley, New York, 1979) ch. 4, and references therein.

[4] J. Yarwood, Ann. Rev. Phys. Chem. C (1979) 99.

[5] J. Yarwood, R. Arndt and G. Döge, Chem. Phys. 25 (1977) 387.

[6] J. Yarwood, A. Khuen and G. Döge, Chem. Phys. 42 (1979) 331.

[7] K. Tanabe, Chem. Phys. 38 (1979) 125;
K. Tanabe and J. Hirashi, Spectrochim. Acta 36A (1980) 665.

[8] J. Schroeder, V.H. Schieman and J. Jonas, J. Chem. Phys. 66 (1972) 3215.

[9] J.E. Griffiths, in: Vibrational spectra and structure, Vol. 6, ed. J.R. Durig (Elsevier, Amsterdam, 1977).

[10] R.E.D. McClung, Advan. Mol. Relax. Inter. Processes, 10 (1977) 83.

[11] W.A. Steele, Proceedings of the NATO Summer School on Vibrational Spectroscopy of Molecular Liquids and Solids, Menton, 1979 (Plenum, New York, 1980) p. 61.

[12] W.A. Steele and A. St. Pierre, Mol. Phys., to be published.

[13] (a) R.M. Lynden-Bell, Mol. Phys. 31 (1976) 1653; 33 (1977) 907; 36 (1978) 1529;
(b) R.M. Lynden-Bell, Chem. Phys. Letters 70 (1980) 477;
(c) L.A. Nafie and W.L. Peticolas, J. Chem. Phys. 57 (1972) 3145.

[14] W.G. Rothschild, G.J. Rosasco and R.C. Livingston, J. Chem. Phys. 62 (1975) 1253.

[15] K. Tanabe and J. Jonas, J. Chem. Phys. 67 (1977) 4222.

[16] K. Tanabe, Chem. Phys. 31 (1978) 319; Chem. Phys. Letters 63 (1979) 43.

[17] M. Schlaak, Ber. Bunsenges. Phys. Chem. 81 (1977) 408.

[18] K. Müller and F. Kneubühl, Chem. Phys. 8 (1975) 468.

[19] M. Gilbert, P. Nectoux and M. Drifford, J. Chem. Phys. 68 (1978) 679.

[20] R. Seloudoux, J. Soussen-Jacob and J. Vincent-Geisse, Chem. Phys. 40 (1979) 257.

[21] C. Dreyfus, C. Breuillard, T. Nguyen Tan, A. Grosjean and J. Vincent-Geisse, J. Mol. Struct. 47 (1978) 41.

[22] M. Bouachir and J. Lascombe, J. Raman Spectry. 7 (1978) 271.

[23] R. Arndt and R.E.D. McClung, J. Chem. Phys. 70 (1979) 5598.

[24] G. Döge and T. Schäffer, Ber. Bunsenges. Phys. Chem. 77 (1973) 682.

[25] M. McClintock, D.A. Jennings and M. Mizushima, Phys. Rev. Letters 21 (1968) 276.

[26] K. Müller and F. Kneubühl, Chem. Phys. 8 (1975) 468.

[27] S. Sunder and R.E.D. McClung, Can. J. Phys. 52 (1974) 1209.

[28] F.J. Bartoli and T.A. Litovitz, J. Chem. Phys. 56 (1972) 404, 413.

[29] R.J.H. Clark and O.H. Ellestad, Mol. Phys. 30 (1975) 1899.

[30] B.T. Bopp, J. Chem. Phys. 47 (1967) 3621.

[31] T.E. Bull, J. Chem. Phys. 62 (1975) 222;
T.E. Bull and J. Jonas, J. Chem. Phys. 53 (1970) 3315.

[32] D.E. Woesner, B.S. Snowden and E.T. Strom, Mol. Phys. 14 (1968) 268.

[33] T.K. Leipert, J.H. Noggle and K.T. Gillen, J. Magn. Res. 13 (1974) 158.

[34] G. Herzberg, Molecular spectra and molecular structure Vol. 2 (Van Nostrand, Princeton, 1945).

[35] F.N. Masri and W.H. Fletcher, J. Raman Spectry. 1 (1972) 221.

[36] H.S. Goldberg and P.S. Pershan, J. Chem. Phys. 58 (1973) 3816.

[37] F.N. Masri, J. Chem. Phys. 57 (1972) 2472.

[38] C. Nakagawe and T. Shimanouchi, Spectrochim. Acta 18 (1962) 513.

[39] A. Bauer and S. Maes, J. Phys. (Paris) 30 (1969) 169.

[40] F.N. Masri and I.R. Williams, Comp. Phys. Commun. 1 (1970) 349.

[41] P. Venkateswarlu, J. Chem. Phys. 19 (1951) 293.

[42] P.S. Hubbard, Phys. Rev. 131 (1963) 1155.

[43] J.E. Griffiths, Chem. Phys. Letters 21 (1973) 354.

[44] J.H. Campbell, J.F. Fisher and J. Jonas, J. Chem. Phys. 61 (1974) 346.

[45] G.T. Evans, J. Chem. Phys. 67 (1977) 2911.

[46] G. Döge, R. Arndt and A. Khuen, Chem. Phys. 21 (1977) 53.

[47] J. O'Dell and B.J. Berne, J. Chem. Phys. 63 (1976) 2376.

[48] C. Breuillard-Alliot and J. Soussen-Jacob, Mol. Phys. 28 (1974) 905.

[49] J. Yarwood, P.L. James, G. Döge and R. Arndt, Faraday Discussions Chem. Soc. 66 (1978) 252.

[50] M. Possiel, unpublished results.